Fabrication of Polymeric Microcarriers with Reduced Permeability Using Layer-by-Layer, Surface-initiated Polymerization and Emulsion Techniques

A Thesis Submitted to University of London for the Degree of Doctor of Philosophy

Li Zhao

Supervisor: Professor Gleb B. Sukhorukov

School of Engineering and Materials Science

Queen Mary University of London

May 2016

Declaration

I certify that the present work is prepared solely by me during the course of my studies at Queen Mary University of London. It has not been submitted for a degree at this or any other university. Any words and /or figures from the work of other people are fully acknowledged according to standard referencing.

This thesis fully complies with the regulation set by University of London and Queen Mary University of London.

Li Zhao

May 2016

Abstract

In recent years, polymeric microcarriers have drawn great attention because of their potential applications in medical, cosmetic and some other industries. A variety of materials, preparation techniques have been explored to endow these microcarriers the desired properties. In spite of encouraging improvements in other properties, the low permeability of microcarriers remains a challenge which results in massive amount of cargo loss due to fast release.

This work aimed to develop microcarriers with reduced permeability by coating with biocompatible and hydrophobic polymers via different techniques such as Layer-by-Layer, surface-initiated atom transfer radical polymerization and emulsion methods.

This thesis starts with an introduction and literature review, which present the background of this work, followed by the description of materials as well as methods used in this work in chapter 3. Chapter 4 studied various parameters for fabricating structurally intact Poly(lactic acid) stereocomplex microcapsules, and demonstrated that heat treatment could significantly reduce the permeability of PLA microcapsules. In chapter 5, Layer-by-Layer and surface-initiated atom transfer radical polymerization techniques were combined to fabricate PMMA coated microparticles with low permeability. A polyelectrolyte macroinitiator and Poly(sodium 4-styrenesulfonate) were first deposited onto $CaCO_3$ particles through LbL process, followed by growing PMMA brush layer via ATRP from the polyelectrolyte precursor. Chapter 6 introduced a simple emulsion method to prepare PLA coated $CaCO_3$ microparticles with low permeability, which can retain bioactive molecules within the particles. It was found that 0.8 was the optimal $CaCO_3$/PLA mass ratio in terms of the low permeability of microparticles as well as high-usage of polymers. In chapter 7, PLA films

were synthesized from two different types of macroinitiators, with one being polyelectrolyte based and the other one being Poly(2-hydroxyethyl methacrylate) polymer brush precursor. The kinetics of PLA film growth from different precursors was compared whilst degradation of PLA films was also studied.

Table of Contents

Acknowledgements

How time flies. It has been three and a half years since I started studying at Queen Mary and my PhD is now about to finish. Looking back to the time I joined, I think that I have gained a lot from which I will be beneficial throughout my entire life. After having prepared for several months, my PhD thesis has been finished and at this moment I would like to thank some people who have been caring about me and supporting me all the time, without which I could not get what I pursued.

First of all, I would like to thank my supervisor Professor Gleb B. Sukhorukov who gave me this opportunity to carry out research in such an excellent environment. Professor Sukhorukov has the common touch and that is why he is so well beloved by all of us. He always guides me, solve my problems with patience, profound knowledge as well as rigorous scientific attitude. I am grateful for everything he has taught me and for the right scientific value he has shown me. It was my honour to have worked in his group, where there are so many talented young researchers that I can learn from and communicate with.

I also would like to thank Dr Julien Gautrot, without whose kind support and fruitful discussion I could not have completed my projects. He is so knowledgeable in polymer chemistry and is selfless to deliver me the techniques and good advice. I was truly inspired by his hard working attitude and desire to the unknown scientific world.

I would like to thank Dr Remzi Becer who has also given me plenty of suggestions and the access to his facilities and Dr Anton Pavlov who taught me the basic techniques of making microcapsules which made the beginning of my PhD much easier.

Many thanks to Miss Burcu Colak for supporting me on the synthesis of polymers and to Dr Nadja Tarakina and Mr Russelle Bailey at Nanovison for the help with SEM and TEM.

I would like to thank all my current and previous colleagues who have accompanied me here at Queen Mary. I would like to give my best wishes to Dr Ran Hao, Dr Weizhi Liu, Dr Devendra Deo, Miss Hui Gao, Mr Yuxiu Chen, Mrs Meiyu Gai, Miss Samantha Gabriel, Miss Valeriya Kudryavtseva.

Finally I would like to thank my families who have been supporting me throughout my life. I would not have had a chance to get to this point without their sincere love. Thank you all and wish myself a bright future.

List of Figures

List of Symbols and abbreviations

AFM - atomic force microscopy

APTES - (3-Aminopropyl)triethoxysilane)

$CaCO_3$ - calcium carbonate

CLSM - confocal laser scanning microscopy

CTA (chain transfer agent)

DCM – dichloromethane

DI H_2O - deionized water

DMAEMA - dimethylaminoethyl methacrylate

DMF - N,N-dimethyl formamid

DMSO - dimethyl sulfoxide

DSC - differential scanning calorimetry

EDS - energy-dispersive X-ray spectroscopy

EDTA - ethylenediaminetetraacetic acid disodium salt

FITC-dextrans - fluorescein isothiocyanate-dextrans

FITC-BSA - fluorescein isothiocyanate-bovine serum albumin

FTIR - Fourier transform infrared spectroscopy

GPC - Gel permeation chromatography

HA - hyaluronic acid

HCl - hydrochloric acid

HEMA - 2-hydroxyethyl methacrylate

HF - hydrogen fluoride

it-PMMA - isotactic poly(methyl methacrylate)

LbL - Layer-by-Layer

LLA – L-lactide

MF - melamine formaldehyde

$MgCO_3$ - magnesium carbonate

MI – macroinitiator

NH_4F - ammonium fluoride

NMR - nuclear magnetic resonance

PAH - Poly(allylamine hydrochloride)

PBS - phosphate-buffered saline

PDADMAC - Poly(diallyldimethylammonium chloride)

PDLA - Poly(D-lactide)

PEC - Polyelectrolyte complex

PEI - Polyethylenimine

PLA – Poly(lactic acid)

PLL - Poly(L-lysine)

PLLA - Poly(L-lactide)

PGMA - Poly(glycidyl methacrylate)

PHEMA - Poly(2-hydroxyethyl methacrylate)

PMA - poly(methacrylic acid)

PMMA - Poly(methyl methacrylate)

PSS - Poly(sodium 4-styrenesulfonate)

PVA - Polyvinyl alcohol

QCM - quartz crystal microbalance

RhB - rhodamine B

RP-LbL - Reverse-Phase Layer-by-Layer

SAM - self-assembled monolayer

SEM - scanning electron microscope

SI-ATRP - surface-initiated atom transfer radical polymerization

SI-CRP - surface-initiated controlled radical polymerization

SI-NMP - surface-initiated nitroxide-mediated polymerization

SI-RAFT - surface-initiated reversible-addition fragmentation chain transfer polymerization

SI-ROP - surface-initiated ring-opening polymerization

$Sn(Oct)_2$ - Tin(II) 2-ethylhexanoate

SPR - surface plasmon resonance

st-PMMA - syndiotactic poly(methyl methacrylate)

T_g - glass transition temperature

TEM - transmission electron microscope

THF – tetrahydrofuran

UV – Ultraviolet

XRD - X-ray diffraction spectrometry

1 Introduction and motivations

As an emerging part of materials science, microtechnology has received great attention in recent decades. Macro/nano delivery systems are of particular interest due to their broad applications. One of the core objectives of developing such smart delivery systems is to protect loading cargos from surrounding environment as well as releasing them in a controlled manner. This is extremely important nowadays as conventional delivery tools usually result in quick release, which is not desired for most applications. Various techniques, including self-assembly, emulsion, Layer-by-Layer (LbL), in-situ polymerization, have been explored to create delivery vehicles at macro and nano scales, such as micelles, polymersomes, liposome, micro/nano capsules or particles. Each of these delivery vehicles has their unique advantages and at the same time flaws depending on the particular application they are used for. The applicability of different delivery carriers is determined by their properties such as size, chemical compositions, hydrophilicity/hydrophobicity, and the way they are fabricated, etc. In general, deliverers made of hydrophilic polymers would lead to faster release whilst microcarriers constructed from hydrophobic materials are likely to have slower release speed.

Layer-by-Layer (LbL) self-assembly technique that introduced by Decher *et al*[1, 2] employs oppositely charged substances to create multilayered thin films by electrostatic interaction. To build up such structure, various charged substances, including polyelectrolytes, proteins, DNA have been used as building blocks[3]. In the late 1990s, Sukhorukov *et al*[4, 5] applied this method on spherical templates to fabricate the so-called LbL microcapsules by depositing oppositely charged polyelectrolytes on templates and later on dissolving the templates, resulting in

hollow microcapsules that can be used to encapsulate a wide range of desired molecules[6, 7]. Recently, some techniques have been combined to make the most of their strengths. For example, Surface-initiated Polymerization was performed to grow thick polymer layer from macroinitiator containing multilayers constructed through LbL process[8]. This combination of different techniques gives a new direction of designing microcarriers.

So far, microcarriers have been widely used in medicine, food as well as cosmetic and other industries. One of the most popular applications of microcarriers is drug delivery, which is of significant importance nowadays as new advanced therapies require more controlled and targeted release of loaded drugs. Take cancer treatment as an example, the traditional chemo therapy would kill both normal human cells and cancer cells. Thereby, drugs are desired to be released only at the place of treatment. Microcarriers are thus becoming a very useful tool as drugs can be protected in the carriers before being navigated to the diseased region. However, most drugs are small molecules which make it difficult for the polymeric carriers to retain them before being triggered to release. Therefore, reducing the permeability of microcarriers is of great interest.

Permeability plays an important role in applications of microcarriers and affects the encapsulation of cargos as well as their controlled release from the microcarriers. There are two possible ways to adjust permeability. On the one hand, permeability largely depends on external factors such as ionic strength, pH value, whilst on the other hand, polymer properties and some other inherent factors can also have influence on it[9, 10]. However, despite the effort made, the fabrication of low permeable microcarriers remains a challenge.

Therefore, this PhD work is dedicated to fabricating polymeric microcarriers with reduced permeability using LbL, surface-initiated polymerization as well as emulsion techniques. The general idea is to create hydrophobic shell structure as depicted in Figure 1.1, which could eventually prevent diffusion of small molecules through the shell of microcarriers. Three types of microcarriers are fabricated using various techniques. The first approach described in chapter 4 is to make Poly(lactic acid) (PLA) microcapsules based on stereocomplexity, followed by heat treatment at different elevated temperatures which has been intensively applied to reduce the permeability of LbL microcapsules. Unlike common LbL microcapsules constructed by oppositely charged polyelectrolytes, Poly(D-Lactide) (PDLA) and Poly(L-lactide) (PLLA) form stereocomplex PLA, leading to a more compact structure. In addition, heat treatment above glass transition temperature (T_g) would rearrange the molecules within the shell structure thus healing the defects. The use of hydrophobic polymer shell could also potentially improve the result by repelling the surrounding water. The second approach is to create an additional layer that is low permeable around the porous particles. Two different methods are described in chapter 5 and 6, respectively. The first one involves both LbL and surface-initiated polymerization techniques. Multilayers that contain polyelectrolyte macroinitiator are first built up through LbL deposition, followed by an ATRP process which generates a Poly(methyl methacrylate) (PMMA) shell from the macroinitiator precursor. The other method is using solid-in-oil-in-water (S/O/W) double emulsion method to create a PLA coating layer on microparticles with an additional Poly(vinyl alcohol) (PVA) surfactant layer that stabilizes the obtained microparticle dispersion.

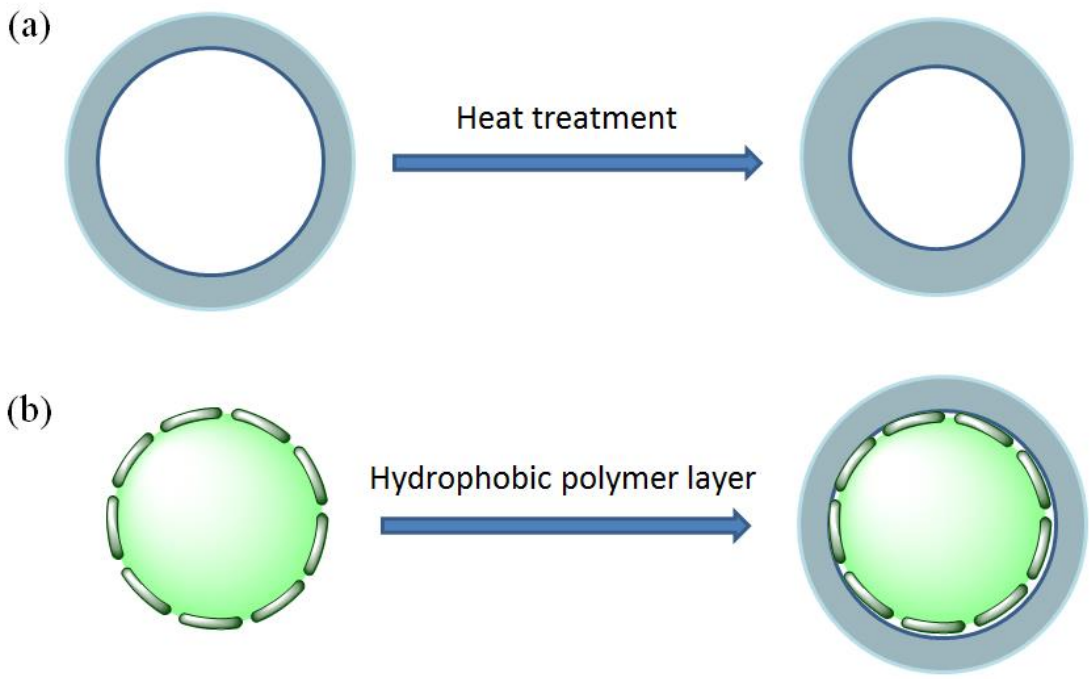

Figure 1.1 General idea of how to achieve microcarriers with reduced permeability, (a) shrinkage of microcapsules upon heat treatment, (b) coating of hydrophobic polymer layer on microparticles. The Size of these microparticles are supposed to be between 1-5 μm depending on the fabrication approach.

2 Literature review

2.1 Polyelectrolyte

Polyelectrolyte is a type of polymer that bears an electrolyte group along its repeating units. Polyelectrolytes appear to be viscous at high concentration in aqueous solution which is similar to polymers and the electrolyte groups it bears dissociate in aqueous medium, making their solutions conductive as ions. Similar to electrolyte molecules, polyelectrolytes could either be polycation or polyanion in aqueous solution, depending on what type of charge groups one has. Polyelectrolytes are also classified as strong polyelectrolyte or weak polyelectrolyte, according to the degree of the dissociation of the electrolyte groups in the aqueous solution. Strong polyelectrolytes are those that dissociate completely at most achievable pH values while the weak ones only partially dissociate at certain range of pH values. Therefore, the dissociation degree of weak polyelectrlytes could be largely affected by several factors including pH value, ionic strength as well as counterion concentration. The equation below is used to describe the reaction of the dissociation of weak polyelectrolytes:

$$HA \leftrightarrow H^+ + A^- \qquad \text{(Eq. 2.1)}$$

Where HA represent weak polyelectrolyte and H+, A- are cation and anion dissociated from HA, respectively. Since weak polyelectrolytes cannot fully dissociate in aqueous medium, the dynamic equilibrium of the dissociation is described by the dissociation constant (*Ka*):

$$K_a = \frac{[H^+]+[A^-]}{[HA]} \qquad \text{(Eq. 2.2)}$$

The degree of dissociation could be easily deduced as:

$$\alpha = \frac{[A^-]}{[A^-]+[HA]} \quad \text{(Eq. 2.3)}$$

And a modified HENDERSON-HASSELBALCH equation could be used to describe the dissociation equilibrium of weak polyelectrolytes:

$$pK_a = pH - n\lg\frac{\alpha}{1-\alpha} \quad \text{(Eq. 2.4)}$$

Where pKa is acid dissociation constant, n is related to the conformation of polymer chains which mainly depends on their charges.

It is very clear from Eq. 2.4 that pH plays a very important role in the dissociation of weak polyelectrolytes. For polyanion, when pH<pKa, the positively charged ions increase in the solution, causing the repression of the dissociation whereas the increase of negatively charged ions when pH>pKa attracts the proton to leave more easily from the electrolyte groups, making the dissociation degree higher. For polycation, the tendency is exactly opposite to that of polyanion.

The conformation of the polyelectrolytes in aqueous medium is, however, difficult to be predicted due to the complication of several affected factors, such as the dissociation degree, the pH, the concentration of other low molecular weight electrolytes. Unlike the uncharged polymers that are of statistically tangled shape, the polyelectrolyte chains tend to have a more asymmetric and untwisted shape due to the electrostatic repulsion which is a type of coulomb interaction created by the charged groups with same electronegativity. Moreover, these differences between polyelectrolytes and polymers without charge groups lead to the differences in other properties, such as viscosity, conductivity, diffusion ability and so on.

Additionally, pH plays an important role in the conformation of weak polyelectrolytes. For polyanion in lower pH condition, the high concentration of protons makes the

dissociation degree of the weak polyelectrolytes lower, leading to the polymer chains present a random shape. When the pH increases, the counterions of the polyions dissociate from the polymer chains and the polyions tend to stretch due to the electrostatic repulsion. In the case of polycation conformation, pH has completely the opposite effect.

Furthermore, the presence of small electrolytes, such as salts, can also influence the conformation through a screening effect on the polyions, resulting in the decrease of electrostatic repulsion and therefore a more bulky shape. The repulsion of polyions disappears when the concentration of salts increases to a critical value and the conformation of the polyelectrolytes is then exactly the same as uncharged polymers.

2.2 **Polyelectrolyte complex**

Polyelectrolyte complex (PEC) will be formed once oppositely charged polyelectrolytes are mixed in the solution.

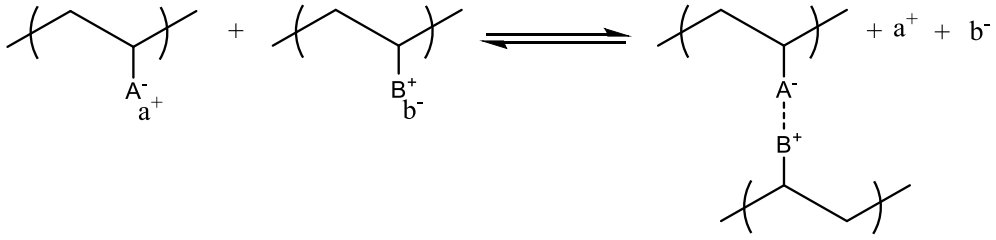

(Eq. 2.5)

This is due to the electrostatic interaction between the positively and negatively charged polyions. The increase in entropy by releasing the counterions is suggested to be the main driving force. The stoichiometric ratio between polycation and polyanion is ought to be 1:1 for strong polyelectrolytes whereas the ratio varies for the weak ones. It mainly depends on the dissociation degree which is why the pH of the solution has an important effect on the stoichiometric ratio between weak polycations

and their counterparts. Apart from the electrostatic interaction, other forces such as hydrogen bonding and hydrophobic interaction are also used for the formation of PECs.

Two models have been introduced to describe the conformation of PECs, ladder like and scrambled egg like structures as shown in Figure 2.1. The ladder model is the structure in which the oppositely charged polyelectrolytes stretch and pair up like zip while polyelectrolytes in random conformation tend to form in the scrambled egg structure. However, it has to be pointed out that both structures of PECs are expected to exist in the solution and the distribution could be adjusted by changing the properties of the solution.

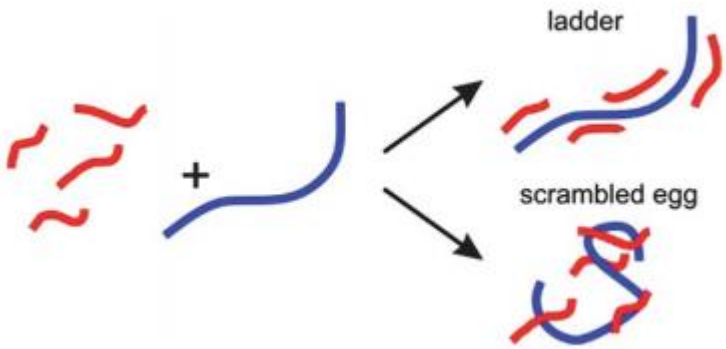

Figure 2.1 Illustration of two classic models for description of the conformation of PECs, ladder model (right top) and scrambled egg model (right bottom)[11].

2.3 **Polyelectrolyte Multilayers**

Self-assembly is an extremely attractive thing in the nature which contributes to a wide range of human activities at macro- or even smaller scale such as self-assembly of DNA. Thus, mimicking the self-assembly process in the biochemistry area is of particular importance. There are three main strategies to create thin multilayered

structure. They are Langmuir-Blodgett technique which is based on hydrophobic effect, chemisorption which is based on covalent bonding and alternative adsorption of oppositely charged polyions[12-14]. The latter one has some advantages over the former two methods in terms of available building molecules, precise control of thickness as well as simplicity. Since the oppositely charged polyelectrolytes are able to adsorb intermolecularly between one another, it offers a great feasibility to build up a number of polyelectrolyte layers through a self-assembly process. Unlike common polymeric layers that have no charges, polyelectrolytes layers could be useful for some biomedical purposes where the charges can interact with certain substances for potential applications.

2.3.1 The layer-by-layer Technique

In the early 1990s, Decher *et al* developed the so-called layer-by-layer technique to build up multi-layered films, which used the principle that differently charged polyelectrolytes can form polyelectrolyte complexes [1, 15]. Take a common process as an example (Figure 2.2), a charged substrate is alternately immersed in positively and negatively charged polyelectrolyte solutions. During each deposition step, charged macromolecules are adsorbed by oppositely charged surface, leading to the reversion of surface charge. After deposition, the substrate should be thoroughly washed to get rid of excess polyelectrolyte molecules, avoiding the formation of non-adsorbed polyelectrolyte complexes on substrate surface in the next step.

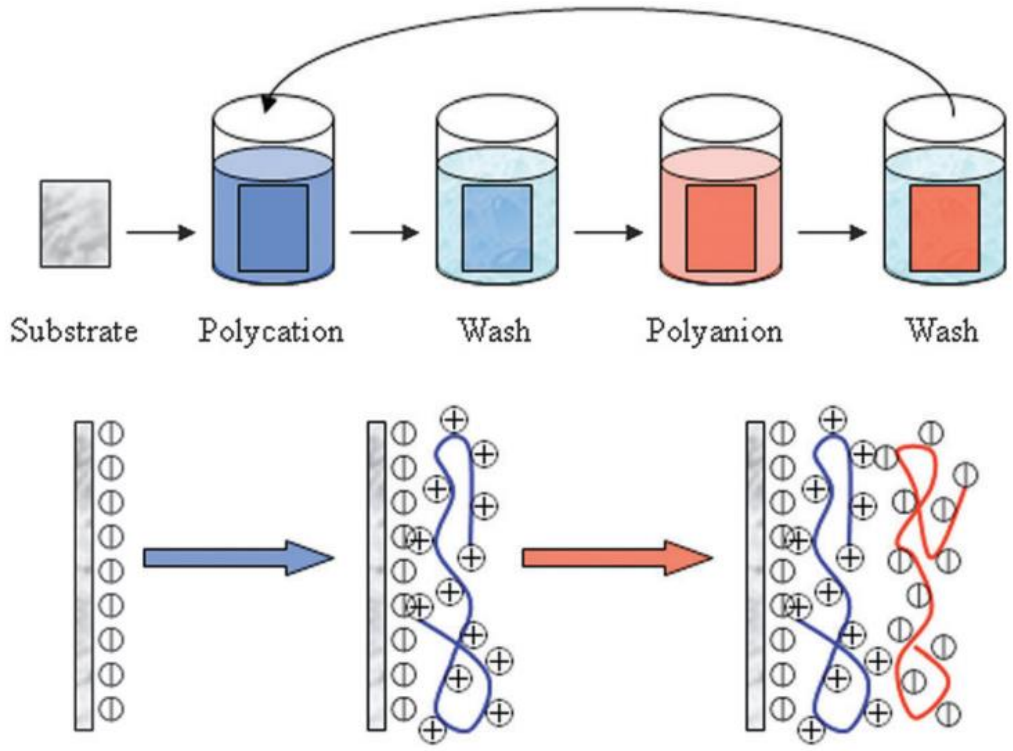

Figure 2.2 Schematic illustration of Layer-by-Layer (LbL) self-assembly by sequential adsorption of oppositely charged polyelectrolytes [16]

The thickness of multilayers could be tuned precisely by controlling the experimental parameters and so far multilayers up to 1000 layers had been successfully made [17]. In addition to the common immersing method, multilayers can also be built up by other means such as spin coating [18] and spraying [19, 20] that cost much shorter preparation time. To ensure the substrate is fully covered, the amount of polyelectrolyte should always be excessive, resulting in uniformly coated surfaces. Since this technique has become a versatile mean of producing thin films, more and more building compositions were introduced to make LbL multilayers. Not only synthetic polyelectrolytes [21] but also a variety of natural macromolecules such as polypeptides, DNA [22, 23] and lipids [24, 25] have been used. For different purposes, some particular substances (eg. dyes [26, 27], metal particles [28-30], carbon tubes [31]) can be incorporated into multilayers, endowing various properties that could be

used for possible applications in biomedical, food as well as cosmetic and other industries [32, 33]. In terms of the interactions that are utilized to build up multilayers, other forces such as hydrogen bonding, hydrophobic interaction have also been employed.

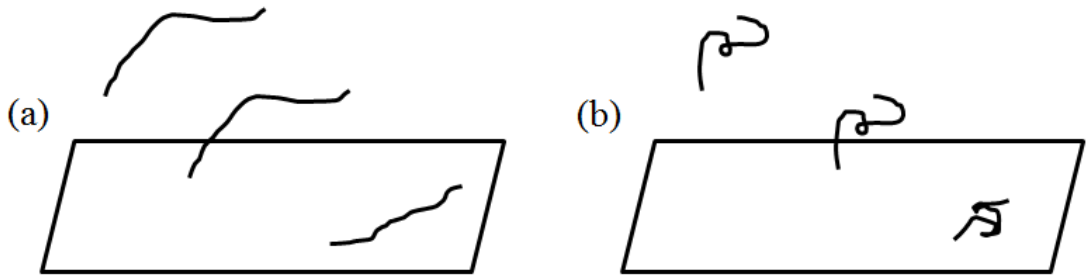

Figure 2.3 Different forms of Polyelectrolyte chains after attaching to charged surface: (a) stretched form, (b) coiled form

As illustrated in figure 2.3 the way the polyelectrolytes adsorbed onto the substrate largely depends on the conformation of their chains as well as the ionic strength. Strong polyelectrolyte with low ion concentration normally leads to a thin film because the polymeric chains are adsorbed in a stretched conformation so that opposite charges on neighbouring layers would pair up nicely. On the other hand, weak polyelectrolyte molecules exist in a coiled form which makes it literally impossible for all of them to pair up with opposite charges in the previous layer. The non-paired charges, depending on their positions on the polymeric chains, are called "loop" or "tail". The loops are those coil-like fragments in the middle of the chains while the tails are the ending parts of the chains whose surrounding area have probably been occupied by other chains. These non-paired charges on the substrate surface which is called "charge overcompensation" are the main driving force for the next deposition step which is why weak polyelectrolytes tend to form thicker

multilayers. Strong polyelectrolytes with high ionic concentration may also deposit in this manner due to the electrostatic repulsion between the ions and the charges of the polymeric chains which causes the polyelectrolytes to have coiled conformation when being adsorbed. This strategy is sometimes used to make thicker layers out of strong polyelectrolyte solution by adding extra salts.

In most cases, the deposition of each polyelectrolyte is very quick, taking only few seconds. However, about 15 minutes are allowed for each deposition step as the polyelectrolyte molecules need more time to rearrange to their favourite conformation. As soon as the whole surface is coated, no further dipping is needed as no more polyions will be further adsorbed. It was found that a precursor layer, mostly Polyethylenimine (PEI) or Poly(sodium 4-styrenesulfonate) (PSS) depending on the surface charge, is often needed as it is difficult to have the substrate entirely coated by other polyelectrolytes as the first layer.

2.3.2 Multilayer growth

As the LbL assembly process carried out, the thickness of the multilayers increases as a function of the layer number. There basically are two different growth patterns of polyelectrolyte multilayers, linear or exponential growth, which depends on the types of the polyelectrolytes. Strong polyelectrolytes tend to grow linearly in which the thickness as well as the mass of formed polymer layer change constantly as a function of layer number, whilst those weak ones usually grow in an exponential fashion and much more rapidly [34-36].

The most popular explanation for this exponential growth phenomenon is based on a diffusion theory[37]. The whole LbL constructed structure is divided by three domains as described in Figure 2.4. Domain I corresponds to the initial stage during

which the polyions anchor onto the substrate. The properties of the substrate play an important role at this stage. Domain III is exposed to the polyelectrolyte solution while domain II is the internal part between Domain I and Domain III. Basically, domain III starts to grow exponentially as soon as domain I is competed. However, as the thickness of domain III increases and by some point when this domain is too thick the free polyelectrolyte molecules can no longer diffuse through the entire multilayer structure, this domain stops growing. A new domain appears and grows linearly which is domain II. From this number of layer on, the increment of each polyelectrolyte bilayer becomes constant.

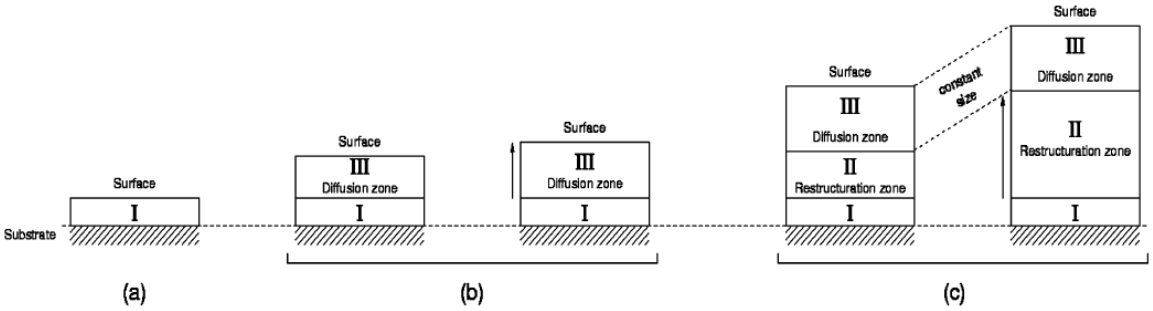

Figure 2.4 Schematic representation of the multilayer buildup mechanism by the model of the three zones: (a) At the beginning of the film buildup, the deposition of the first layers strongly depends on the properties of the substrate surface. This region is composed of only the first pairs of layers in the vicinity of the substrate surface and corresponds here to domain I. (b) The number of deposition steps increases, and the diffusion process takes place in domain III, leading to exponential growth of the film thickness. (c) As the construction goes on, the film undergoes a restructuring of the bottom layers of zone III, leading to the formation of a restructured zone denoted as zone II. Because this new zone is supposed to become impermeable for the diffusion process, domain III reaches a limited thickness, and the film grows linearly with the number of deposition step[37].

The rearrangement of the complexed polyion chains is thought to be another factor that contributes to this process. As domain III becomes thicker and the polyelectrolytes chains rearrange themselves, the polymer network becomes denser and less permeable which makes the incoming polyelectrolyte more difficult to diffuse through multilayers. Thereby, domain III stops growing once the free polyelectrolyte cannot travel through or penetrate domain III.

In the case of the hyaluronic acid (HA)/ poly(L-lysine) (PLL) multilayers build-up process[34, 38], HA interacts only with the previous layer during each deposition step, whereas PLL travels all the way through the entire multilayer domain to the substrate. Some of these free PLL molecules get trapped during the washing step due to the electrostatic barrier and then form complex with HA at the outer layer once they travel back to the interface in next deposition step. Hence, the structure of these exponentially grown multilayers is quite different from that derived from multilayers grown linearly. The exponential-to-linear transition for (HA/PLL) multilayers occurs after 12 bilayers. Study also demonstrates that the use of different deposition methods or adjusting the parameters will not change the exponential-to-linear transition point after which layer the thickness of domain III stops increasing[37].

Despite these common findings, it is oversimplified to classify PEM films into two categories. In fact, the complexing behaviour of a certain pair of oppositely charged polyelectrolytes can be significantly changed by other parameters such as salt concentration and temperature[39, 40]. For example, the (PSS/PAH) and (PSS/PDADMAC) multilayers normally grow linearly which favours room temperature and moderate salt concentration. However, this growing process can be forced to be exponential in the presence of high salt concentration[41, 42]. It was observed that raised temperature also has a similar effect in this aspect[40]. These

subtle influences can be very useful in terms of fabricating multilayers with ideal structures.

2.3.3 Stability of polyelectrolyte multilayers

Unlike multilayers that firmly attached by covalent bonding which is difficult to be broken by physical means, the driving force for the polyelectrolytes multilayers assembled through LbL process is normally based on electrostatic interaction between oppositely charged polyions. Hence, any factors that can affect this interaction would influence the stability of the multilayer structure.

Undoubtedly, ion concentration plays a pivotal role in this aspect. When the polyelectrolyte multilayers are exposed to medium that contains high salt content, they may disassemble due to the over screening caused by the external ions spread within multilayers. To explain in the thermodynamics way, the assembly and the disassembly of polyelectrolyte complex is a reversible process which has been expressed in Eq.2.5, the addition of salt would help the equilibrium move towards the left direction and cause the polyelectrolytes complex to dissociate into free polymer chains.

Besides, pH is another important factor that affects the stability of multilayer structure when either or both of the constituent polymers are weak polyelectrolyte. At certain pH value, weak polyelectrolyte may combine with hydrogen ions in the solution which leads to the disassembly of multilayers. In some circumstances, pH may also affect the stability of multilayers constructed via hydrogen bonding.

2.3.4 Characterizations for polyelectrolytes multilayers

Polyelectrolytes multilayers have been extensively researched by different characterization techniques. To study the LbL build-up process, quartz crystal

microbalance (QCM) is used to measure the mass gain by converting frequency signal after each deposition step [43]. However, QCM may not be able to tell the thickness increase as the density of the polymer layer is hard to know. Thus, ellipsometry is more efficient in terms of monitoring thickness changes as it directly shows the thickness of the sample being tested [44]. Ellipsometry is also capable of monitoring the degradation process of polymeric multilayers which degrades evenly throughout the sample surface[45]. In contrary, QCM is more universal for degradation study. In addition, UV-vis is also a conventional instrument for monitoring the LbL build-up process as the change in functional groups on the polyelectrolytes could be closely detected by the machine[46]. Due to the technical restriction, zeta-potential measurement which gives the information of surface charge of the polyelectrolyte coated samples and hence can confirm the charged reversal after each deposition step cannot be used for multilayers fabricated on planar substrates.

Since most polyelectrolytes multilayers are extremely thin which makes them difficult to be observed under scanning electron microscope (SEM), atomic force microscopy (AFM) is more often applied to image the surface morphology of these thin films. Furthermore, AFM can also be used to know the mechanical properties of polymer layers by tapping the surface with its tips. Other instruments including confocal laser scanning microscopy (CLSM), surface plasmon resonance (SPR) and optical waveguide light-mode spectroscopy (OWLS) are widely used for different purposes too.

2.4 Polyelectrolyte microcapsules

2.4.1 Adsorption of multilayers onto templates

In the late 1990s, Sukhorukov *et al.* successfully employed the LbL technique on the colloidal particles [4, 5, 47]. Theoretically, any charged surface could be used as substrates for LbL assembly, regardless of their morphologies, chemical compositions or other properties. The deposition process follows exactly the same way as used for planar substrate. Once the desired number of layers is deposited, template dissolving process is carried out in order to obtain hollow capsules.

Microcapsules can be constructed by two different self-assembly means: (1) sequential adsorption of polyelectrolyte, followed by centrifugation and washing steps to get rid of excess polymers [47], or (2) using a micro-filtration setup [48] in order to remove the supernatant without centrifugation, which is an ideal method to prevent microparticles from aggregations. Sufficient washing is necessary to remove unattached polyelectrolytes so that polyeletrolyte complexes will not form after addition of subsequent oppositely charged solution. Theoretically, it is possible to calculate the exact amount of polyelectrolytes that need to be added, avoiding washing steps that could damage fragile substances. However, due to the difficulty in determining the total surface area of microparticles, it is practically infeasible for the case of LbL microcapsules [49].

2.4.2 Template dissolution

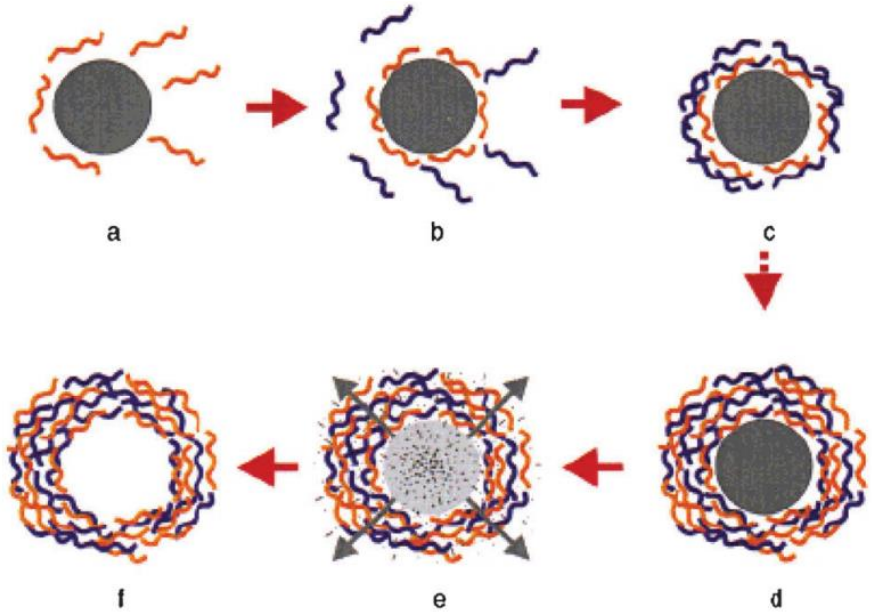

Figure 2.5 Schematic diagram of the polyelectrolyte deposition and subsequent core removal process resulting in hollow microcapsules [5]

Different organic and inorganic templates have been employed for the preparation of microcapsules, including calcium carbonate ($CaCO_3$)[50-52], melamine formaldehyde (MF) particles [4], silica particles [53, 54], microbubbles [55-57], and even cells [58-60]. In terms of particular aims, templates can be chosen according to their advantages and disadvantages. So far, microparticles are more commonly used as the templates than other objects. The size of templates normally ranges between 15 nm to 1mm [61]. Capsules might be destroyed due to either the unstability when the diameter is below 15nm or the high pressure when the diameter is above 1 mm [55, 62].

Monodisperse organic microparticles such as MF microparticles are can be easily handled for the LbL assembly[63, 64]. However, MF particles can be rapidly dissolved by HCl or polar organic solvents such as N,N-dimethyl formamid (DMF)

and dimethyl sulfoxide (DMSO), resulting in oligomers being trapped in the cavity of the capsule which may probably rupture the capsule due to high pressure or leave a significant number of residual inside capsules, affecting their properties[65, 66].

In comparison with organic particles, inorganic particles such as $CaCO_3$, magnesium carbonate ($MgCO_3$) as well as silica microparticles can be fully dissolved, turning into ions and carbon dioxide that can release from the polymeric shell pores without any difficulty during dissolution process[7, 62]. The dissolution of carbonates usually employs either a mildly acidic environment or ethylenediaminetetraacetic acid (EDTA). These carbonate microparticles tend to be highly porous and irregular, which leads to the formation of irregularly structured microcapsules. Silica particles are normally monodisperse and not porous, but requiring hazardous chemicals such as ammonium fluoride (NH_4F) or hydrogen fluoride (HF) for template removal which probably cause the restriction of further applications as well as the aggregation of weak polyelectrolyte capsules[54, 67].

2.4.3 Encapsulation in microcapsules

The possibility of entrapping substances in the cavity of microcapsule promotes the level of functionality to the hollow multi-layered polyelectrolytes shells with regard to their further applications. Thus, a series of encapsulation methods have been developed, which can be classified into two main groups, depending on when the encapsulation is carried out during the capsule fabricating process. Substances can either be co-precipitated during the formation of $CaCO_3$ cores or diffuse into cavities through the capsule shells by adjusting the shell permeability after the templates are dissolved.

2.4.3.1 Encapsulation by co-precipitation in $CaCO_3$ particles

Co-precipitation of desired substances in $CaCO_3$ particles is the most commonly used mean for encapsulating substances that are too big to diffuse through the capsule shell [68]. Some insoluble substances such as certain type of crystals, nanoparticles can be employed as templates directly for LbL assembly[69, 70]. During the co-precipitation, the desired molecules are first added to one of the $CaCl_2$ and $NaCO_3$ solutions, followed by mixing the two salt solutions to form $CaCO_3$ suspension. If necessary, co-precipitation could be repeated more than once, resulting in multi-compartment microcapsules [71, 72].

2.4.3.2 Encapsulation by tuning the microcapsule permeability

Another strategy of encapsulation is employed by changing the shell permeability after capsules are produced. Only substances that can diffuse through the capsule shell are applicable for this technique. PH, ionic strength, solvent change as well as temperature are the primary factors that influence shell permeability [73-76].

2.4.3.2.1 pH

PH value could be adjusted to achieve the encapsulation when, at least, one of the shell constituents is weak polyelectrolyte, which makes capsules stable only within a certain pH range[62]. Take PSS/PAH shells as an example, this shell is permeable for high molecular weight substance at alkaline conditions and encapsulation could be completed by adjusting pH to acidic conditions, inducing the shrinkage of microcapsules and the decrease of permeability [10]. When the pH value is adjusted beyond this certain range, the charge density of one of the polyelectrolytes and also the electrostatic attraction between layers decrease, resulting in the decrease of the shell density and increase of the shell permeability [73, 77, 78]. If leaving

microcapsules in a solution with inappropriate pH for a long period of time, the polymeric shells might experience an irreversible process of disassembly.

2.4.3.2.2 Ionic strength

Ionic strength of the polyelectrolyte solution can be adjusted by adding salts, enabling large molecules that normally cannot diffuse through the polymeric shells to penetrate into capsule cavity. At low ionic strength, capsules tend to be more permeable because of the weakened interaction between polyions while high ionic strength leads to the shrinkage of the capsules as the hydrophobic polymeric chains become an important force, making the capsules less exposed to water [79, 80].

2.4.3.2.3 Solvent

Resuspending microcapsules in a polar organic solvent also could significantly change the shell permeability. Dispersing microcasuples in polar organic solvent and followed by resuspending in water noticeably thin the shells whilst the diameter keeps constant. This is because the electrostatic interactions between polyions change as the solvent dielectric constant changes. However, the reversibility of changing the shell permeability by using the solvents exchange process remains in doubt [81]. Practically, this method was once employed to make PSS/PAH shells penetrable for urease by dispersing the capsules in ethanol, allowing urease to diffused into capsules and blocked the encapsulated urease in the cavity by resuspending capsules into water [82].

2.4.3.2.4 Temperature

The influence of temperature on the LbL multi-layered surfaces has been studied by several researchers [83]. Both weak and strong polyelectrolytes made capsules are sensitive to temperature, indicating the electrostatic interactions are not affected

whereas some secondary interactions may be impacted [84, 85]. Köhler *et* al[83, 86] found that as the temperature increases, capsules can either shrink or swell which probably depend on the constitution. Capsules can shrink upon heating if the shells consist of even number of layers and are present in appropriate environment, leading to decrease of the shell permeability that caused by the increment in the thickness and density of the capsule shells [86-88]. However, neither process can happen below the glass transition temperature (T_g), because the polymer chains are not flexible for reconstruction. Above the T_g, one can be categorized into two distinct situations, capsules with even number of layers or capsules with odd number of layers. When the number of capsule layers is even, the charge of shells is nearly neutral so that the electrostatic repulsion within the shells is assumed be neglected. Under this condition, the hydrophobic force upon heating tend to make the shells shrink, decreasing the surface area of capsules. Oppositely, when the number of capsule layers is odd, the electrostatic repulsion is more influential, inducing the polyions stretch and repel each other which makes capsules swell or even rupture. Therefore, heating could be introduced to encapsulate substances due to the reasons listed above.

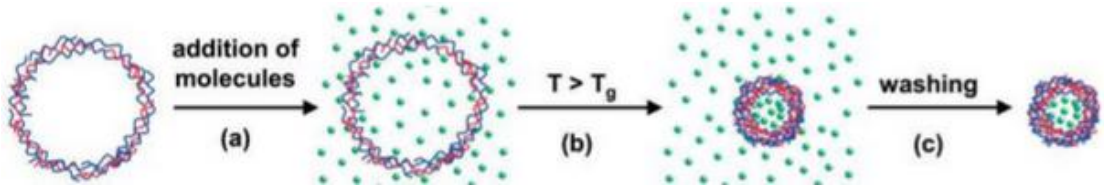

Figure 2.6 Schematic diagram of the thermal-induced encapsulation procedure[67]

2.4.3.2.5 Ultraviolet (UV) crosslinking

The aforementioned four encapsulation strategies are all largely influenced by external environment which would possibly cause undesired release. Thus, the irreversible encapsulation methods are also important. One of these approaches is

making UV-responsive microcapsules, for which their porosity can be reduced through molecular rearrangement by responding to external UV irradiation at certain wavelength. The loading cargos can simultaneously be sealed in the cavity.

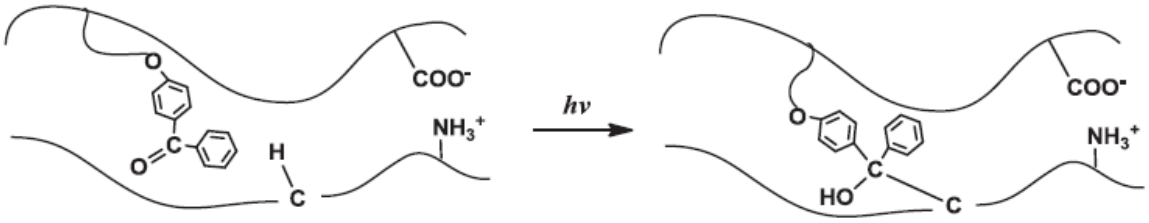

Figure 2.7 Schematic illustration of benzophenone-related crosslinking reaction within microcapsule shells[89]

Yi[89] introduced benzophenone chromospheres groups to poly(methacrylic acid) (PMA) chains, which was later assembled with PAH to form multi-layered microcapsules. Upon exposure to UV at 275 nm, the benzophenone groups crosslinked with the C-H bonds on the PAH chains, resulting in a much denser shell structure. As depicted in Figure 2.8, small fluorescent molecules can be encapsulated after $(PAH/PMA\text{-}BP)_4$ microcapsules being irradiated under UV for 15 min compared to the initial microcapsules which cannot retain those molecules after washing.

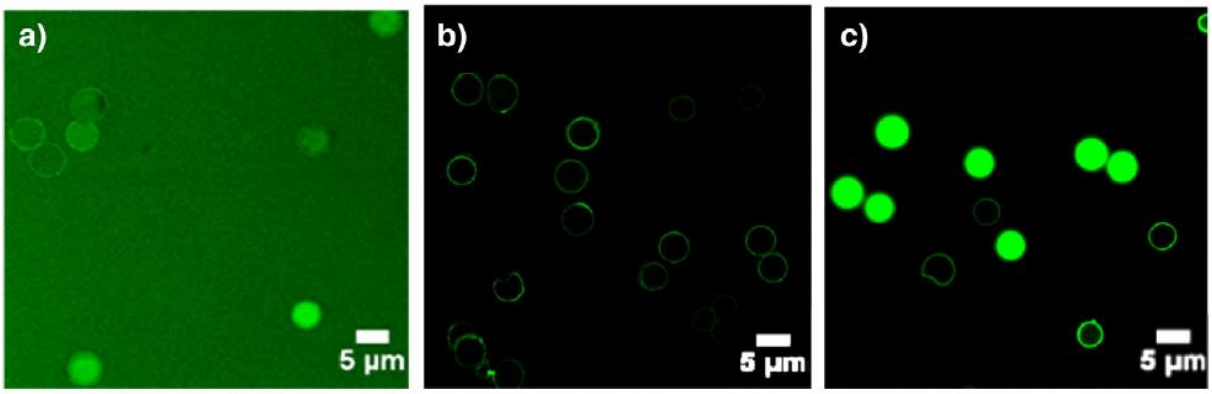

Figure 2.8 Confocal laser scanning microscopy (CLSM) images of cargo encapsulation of $(PAH/PMA\text{-}BP)_4$ microcapsules in the presence of a AF488-dextran. (a) Before UV irradiation, the fluorescent polymer can permeate into the hollow microcapsules, (b)

fluorescent molecules cannot be retained after direct washing, (c) fluorescent molecules can be encapsulated after microcapsules being exposed for 15 min[89].

2.4.4 Triggered release from encapsulated microcapsules

LbL assembly, core removal, substances encapsulation and release consist of the whole process of controlled delivery. Hence, the release means for capsules is one of the major missions should be addressed. In terms of microcapsules, the release of cargos could be implemented either by adjusting the shell permeability or by breaking the shells. In addition to several simple methods aforementioned, this aim can also be achieved irreversibly by some external triggers (eg. light, ultrasound, magnetism).

2.4.4.1 Laser irradiation

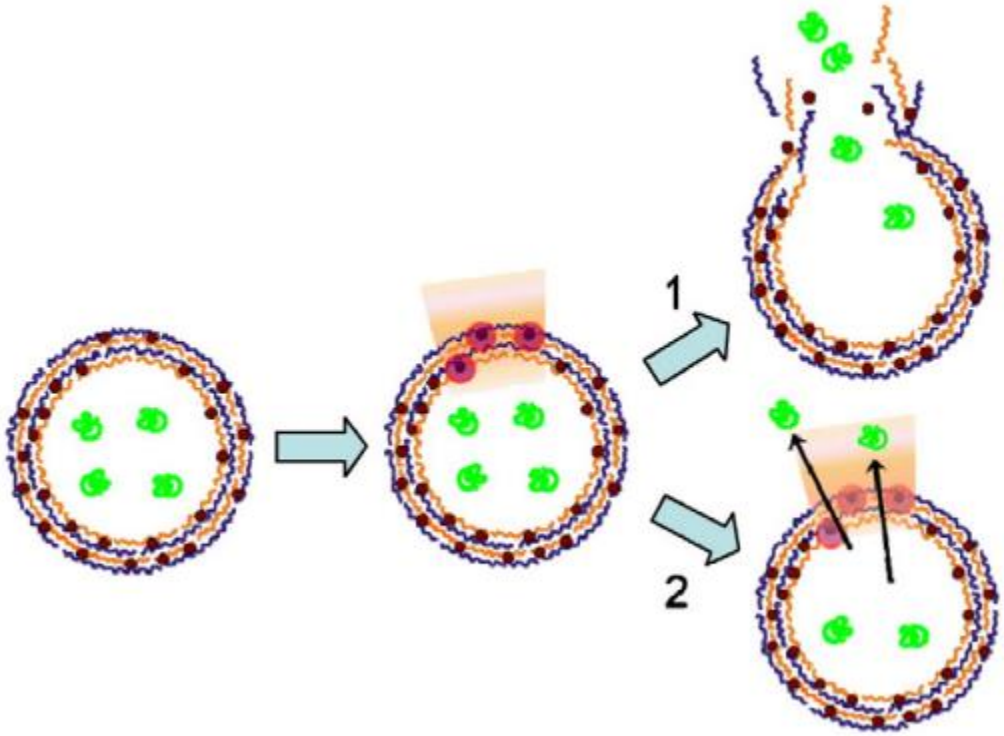

Figure 2.9 Schematic illustration of two possible release scenarios of encapsulated substances by the laser irradiation[90]

Laser irradiation could be carried out by heating upon particular substances which can break the shells under irradiation. It involves some substances that can absorb laser energy and be incorporated within the microcapsule shells, which is different from those microcapsules that release loading cargos by changing their own permeability in response to external stimuli. Generally, any kind of substances that is applicable to the requirements above can be candidates for this method. However, these substances should meet the requirements of size and charge which enable them to be incorporated during LbL process. As illustrated in figure 2.9, there are two ways to trigger release microcapsules by laser treatment. Once the microcapsules receive a large amount of laser irradiation and assimilate the heat, the shells of microcapsules would be broken, resulting in the release of loading cargos. When the accumulated energy is not enough to break the shells, it is still possible that the shell permeability would increase due to the more flexible polymer network, allowing for the cargos to release [91, 92].

2.4.4.2 Ultrasound

Ultrasound with high frequency and low power has been broadly utilized for imaging and diagnosis in medicine area and attracted great attention for their potential applications of being used for cure of ill body or organs.

The most important advantage of high frequency and low energy ultrasound is that it can be used for targeted applications at a specific location in human body[93]. The use of high energy ultrasound could be hazardous and inevitably damage human tissues, which has been proven by several publications with regard to the application of high power ultrasound[94, 95]. In addition to targeted release, ultrasound can also be employed as a motive force for the targeted delivery of microcapsules throughout body, especially in the blood vessels[96].

2.4.4.3 Magnetic

Microcapsules with magnetic properties were also found to be promising vehicles for remotely navigated delivery system. A versatile way to endow microcapsules with these properties is incorporating magnetic iron oxides such as Fe_3O_4, $MeSO_4$ within the shells. The first successful case of this method was using alternative absorption of negatively charged Fe_3O_4 particles and positively charged PAH on polystyrene latex beads[97]. Microcapsules with magnetic properties can either be remotely navigated or remotely triggered. Fe_3O_4 functionalized PSS/PAH capsules were injected into a flow channel system and located at the bottom after some time where a magnet placed[98] whilst several groups have found that certain magnetic field can lead to magnetic particles embedded microcapsule shells becoming loose and more permeable for encapsulated substances[99-101]. Furthermore, magnetic microcapsules can potentially be used for magnetic resonance imaging, either for addressed delivery of contrast agents or for visualization of drug delivery[102].

2.5 Layer-by-Layer assembly in Organic Phase

2.5.1 Reverse-Phase Layer-by-Layer (RP-LbL)

However, some shortages have been found when LbL process performed in aqueous phase, such as low encapsulation efficiency of hydrophilic cargos and limitation of templates. Besides, water-sensitive substances cannot be encapsulated as they would be inevitably damaged when being exposed to water. Some other drawbacks have also been pointed out[102].

Recently, a novel approach called Reverse-Phase Layer-by-Layer (RP-LbL) Encapsulation has been developed by the group of Trau[103]. In contrast to the conventional aqueous medium based LbL process, this technique can be carried out in

various organic solvents, mainly in aliphatic alcohols due to their excellent biocompatibility. The polymers used for this approach are usually polyamines and polyacids as pairs. They can readily be obtained from their polyelectrolyte forms using acid-base chemistry to remove small conterions, thus making these polymers non-ionized. The polyamines and polyacids used in RP-LbL are in free base and acid forms, respectively. These non-ionized polymers are thereby soluble in inorganic solvents.

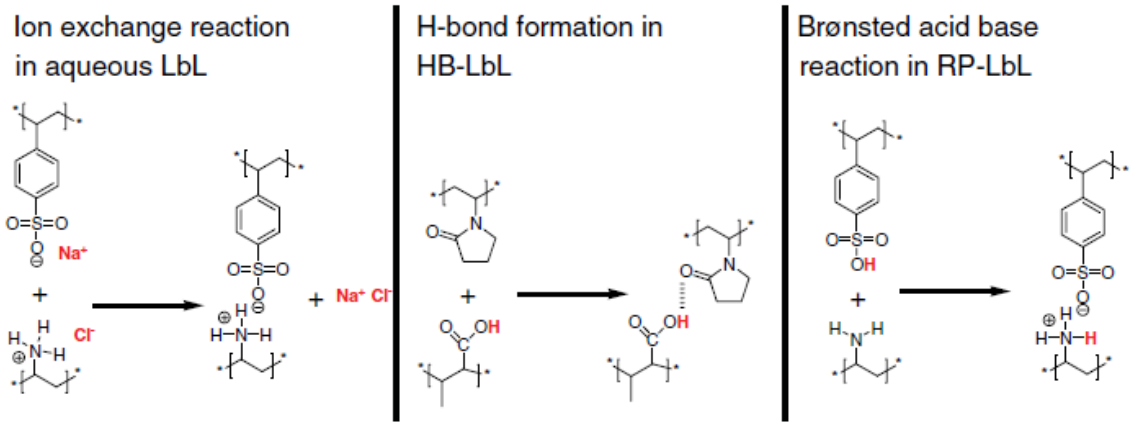

Figure 2.10 Molecular interactions between polymers in the aqueous LbL, HB-LbL and RP-LbL techniques[104]

The polyamines do not have many charges in organic solvent and can be regarded as neutral, whereas the polyacids carry very low charge under low degree of protolysis in organic solvents. In a typical deposition process, a *BrØnsted* acid-base reaction in which the non-dissociated proton of the polyacid protonates the amine and form the corresponding ammonium salt, takes place between the polyamine and the polyacid pair. The multilayers are built up and hold together because of the electrostatic interaction which has been illustrated in Figure 2.11, Compared to the polyelectrolytes that carry a large amount of charged species and normally exhibit quite stretched chain conformations in aqueous solutions, the significantly less

amount of charges these polyamines and polyacids have in organic solvents result in their much more coiled conformations. Therefore, the thickness of multilayers built by RP-LbL is dramatically higher which is usually achieved by addition of salts in the case of polyelectrolyte multilayers formation.

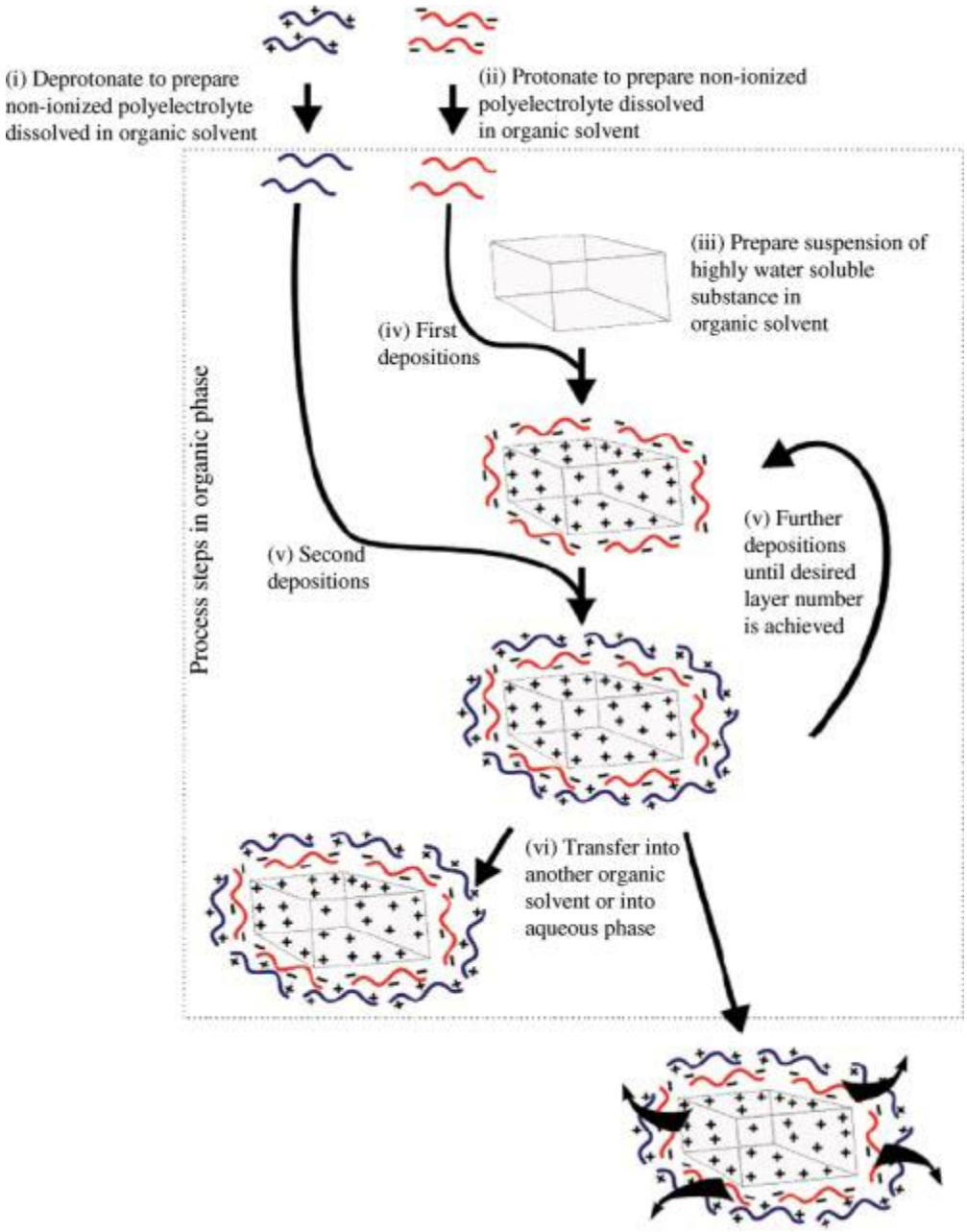

Figure 2.11 Schematic diagram of the RP-LbL process[103]. The particle size are 5-20 μm.

The use of this RP-LbL encapsulation process of water-soluble or water-sensitive substances in organic solvents avoids some intermediate steps, such as removal of template and loading of cargos. By using this novel approach, powders of microcapsules loaded with desired substances can be obtained after simple evaporation of organic solvents.

However, despite having various advantages, this approach does not change inherent properties of the shell materials. Thus the permeability of the resulting microcapsules is as high as those compose of polyelectrolyte multilayers. Once these microcapsules are transferred into water, the small molecules loaded will still diffuse into the medium very quickly.

2.5.2 Layer-by-Layer assembly through stereocomplex in organic phase

In addition to conventional interactions such as electrostatic interaction, covalent bonding and some other forces, the van der Waals interaction is also worth discussing as it provides some unique advantages. Van der Waals force is the sum of the attractive or repulsive forces between molecules or between parts of the same molecule, and thus this weak force plays a crucial role in polymer properties (e.g. specific structure, morphology) because of the massive amount of the influencing macromolecules. Thus, the microcapsules that consist of non-ionic polymers can be expected to have extraordinary shell permeability and morphology.

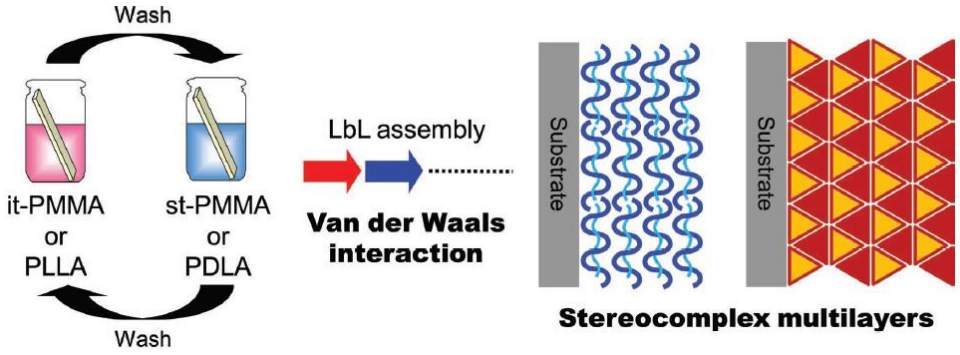

Figure 2.12 Schematic illustration of LbL assemblies using van der Waals interactions between Isotactic (it)-/syndiotactic (st)-poly(methyl methacrylate) (PMMA) or poly(L-lactide) (PLLA)/poly(D-lactide) (PDLA)[105]

Stereocomplexes is a type of polymer complexes that formed between stereoisomers through van der Waals interaction. Different stereocomplexes have been assembled from structurally well-defined synthetic polymers such as isotactic (it) / syndiotactic (st) PMMAs[106-108], it-PMMA/st-alkyl methacrylate[109], enantiomeric PLAs[110] and poly(-benzyl L-/D-glutamate)[111, 112].

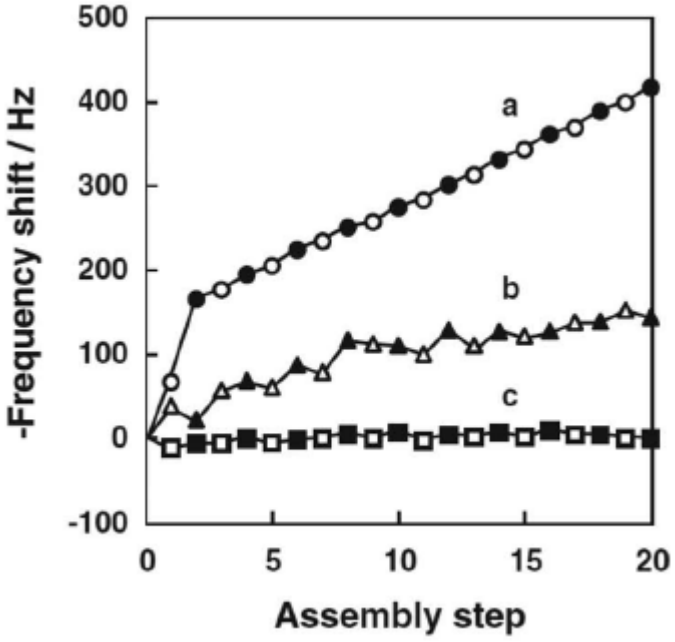

Figure 2.13 Frequency shift of QCM measurement during the sequential LbL assembly of it-PMMA and st-PMMA in (a) acetonitrile, (b) acetone, (c) DMF solutions[113]

The PMMA stereocomplex has attracted particular interest from researchers. It was found that the formation of it-PMMA and st-PMMA stereocomplex is highly dependent on the solvent in which this process takes place. Solvents such as acetonitrile, acetone and DMF are considered to be good complexing solvents[114]. However, the results show in Figure 2.13 suggest that the selection of solvent for the

stepwise deposition of PMMA stereocomplex is the key factor as the assembly carried out in acetonitrile shows a much higher frequency shift in QCM measurement than those in acetone and DMF[113]. Therefore, the formation of PLA stereocomplex between enantiomers was also performed in acetonitrile[115].

After stereocomplex multilayer films composed of non-ionic polymers were successfully assembled through their van der Waals interaction, the same procedure was applied to prepare stereocomplex hollow capsules. Both PMMA and PLA stereocomplex were fabricated[116, 117]. However, the use of silica particles as the template causes an inevitable problem due to the residual HF left in the cavity of capsules after core dissolution, which makes the capsule not suitable for biomedical applications. Thus, the use of a bio-friendly template such as $CaCO_3$ would be an appropriate alternative as its residues upon dissolution are not harmful to living tissues.

2.6 **Microcapsules with reduced permeability**

As one of the most important properties of microcapsules that are being widely studied, permeability is of particular importance. One of the major problems for microcapsules is high permeability, which causes fast release. There are generally two strategies to obtain microcapsules with reduced permeability, either use specific building materials which help achieve low permeability or construct microcapsules through specially designed processes which differ from those conventional ones.

Some of the stimuli that can change the microcapsule permeability have been discussed as means of encapsulation and release. Meanwhile researchers have also explored many other ways to reduce the microcapsule permeability in order to entrap small molecules.

Some charged small molecules were complexed with polyelectrolytes via electrostatic interaction by Radtchenko et al. However, the obtained complexes are not stable at a wide range of pH due to their binding force being the electrostatic interaction. Similar process was conducted by Yan in which hydrogen bonding was used as driving force instead of electrostatic interaction[118]. It was found that hydrophilic small molecule drugs release from the microcapsules much slower which can be further decelerated after crosslinking of shells. Nonetheless, the majority of small molecules that are to be encapsulated may not have such interactions with the shell materials, which makes this method less applicable.

A pre-coating layer which has long alkyl chain before deposition of polyelectrolytes multilayer would reduce the release speed of small molecules[119]. This is apparently attributed to the hydrophobicity of the pre-coating layer that makes it more difficult for the small molecules to penetrate. Tong and co-workers used micelles as a reservoir for small molecules and doped them within the $CaCO_3$ cores before polyelectrolytes shell build-up[120]. Since micelles are of much bigger size and will not diffuse out easily, it is an efficient way to retain small cargos in the capsule cavity.

Since the discovery of click reaction, it has been one of the most important ways to create microcapsules via covalent bonding. Microcapsules built up by electrostatic interaction carry numerous charge species which makes them high permeable to small molecules. In contrast, microcapsules constructed by covalent bonding normally have more hydrophobic and compact shells, which apparently reduce their permeability. Huang synthesized poly(N-isopropylacrylamide)s that bear different clickable groups and assembled them into microcapsules using step by step click reactions[121]. The obtained microcapsules showed reduced permeability due to the non-charged shell structure as well as the thermo sensitivity.

In addition to polymers which are most widely used building materials for microcapsule construction, composite materials such as silica, titanium oxide, carbon, are also common options due to their unique properties. These materials endow microcapsules various responsiveness, such as laser, ultrasound sensitivity. They can also make the shell less permeable. Gao synthesized silica particle layer via direct *in situ* hydrolysis reaction at the (PSS/PAH) polyelectrolyte microcapsule/water interface[122]. Small molecule Rhodamine B was mixed with the reaction solution and sealed in the modified microcapsules after the formation of silica layer. This silica reinforcing layer significantly reduced the permeability of the original polyelectrolyte microcapsules. When exposed to ultrasound at suitable strength, the silica shell will break up into debris during which the release of small molecules is achieved simultaneously.

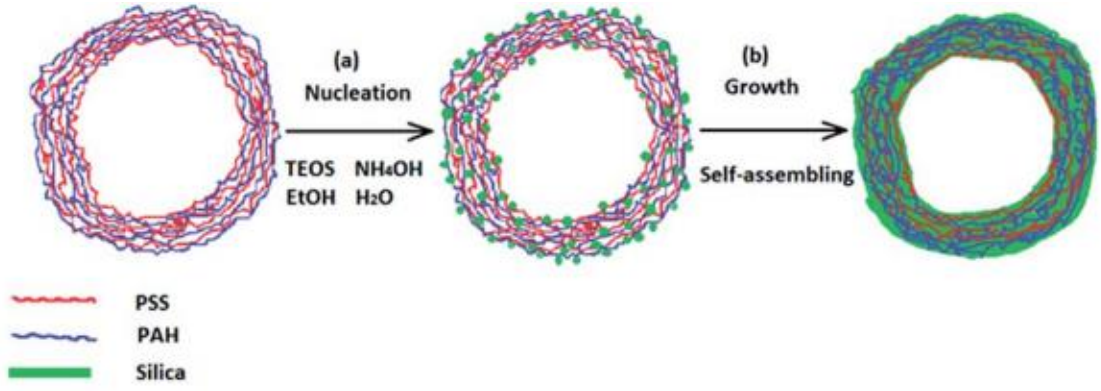

Figure 2.14 Schematic illustration of $(PSS/PAH)_4$ microcapsules incorporated and strengthened by in situ formed silica nanoparticles: (a) silica nucleation and deposition; (b) growth and ripening process[122].

2.7 **Coating on surface**

Thin film coatings on the surface of an object can significantly change the properties of the objects as they create a barrier between the coated objects and the environment.

Since very early ancient time, human beings had applied different coatings onto the target surfaces as a protective layer against environmental erosions or for simple decoration purposes. Today, the range of applications of surface coating has developed from protection and decoration usages to various cutting-edge areas including computer industry, manufacturing, bio-engineering, etc. An important fact that needs to be pointed out is that, an organic thin film is fairly efficient in terms of influencing the interaction between the underlying material and the environment that even the its thickness is less than 1 nm, it can completely isolate the covered surfaces. This character has broadened the use of thin film coating from only being an inert protective layer to functionalization of the coated materials. For example, a specifically designed coating layer on the artificial materials can significantly improve the biocompatibility of an exogenetic implant. As a result of this development, different techniques of surface coating formations have been widely explored, among which the surface-initiated polymerization is of particular interest which will be broadly discussed in this literature review.

There are two types of strategies that are used to make interactions between the molecules which constitute the organic coating and the surface materials. One of the routes is physical interactions in which the molecules form physical bonds with surfaces of the target objects whilst chemical interaction between coating molecules and substrates is the other strategy.

The commonly used techniques for fabrication of surface coatings using physical interactions include spin coating, spray coating, painting, etc. The processes of these techniques are quite different from one another. However all of them involve two steps which are deposition of molecules containing solution as well as solvent drying. If the whole process of coating is well controlled, the ideal thickness and homogeneity

can be achieved. Recently, more sophisticated technique including Layer-by-Layer assembly has been developed. These new techniques allow much higher precision over the thickness of the coating and better control of the structure of the coated layers. Due to the nature of the physical forces, the interactions between the coating layers and the substrates are rather weak. This is desirable in some circumstances. However it may not be the case when the applications where strong attachment of the coated layers to the substrates are designed.

Alternatively, the enhancement of the long-term stability of the coatings can be achieved by chemically bonding the molecules of the coating material to the substrates. A prevalent way to create covalent bonding is the deposition of self-assembled monolayer (SAM) which involves molecules that have reactive groups to form robust chemical bonds with the functional moieties on the surface of the substrate[123]. The density of the coating materials directly depends on the density of the functional groups on the surface of substrate. Ideally, coating can be continued as long as there are free groups accessible. However, the surface of the substrate may not be densely coated if the coating molecules are spatially too big which leads to the repulsion between the attached molecules.

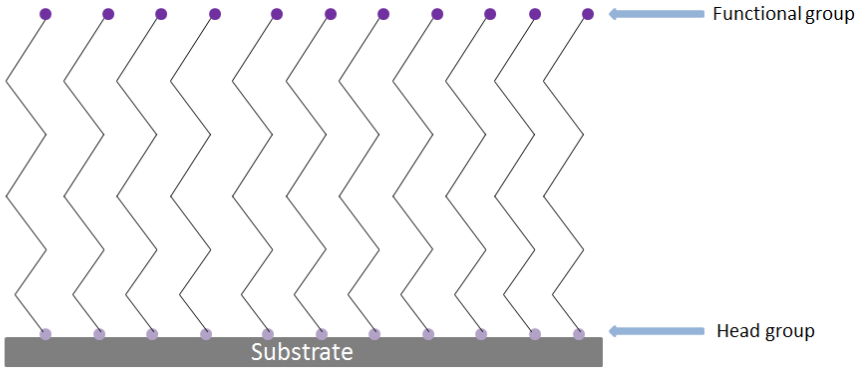

Figure 2.15 Schematic illustration of self-assembled monolayer on substrate.

2.8 **The overview of polymer brushes**

The term "polymer brush" is defined as a structure of polymer chains that are tethered to a surface. The conformation of polymer brushes can be various mainly depending on the graft density of polymer chains. When the graft density is low, that is the distance between two neighbouring attached points is larger than the size of graft polymer chains, the individual chains do not have any interaction or contact with each other. There could be two different conformations of one-end tethered polymer chains, depending on the strength of the interaction between the polymer chains and the surface. If the interaction is weak, the polymer chains present a coil conformation with one end linked to the surface. The term "mushroom-like" is given to this conformation as shown in Figure 2.16 (a). In contrast, if the interaction is strong, a "pancake-like" (Figure 2.16 (b)) conformation will form as the attached polymer chains are strongly attracted by the surface. When the graft density of polymer chains is high, the repulsion between each polymer chain increases, resulting in the polymer chains trying to avoid each other and stretching away from the surface. The "brush-like" conformation forms as shown in Figure 2.16 (c).

Figure 2.16 Schematic illustration of possible conformations of surface attached polymer chains: (a) mushroom-like, (b) pancake-like, (c) brush-like[124].

2.9 Synthesis of polymer brushes

2.9.1 Substrates used for the polymer brushes growth

Polymer brushes can be grown from various surfaces. Although silicon and gold substrate are predominantly used as the grafting surface[125-128], many others including clay mineral[129], carbon[130], other metal oxide[131] and polymer[132] based substrates have also been explored. Polymer brushes can be directly grown from surfaces where initiators for Surface-initiated Controlled Radical Polymerization (SI-CRP) are available. However, SI-CRP can still be performed after initiators are pre-attached to the surfaces without available initiating species via one- or multi-step modifications. The possibility of growing polymer brushes from a wide range of surfaces with different chemical compositions has certainly broadened the usage of polymer brushes, as polymer brushes with different substrates can be developed for specific applications. The combination of substrates, polymer brushes, the grafting strategy and the polymerization techniques offers great opportunities for tailored design of this system.

2.9.2 Strategies for synthesis of polymer brushes

The polymer brush structure can be formed by either of two approaches, physisorption or chemical bonding. For the former type, a precursor polymer which consists of two components is needed. One of the constituent part is intended to strongly adsorb onto the surface whilst the other one is used to initiate the polymerization by different techniques[133]. Due to the fact that polymer brushes and surfaces are connected by physical adsorption which is thermally, mechanically unstable, this approach may not be suitable for applications that need additional stability against heating and other external forces. However, the most commonly used

approach is the chemical bonding linkage in which the polymer chains are covalently bonded to the surface. For the formation of polymer brush chains that are covalently attached to the surfaces, one can either use "grafting to" or "grafting from" approach as illustrated in Figure 2.17.

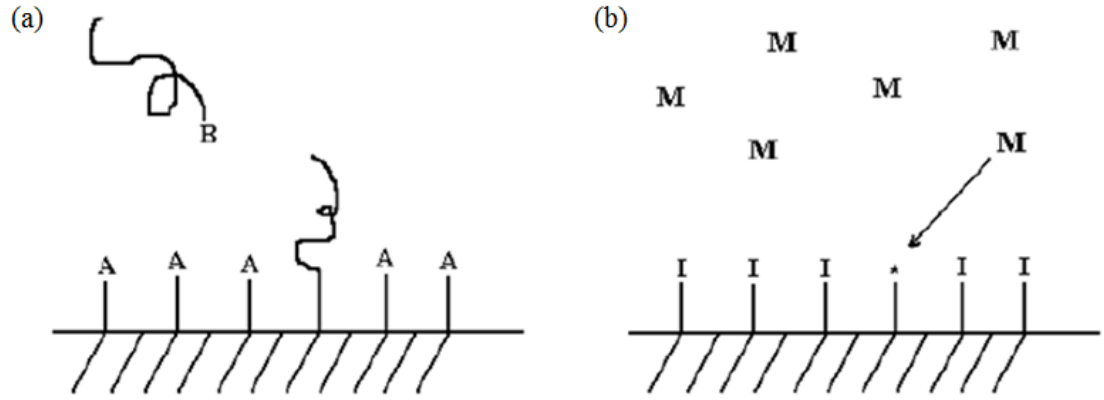

Figure 2.17 Schematic illustration of (a) "graft to" approach and (b) "graft from" approach.

2.9.2.1 "Grafting to" synthesis approach

The "grafting to" approach involves prefabricated polymer chains and a surface where reactive groups exist. Once the end groups of polymer chains connect to the surface via covalent bonding, the polymer brushes are formed. In spite the stability of polymer brushes prepared by this approach, the "grafting to" approach however suffers from several drawbacks, resulting in the difficulty of obtaining thick and dense polymer brushes. The main cause is the steric repulsion which hinders free polymer chains from attaching to the surface[134, 135]. Moreover, the molecular weight of macromolecules to be attached also plays an important role in the grafting density as longer polymer chains generate more steric hindrance. The longer the polymer chains are, the lesser surface area will be covered by the polymer chains.

The preformed polymer chains can be synthesized via different techniques including anionic, cationic, living free radical polymerizations. One should always bear in mind

that the molecular weight distribution of these preformed macromolecules must be extremely low in order to obtain uniformly long polymer brush layers. For substrates like silica or gold which already have active functionalities, the reaction can be carried out straight away. However, for substrates that do not functional sites, corresponding coupling groups which can react with the end group of polymer chains must be anchored on the surface prior to the attachment of macromolecules.

In comparison to the "Grafting to" approach in which attachment of large molecules to the substrate surface is difficult, a "Grafting from" approach which involves attachment of small monomers to substrate surface might be much easier due to the less repulsion between small molecule initiators. Thus, "Grafting from" approach is more suitable for growth of polymer brush where higher brush density is desired.

2.9.2.2 "Grafting from" synthesis approach

In a "grafting from" process polymer chains are directly synthesized on the initiator functionalized surface. Unlike "grafting to" strategy where only small portion of polymer chains can reach the functional sites on the surface, the density of polymer brushes via "grafting from" strategy is mainly determined by the density of the initiators that are pre-anchored on the surface. Due to the nature of small molecules that they have less steric repulsion, high density of brush coverage can be readily achieved which enables much thicker polymer brushes[136]. In order to use this strategy, many polymerization techniques have been performed[137-139], among which the controlled/"living" polymerization technique is of particular importance as they are able to precisely control the thickness, composition as well as the architecture of the polymer brushes[140-145]. Besides, the controlled radical polymerization (CRP) is compatible with a wider range of monomers compared to other technique such as anionic polymerization with which only some particular monomers can be

polymerized. The categories of the CRP techniques will be discussed in details in the following context.

In summary, the characters of both "Grafting to" and "Grafting from" approaches have been introduced. Either or a combination of the two can be applied according to the actual purposes.

2.9.3 Synthesis of polymer brushes via surface-initiated polymerization

The controlled/"living" radical polymerization is the most commonly used technique among controlled/"living" polymerization due to some unique advantages, such as wider range of solvents and monomers being used. Three most important controlled free radical polymerization techniques are introduced below.

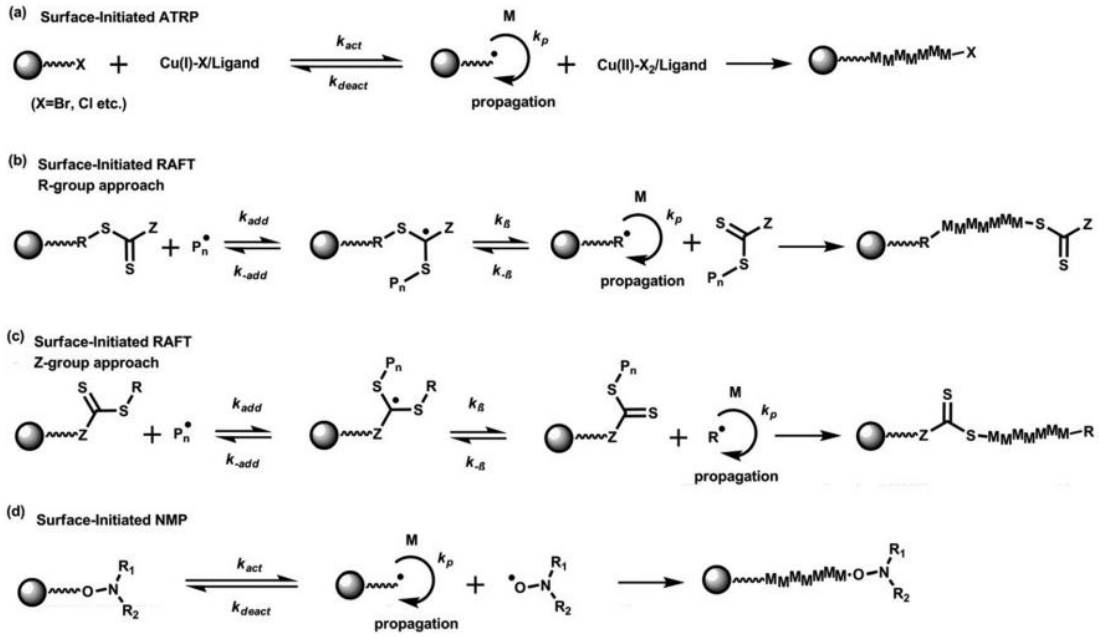

Figure 2.18 General mechanisms of polymerizations for the growth of polymer brushes: (a) surface-initiated ATRP, (b) surface-initiated RAFT polymerization with R-group approach and (c) Z-group approach, as well as (d) surface-initiated NMP. M represents monomers, and k_p is the propagation rate constant. In (a) and (d), the kinetic parameters k_{act} and k_{deact} represent the rate constants of activation and deactivation, respectively, in surface-initiated ATRP and

NMP. In (b) and (c), R- represents the R-group while Z- is the stabilizing group in the CTA (chain transfer agent) for RAFT polymerization. k_{add} and $k_{-\beta}$ are the rate constants for the addition reaction of CTA with the propagating (or initiator-derived) radicals, whereas k_{-add} and k_{β} are the fragmentation rate constants for the intermediate radicals[146].

2.9.3.1 Surface-Initiated Atom Transfer Radical Polymerization (SI-ATRP)

Atom transfer radical polymerization (ATRP), discovered by Matyjaszewski, is a revolutionary method for the synthesis of well-defined polymer with predetermined molecular weight and narrow molecular weight distribution. Since it was first introduced for the preparation of polymer brush[147], it has been the most widely used technique in this area due to some extraordinary advantages such as simplicity of preparation and good tolerance of a wide range of functional groups. SI-ATRP can be carried out on any shape of surfaces such as planar substrates, spherical particles.

Four components are required for an ATRP process: monomer, initiator, catalyst and solvent, all of which play important roles. In a typical ATRP process, the dormant species is initially activated by the transition metal complex to generate the radicals in a one electron transfer step whilst the transition metal itself is oxidized to the higher oxidation state. The number of polymer chains depends on the number of initiators. However, all the growing chains are similar in terms of the probability to propagate with the next monomers and form longer polymer chains, which result in the polymers having narrow molecular weight distribution.

Unlike the ATRP polymerization in bulk solution, the SI-ATRP suffers from the low concentration of initiating groups on the surface which results in difficulty in reversibly trap the propagating radicals once halogen atoms complexes with transition metal catalyst. Some researchers found that addition of a free sacrificial initiator or

directly adding deactivating Cu^{II} species to maintain an appropriate deactivator concentration is essential to have a controlled SI-ATRP polymerization[141, 148]. The effect of the concentrations of Cu^{I} and Cu^{II} have been studied by performing SI-ATRP process with different ratios of catalysts[149]. The best result was found when the concentration of was Cu^{I} 0.1 mM whilst the concentration of Cu^{II} being at 30 % relative to complex. Higher Cu^{I} concentration can still lead to excessive chain termination even in the presence of deactivators. Thus, the dilution of catalysts may help achieve a controlled SI-ATRP process which was confirmed by Wirth et al[148]. The addition of free initiators also provides sufficient deactivators by generating a large amount of persistent radicals in the reaction solution[141]. Besides, the free polymers formed in the solution facilitate the characterization of polymer brushes as in some cases the molecular weight and polydispersity of free polymers are similar to those of polymer chains grown on substrates[150].

There are also some techniques to speed up the SI-ATRP polymerization rate, among which the most efficient one is to perform the reaction in polar solvent, especially in aqueous media[151, 152]. PMMA and poly(2-hydroxyethyl methacrylate) (PHEMA) were both grown rapidly in water containing mixture solvent or pure water[153, 154]. A mixed $Cu^{I}Cl/Cu^{II}Br_2$ halide catalyst combination is also helpful in getting quicker reaction rate[155].

The thickness of the resulting polymer brush and their conformation are significantly affected by the surface coverage of initiators. The Langmuir-Blodgett technique provides denser deposition of initiating groups on the surface which leads to high grafting density of polymer brushes whilst the usage of a blend of active ATRP

initiators and inactive coupling agents offers the feasibility of preparing polymer brushes with controlled coverage[156, 157].

Due to the use of copper catalyst, concerns have been raised towards the polymer brushes synthesized via SI-ATRP which will be later used for biomedical applications. Accordingly, an ATRP variant called Activator Generated by Electron Transfer (AGET) ATRP which usually uses a reducing agent such as ascorbic acid or Cu^0 to constantly regain Cu^I from Cu^{II} has been explored[158-161]. This improved technique has helped reduce the final concentration of copper catalyst within the obtained materials to a very low value as well as enhancing the capability of reaction system in terms of its tolerance of unavoidably introduced oxygen.

In summary, SI-ATRP has successfully shown its simplicity and excellence in preparing polymer brushes. After having been widely used for years, ATRP has been proven to be a chemically versatile and compatible with a wide range of monomers and tolerant with impurities. Particularly, the use of mixed catalyst has made ATRP relatively insensitive to low amount of oxygen due to the immediate oxidation of the catalyst upon the contact with oxygen. Furthermore, most of the chemicals an ATRP process needs can be directly purchased or can be readily synthesized in a standard chemistry laboratory which makes it more convenient from polymer chemists' perspectives. However, one can still find some limitations of ATRP technique which narrows its application. For example, some monomers, such as pyridine containing or acidic monomers, may react or form complex with catalyst or ligand which results in the failure of the polymerization. Thus, adjustment of catalysts or ligands has to be made accordingly[162, 163].

2.9.3.2 Surface-Initiated Reversible-Addition Fragmentation Chain Transfer Polymerization (SI-RAFT)

In comparison to ATRP, in which the amount of the active and dormant propagating chains is controlled by reversible termination, reversible chain transfer is the main principal of the Reversible-Addition Fragmentation Chain Transfer (RAFT) Polymerization[164, 165]. RAFT polymerization is a relatively simple and versatile technique as addition of a suitable RAFT agent can convert a conventional free radical polymerization into a RAFT polymerization while other chemicals being used in the reaction remain the same. The RAFT agents that are widely used include dithioester, dithiocarbamate, and trithiocarbonate compound. Same to ATRP, RAFT technique has also been applied to grow polymer brushes on surfaces where polymerization is feasible. There are two kinds of species which can be immobilized on a surface and thereafter trigger a surface-initiated RAFT polymerization: conventional free radical initiators and RAFT agents. Addition of free initiators can sometimes be helpful when free radical initiators are immobilized to start the SI-RAFT polymerization as the initiator concentration on the substrate is extremely low compared to other reagents in the solution which may lead to early termination of the reaction[166].

Apart from the surface immobilized free radical initiators, RAFT agents can also be immobilized onto a surface for a SI-RAFT process as discussed above. There are two approaches which are defined as R-group and Z-group respectively. The difference is that the former approach involves the attachment of RAFT agent via the leaving and reinitiating R group whilst the stabilizing Z group is used to anchor on the surface in the latter approach. Both routes have been used to prepare different polymer brushes as per the needs[167-170].

Therefore, RAFT technique is highly versatile and will not affect a broad range of monomers which have sensitive functional groups. However, the use of a RAFT agent which is usually not commercially available and has to be synthesized via multistep reactions has certainly limited its application. In comparison to SI-RAFT process that starts from the surface-immobilized initiators, the SI-RAFT polymerization uses surface-immobilized RAFT agent has particular drawbacks. The R-group strategy in which the RAFT agent detach during the polymerisation may broaden the molecular weight distribution by bimolecular termination, whereas the Z-group strategy suffers from low polymer brush density as the RAFT agent attached on the surface will be less accessible as polymer brushes grow.

2.9.3.3 Surface-Initiated Nitroxide-Mediated Polymerization (SI-NMP)

Nitroxide-mediated polymerization involves use of nitroxide radicals to control a reversible activation/deactivation of growing polymer chains[171]. The first successful case of polymer brush growth by NMP technique from surface was made by the group of Husseman, in which 120 nm long polystyrene (PS) brushes was synthesized from 2,2,6,6-tetramethylpiperidinyloxy(TEMPO) deposited silicon substrate[172]. Due to the relatively low amount of anchored initiators on substrates surface which limits the concentration of persisting radicals, the reversible capping becomes slow because of the diluted persisting radicals in the reaction solution. Similar to the case in SI-RAFT, this problem was subsequently addressed by adding a known amount of free initiators into the reaction solution. As a result, the retrieved flat substrates need to be washed with a large amount of solvent that dissolves the physisorbed polymers on the substrates which formed by the free initiators. As the technique developed, the PS brushes have been grown from various surfaces including carbon[173], carbon MWNTs[174], magnetite[175], etc. Moreover, other

polymer brushes such as poly(3-vinylpyridine)[176], poly(4-vinylpyridine)[177] have also been synthesized from TEMPO containing substrates by SI-NMP.

However, being only able to grow styrenic polymer brushes has significantly narrowed the use of SI-NMP. Hence, efforts were made to study other more conventional alkoxyamine initiators which can replace the TEMPO initiator[178]. As a matter of fact, α-hydrido nitroxide, *N*-*tert*-butyl-*N*-[1-diethylphosphono-(2,2-dimethylpropyl)] nitroxide have both found to be capable of replacing TEMPO initiator[179, 180].

In spite of the drawbacks of the SI-NMP which are the use of relatively high reaction temperature, the limited options of mediating nitroxide for specific monomers and the need of synthesizing the mediating radicals, the advantage of not using any catalysts still makes SI-NMP a competitive candidate for growing certain type of polymer brushes for the electronic and biomedical related applications where impurities are strictly controlled.

2.9.4 Polymer brushes by ATRP polymerization from macroinitiator deposited surfaces

For an SI-ATRP process, the presence of suitable initiators on the substrate surface is essential. Two different approaches have been used to attach the initiators onto the substrate surface. The first approach involves chemical interactions between initiators that possess end functional groups and their counterparts that naturally occur on the substrate surface. The other way is based on the formation of a SAM comprising terminally functionalized initiators such as amine, epoxide, etc. Silane and thiol chemistries are commonly used for grafting initiators on silicon and gold substrate, respectively.

In addition to the attachment of small molecule initiators on the substrate surfaces, the formation of a polymer layer which can be post-modified to have initiating sites on the substrate surface is an alternative way to graft initiators. The modified polymer which subsequently possesses a wealth of initiators is called microinitiator. For example, poly(glycidyl methacrylate) (PGMA) which has quite reactive epoxy groups, can be chemically anchored onto the silicon substrate where hydroxyl groups are naturally present, followed by attachment of small molecule initiators via chemical bonding.

There are also two different approaches to form the PGMA precursor on the substrate, being called dip-coating and adsorption from the polymer solution respectively. It was found that the former method is more suitable in terms of obtaining more uniformly coated and precisely controllable polymer layer[181].

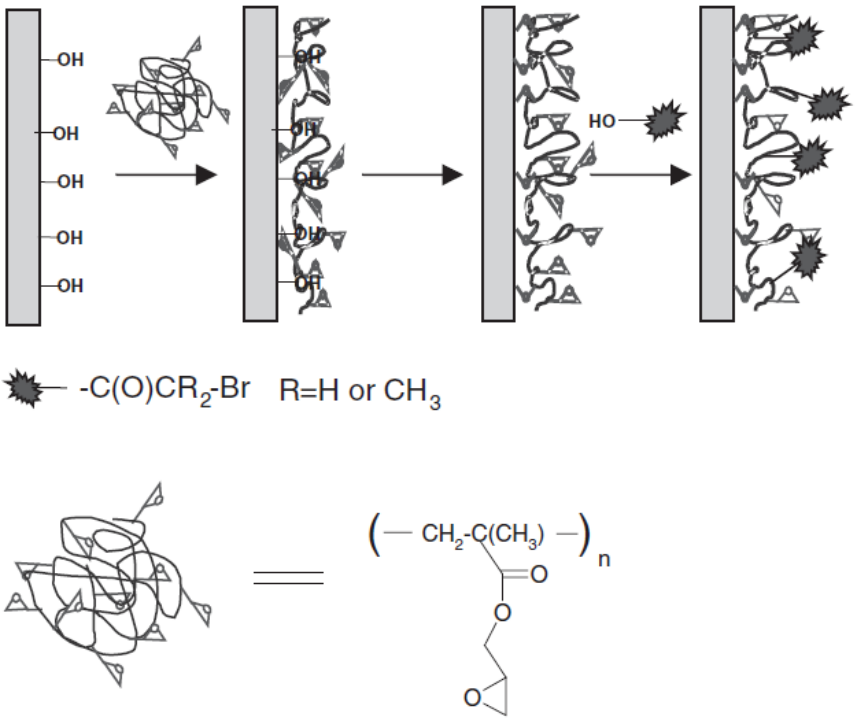

Figure 2.19 Schematic illustration of attachment of poly(glycidyl methacrylate)/bromoacetic acid macroinitiator on substrate surface[182].

As shown in Figure 2.19, after the attachment of PGMA on the substrate surface, bromoacetic acid (BAA) is used to "open" the epoxy groups of PGMA precursor as the resulting α-bromoester is known as an effective initiator for ATRP of a wide range of monomers. The attachment of BAA to the PGMA pre-formed surface is normally carried out in argon atmosphere at 110 ℃. Ellipsometry results showed an approximately 1.5-fold thickness increase after the BAA attachment, indicating that a great number of BAA molecules have been incorporated into the PGMA layer structure[181]. The amount of BAA attached was also found to be linearly dependent on the thickness of PGMA precursor layer which allows for precise control over the number of initiators. The surface density of the macroinitiator are higher than that of self-assembled monolayer of small molecule initiators which facilitates the polymer brush growth[183]. Thereby, a proper macroinitiator containing substrate for SI-ATRP is prepared. Similar to SI-ATRP initiated by small molecule initiators on the substrate surface, the macroinitiator also needs the assistance of free initiator as well as Cu^{II} deactivator in order to maintain a controlled growth speed of polymer brushes[184].

In addition to the aforementioned PGMA/BAA macroinitiator, another type of macroinitiator that contains polyelectrolyte chains has also been developed as depicted in Figure 2.20[185]. This polyelectrolyte macroinitiator only attach to the surface by physisorption between oppositely charged polymer chains and substrate surface instead of forming chemical bonds between PGMA/BAA macroinitiator and substrate surface.

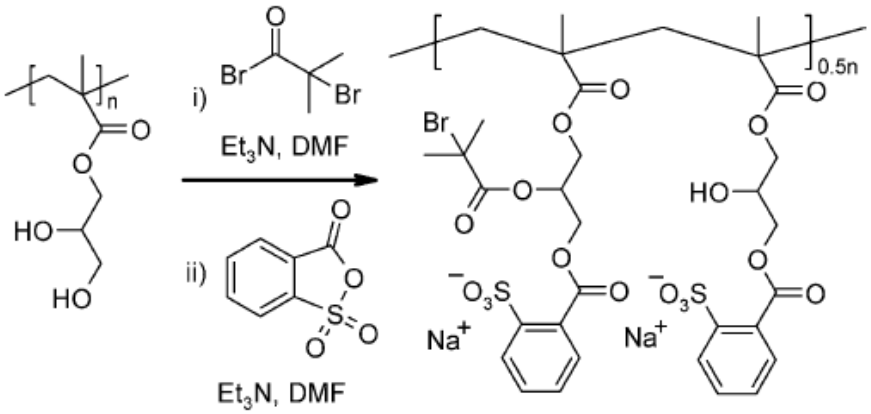

Figure 2.20 Schematic illustration of synthesis of an anionic macroinitiator[185].

The most important advantage of these ionic macroinitiators compared to other macroinitiator is the control over the amount of initiators coated onto the surfaces and thus the thickness of polymer brush can be easily designed. As LbL process can be performed for indefinite circles between either two oppositely charged macroinitiator or a pair of macroinitiator/conventional polyelectrolyte, resulting in the easy manipulation of the amount of initiating sites on the surfaces, the growth of extremely thick polymer brush becomes possible.

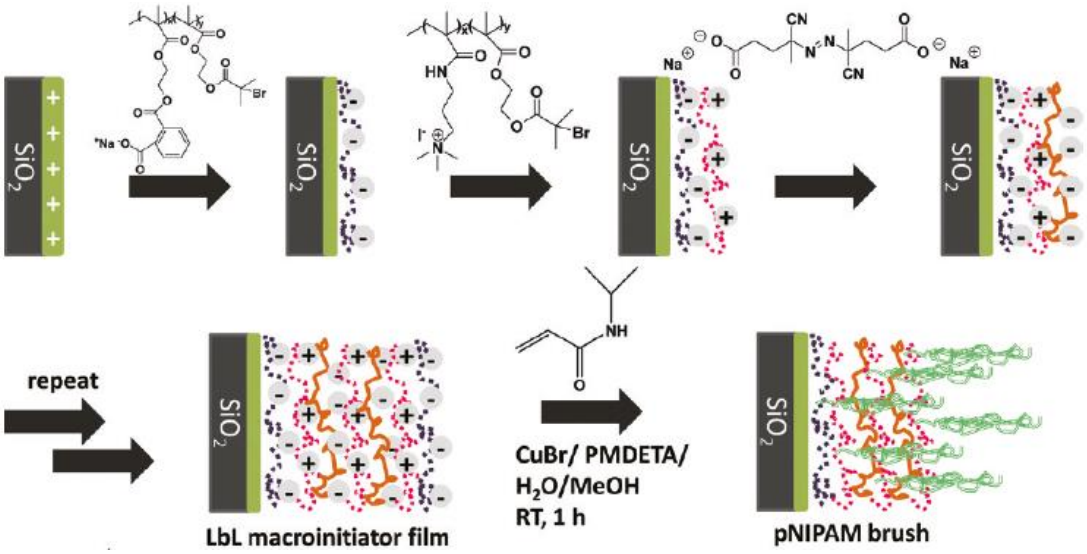

Figure 2.21 Schematic illustration of growth of Poly(N-isopropylacrylamide) (PNIPAM) brush from LbL macroinitiator precursor[8].

Estillore synthesized two oppositely charged polyelectrolyte macroinitiator and constructed their multilayers through LbL process. PNIPAM brushes were then grown from this macroinitiator containing LbL multilayers which is illustrated in Figure 2.21.

2.9.5 Synthesis of polymer brushes via surface-initiated ring-opening polymerization (SI-ROP)

Ring-opening polymerization is a standard technique for synthesizing biodegradable polyesters. The monomers normally used for SI-ROP are cyclic esters including lactide, caprolactone, dioxanone, butyrolactone, etc and this process has been carried out from a variety of surfaces such as cellulose[186], polymer film[187], carbon nanotubes[188], silicon and gold substrate, silica and magnetite particles where hydroxyl groups are present. Since the Au-initiator layer bond is unstable over 60 ℃, the reaction temperature should be set lower than that. Thus, silicon substrate is more prevalent for the growth of PLA brushes, which is usually carried out at a high temperature (>80 ℃). The thicknesses of polymer brushes grown from silicon substrates have also been found to be longer than those from gold substrates. Based on the previous result that hydroxyl and amine groups have roughly the same efficiency in initiating ROP of cyclic esters whilst temperature is believed to play an important role in this polymerization[189].

For a SI-ROP process, an anhydrous reaction atmosphere is pivotal as water molecules could act as competing initiators, leading to the failure of propagating macromolecular chains. Thus, reactants especially the solvent has to be dried properly prior to the polymerization. Ideally, the solvent should be refluxed over CaH_2 or sodium metal depending on the quality needed, followed by distillation under protection of inert gas. However, if the required equipment is unavailable, storing

solvents over activated molecular sieves may be used as an alternative way of drying the solvent. Normally size 4 Å sieves are enough for most solvents, but size 3 Å sieves should be used when drying solvents that have smaller size.

The most commonly used catalyst for SI-ROP is Tin(II) 2-ethylhexanoate ($Sn(Oct)_2$) which is also a popular catalyst for synthesis of PLA in bulk polymerization. It is quite efficient at higher temperature. However, being a metal based catalyst that will be an impurity existing in biomaterials has raised many concerns. Alternatively, some particular enzymes such as lipase B could also be used as a catalyst for ROP[190]. Recently, triazabicyclodecene (TBD) which is a guanidine base catalyst and is able to catalyse the ROP at room temperature has been proven to be an extremely efficient catalyst for SI-ROP[186]. In comparison to aforementioned conventional catalysts which need a long time to reach a high conversion, polymerization that uses TBD only need few minutes to complete the reaction[191].

The impurity of monomer can affect the ROP greatly. Thus, repeated recrystallization (ideally at least twice for a 98 % purity product) of lactide monomer in toluene should be carried out as a standard procedure. In order to avoid absorbing water moisture, the recrystallized monomers should be stored in a desiccator along with silica beads as drying agents prior to use.

In addition to the approach that polyester brushes are synthesized from initiators pre-assembled on the substrates, the SI-ROP can also be carried out from catalyst immobilized substrate with addition of free initiator in the reaction solution[192]. Unlike the traditional metal-catalysed SI-ROP that the metal catalyst is located at the outer end of chain after brush growth, this alternative approach leads to polymer

brushes that have the metal catalysts at the inner end which could potentially reduce the toxicity for biomedical applications.

As a degradable polymer, the degradability of PLA brushes has been extensively studied. A backbiting mechanism was introduced to explain how polyester brushes degrade. It was found that the degradation rate of PLA brushes is significantly slower than that of PLA layer formed by spin coating, due to the increased packing density of PLA brushes[193]. Solvent, pH as well as temperature all have great impact on the degradation kinetics[193, 194]. The addition of methanol can help accelerate the degradation by solvating the polymer brushes. The rate of degradation also increases at higher temperature and the degradation was observed only take place in neutral or basic conditions.

Besides, protein resistance of polyester brushes has also been studied. Bovine serum albumin (BSA) was found to be rapidly adsorbed by polyester brushes. The rate of adsorption is related to the hydrophobicity of the brush chains. Also, the adsorption of BSA could effectively slow down the degradation process of these brushes which is similar to the effect of an outer layer of oligo(ethylene glycol).

2.9.6 Post-modification of polymer brushes

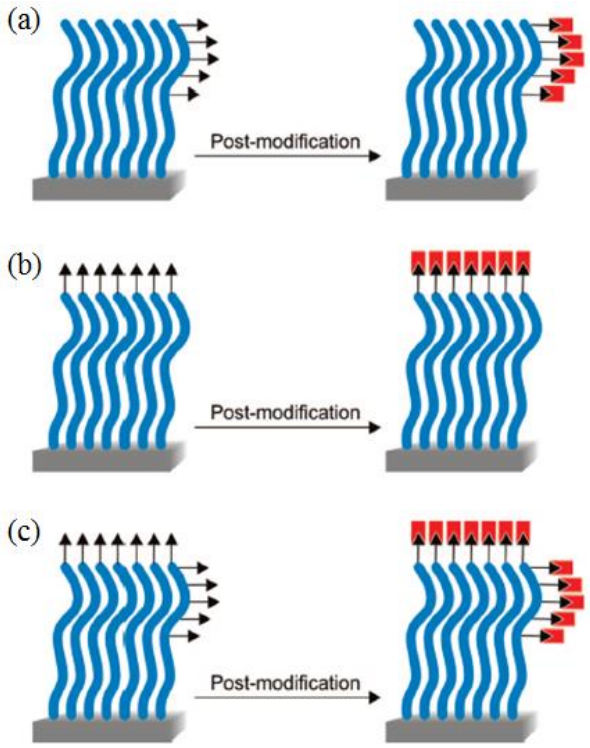

Figure 2.22 Post-modification of polymer brushes, from (a) side chains, (b) chain ends and (c) both side chains and chains ends[195].

The SI-CRP has shown excellent tolerance for a wide range of functional groups, however there are still some monomers with particular sensitive functional groups that cannot be grown directly via polymerization as the sensitive groups may react with other reactants such as initiating radical and catalysts during the polymerization. This problem can be addressed by post-modification of the polymer brushes which have reactive groups that can be attached by the target groups. As shown in Figure 2.22, there are three strategies for post-modification which are attachment of target groups with the functional groups of polymer brushes on the side, at the end of brush chains as well as the combination of both[195].

The functional groups that can act as precursor for further modification include hydroxyl groups, carboxylic acid groups, carboxylic ester groups, epoxide groups, etc.

Some hydrophobic groups have been attached to hydroxyl containing polymer brushes by reacting with corresponding acid chlorides[196]. This is a good tool to tailor the surface properties of polymer brushes such as wettability and barrier property. In addition, halogen moieties can also be introduced onto polymer brushes via modification of hydroxyl groups[197]. This has offered a way to generate comb-like brushes by carrying out second polymerization from the attached halogen initiators. Another interesting application of hydroxyl containing polymer brushes is acting as a platform for immobilization of bioactive groups such as proteins and peptides[198].

Polymer brushes with carboxylic acid groups on the side chains can be prepared via surface-initiated polymerization of monomers such as acrylic acid and methacrylic acid[199, 200]. Alternatively, these polymer brushes can be obtained from deprotection of other brush precursors on which the functional groups have been pre-protected by non-reactive groups. Similar to hydroxyl groups, carboxylic groups on the side of polymer brush chains can also be modified with bioactive molecules[201] and the functionalized polymer brushes are attractive for biosensing and cell adhesion-related applications[202].

Different from hydroxyl and carboxylic acid groups which are reactive and are extensively used for bonding target molecules, carboxylic ester containing polymer brushes are usually seen as a precursor for carboxylic acid containing polymer brushes, where direct polymerization of carboxylic acid containing monomer is unachievable[203].

In addition to the above three functionalizable polymer brushes, epoxide-functionalized polymer brushes such as PGMA is another versatile toolbox that can be

post-modified. Generally, these polymer brushes can be used for three purposes: (1) preparation of cross-linked polymer brushes[204], (2) immobilization of bioactive molecules[205] and (3) being a precursor for the synthesis of macroinitiators[206]. These processes all involve a ring-opening reaction of the epoxide groups.

2.9.7 Architectures of polymer brushes

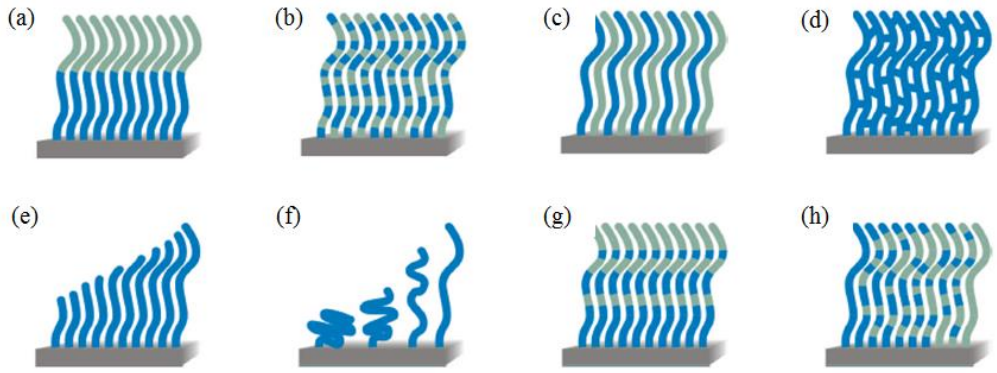

Figure 2.23 Different polymer brush architectures: (a) block copolymer brush, (b) random copolymer brush, (c) binary mixed brush, (d) cross-linked polymer brush, (e)-(f) molecular weight gradient polymer brush, grafting density gradient polymer brush and chemical composition gradient polymer brush, respectively[195].

Surface-initiated polymerization can not only precisely control the thickness of polymer brushes, but also allows the design of their architectures. As depicted in 2.23, the common architectures of polymer brushes range from block or random copolymer brushes to binary, branched brushes as well as some other complex structures.

The preparation of block copolymer brushes involves a two-polymerization process in which each block of polymer brush chains are synthesized in separate reactions compared to random copolymer brushes which is synthesized by direct polymerization of two monomers. It is noteworthy that adding $CuBr_2$ to quench the polymerization will result in more than 95% active chain ends being still able to

reinitiate the next reaction whereas only 85-90% of the chain ends are available for the second block if the first polymerization was stopped by simply rinsing with solvent[207]. Block copolymer brushes are useful in terms of combining different functional groups for further modifications.

Binary polymer brushes contains two different types of polymer chains that are synthesized via two separate polymerizations but are both directly attached to the surface immobilized initiators.

In addition to above three linearly grown polymer brushes, some architecturally more complex brushes have also been fabricated via SI-CRP. Comb-like polymer brushes can be obtained by polymerization of the main brush chains followed by the attachment of initiators on the sides of brush chains and finally the polymerization of arm chains from the side initiators[208]. There are three routes to prepare cross-linked polymer brushes with homopolymerization of ethylene glycol dimethacrylate derivatives via SI-ATRP being the easiest approach[209]. It can also be achieved by post-modification of PGMA brushes[210].

The gradient polymer brushes are those have gradient change of chemical composition[211], grafting density[212] or molecular weight[213] along the brush chains. A combination of these three different gradient factors has successfully been introduced to one brush system[214].

2.10 Characterization techniques for polymer brushes

Precise characterization of polymer brushes is challenging, as brushes are normally very thin and covalently bonded to the surfaces. A group of techniques have been applied to study different properties of polymer brushes.

The chemical composition is probably one of the first properties that researchers want to know after synthesis of polymer brushes. FTIR which can confirm the presence of different functional groups is an efficient tool in this case. Even if the polymer brushes is very thin, the use of some special modes of FTIR such as transmission or grazing angle reflection can assure the sensitivity. X-ray photoelectron spectroscopy (XPS) is another technique to study the chemical composition, which can also be used to investigate the chemical structure of the polymer brushes. A unique advantage of XPS is that it is also able to do the depth profiling as well as the mapping analysis[215, 216]. ^{1}HNMR is also a useful technique for characterization of chemical composition. Since the polymer brushes are covalently attached to the planar substrates or other shapes of surface, the polymers need to be detached from the surface prior to the characterization.

Gel permeation chromatography (GPC) is the preferred instrument for analysing molecular weight and its distribution of the polymer brushes. A very straightforward way of getting the polymer sample is cleaving the brushes off the substrates which may involve the use of strong acids. However in some cases where obtaining enough samples are difficult, researchers also add free initiators into the reaction solutions to get free polymer as a bypassing approach. Marutani and coworkers did found that the molecular weight of the polymer initiated by the sacrificial initiators is in extraordinary agreement with that of polymer brushes cleaved off the substrates[217]. However this theory is still under debate as some other groups claim that surface-initiated polymerization is a heterogeneous process compared to solution polymerization which is homogeneous[218]. The distributions of reactants in both processes are significantly different from one another. In addition, other factors such as the geometry of substrate surface also play a decisive role[219].

However, some characterization techniques can only be used for polymer brush on planar substrates due to the limitation of technology. Ellipsometry is undoubtably the most convenient tool for the measurement of polymer brush thickness grown from planar substrate. It takes very short time whilst offers great accuracy. AFM is another technique being used to measure the thickness. But the drawbacks such as underestimation of the brush thickness when used in special conditions have surely limited its performance[220, 221]. Despite having poorer performance in the thickness characterization, AFM however has been a predominant tool for analysing the surface topography of polymer brushes on planar substrate[216] compared to some counterparts such as SEM, fluorescence and optical microscopy.

Apart from understanding the properties of polymer brushes in dry condition, the study of polymer brushes in swelling condition while exposed in appropriate mediums is also essential. Not only the dry thickness of polymer brushes but also the thickness in the swelling condition can be measured by ellipsometry. Surface plasmon resonance (SPR) is an attractive tool for studying the conformational change of polymer brushes in dry and different liquid mediums[222]. It can also be used to study the protein resistance property of polymer brushes[223].

An inevitable study of polymer brushes is the kinetics which gives researchers an idea about how thick the polymer brushes can be grown with time. This can be accomplished by simply doing a series of reactions and stopping each polymerization at certain time points accordingly.

Since some of the brushes are formed from electrolyte monomers, the electronic properties of the polyelectrolyte brushes need to be explored as well. Electrochemical impedance spectroscopy (EIS), chronoamperometry, cyclic voltammetry (CV) have

shown their capability of monitoring the swelling/collapse process of polymer brushes upon ion exchange[224] or ionic strength variation[225].

2.11 Fabrication of microcarriers by emulsion method

Emulsion method, which was first introduced by Vanderhoff[226], is another versatile method for preparation of macro/nano particles. The mechanism is rather simple for a single emulsion process which is illustrated in Figure 2.24: a polymer is dissolved in a volatile solvent, which will then be emulsified in an aqueous solution that contains surfactant. As the organic solvent slowly evaporates, the polymer molecules nucleate at the water-solvent interface or precipitate onto the loading cargo. After evaporation of the solvent, the particle dispersion could be filtrated or dialyzed to get rid of residual polymers.

Size is among one of the most important properties of particles. Since particles are resulted from droplets in an emulsion process, the size of particles is mainly dependent on the size of droplets, which is primarily controlled by the concentration of surfactant[227]. In addition, other factors including the stirring rate, ultrasonication time as well as the nature of the solvent also play important role in the particles size and its distribution[228, 229]. The advantages of this method as contrasted with other techniques for fabrication of microparticles are the versatility in respect with the types of polymer that can be used, the less amount of time spent, the simplicity of the preparation process as well as the post treatment. However, the size distribution of the particles prepared by emulsion method is comparatively broad. The volatile solvent used as the oil phase should be of low boiling temperature in order to accelerate the evaporation of residual solvent. Commonly selected solvents include chloroform, dichloromethane, ethyl acetate, acetonitrile and so on.

2.11.1 Single emulsion method

There are two types of emulsion methods, single and double emulsion process. The process of the single emulsion method has been aforementioned. It is mainly used for encapsulation of hydrophobic substances. However, this method is not efficient for encapsulation of hydrophilic substances due to the rapid diffusion of encapsulated cargos into aqueous medium. Thus, double emulsion processes were developed.

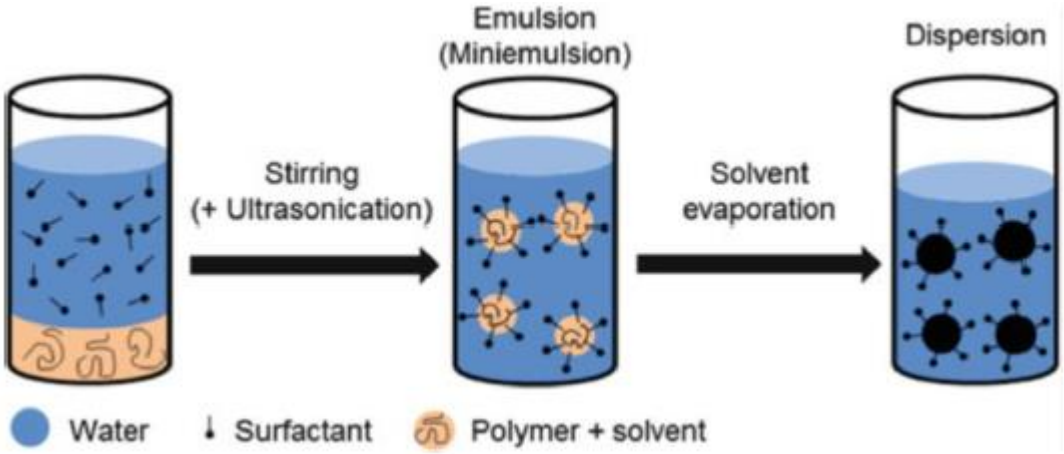

Figure 2.24 Schematic illustration of single emulsion process[230].

2.11.2 Double emulsion method

The process of double emulsion method is almost as simple as that of single emulsion method and it is able to retain highly water soluble drugs in the particles. There are few types of double emulsion processes.

In a water-in-oil-in-water (W/O/W) double emulsion evaporation process (Figure 2.25), an aqueous solution of the intended loading molecules is emulsified in an organic solution containing polymers, resulting in a primary emulsion (W/O). This emulsion is then dispersed in another aqueous solution that contains surfactant to form double emulsion. In this process, the oil layer acts as a liquid membrane and water

soluble substances can be sealed in the internal aqueous phase which significantly improves the encapsulation efficiency.

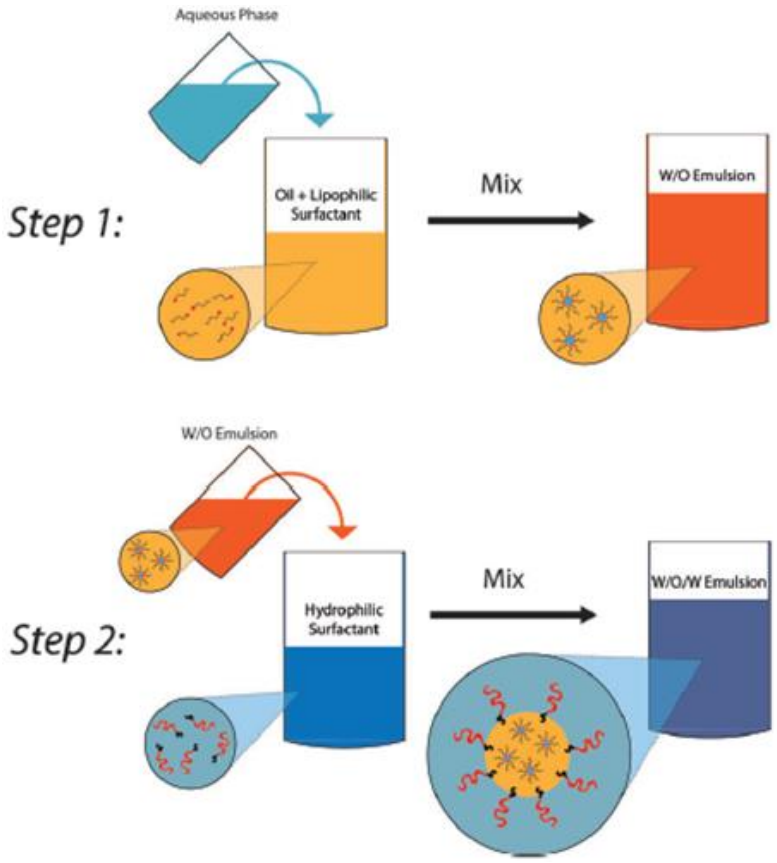

Figure 2.25 Schematic illustration of double emulsion process, step 1: creation of the water-in-oil (W/O) droplets, step 2: creation of water-in-oil-in-water (W/O/W) droplets[231].

Some other double emulsions such as W/O/W double emulsion solvent extraction method, solid-in-oil-in-water (S/O/W) double emulsion method, have also been developed. The former technique employs a third solvent which is miscible with both oil and aqueous phase to extract the organic solvent after the formation of the double emulsion.

In an S/O/W process, solids are uniformly dispersed in oil phase which forms a primary emulsion. Afterwards, the first emulsion is added into an aqueous solution containing surfactant, following by stirring or sonication to form the final emulsion.

Although the W/O/W double emulsion method is the most widely used encapsulation technique, it may not be suitable for certain type of proteins which will be aggregated at the oil/water interface under high shear during the emulsion process. In such cases, S/O/W technique could be applied alternatively to improve the protein stability by avoiding the first W/O emulsification. Takada *et al*[232] achieved high loading efficiency as well as sustained release of recombinant human growth hormone (rhGH) using this technique. Apart from encapsulation of biomolecules, inorganic particles can also be encapsulated into polymer shell through this process, forming inorganic-organic hybrids which have various applications.

2.12 **Conclusions and aims for this research**

In the literature review, three different approaches of fabricating polymeric microparticles have been broadly discussed. For LbL process, most studies are currently focused on using hydrophilic polyelectrolytes which significantly increase the permeability of microcapsules. Since stereocomplex polymers have been used for LbL assembly, the fact that these polymers are hydrophobic and biocompatible is of great interest. The use of $CaCO_3$ microparticle as the template during the assembly process could lead to a completely biocompatible protocol. Also, combining with the conventional heat treatment, a hydrophobic microcarrier system with reduce permeability is very likely to be harvested.

Surface initiated polymerization (SIP) is another popular approach used to synthesize polymer films. The applications of polymer brush layer range from membrane science, biosensing to cell culture as well as antibacterial coatings. Recently the development of polyelectrolyte macroinitiator provides a way to combine LbL as well as SIP to fabricate polymer films with tailored thickness. By using this idea, one can synthesize

thick hydrophobic shells, which would potentially have low permeability. One of the most important advantages of this approach is that a great number of monomers can be chosen which leads to a broad range of polymer shells can be fabricated according to the needs.

In addition to the two aforementioned approaches, the emulsion method is probably a much simpler and more straightforward process, which only takes few minutes. Biodegradable polymers such as PLA, PLGA have been used to either form pure polymer particles or encapsulate inorganic cores or other substances. Here, we propose to use PLA to encapsulate $CaCO_3$ cores, which is the most widely used template in LbL process. This could potentially enable the encapsulation of a wider range of substances as they can be co-precipitated into $CaCO_3$ cores prior to the emulsion process. The resulting microparticles covered by PLA are also intended to have reduced permeability.

3 Materials, Methods and Instruments

3.1 Materials

3.1.1 Chemicals

2,2′-Bipyridyl, 2-bromoisobutyryl bromide, benzyl alcohol, calcium chloride, $CuBr_2$, CuBr, ethylenediaminetetraacetic acid (EDTA), methyl iodide, sodium carbonate, sodium hydroxide, silica gel, triethylamine, Tin(II) 2-ethylhexanoate were all purchased from Sigma and were used as received.

L-Lactide, D-Lactide monomers used for synthesis of PLAs and N,N-Dimethylaminoethyl Methacrylate (DMAEMA), 2-hydroxyethyl methacrylate (HEMA), Methyl methacrylate (MMA) used for the synthesis of macroinitiator and polymer brushes were bought from TCI UK and Sigma, respectively.

Poly(L-lysine hydrobromide) (PLL, Mw = 30,000-70,000), Poly(sodium 4-styrenesulfonate) (PSS, M_W~70,000), Poly(allylamine hydrochloride) (PAH, M_W~58,000), Polyvinyl alcohol (PVA, M_W~89,000-98,000), Poly(diallyldimethylammonium chloride) solution (PDADMAC, average M_W 200,000-350,000, 20 wt. % in H_2O) were all purchased from sigma.

Solvents including acetone, acetonitrile, dimethylformamide, dichloromethane, diethyl ether, ethanol, n-hexane and tetrahydrofuran were bought from fisher chemical and were used as received. Anhydrous toluene was bought from sigma and stored over activated molecular sieves.

Molecular sieves, schlenk flask were also purchased from sigma. Silicon wafers and monodisperse 4.96 µm silica particles (SiO_2, 5% weight dispersion) were bought from Pi-kem Ltd and Microparticles, GmBH (Germany), respectively.

The deionized water used in this study was produced by a Millipore ultrapure water remote dispenser and has a resistivity of 18.2 Ω·cm.

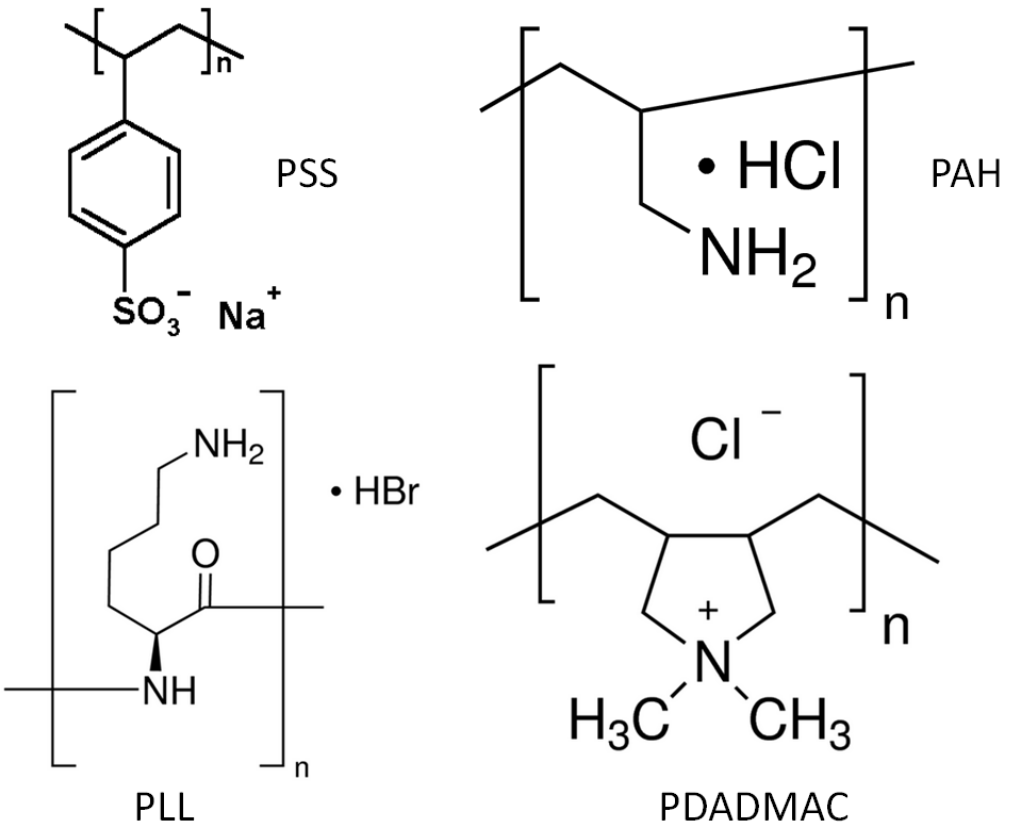

Figure 3.1 Structural formulae of polyelectrolytes used in this study.

3.1.2 Consumables

Different sizes of Eppendorf tubes and pipettes were used for microcapsules preparation throughout this work. 15 ml and 45 ml centrifuge tubes were purchased from Corning Inc.. Plastic syringes with various volumes and microliter syringes were bought from BD medical technology company and Hamilton company, respectively. Needles for plastic syringe were bought from B. Braun Melsungen AG while the 0.22 µm syringe filter were bought from sigma. 25 KD cut-off dialysis bag was purchased

from Roth. Zeta-potential cuvettes were purchased directly from the instrument manufacturer Malvern. Desiccator that used for storing moisture sensitive chemicals was purchased from sigma. Filter paper and glass bottles were from Whatman and VWR, respectively. Steinel HL 1610S heat gun was used for heating and drying purposes.

3.1.3 Polymer synthesis

3.1.3.1 Synthesis of Poly(lactic acid)s

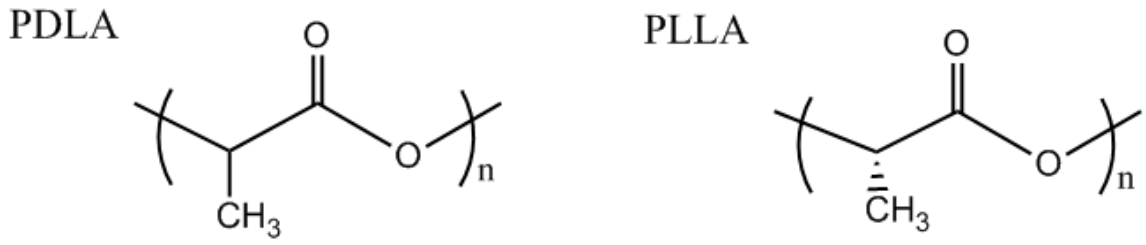

Figure 3.2 The structural formulae of PDLA and PLLA

Poly(L-lactide) and Poly(D-lactide) were synthesized via ring-opening polymerization. Briefly, a schlenk flask which had been pre-dried in oven at 100 ℃ was connected to schlenk line and heated under vacuum to remove the residual water moisture. Afterwards, the flask was quickly charged with monomer and Tin(II) 2-ethylhexanoate catalyst under the protection of inert argon flow. This chemicals loaded flask was further vacuumed at room temperature for another 60 minutes. A small amount of benzyl alcohol initiator was finally injected into the flask to start the polymerization. The reaction was kept at 125 ℃ for 24 hours. After the reaction was stopped and the chemicals cooled down, dichloromethane was added to dissolve the obtained products. The purified polymer was obtained by precipitating this dichloromethane into large excess of diethyl ether and drying under vacuum. This

precipitation procedure should be carried out for three times to ensure the purity of the final polymers.

3.1.3.2 Synthesis of macroinitiator for atom transfer radical polymerization (ATRP)

The macroinitiator was synthesized according to the literature[233]. A polymerization step and two modification steps were carried out as illustrated in Figure 5.4. Firstly, a random copolymer of DMAEMA and HEMA was obtained via ATRP polymerization, followed by esterification of PolyHEMA in order to graft Br initiator onto the polymer side chains and quaternization of PolyDMAEMA as the last step to make the copolymer positively charged. A typical procedure for the synthesis of the macroinitiator was as follows. HEMA, DMAEMA, $CuBr_2$, ethonal, 2-(N-morpholino)ethyl bromoisobutyrate, and 2,2'-bipyridine were added into a round-bottom flask before being degassed for 30 minutes with nitrogen flow and gentle stirring at ambient temperature. CuBr catalyst was at the same time being degassed in another flask for a same period of time. This solution was finally transferred to the main solution to start the polymerization. The reaction was left overnight and was stopped by bubbling with compressed air next day. The remaining solvent was removed by rotary evaporation. In order to get rid of the oxidized catalysts, the mixture was diluted with a large amount of THF and passed through a silica gel column. The obtained mixture was then concentrated and precipitated into excess *n*-hexane, resulting in light-yellow precipitations. The precipitation process was repeated 3 times to remove impurities and the purified products was then filtered and dried in vacuum at room temperature. In next step, the hydroxyl groups in Poly(HEMA-*co*-DMAEMA) copolymer was esterified. The acetone solution which contained triethylamine and DMAP was cooled in ice bath and kept at 0 ℃ before the

addition of excess 2-bromoisobutyryl bromide. Then a solution of the copolymer in acetone was added dropwise into reaction mixture within 1 hour under nitrogen protection. The temperature of water bath was then allowed to return to room temperature and the reaction lasted for another 24 hours. The resulting polymer which was insoluble in acetone was separated by centrifugation, followed by three circles of re-dissolution in water and precipitation into excess acetone in order to get rid of the impurities. The esterified and purified copolymer was again dissolved in water and freeze dried for 3 days. In the final quaternization step, the copolymer was dissolved in water and the pH of the solution was adjusted to approximately 8.8. Subsequently, methyl iodide was added into the solution and the reaction was lasted for 24 hours at room temperature. After that, the reaction mixture was added into a large excess of acetone and the crude product was re-dissolved in water and freeze dried for 72 hours to obtain purified macroinitiator copolymer. Products after each step were all characterized by both H^1NMR spectroscopy for chemical composition and GPC (DMF as eluent and PMMA as calibration standard) for molecular weight and distribution.

3.1.3.3 Synthesis of macroinitiator for ring-opening polymerization (ROP)

The macroinitiator for the ROP was synthesized in a similar fashion as that for ATRP polymerization. As the hydroxyl groups on PHEMA can be used as initiator of ROP, quaternization was carried out direct after synthesis of the copolymer.

3.2 Methods

3.2.1 RCA cleaning protocol

In order to remove the organic contaminants from the surface of silicon substrate, the RCA cleaning protocol was carried out before silicon wafer being used. The

substrates were immersed into a mixture of deionized water, NH_4OH, H_2O_2 in ratio of 5:1:1 and kept at 75 ℃ for 15 minutes. Afterwards, the substrates were taken out from the solution and rinsed with DI H_2O thoroughly before being dried with nitrogen flow.

3.2.2 Layer-by-Layer deposition of PLLA/PDLA stereocomplex multilayers on silicon substrate

To form PLA stereocomplex films with polyelectrolytes precursor, PSS and PAH multilayers were firstly deposited using conventional LbL process. The silicon chips were alternatively immersed in PSS and PAH solutions with a concentration of 2mg/ml for 15 min, and thoroughly rinsed before next immersion. This circle was repeated until the desired number of polyelectrolytes multilayers was obtained. Prior to fabricating PLA multilayers, Poly(L-lysine) was always deposited as it has better attachment with both polyelectrolytes and PLAs. PDLA and PLLA were then deposited consecutively in acetonitrile at 45 ℃ for 1 h for each layer.

3.2.3 Fabrication of Poly(lactic acid)s microcapsules

$$CaCl_2 + Na_2CO_3 \rightarrow CaCO_3 + 2NaCl \qquad \text{(Eq. 3.1)}$$

The synthesis process of $CaCO_3$ templates is formulated as Eq. 3.1. Equal volumes of $CaCl_2$ and $NaCO_3$ solutions were mixed in a beaker and stirred for approximately 25 seconds at predetermined speed. The fresh $CaCO_3$ suspension was then centrifuged immediately and washed with DI H_2O for 3 times in order to get rid of small particles. The centrifuge/wash step has to be taken as soon as the stirring stops as $CaCO_3$ particles will transform from spherical shape into square shape very quickly.

After the synthesis of $CaCO_3$ templates, the PLA multilayers with and without polyelectrolytes precursor were deposited in the same way as it was done on planar substrates. After each layer, triple wash/centrifuge circles were performed to remove

the excess polyelectrolyte molecules. After having constructed the polyelectrolyte multilayer structure, the $CaCO_3$ cores were removed by using EDTA in different ways including vortex shaking and dialysis in order to compare the impact of them on the morphologies of resulting microcapsules.

3.2.4 Encapsulation of fluorescent molecules and heat treatment for PLA stereocomplex microcapsules

PLA microcapsule suspension was first centrifuged and the supernatant was discarded before addition of the fluorescent dye solutions. These mixtures were then left on vortex shaker for 3 hours. Afterwards, microcapsule suspension which underwent heat treatment was placed in an oven overnight. All microcapsule suspensions were finally washed with DI H_2O to remove excess dye molecules.

3.2.5 Deposition of silane initiators on silicon substrates and silica particles

The initiator solution consisted of silane initiator, triethylamine and toluene (2:5:100 in volume ratio). The silicon substrates and the silica particles were then incubated in this mixture solution overnight. Afterwards, samples were washed with large amount of toluene and ethanol. These initiator deposited substrates and particles were finally stored in desiccator and refrigerator, respectively.

3.2.6 Deposition of (3-Aminopropyl)triethoxysilane (APTES) on silicon substrates

ATPES was deposited on the surface of silicon substrates to ensure better attachment of polyelectrolytes multilayers to the substrate surface. The silicon substrates were incubated in an APTES containing toluene solution (ratio of ATPES to toluene was 1:10) and left overnight. The substrates were then taken out and rinsed thoroughly

with excess toluene and ethanol to remove unattached ATPES molecules before being stored in vacuum environment.

3.2.7 Deposition of polyelectrolyte multilayers on silicon substrate and $CaCO_3$ templates

PSS and macroinitiator were deposited alternately on silicon substrate which had been previously coated with APTES. The wafer was first immersed in PSS solution with concentration of 5 mg/mL for 15 minutes and rinsed afterwards with DI H_2O to remove the unattached polymers. Then the chips were incubated in macroinitiator solution with the same concentration for another 15 minutes and washed accordingly. This immersion/washing circle was repeated until the desired number of polyelectrolyte multilayers was achieved. The deposition of polyelectrolyte multilayers on $CaCO_3$ microparticles was conducted in the same manner.

3.2.8 Purification of methyl methacrylate

In order to remove the inihibitors in methyl methacrylate, the monomers were passed through a Al_2O_3 column (10 g Al_2O_3 basic powder for 20 mL monomers) under argon flow which creats a strong pressure to push the liquids out of Al_2O_3 column. The purifed monomers were then stored in refrigerator before use.

3.2.9 ATRP of methyl methacrylate (MMA) to make Poly(methyl methacrylate) (PMMA) shell on macroinitiator covering inorganic templates

This procedure was taken place on a radleys carousel 12 plus reaction station. Specifically, the polymerization solution and the macroinitiator deposited templates need to be degassed before being mixed together as the reaction starts once the initiators encounter the reaction mixture. Firstly, the reaction mixture comprising methyl methacrylate, $CuBr_2$, 2,2′-Bipyridyl, DMF, DI H_2O was added into a round

bottom flask before being degassed by bubbling with argon for approximately 30 minutes. Afterwards, CuBr was quickly added into the solution, followed by a further 15 minutes degassing to ensure the oxygen was thoroughly expelled. At the same time, the suspension of macroinitiator covered $CaCO_3$ particles was transferred into the reaction tube and bubbled with argon for 15 minutes to get rid of oxygen. Upon the completion of the degassing of both the particle suspension and reaction solution, the reaction solution was injected into each reaction tube, triggering the polymerization of MMA on the surface of the particles. At each time interval, the reaction was stopped by bubbling the reaction solution with compressed air and the resultant was collected after several washing cycles. The obtained particles were stored at 4 ℃ before further characterizations.

Figure 3.3 A image of a radleys carousel 12 plus reaction station [234]

3.2.10 Labeling of BSA with FITC

160 mg of BSA was dissolved in 40 ml of PBS which was at pH 8. In the meantime, 5 mg of FITC was dissolved in 5 ml of ethanol. These two solutions were then mixed and incubated in refrigerator for 12 hours, followed by dialyzing against DI H_2O for 72 hours. The obtained solution was stored in dark before further use.

3.2.11 Co-precipitation of BSA-FITC in $CaCO_3$ microparticles

0.615 ml of $CaCL_2$ (1M) and Na_2CO_3 (1M) were mixed with 1 ml of BSA-FITC solution and 1 ml of DI H_2O. The mixed solution was then vigorously stirred for 30 sec before being washed with DI H_2O for 3 times. Afterwards, the microparticle dispersion was centrifuged and the supernatant was discarded. Finally, the obtained microparticles were dried in oven overnight.

3.2.12 Fabrication of PLA coated $CaCO_3$ particles via emulsion method

$CaCO_3$ particles were first synthesized using the conventional procedure described previously and were dried in oven overnight. PLA/DCM and PVA/H_2O solutions with different concentrations were also prepared beforehand. Afterwards, $CaCO_3$ particles were dispersed in a small amount of DCM and sonicated, following by adding PLA solution into the $CaCO_3$ particle dispersion. This mixture was also sonicated in order to obtain a homogeneous particles/polymer mixed dispersion. PVA/H_2O solution was then added which formed a two phase separation with the pre-added dispersion. Finally, this two phase mixture was mechanically sonicated for 30 seconds at a frequency of 20 Hz. The resulting dispersion was stirred vigorously and left at room temperature to allow the solvent to evaporate. After evaporation of solvent, this dispersion was washed with deionized water and stored in refrigerator before further use.

3.2.13 Permeability test of polymer coated microparticles

In order to assess the permeability of the PMMA and PLA coated microparticles, the retrieved microparticles were dispersed into 0.2 M EDTA solution and were shaked on a vortex shaker for 2 hours. This was carried out in order to see whether $CaCO_3$ microparticles would be dissolved in EDTA solution. Finally, the solution was centrifuged and washed with DI H_2O for 3 times to remove excess EDTA and other residues. The obtained particles were dispersed in DI H_2O again and stored at 4 ℃ for further characterizations.

3.2.14 Drying of solvent

For ROP, anhydrous solvent is required as any water molecules left in the reaction system could act as competing initiator. For long term use, the commercial anhydrous solvent should be re-stored over active molecular sieves in order to avoid absorption of water into the solvent. The whole drying process was done with a schlenk line system. Firstly, molecular sieves were filled into a clean pre-dried schlenk flask to a third of its volume. The flask was baked in a heating mantle under vacuum for about 4 hours to fully activate the sieves. When then activation is done, the heating mantle was moved away and the flask was let to cool down in air for 30 min. Afterwards, the flask was purged for at least 3 times and was protected in argon environment before transfer of solvent.

The needle which connected the schlenk line and the flask was purged for 10 min to get rid of air before being inserted it into the solvent bottle. Then, insert a long needle into the bottle and remain its head above the solvent to get rid of air in the long needle. Subsequently, take off the lid of the solvent flask and replace with a rubber septum onto which a small needle is inserted to let the argon flow out. The other side of the long needle was then inserted into the solvent flask, followed by closing the tap on the

schlenk line to stop argon flow coming into the solvent flask, creating a positive pressure of the solvent bottle against the solvent flask. Finally, the long needle was inserted to the bottom of the solvent and the solvent was immediately transferred into the flask.

Upon the completion of solvent transfer, the tap on the schlenk line was open again to eliminate the pressure difference between the solvent bottle and flask before taking away the long needle. The solvent flask was resealed tightly by the lid and was left for 1 week before use to ensure all remaining water molecules have been absorbed properly by the molecular sieves.

3.2.15 Purification of LLA monomer

Purification of LLA monomer was done through a recrystallization procedure. In a typical procedure, 10 g of LLA monomer and 15 ml of toluene were added into a round bottom flask, followed by being gently heated by a heat gun until the monomer was completely dissolved in toluene. The flask was then left at room temperature to cool down until most of the monomer precipitated. The flask was stored in refrigerator overnight to ensure a maximum recovery of monomer from the solvent. The supernatant in the flask was finally discarded. This procedure should ideally be repeated for three times in order to have a higher purity of monomer.

3.2.16 Preparation of Macroinitiator-PLA copolymer micelles

5 mg of the copolymer was first dissolved in 1 ml of THF. Afterwards, the polymer containing solution was slowly dripped into 10 ml of DI H_2O with vigorous stirring. Light blue colour can be observed as more polymer solution dripped in as a result of the formation of micelles. The micelle solution was then left in air for 3 days for the

solvent to fully evaporate before being stored in refrigerator before further characterisations.

3.2.17 Synthesis of PHEMA brush

The synthesis of PHEMA brush follows a typical procedure that has been described in the formation of PMMA brush. However, the composition of reaction chemicals differs from the previous polymerization. In this case, 10 ml HEMA monomer, 10 DI H_2O, 0.5 mmol CuCl, 0.06 mmol $CuCl_2$ and 0.6 mmol BiPy were used for 6 reaction tubes.

3.2.18 Growth of Poly(lactic acid) brushes on planar substrates

The growth of PLA brushes was taken place in a schlenk flask. Prior to the experiment, all the glassware were pre-dried in an oven at 100 ℃ overnight. During the preparation stage, the flask was dried again by a heat gun for at least 3 times to ensure that no moisture was left in the flask. Then, initiator coated planar substrate as well as a pre-determined amount of L-lactide monomer were put into the flask. The charged flask was vacuumed for another 2 hours to get rid of any water moisture that got into the flask during the addition of reactants. Afterwards, benzyl alcohol free initiator, catalyst as well as solvent were added and the flask was refilled with argon before being immersed into the oil bath. The reaction was then kept at 100 ℃ for a pre-determined duration. After the reaction is finished, the flask was lifted up and left in air to cool down. Dichloromethane was then added to dissolve the free polymer in the solution. The substrates were finally immersed in DCM, acetone and ethanol in sequence to remove any polymer or other chemical compounds that were physisorbed on them and dried with nitrogen flow before further measurements.

3.2.19 Preparation of phosphate-buffered saline solution

PBS solution was made by directly dissolving tablets purchased from sigma in DI H_2O. PH values of the obtained solutions were adjusted by adding HCl or NaOH accordingly.

3.2.20 Degradation of PLA brushes

The degradation of PLA brush film was studied in PBS solutions at different temperatures as well as at various pH values at 37℃. For the former degradation study, experiments were carried out at 20, 37 and 60 ℃. For the latter one, PLA degradation was studied at pH = 3, 6, 7.4 and 9 at 37℃. In a typical procedure, the substrates with PLA films were incubated in a PBS solution in corresponding experimental conditions. The substrates were then taken out for thickness monitoring at pre-determined time intervals. The thickness measurement throughout the degradation process was made by ellipsometry and the substrates were thoroughly washed with DI water before and after thickness measurements. It is also noteworthy that the solutions used for degradation studies should be refreshed every 2 days in order to maintain a consistent environment for PLA films.

3.3 Instruments

3.3.1 Nuclear magnetic resonance spectroscopy

Nuclear magnetic resonance spectroscopy, commonly referred to as NMR, is a technique used in chemistry related areas that investigates the magnetic properties of atomic nuclei. Nuclear magnetic resonance is a physical phenomenon which occurs when nuclei is exposed in a magnetic field where the nuclei absorb and re-emit electromagnetic radiation. Being based on the phenomenon of nuclear magnetic resonance (NMR), it can exploit a variety of information about the tested molecules

(e.g. the chemical structure, dynamics,). NMR spectroscopy is an extremely convenient and versatile characterization method in chemistry which can detect a wide range of samples containing nuclei possessing spin. It studies the chemical properties of organic compounds, with the help of NMR active nuclei (e.g., ^{1}H, ^{13}C, ^{31}P, ^{15}N, ^{29}Si). ^{1}H NMR and ^{13}C NMR are the two most commonly used types of NMR spectroscopies, with ^{1}H NMR being more frequently used.

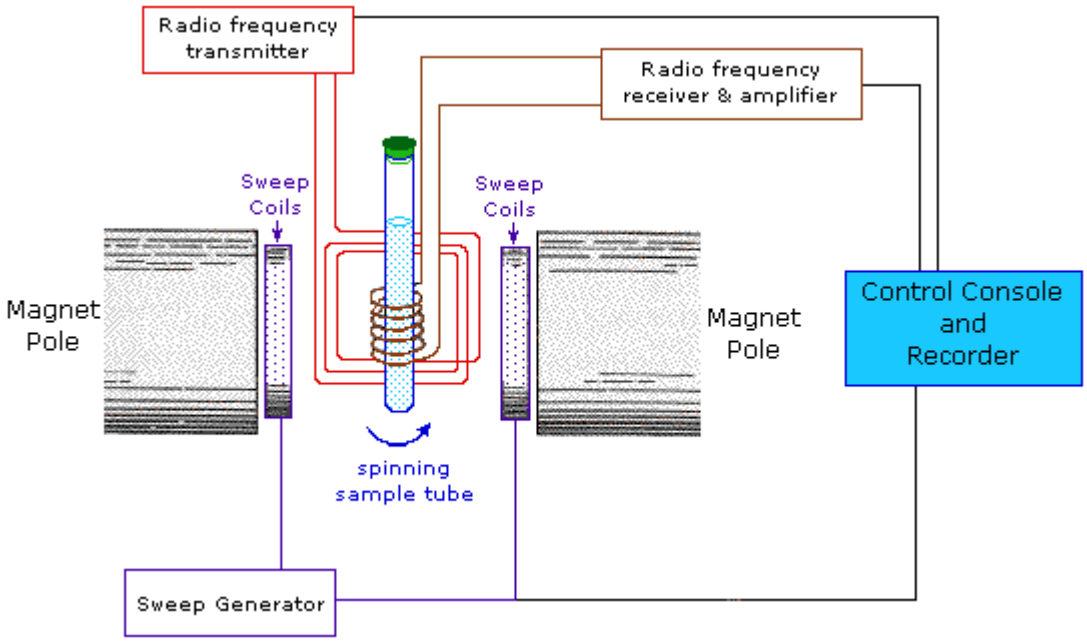

Figure 3.4 Schematic illustration of nuclear magnetic resonance [235]

For a real molecule, a particular nucleus can not only be affected by the applied field, but also be influenced by the magnetic effect of neighbouring nuclei and electrons. This leads to the signal being absorbed at a slightly different frequency than that for a single atom. A NMR spectrum, which contains a series of peaks belonging to different compounds, can be obtained after plotting the data from those absorptions. The difference from the zero point is referred to as the chemical shift (δ). The zero point is customary on the right end of the spectra, with the values increasing to the left.

In this work, proton nuclear magnetic resonance (^{1}H NMR) characterization was carried out by a Bruker AV spectrometer at frequency of 400 MHz at room temperature. Deuterated chloroform ($CDCl_3$) and tetramethylsilane were used as solvent of sample and internal reference, respectively. The concentrations of samples were all set to be 10 mg/mL.

3.3.2 Gel Permeation Chromatography

Gel Permeation Chromatography (GPC) is a type of high performance liquid chromatography (LC), which is performed in a wide range of solvents for the separation of organic polymers. It is a separation technique based on the molecular size of components and is achieved by packing the columns with very small and porous particles to separate molecules dissolved in the solvent that is passed through. It is also used to determine the molecular weight distributions of polymers. The filled materials in the columns are made from polymers that have been crosslinked to make them insoluble and non-adsorptive with the samples. GPC uses a stagnant solvent present in the pores of packed particles as the stationary phase and a flowing liquid as the mobile phase. The mobile phase can thus flow in and out of the pores in the particles and also between the particles.

A GPC instrument comprise a pump to push the solvent through the device, an injection port to lead the samples into the column, a column to hold the stationary phase, several detectors to detect the components as well as a software that controls the device and processes the data. During the test, the polymer sample is first dissolved in a proper solvent before being injected into the machine. The polymer containing solution will then move across the beads as the mobile phase carries them down the column. Afterwards, the data generated is compared with the calibration curve that has been made beforehand, giving the users the information about the

molecular weight and its distribution of the polymer. The larger the macromolecules are the quicker they will be detected in the column.

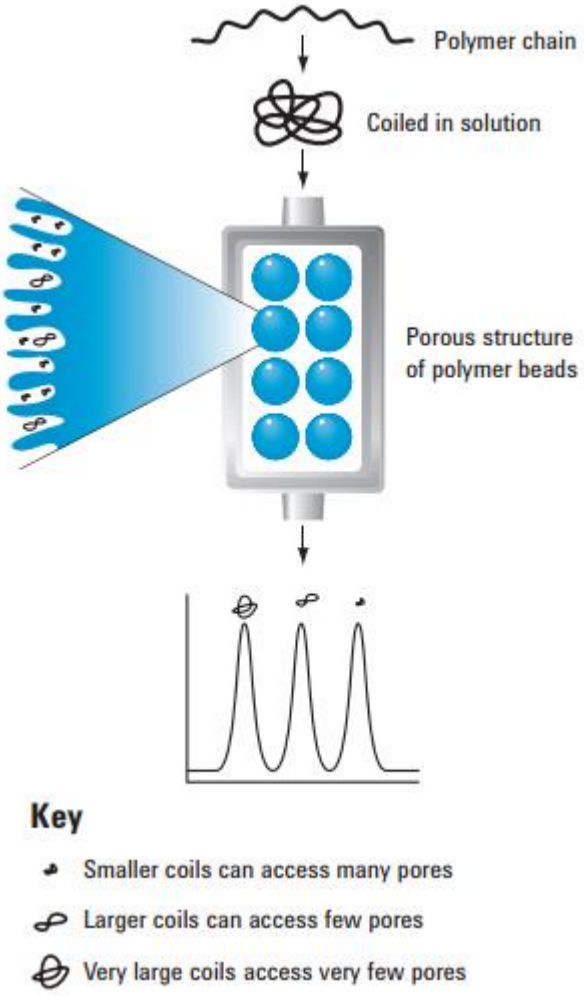

Figure 3.5 Schematic illustration of how gel permeation chromatography separates molecules with different sizes [236]

GPC is considered the only technique available to characterize the molecular weight distribution of polymers, which is an important property of polymers. Moreover, a polymer mixture could be separated into individual components. GPC is frequently combined with some other techniques to further separate molecules by other characteristics, such as charge, acidity, basicity and affinity.

As it has been described above, a calibration of known molecular weights has to be carried out in order to have a standard for the calculation of the molecular weight of the polymer samples. These standard materials must be of very high quality and with extremely narrow molecular weight distributions. The molecular weight is then determined from the calibration curve.

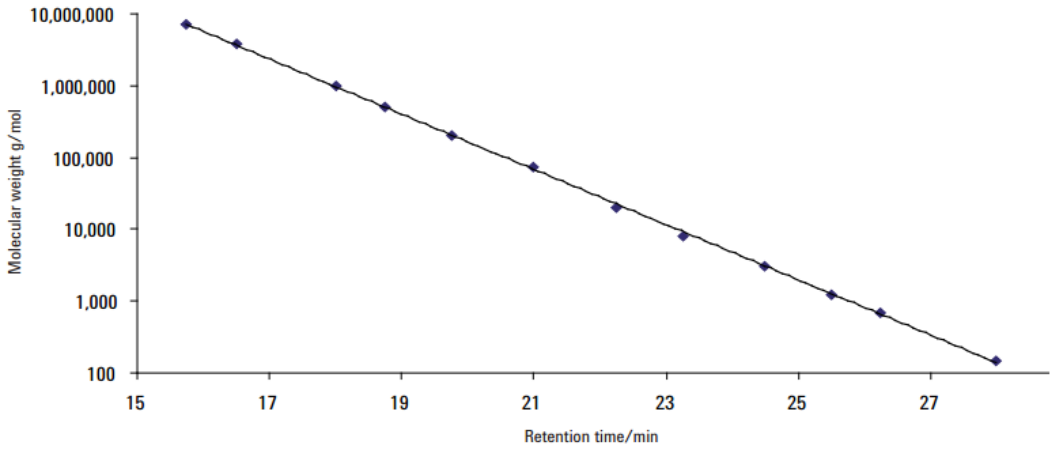

Figure 3.6 A typical calibration curve to determine the molecular weights of polymers from the retention time [236]

The most commonly calculated average molecular weight is the number average molecular weight, abbreviated as Mn and usually represents the thermodynamic properties of the molecules. As it can be seen in Figure 3.7, the Mn value is the critical point at which there are equal amounts of molecules on each side. There are also some other descriptions for average molecular weight, including weight average molecular weight which is abbreviated to Mw and is defined as the value at which there are equal masses of molecules on each side. Theoretically, Mw is always greater than Mn unless the polymer is completely monodisperse. Z-average molecular weight (Mz) as well as Mz+1 are also used to calculate the average molecular weights. Mz is more affected by viscoelasticity and melt flow behaviour. The ratio of Mw/Mn is defined as the polydispersity index (PDI) of the macromolecules, which indicates the

range of molecular mass of the sample. In another word, the larger the PDI is, the broader the molecular weight distribution will be.

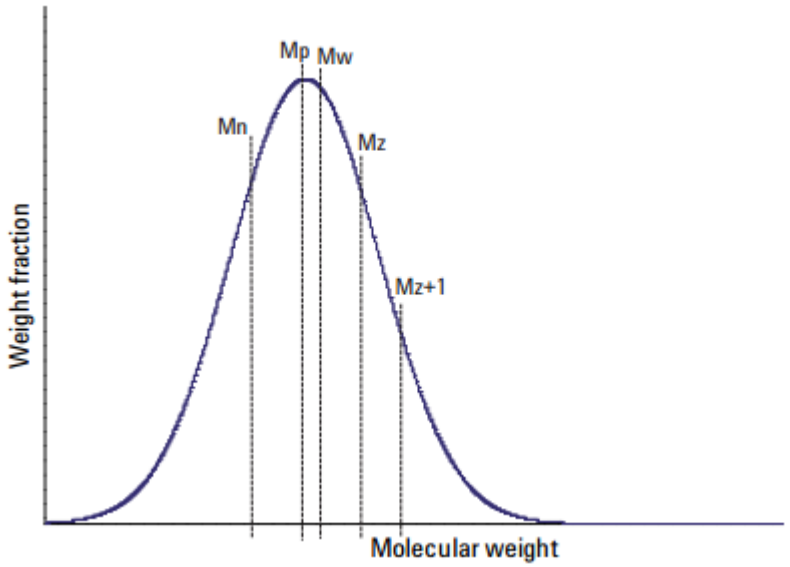

Figure 3.7 Different average molecular weights of monodisperse polymer [236]

During the sample preparation, 2 mg of each polymer sample was dissolve in 2 ml of proper solvent that also contains 2 % of TEA. The dissolved solutions were then filtered through a syringe with filter paper to remove any impurity before sample being submitted to the machine.

3.3.3 Differential Scanning Calorimetry

Different Scanning Calorimetry, known as DSC, is a thermo analytic technique that detects the amount of heat that materials need to change their temperatures as temperature increases. Each sample with known mass can be heated up during which the heat capacity of the sample can be quantified. Heat capacity is a measureable physical quantity that an object absorbs or releases which results in temperature change. Depending on whether the sample absorbs or releases heat, a phase transition process is either endothermic or exothermic. For example, a melting process, in which

more energy is absorbed by the sample to increase its temperature, is an endothermic phase transition. This unique principal allows researchers to monitor the transitions of materials such as melting process, glass transition and phase changes. Glass transition and melting process are the basic characterizations in polymer chemistry and understanding the phase changes of liquid crystals, metals, etc enables analysts to know the degree of the purity of the tested materials. Thus, DSC has been widely used for characterizations of polymers, liquid crystals as well as for the industrial tests such as oxidative stability, drug and chemical analyses. Besides, getting an idea about how much the heating capacity of a material exactly is also helps operate industrial process more efficiently. The rate of temperature increase during the heat process can be simply set in the controlling software according to the need which helps users save a considerable amount of time.

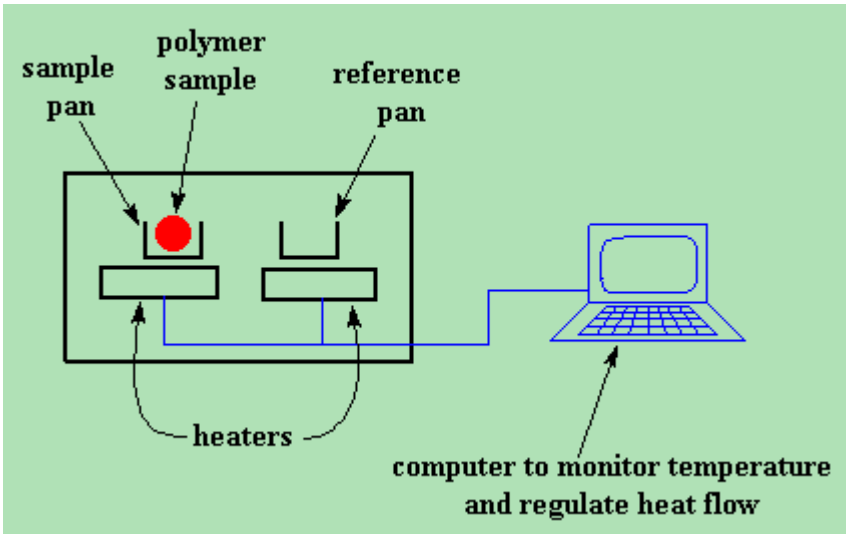

Figure 3.8 Schematic illustration of a different scanning calorimetry setup[237]

In this work, the melting points of different PLA samples were characterized by a Mettler Toledo DSC822e equipment. The polymer powder was first filled into a steel

sample holder and then was sealed by immobilizing a cap before being put into the instrument.

3.3.4 Fourier Transform Infrared Spectroscopy

Fourier Transform Infrared Spectroscopy (FTIR) is a technique that can be used to analyse the chemical composition of a sample by recognizing molecular bonds present in the detected infrared spectrum. The chemicals being analysed can be in any form of solid, gas or liquid, depending on their status.

Basically, FTIR measures how much of light a sample absorbs at each wavelength. In detail, the light source within the FTIR equipment which contains the full spectrum of wavelength to be measured irradiates a beam into a Michelson interferometer-consists of several stationary mirrors as well as a moving mirror. As the mirror moves, each wavelength of light is periodically blocked and transmitted by the interferometer which leads to the separation of the light and wavelength being modulated at different rates. Finally, the collected raw data of light absorption is processed by a computer and converted into a spectrum. Due to the use of a mathematical process called fourier transform to turn the raw data into the desired spectrum, this method was then named Fourier Transform Infrared Spectroscopy.

The obtained spectrum of the measured sample shows the information of the chemical bonds vibrating at different frequencies. The existing functional groups in the measured samples can then be identified by comparing the spectrum with the infrared spectra of the known compounds as standards. It is worth noting that FTIR is a quantitative analysis technique because of the fact that absorption intensities are proportional to the concentrations of the corresponding functional groups.

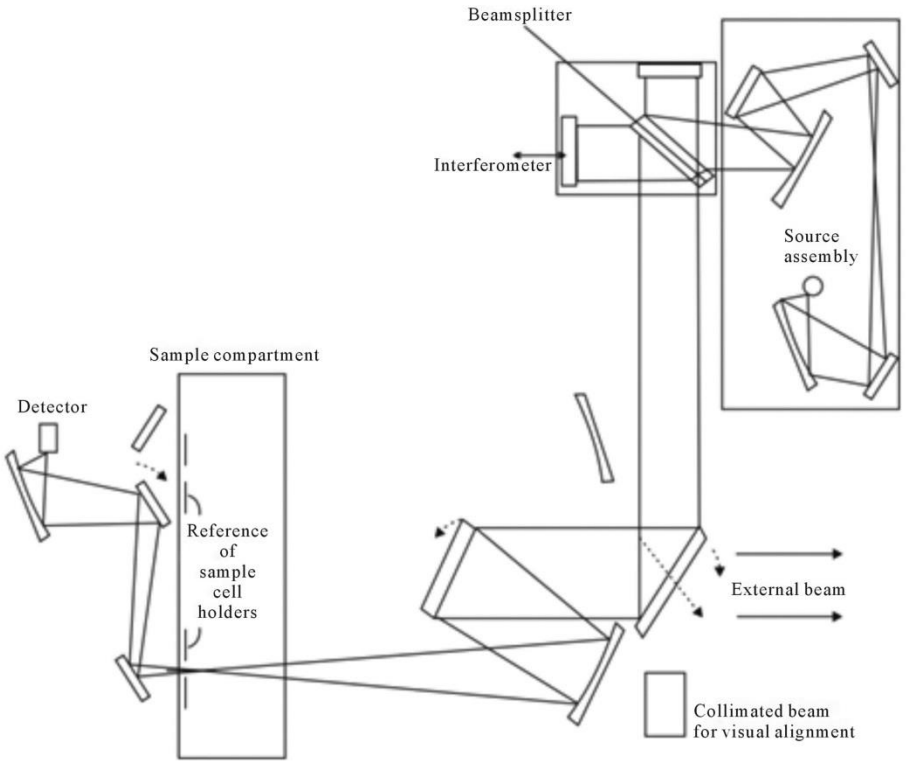

Figure 3.9 Schematic diagram of fourier transform infrared spectroscopy (FTIR) [238]

In this work, the chemical compositions of different samples were characterized with a Bruker Tensor 27 FTIR system. It is equipped with a room temperature DTGS detector, mid-IR source ranging from 4000 to 400 cm^{-1}, and a KBr beamsplitter. The maximum resolution is 1 cm^{-1} and a background spectrum was run prior to each measurement session. For some samples containing water medium, proper drying should be done before measurement to prevent disfavoured interference.

3.3.5 X-ray diffraction spectrometry

X-ray diffraction (XRD) technique is a non-destructive analytical tool that investigates the crystal structure, chemical composition as well as physical properties of given materials. The analysed materials should be finely ground and homogenized.

In 1912, Max von Laue discovered the phenomenon that crystalline substances can act as diffraction grating for X-ray wavelengths. So far, X-ray diffraction has been a

common technique for the characterization of crystal structure as well as atomic spacing. All diffraction methods are based on X-ray, which will be led to the samples where the diffracted rays occur and will be later collected by a detector. The interaction between the incident rays and the samples generate constructive interference when the conditions for the Bragg's law ($n\lambda=2d\sin\theta$) which relates the wavelength of electromagnetic radiation of the diffraction angle and the lattice spacing in a crystalline sample are met. All diffraction directions of the lattice should be detected after samples being scanned through the whole range of 2θ angles.

Basically, an X-ray diffractometer comprise four constituent parts, which are: a highly stable X-ray source, a sample holder that can adjust the sample position, an X-ray detector as well as an analysing system. During a measurement, X-rays are generated by a cathode ray tube where electrons are produced by heating a filament. Then these electrons are accelerated under voltage to bombard the target materials. If the energy the electrons carry is enough, the electrons in the inner shell of the target materials will be dislodged and thus creating characteristic X-ray spectra. The intensity of the reflected X-ray will be recorded as the sample and detector rotating.

Characterization of unknown or known solid is crucial to research in materials science. Since XRD can distinguish different crystallinity, it is a suitable technique to study the change in the crystallinity of a known material. Other applications of XRD include determination of unit cell dimensions, sample purity, etc.

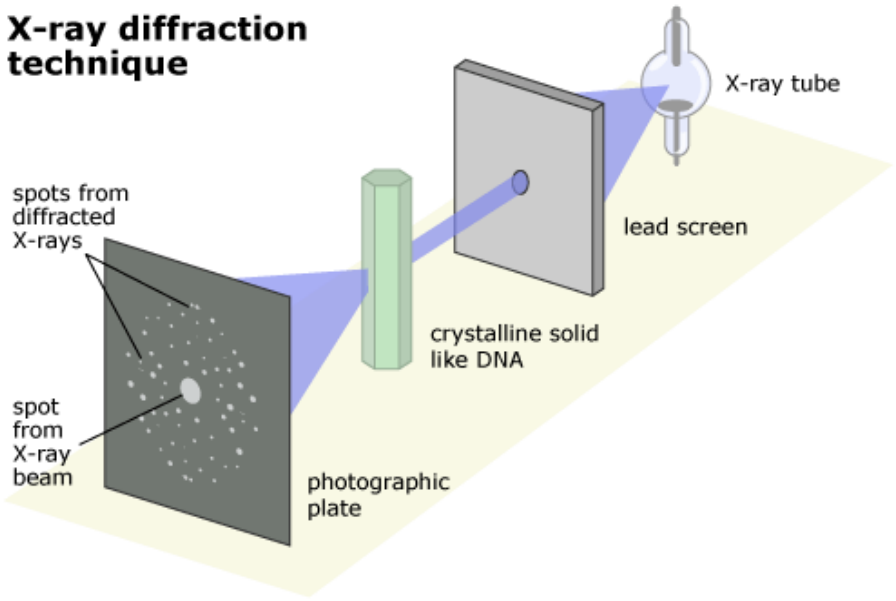

Figure 3.10 Schematic diagram of X-ray diffraction [239]

3.3.6 Ellipsometry

Ellipsometry is an optical technique which studies the dielectric properties of thin films and is widely employed for material characterizations such as thickness, roughness, composition, electrical conductivity and some other properties.

Since ellipsometry is a sensitive and contactless approach which can directly give the value of film thickness upon measurement without any calculation by the operator, it is much more convenient to use it for thickness measurement than methods such as SEM and AFM, especially when the film is very thin. Ellipsometry measures the thickness based on the change of polarization upon reflection or transmission which will then be compared with a pre-created model. It determines film thickness by interference between light reflecting from the surface and light traveling through the film. Depending on the relative phase of the re-joining light to the surface reflection, interference can be defined as constructive or destructive. The interference involves

both amplitude and phase information. The phase information is very sensitive to films down to sub-monolayer thickness.

This technique is normally used to measure thickness of thin film between a few angstroms and microns. It is, however, not suitable for films whose thicknesses are more than tens of microns as interference oscillation will be extremely difficult to resolve in such circumstances. Alternative characterization techniques should then be applied.

The use of ellipsometry to measure the thickness also requires at least partial light being able to travel through the entire film and then return to the surface, which may lead to the limitation of not being able to measure samples made of materials that can adsorb light. This can sometimes be addressed by using different wavelength as materials absorb light very differently at various wavelengths.

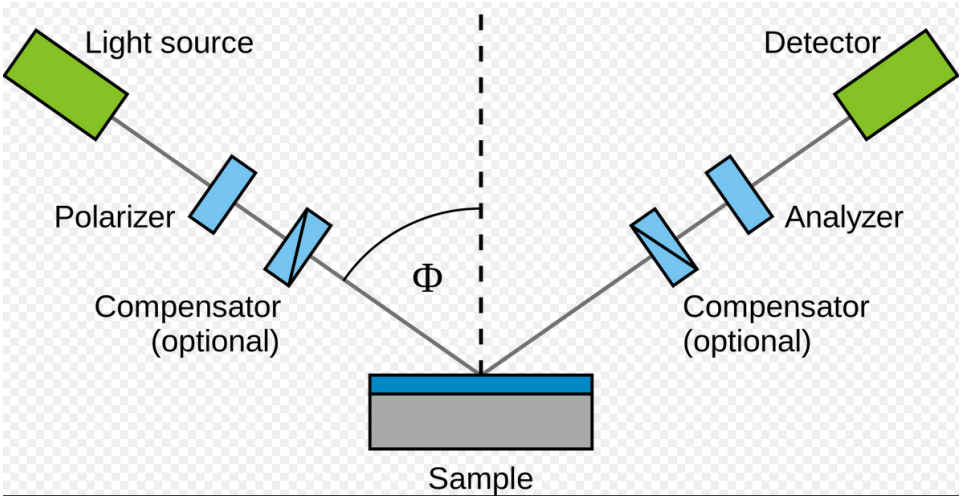

Figure 3.11 Schematic illustration of ellipsometry [240]

In this work, the films thicknesses deposited on Silicon substrate were measured with a J.A.Woollam alpha-SE Ellipsometer. A proper model should be chosen before the measurement to fit the certain substrate. After having placed the substrate at the

measuring area and given the order to the software, data was shown within few seconds.

3.3.7 Zeta potential

Zeta potential refers to electrokinetic potential in colloidal dispersion and is a parameter representing net charge between the slipping plane of colloidal particles and the dispersion medium. It differs from stern potential or electric surface potential as they are defined at different locations. When charged particles are dispersed, a double layer structure of ions is formed at particle/liquid interface as counterions are attracted to the particle surface. The double layer comprises two parts: the inner region where ions are tightly bounded to the particles and the outer region in which ions are less bounded. The boundary of these two regions and the interface between this double layer and the medium are called stern layer and slipping plane, respectively.

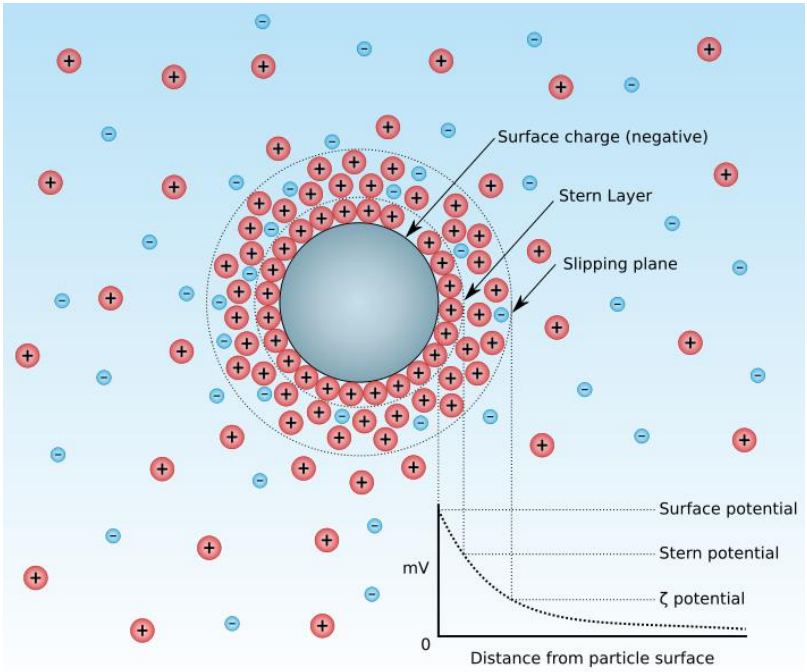

Figure 3.12 Diagram showing the ionic concentration and potential difference as a function of distance from the charged surface of a particle suspended in a medium [240]

Zeta potential is an important indicator of the stability of the particle dispersion as it reflects the repulsion between particles within the medium. Colloidal dispersions that have a zeta potential value of greater than ±30 mV are considered to have good stability whereas particles can easily form aggregation if their zeta potential values are between -5 mV and 5mV. Particle dispersions with a zeta potential value between -30 and -5 mV or between +5 and +30 mV are also likely to be quite instable. Thus, the stability of colloidal dispersions can be adjusted according to the zeta potential value.

Some factors including pH of the medium where the colloidal particles suspended can significantly affect the zeta potential value. As shown in Figure 3.13, zeta potential remains high above zero at low pH as there are a great number of positive charged groups adsorbed at the surface of particles. On the other side, zeta potential will be very low at high pH as a result of negative –OH groups adsorbing on the particles. An isoelectric point is a pH value at which the particles are neutralized and are least stable.

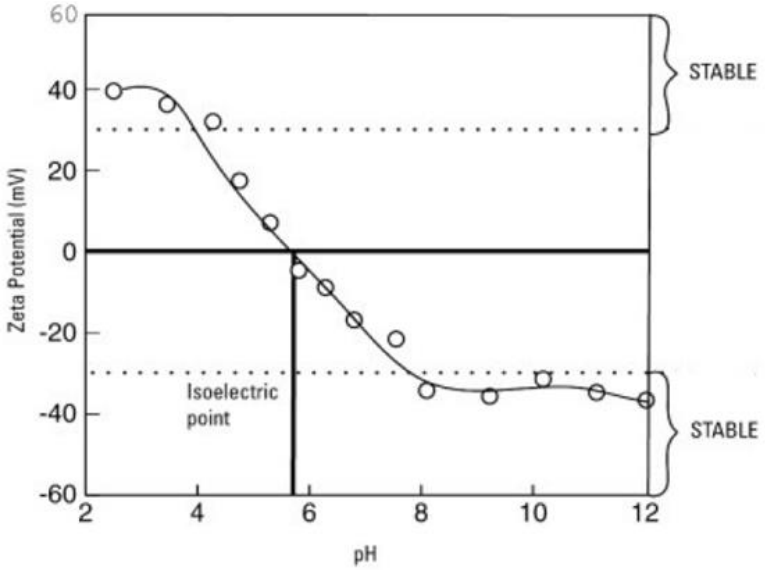

Figure 3.13 Dependence of zeta potential on pH [241]

When an electric field is applied to a colloidal dispersion, the charged suspended particles will be attracted to the electrodes. The velocity of the particles will be constant when equilibrium between the electronic forces and the viscous forces which opposes the movement of particles is reached. The velocity of a particle in a unit electric field is defined as electrophoretic mobility. The relationship between zeta potential and electrophoretic mobility is formulated as Smoluchowski equation:

$$U_E = \frac{2\text{Ɛ}Zf(\kappa a)}{3\eta}$$

UE: electrophoretic mobility, Z: zeta potential, Ɛ: dielectric constant, η: viscosity, f(κa): Henry's function. Smoluchowski's theory is fairly useful as it can be applied to colloidal dispersions of any shape and concentration.

Zeta potential in this work was obtained by using a Malvern nano zetasizer instrument. Average zeta potential was calculated from 3 independent measurements, with each of them having 10 single runs.

3.3.8 Scanning Electron Microscope

Scanning Electron Microscope (SEM) is one of the most commonly used electron microscopes, which images the sample surfaces and characterize surface morphologies by scanning them with a beam of electrons. It is an efficient tool to investigate the microstructure as well as chemistry of different types of materials.

An SEM system usually includes: electron source, electron lenses, electron detector, sample chamber, display and data processing devices as well as some other infrastructure components. There are different detectors for SEM, with secondary electron detector and backscatter detector being the most widely used ones. The former one can attract electrons by charging with a positive voltage which helps

improve the signal. The latter one can be either scintillator or solid-state detectors. The specific usage of a particular SEM machine is entirely dependent on which detector it equips. The interior of the machine is normally evacuated at a moderate vacuum when it's being used which allows the electrons to travel in their route without obstruction.

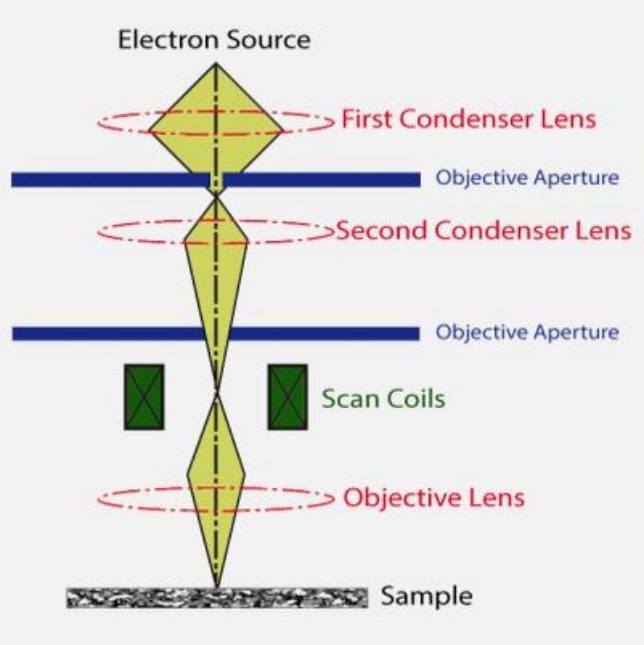

Figure 3.14 Schematic illustration of scanning electron microscope [242]

Before the observation, samples have to be sputter coated with a thin conductive film which enables the electrons to travel through. Gold and carbon are usually used as the coating materials. Any damages on the coating layer will likely cause image defects. During the observation, a beam of incident electrons are firstly generated by a thermal emission source, which can be a heated tungsten or a field emission cathode. The electrons were then accelerated down to pass through several electromagnetic lenses which produces a focused beam of electrons. These electrons will thereafter be directed by the scanning coils near the end of the column to bombard the surface of the sample. In order to create the SEM images, the electron beam is scanned in a

raster pattern across the sample surface. The emitted electrons and their intensity are detected by a detector and will later be processed. The signals are obtained from the interaction between the electrons and the atoms at different areas of the sample.

SEM is frequently applied to obtain high-resolution images of characterized samples. It can also analyse the chemical composition by using Energy-Dispersive X-Ray Spectroscopy (EDS) accessories. An EDS detector can display different elements into an energy spectrum by separating their characteristic x-rays. It is able to analyse the chemical composition of characterized materials in the size of few microns, providing essential compositional information for a wide range of materials.

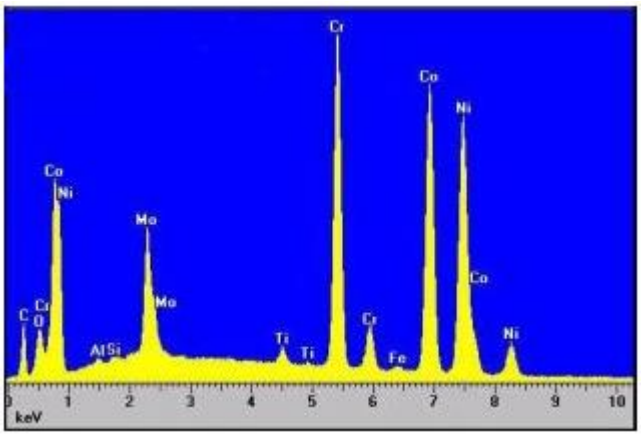

Figure 3.15 A typical spectrum of energy-dispersive X-Ray spectroscopy [243]

In this study, the surface morphologies of polymeric microcontainers were studied by using an Inspect FEI SEM system. A drop of diluted microcapsule solution was dispersed on a round flat glass slide which was attached on a stud and dried in air before being coated with gold.

3.3.9 Transmission Electron Microscope

The transmission electron microscope operates on the same basic principal as the light microscope, but using electrons as the "light source" instead of light. The relatively

big wavelength of light limits the size of sample that operators can see. In contrast, the short wavelength of electrons significantly improves the resolution of the microscope, enabling operators to see much smaller objects at the size of down to a few angstrom (10^{-10}m).

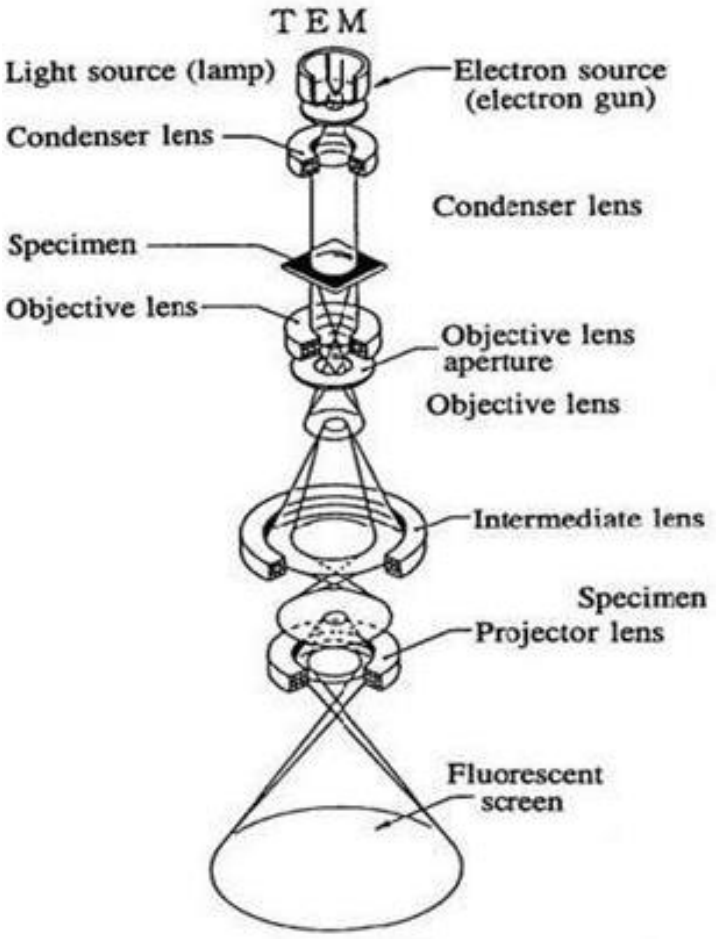

Figure 3.16 Schematic illustration of TEM [244]

During the observation, the electrons were firstly emitted from a cathode at the top of the column. They then travel through the evacuated column and a series of electromagnetic lenses which focus them into a very narrow beam. Afterwards, the focused electron beam travel through the specimen that previously positioned in the microscope. The resulting beam will then be magnified by a couple of objective

lenses before finally hitting on a fluorescent screen, which generates an image of the sample with varied darkness, depending on the sample density.

In this work, a JEOL 2010 TEM was employed to image. A droplet of the diluted dispersion was added onto a copper grid and then left in air overnight to dry before the observation.

3.3.10 Water Contact Angle Measurement

Measuring the contact angle is an efficient way to characterize the surface wettability. Contact angle is an angle which a liquid droplet exhibits on a solid surface when they are in contact. Not only can the properties of the solid and the liquid determine this angle, but the interaction between the two phases also plays an important role. The value of contact angle demonstrates the ability of the liquid spreading on the solid surface.

Figure 3.17 shows the instrument used in this work for water contact angle measurement. The process of measuring the contact angle on a substrate is rather simple. The substrate which contains the characterizing surface is placed on the sample platform, a small water droplet was then dropped onto the surface, followed by focusing them with camera that is connected to the computer. Once the images are captured, choose a model and the contact angle (θ) is given automatically. Hydrophilic surfaces tend to have higher affinity with the liquid which shows a faster spread speed, smaller contact angle as well as better wettability. On the other hand, the hydrophobic surfaces have the opposite effects.

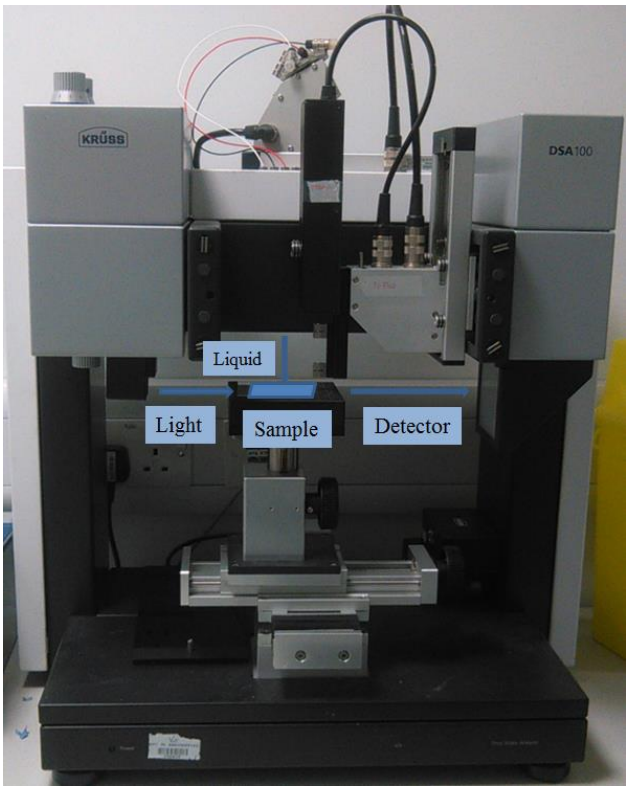

Figure 3.17 Schematic illustration of the setup for water contact angle measurement

3.3.11 Mechanical sonication

Sonicator is an important lab device, which uses sonication to break apart objects. The main component of a sonicator is the ultrasonic electric generator, which can produce a signal that drives the transducer to convert the electric signal into physical vibration. This physical vibration exists at the molecular level and could be amplified by the sonicator. The amplified vibration will then be delivered to the probe and ultimately be transmitted to the solution being sonicated by constant mechanical vibration of the probe.

The vigorous vibration of the probe results in cavitation, which is a phenomenon of formation and violent collapse of microscopic bubbles. Massive energy is released during the collapse of these micro bubbles in the cavitation field, within which the target objects are processed.

There are different sizes of probes available for different types of sonication processes. The big-sized probes have a more effective acting area which makes them able to process larger volumes. But their reaction intensity is relatively low, whereas the small-sized probes have a contrary effect.

3.3.12 General lab equipment

IKA Werke RET basic C magnetic stirrer, Elma S15H Elmasonic ultrasound bath, Salter-And ER-180A electronic balance, Mettler Toledo pH meter, Nikon Labophot optical microscope, Buchi Rotavapor R-210, Edwards RV3F pump, Diener plasma cleaner, Binder incubator, fume hood, Millipore ultrapure water remote dispenser, IKA vortex Genie 2 and IKA vortex Genie 3 shakers, Eppendorf 5417C and Eppendorf 5418 centrifuge were used for various experiments and lab work.

4 Fabrication of Poly(lactic acid) stereocomplex microcapsules with reduced permeability using Layer-by-Layer technique in non-aqueous medium

In recent decades, Layer-by-Layer microcapsule, which is a multi-layered polymeric capsule system created by different driving forces between polymer pairs, has been a promising candidate for controlled release and some other biomedical applications[245, 246].

Various polymers have been used as shell materials to build up multilayer polymeric containers. Among the non-water soluble polymers, Poly(lactic acid)s which is an aliphatic polyester, has been widely studied and used as biomedical materials in recent decades due to their extraordinary biocompatibility, biodegradability and mechanical properties[247, 248]. Lactic acid, which is the degradation product of PLA, is fully biocompatible in human bodies, leading to a high demand of medical materials made from PLA such as surgical suture, implant, as well as drug carriers.

Stereocomplex formation is a process during which two enantiomeric polymers form their stereocomplex in an appropriate organic solvent. PLA microcapsules have been prepared through this interaction[117]. However, the utilisation of SiO_2 templates and thus the involvement of hydrofluoric acid would lead to toxic residual left in the microcapsules which limits the application of the PLA stereocomplex microcapsules in biomedical area. Thus, fabrication of PLA microcapsules made by LbL technique with a biocompatible procedure is of great interest.

Therefore, here we propose a fully biocompatible LbL fabrication procedure of PDLA/PLLA stereocomplex microcapsules using $CaCO_3$ as template. Different layer numbers, adsorption ways of first PLA layer as well as template removal methods and the effect of polyelectrolyte precursor will be studied. The effect of heat treatment on the permeability of PLA microcapsules will also be investigated.

4.1 Synthesis of Poly(lactic acid)s for LbL assembly

In order to construct PLA stereocomplex multilayers, the enantiomeric poly(lactic aicd) polymers were firstly synthesized via a typical ring-opening polymerization process. Poly(L-lactide) and Poly(D-lactide), which are two enantiomers of poly(lactic acid), were prepared from L-lactide and D-lactide monomers, respectively. As the most commonly used initiator and catalyst for ring-opening polymerization of cyclic esters, benzyl alcohol and $Sn(Oct)_2$ were used in this work. No solvent was used for this bulk polymerization, which was carried out at 125 °C for 24 hours. The crude polymers were dissolved in DCM and precipitated in cold diethyl ether. This was repeated for three times to ensure the high purity of obtained polymers for the LbL assembly.

The chemical structure of PDLA and PLLA were determined by ^1H NMR. As can be seen in Figure 4.1(a), the peak at 1.61 ppm belongs to methyl group while the 5.19 ppm peak was assigned to the protons of $-CH_2-$ group. The last small peak between 7-8 ppm was for $CDCl_3$ solvent. Figure 4.1(b) shows a similar spectrum as Figure 4.1(a), with all of the peaks at the same positions, meaning that two polymers with the same chemical composition were synthesized.

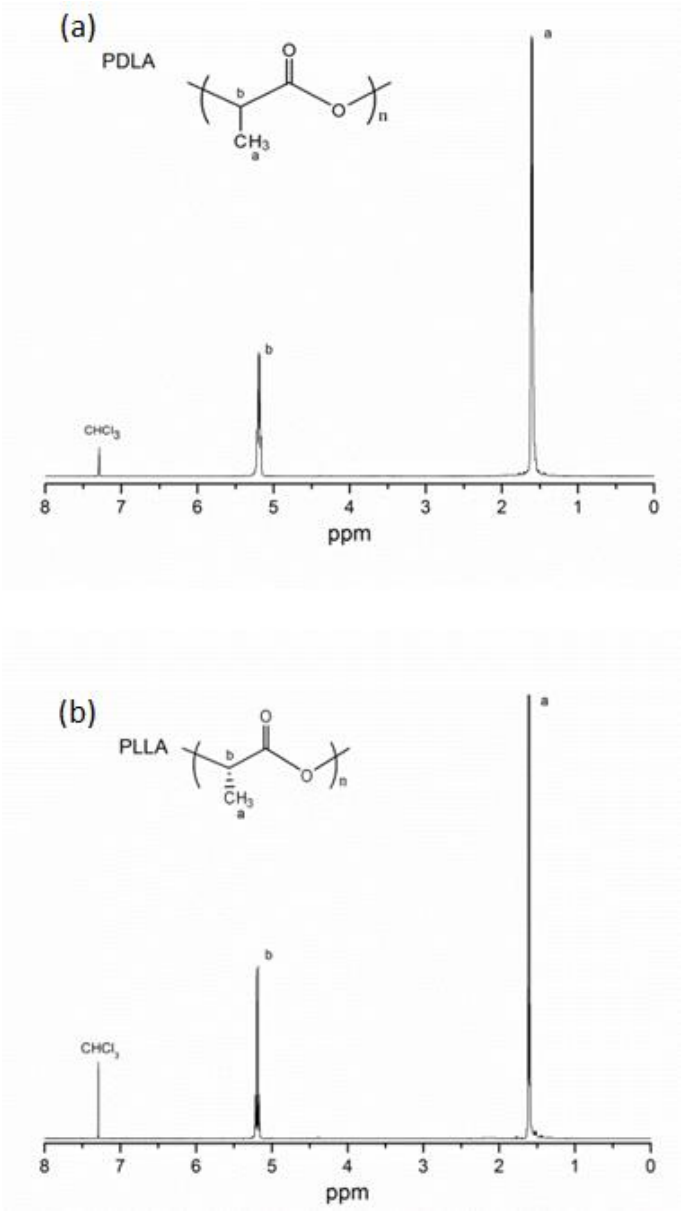

Figure 4.1 The NMR spectrums for (a) PDLA and (b) PLLA

GPC curves in Figure 4.2 showed that both PDLA and PLLA that have a relatively narrow molecular weight distribution were obtained via ring-opening polymerization. The molecular weight of PDLA and PLLA are 37,500 and 59,200, respectively, which were suitable for our usage due to the use of polymers with similar molecular weights in Layer-by-Layer assembly[249]. Thus, these polymers were used for LbL assembly directly after synthesis and purification.

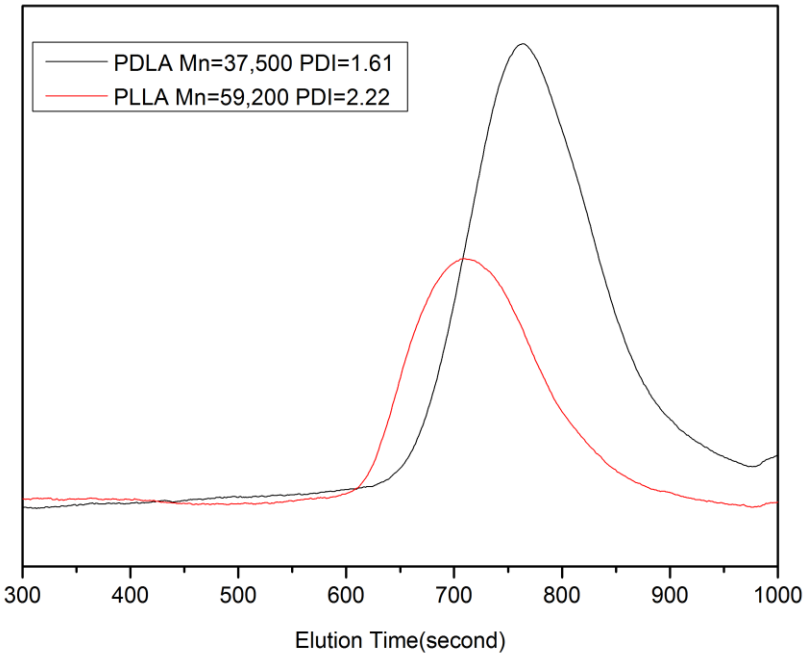

Figure 4.2 GPC curves of the synthesized PLLA and PDLA

4.2 Layer-by-Layer assembly of Poly(lactic acid)s stereocomplex multilayers on planar substrate

4.2.1 The effect of polyelectrolytes precursors on the thickness of Poly(lactic acid)s multilayers

The kinetics of the growth of PLA films on planar silicon substrate was studied. Two samples were compared, PLL/$(PDLA/PLLA)_5$ multilayers with and without $(PAH/PSS)_4$ PEMs precursor, which was pre-deposited on the bare substrate.

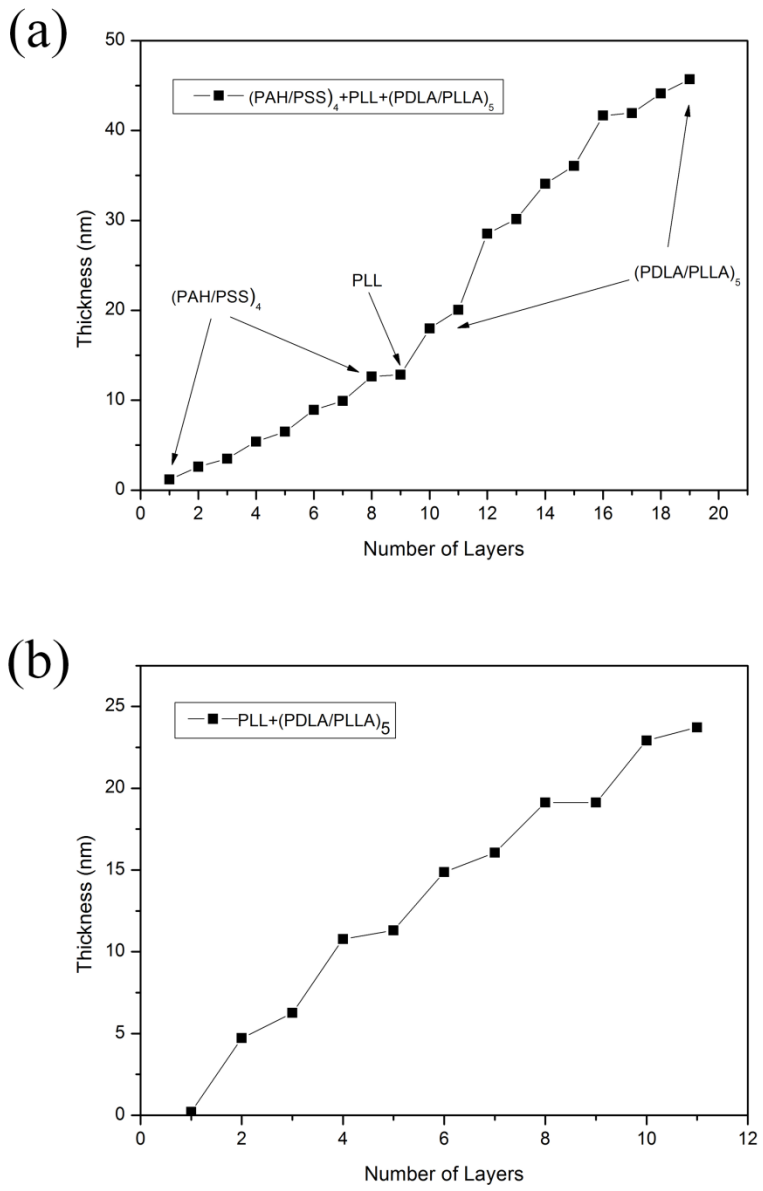

Figure 4.3 Growth pattern of PLA stereocomplex films on substrate

The thickness of PLL/$(PDLA/PLLA)_5$ multilayers assembled onto $(PAH/PSS)_4$ PEMs precursor as shown in Figure 4.3(a) was found to be 22.84 nm while the thickness of PLL/$(PDLA/PLLA)_5$ multilayers deposited onto bare substrate without $(PAH/PSS)_4$ PEMs precursor (shown in Figure 4.3(b)) was 23.5 nm, indicating that Polyelectrolytes multilayers precursor has no particular effect on the thickness of the PLA stereocomplex films. Another phenomenon that was observed is that an odd

number of PLA layers are always thicker than an even number of PLLA layer. This is due to the "dotted-structure" formation during the assembly of PLA multilayers[249]. As the process of each PLA deposition takes longer than polyelectrolytes assembly, each odd number layer can hardly cover the whole substrate surface uniformly within each deposition. Hence, the next even number layer has to deposit on the uncovered surface during their formation of the stereocomplex with the former layer, which is reflected as a thinner layer after each deposition circle.

4.3 Fabrication of Poly(lactic acid)s stereocomplex microcapsules

Poly(lactic acid) stereocomplex microcapsules were prepared through LbL process in acetonitrile using $CaCO_3$ particles as templates and PLL, PDLA, PLLA as shell materials, followed by template removal by EDTA as illustrated in Figure 4.4. All PLA deposition processes were carried out at 45 ℃ as indicated in previous study[6].

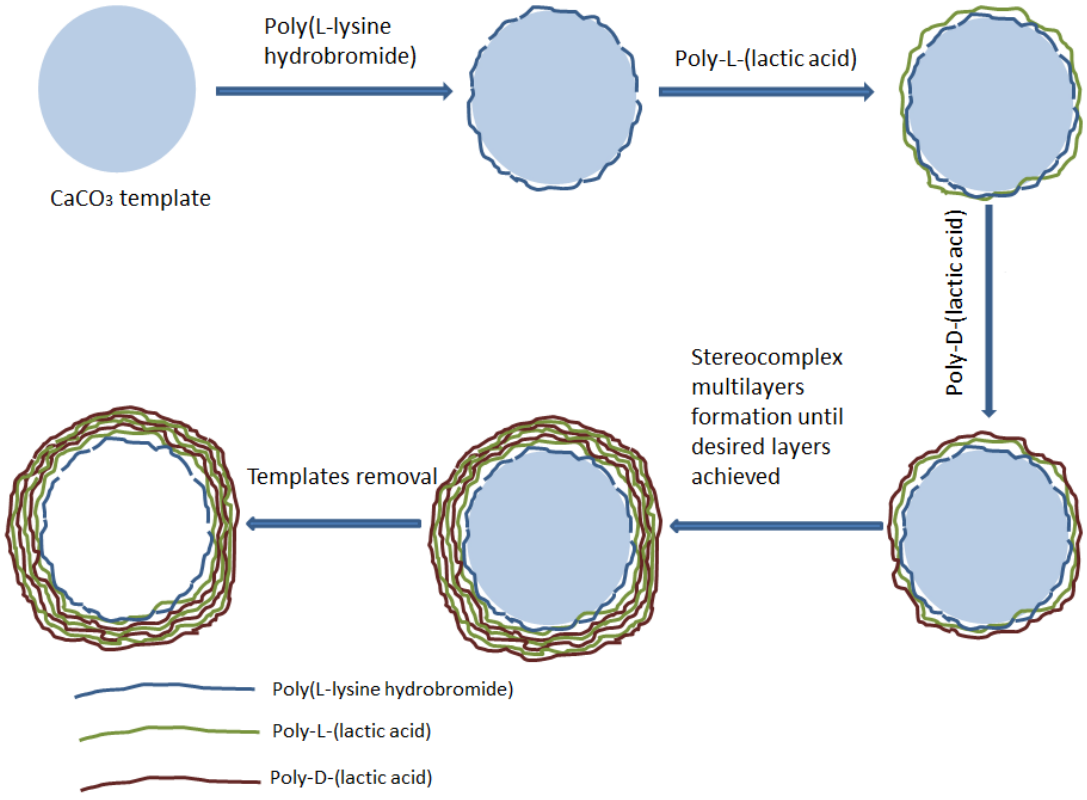

Figure 4.4 Schematic illustration of fabrication of PLA stereocomplex microcapsules

4.3.1 Analysis of chemical composition of Poly(lactic acid)s stereocomplex microcapsules

XRD is a conventional tool to characterise crystallinity. Since the change in crystallinity is one of the differences that occurred during the formation of the stereocomplex polymer, XRD was applied to confirm the successful formation of the PLA stereocomplex microcapsules [116]. It can be seen in Figure 4.5 that PDLA and PLLA polymers have the same diffraction peaks in the spectrum which are at θ=15.1˚, 16.5˚, 18.1˚ and are the typical peaks of polylactic acid. The diffraction peaks of the PDLA/PLLA film are at θ=12˚and 22.1˚(which is an overlap of the peaks at 20.8˚ and 24.1˚). The peaks of microcapsules situate at θ=12˚, 20.8˚ and 24.1˚, which are uniquely assigned to PLA stereocomplex, demonstrating that the PLA microcapsules fabricated are in the structure of stereocomplex[250].

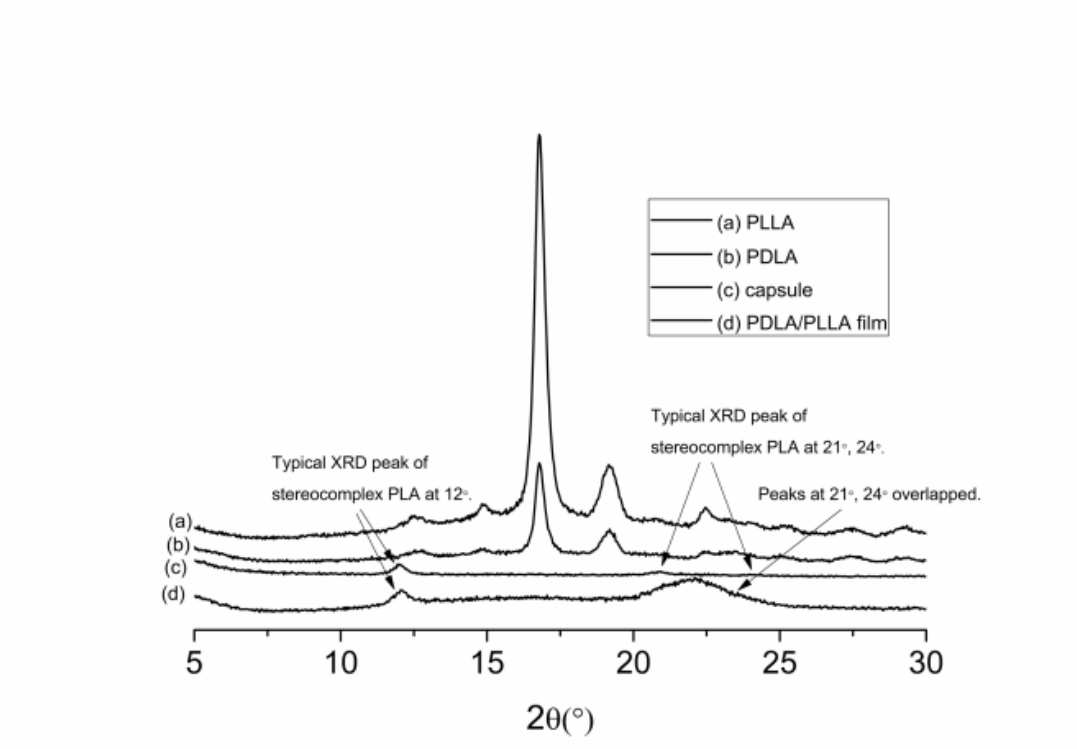

Figure 4.5 The XRD spectrums of (a) PLLA, (b) PDLA, (c) PDLA/PLLA stereocomplex capsules and (d) PDLA/PLLA stereocomplex film

Moreover, it is known that the melting point will shift to a higher degree once two enantiomeric polymers have formed their stereocomplex polymer due to the increased crystallinity. This is because the enantiomeric polymers attract each other with Van der Waals force, creating a more complementary and rigid structure which leads to a higher melting point.

In order to know whether the PDLA/PLLA complex had been formed after the PLA microcapsules were obtained, DSC was used to measure the melting points of four different samples (Figure 4.6). As described in literature, the melting points for PDLA and PLLA are approximately 170℃, which is very close to the melting points of the PLA polymers measured in our experiment[249]. The melting points for PDLA/PLLA stereocomplex films and microcapsules are 213.4℃ and 213.1℃, respectively. This result indicated that the PLA complex microcapsules had been obtained during the LbL process as the melting point of the PDLA/PLLA stereocomplex is at approximately 210-220 ℃[249].

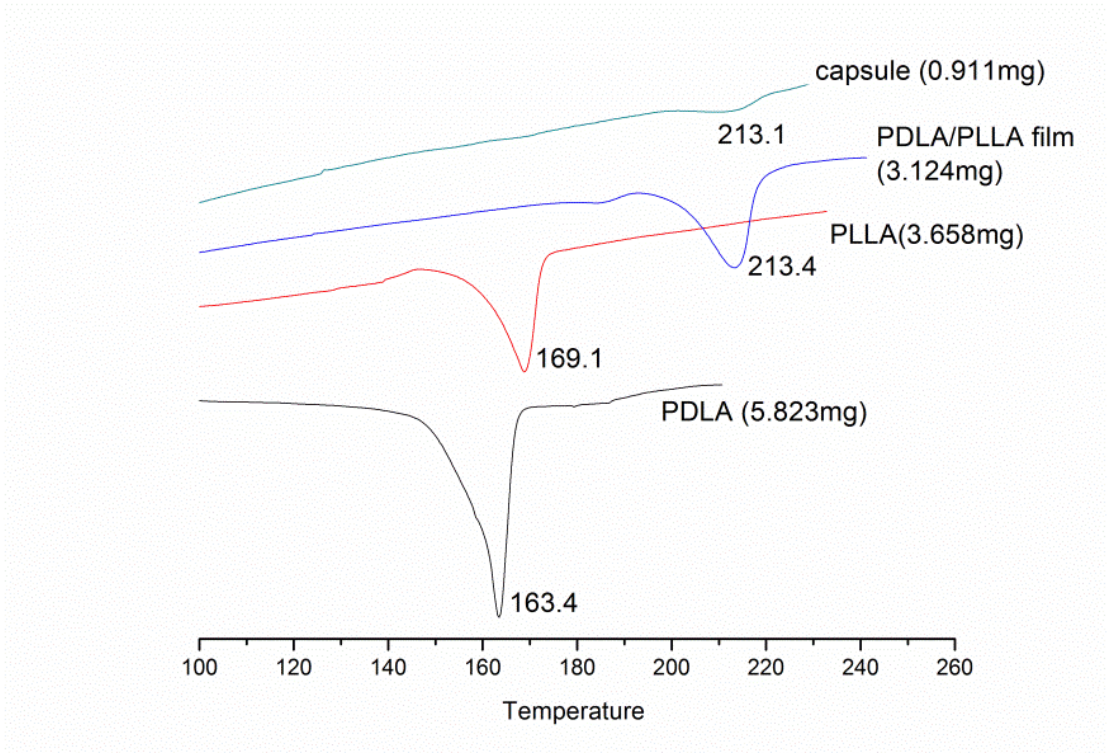

Figure 4.6 The DSC curves of PDLA, PLLA, PDLA/PLLA complex film and PDLA/PLLA complex microcapsules

The PDLA/PLLA stereocomplex formation was also monitored by ATR-FTIR. Figure 4.7 shows the PDLA/PLLA stereocomplex spectrum obtained by mixing 1:1 solutions at 45 ℃. As previously reported[251], the 1:1 blend of low molecular weight PLLA and PDLA solutions in acetonitrile is desired for the stereocomplex crystallite formation. The crystallization promotes the v(C=O) spectral band at 1748 cm^{-1}, clearly visible in Figure 4.7. Furthermore, two peaks at 909 and 1040 cm^{-1} can be identified, which are the characteristic bands of the PDLA/PLLA stereocomplex. C–O–C and C–C peaks were also visible at 1182 and 1209 cm^{-1}, respectively. Finally, bands at 2995 and 2944 cm^{-1} can be assigned to the CH_3- asymmetric stretching and CH_2- stretching, respectively, which confirmed the successful stereocomplex formation[147, 252]. In the case of PDLA/PLLA stereocomplex microcapsules, PDLA and PLLA were not mixed but rather adsorbed onto the PEM capsules by the LbL technique. Figure 4.7 shows the comparison between the spectrums of the PDLA/PLLA stereocomplex and the capsules with PDLA/PLLA stereocomplex as outer layers. The characteristic peaks of the stereocomplex were detected, confirming the successful LbL deposition of PLAs on the polyelectrolyte precursor.

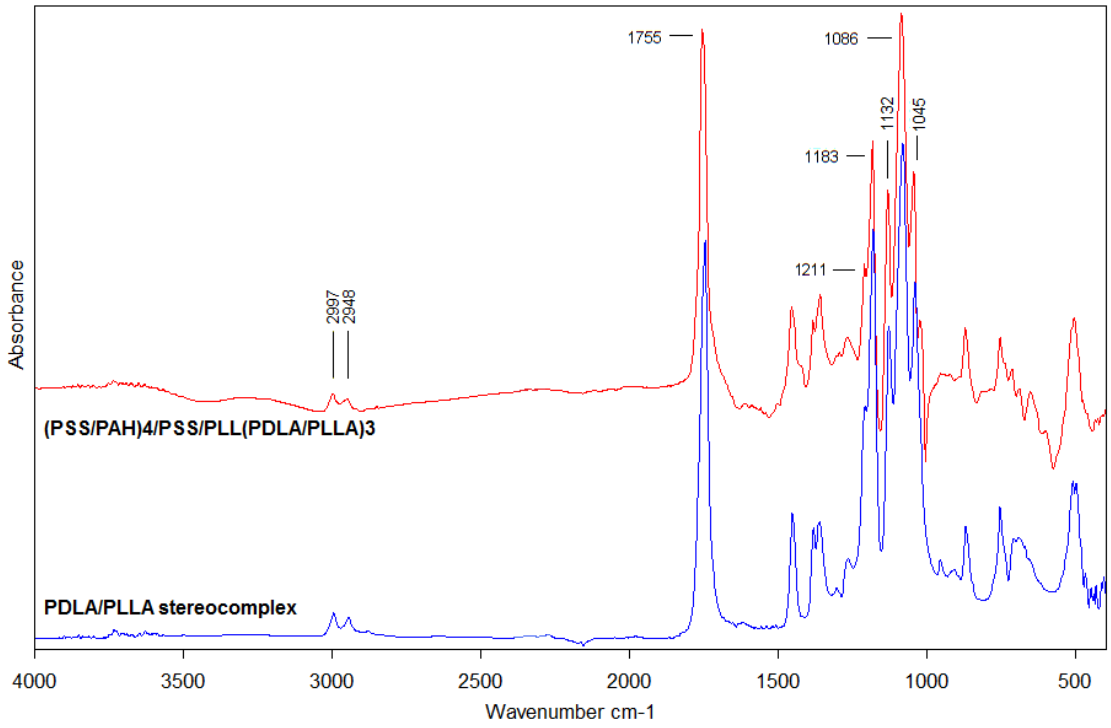

Figure 4.7 The FTIR spectrums of PDLA/PLLA stereocomplex film and PDLA/PLLA stereocomplex microcapsules

From the results of DSC, XRD as well as FTIR, it is clear that the PLA stereocomplex microcapsules were successfully fabricated in non-water medium through LbL technique.

4.3.2 Poly(lactic acid)s stereocomplex microcapsules with different number of layers

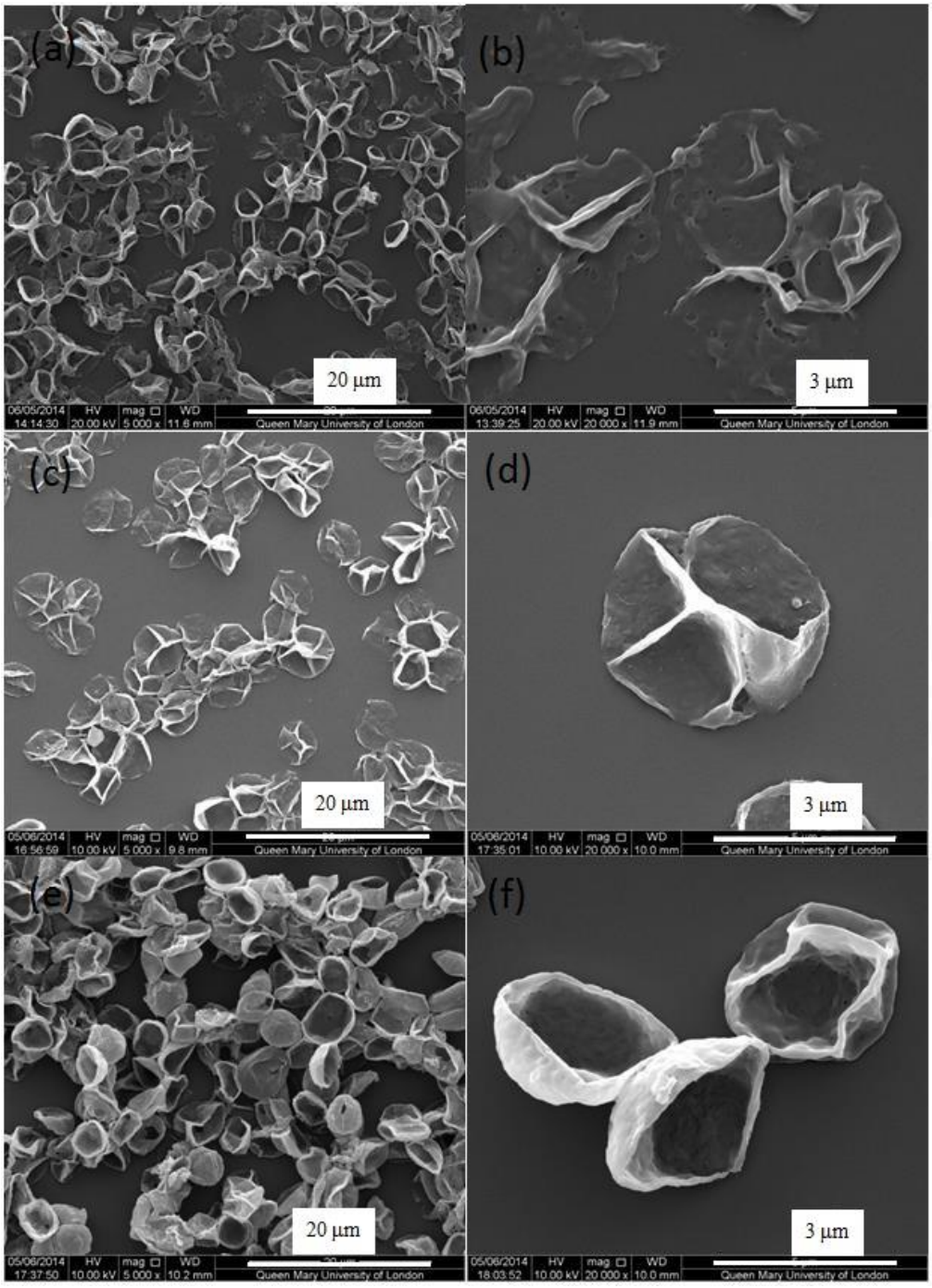

Figure 4.8 SEM images of PLA microcapsules with different layers: (a) (b) 10 layers, (c) (d) 20 layers, (e) (f) 30 layers.

The surface morphologies and inner structure, shell thicknesses of PLA stereocomplex capsules with different layers were observed by SEM and TEM,

respectively. In order to investigate the influence of different layer numbers, microcapsules with different multilayers were assembled. It is clearly shown in Figure 4.8 (a), (b) that 10 PLA layers were not enough to create an intact microcapsule structure as there were lots of defects on the surface as well as at the edges. Since these PLA microcapsules were assembled via weak Van der Waals force, which is less efficient than traditional electrostatic interactions between two oppositely charged polyelectrolytes in terms of the amount of adsorption and coverage[43], more polymer layers are required to build up structurally complete microcapsules. After the number of PLA multilayers increased to 20, a relatively intact capsule structure was obtained with few small holes appearing on the shell as shown in Figure 4.8 (c) and (d). This could also be found in the corresponding TEM images in Figure 4.9 (a), where some transparent defects were observed. Thus, microcapsules with 15 PDLA/PLLA bilayers were fabricated which are shown in Figure 4.8 (e), (f), where most of the microcapsules seem to be intact and defects cannot be seen in the corresponding TEM images (Figure 4.9 (c)), indicating that 15 PDLA/PLLA bilayers are enough to make structurally perfect PLA stereocomplex microcapsules.

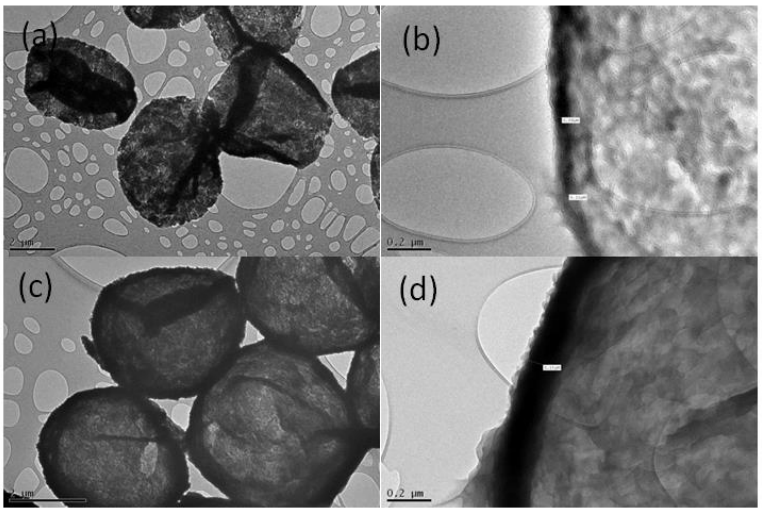

Figure 4.9 TEM images of PLA microcapsules with different layers: (a) (b) 20 layers, (c) (d) 30 layers.

Importantly, thicknesses of two batches of microcapsules were roughly measured under TEM. The reason why AFM was not applied to measure the thickness of these PLA microcapsules was because most of the 15 bilayers microcapsules were folded up whereas AFM requires the samples being detected to be even. As can be seen in Figure 4.9 (b) and (d), thicknesses of 10 bilayers and 15 bilayers PLA capsules are approximately 75 nm and 150 nm, respectively. Hence, the thickness of each PDLA/PLLA bilayer is estimated to be about 7.5-10 nm, which is very different from the thickness of PDLA/PLLA multilayers deposited on planar substrate. The reason for this is that $CaCO_3$ particles are quite porous and their surfaces are rough which enable them to adsorb more polymer molecules. In contrast, planar substrates are fairly smooth and thus are less able to adsorb polymer molecules.

It is worth mentioning that, different from normal polyelectrolyte microcapsules which have charge repulsion between microcapsules, PLA microcapsules do not carry any charges which makes them easier to form aggregations. Hence, 1 min sonication before each deposition step was applied in order to improve the dispersion of colloidal particles.

4.3.3 Effect of different ways of adsorption of PLA onto $CaCO_3$ template on the morpologies of PLA stereocomplex microcapsules

In order to achieve the best adsorption of polymer multilayers, it is extremely important to have a good attachment of the first polymer layer on the particle surface. Therefore, we studied the influence of different ways of adsorption of PLA onto $CaCO_3$ template on the formation of microcapsule. Due to the porosity and roughness of $CaCO_3$ particles, polymeric molecule could be adsorbed as the first layer via solely physisorption. Different from conventional LbL assembly that based on electrostatic interaction, PLA is a neutral polymer that carries no charges. Therefore, another

strategy of fabricating PLA multilayers on $CaCO_3$ particles is to use a "bridge" which can form interaction with both $CaCO_3$ particles and PLA polymers. Positively charged Polylysine was found to be a suitable candidate for this as it can deposit onto $CaCO_3$ particles because of the electrostatic interaction as well as forming polymer complex with PLA through Cation-Dipole interactions between the positive charge on the amino nitrogen atom of PLL and the lone pairs of the carbonyl oxygen atom of PDLA[43].

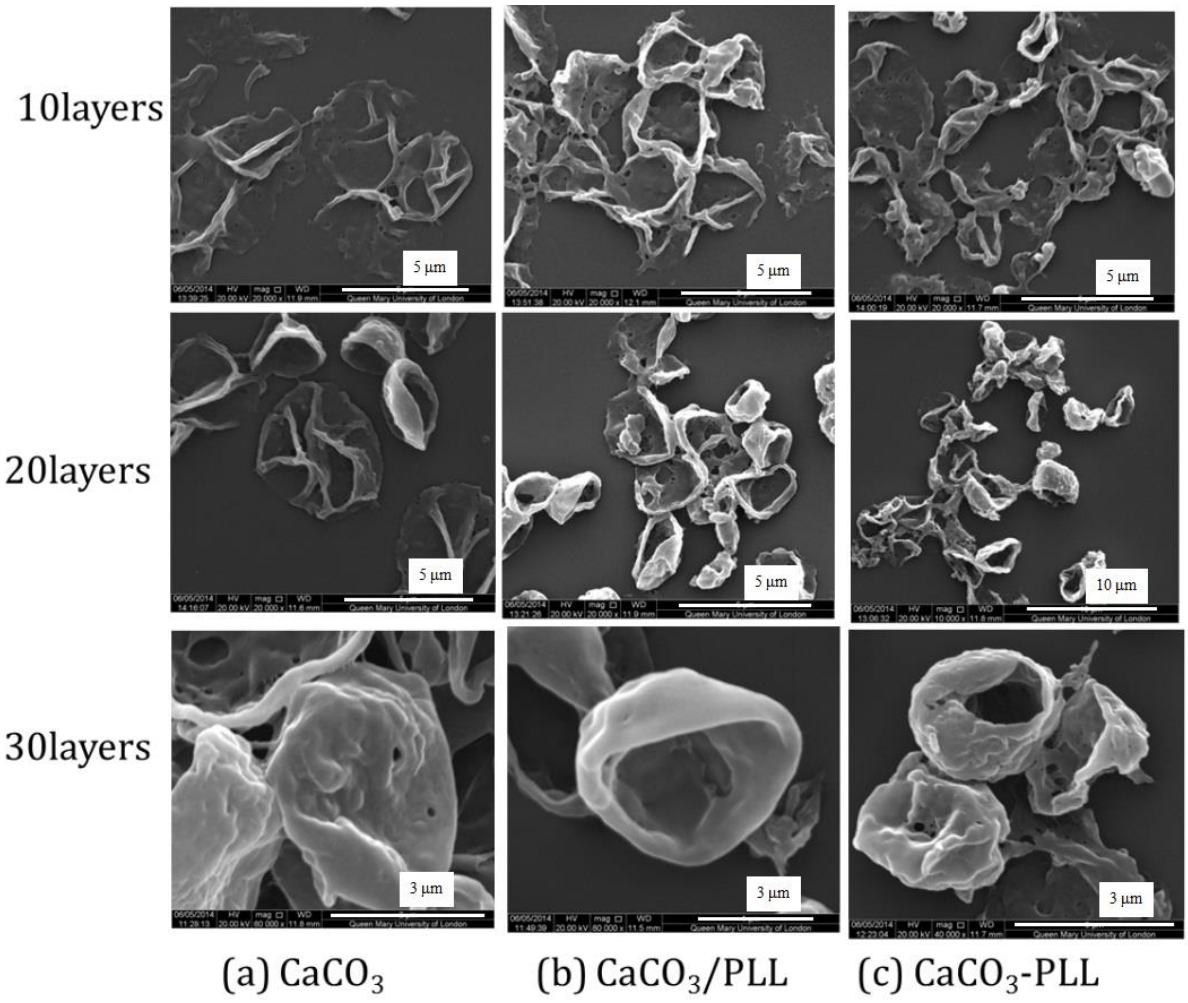

Figure 4.10 SEM images of PLL/(PDLA/PLLA) microcapsules assembled using different adsorption ways of first PLA layer , (a) (PDLA/PLLA) multilayers directly adsorbed onto $CaCO_3$ particles, (b) PLL adsorbed onto $CaCO_3$ particles as the first layer followed by

adsorption of (PDLA/PLLA) multilayers, (c) PLL co-precipitated in $CaCO_3$ particles before adsorption of (PDLA/PLLA) multilayers.

Here we used two ways to form $CaCO_3$ particle/PLL complex: direct deposition of polylysine onto $CaCO_3$ particle surface as well as co-precipitation of polylysine during the formation of $CaCO_3$ particles. Afterwards, PLLA/PDLA multilayers were then assembled onto these three different types of template particles, eventually leading to microcapsules that have different morphologies after certain amount of deposition circles. Results are shown in Figure 4.10. Unsurprisingly, PLA microcapsules without PLL layer have the poorest structural integrity. This is due to the weaker physisorption compared to electrostatic interaction, which makes $CaCO_3$ particles adsorb lesser amount of PLA molecules onto their surfaces. Deposition of PLL on $CaCO_3$ particles was found to be better than co-precipitation. This can be explained as higher and denser coverage of PLL on particle surface using direct deposition in comparison with co-precipitation of PLL which leads to a great number of PLL molecules being stored inside the particles other than on the surface.

4.3.4 Effect of different methods of template removal on morphology of microcapsules

It is known that the dissolution of $CaCO_3$ cores would cause high osmotic pressure due to the generation of CO_2 which may rupture microcapsules. For most polyelectrolyte microcapsules that have very porous structure, the gas could release easily without breaking the walls of microcapsules. However, PLA microcapsules tend to have more rigid and less porous structure due to the rearrangement of the polymeric chains during the formation of stereocomplex of PLLA and PDLA. Thus, adding EDTA solution directly into PLA microcapsules may result in capsule walls being broken by the CO_2 gas. We considered a milder way to remove the $CaCO_3$

templates which is dialysis of microcapsule dispersion against EDTA solution. The slow diffusion of EDTA into the dialysis bag, which contains microcapsules, would significantly reduce the speed of CO_2 generation.

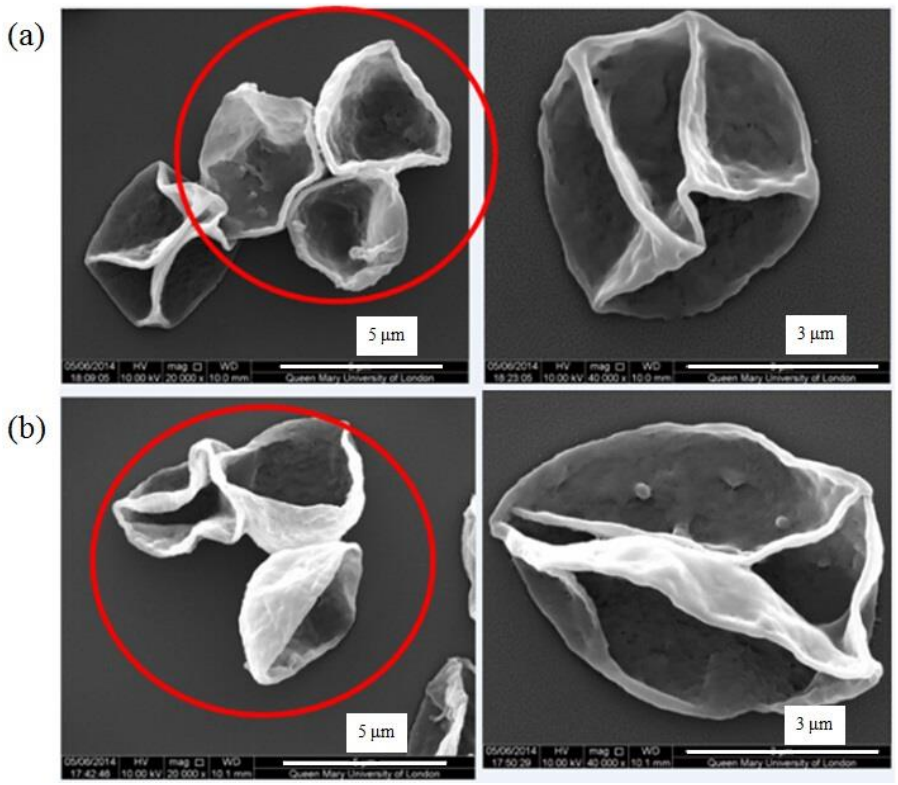

Figure 4.11 SEM images of PLL/$(PDLA/PLLA)_{15}$ microcapsules obtained after template removal by (a) 0.2 M EDTA solution, (b) dialysis of microparticle dispersion against 0.2 EDTA solution for 3 days.

Therefore, both two ways of template removal were studied and the morphologies of the obtained PLA microcapsules were imaged by SEM for comparison. Figure 4.11 (a) are SEM images of the microcapsules obtained by dissolving the template with lower concentration of EDTA (0.2 M concentration) whilst figure 4.11 (b) is SEM images of the microcapsules obtained by using dialysis method (against 0.2 M EDTA solution for 3 days) to remove $CaCO_3$ templates. Both batches of microcapsules seemed to be structurally intact. However, some small holes were randomly found on the microcapsules obtained by the direct dissolution method whereas no such defects

were observed on their counterparts resulting from dialysis dissolution method. Thus, a mild way of template removal would be preferred for the preparation of PLA stereocomplex microcapsules.

4.3.5 Effect of heat treatment on morphology of microcapsules

Heat treatment is well-known to be effective in reducing the permeability of polymeric microcapsules[67]. When the temperature is above the glass transition temperature (T_g), the polymer chains start to move and rearrange. They may move to the defective area and thus heal it. When the heat treatment is finished and temperature cools down, these polymer chains will remain in the position and thus form more intact and rigid structure.

As the T_g of stereocomplex PLA is between 65-70 ℃, the heating treatment was carried out at 75 ℃ overnight in this experiment followed by gradually cooling down in ambient temperature. PLL/(PLLA/PDLA)$_{10}$ microcapsules were used here as they had defective structure which might be improved after heat treatment compared to PLL/(PLLA/PDLA)$_{15}$ microcapsules that already had intact morphologies before heat treatment.

As expected, SEM images in Figure 4.12 showed significant improvement in the integrity of microcapsules. These PLL/(PLLA/PDLA)$_{10}$ had quite a lot of broken edges before being heated whereas after heat treatment microcapsules became completely intact without any obvious defects, meaning the defective areas have been filled. The reason why the capsules become more intact at elevated temperature is because once the temperature is above T_g, polymer chains start to rearrange and move to the less compact area. After enough time, the chain rearrangement will end, forming a more rigid structure than before. This encouraging result demonstrated the

possibility of using heat treatment to reduce the permeability of PLA microcapsules and thus increase their loading and retention capacity.

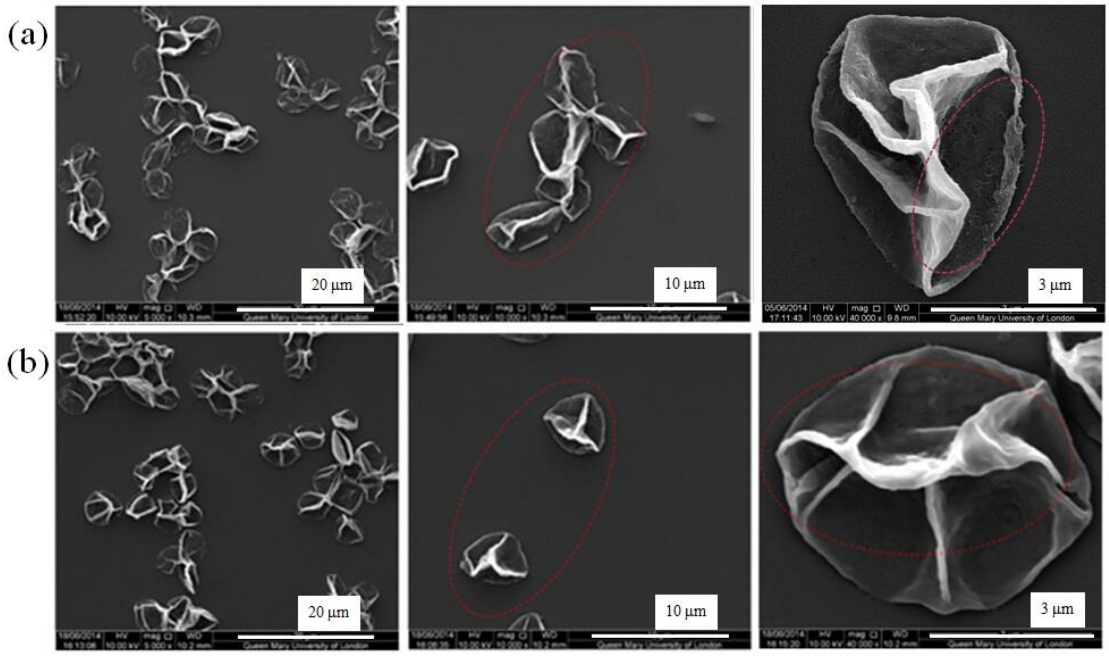

Figure 4.12 SEM images of PLL/(PDLA/PLLA)$_{10}$ microcapsules, (a) before and (b) after heat treatment at 75 ℃

4.4 Loading of dye labelled molecules into PLA stereocomplex microcapsules using heat treatment

After having shown a positive effect of heat treatment on improving the integrity of the PLA microcapsule structure, fluorescent molecules were used to be loaded into these microcapsules. Three kinds of fluorescent dyes were chosen for this encapsulation experiment, which were rhodamine B and two fluorescein isothiocyanate-dextrans (FITC-dextrans) with molecular weight (Mw) of 4400 and 65,000~85,000 respectively.

As a control, the permeability of PLL/(PLLA/PDLA)$_{15}$ microcapsules without heat treatment was first examined. This was accomplished by incubating the microcapsules

in each dye solution for 3 hours and then washing with water for 3 times to remove the excess dye molecules. The resulting dye loaded microcapsules were observed under CLSM. It can be seen in Figure 4.13 that only FITC-dextran with Mw 65000~85000 could be encapsulated into the microcapsules without heat treatment which indicates these PLA microcapsules have similar permeability and retention capability with common polyelectrolyte microcapsules.

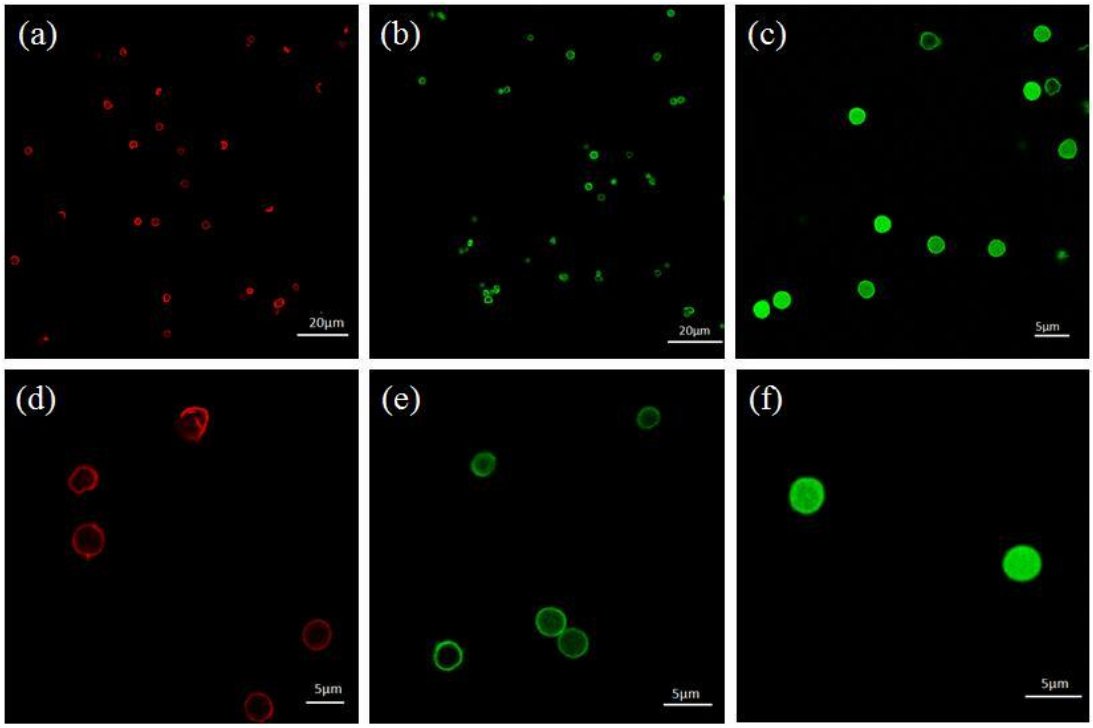

Figure 4.13 CLSM images of PLA stereocomplex microcapsules encapsulated with: (a), (d) RhB, (b), (e) FITC-dextran with MW 4400, (c), (f) FITC-dextran with MW 65,000-85,000 without heat treatment.

The heat treatment of microcapsules was then carried out again at 75 ℃. The microcapsules were incubated in each dye solution at room temperature for 3 hours and then kept at 75 ℃ in an oven overnight before being washed with water. The CLSM images in Figure 4.14 shows that after heat treatment at 75 ℃ two FITC-dextrans with different molecular weights could be encapsulated in the microcapsules,

demonstrating a remarkable reduction in permeability and increase in retention capability of PLA microcapsules. However, small molecular dye still could not be retained within the microcapsules after intensive wash with water. This result indicates that heat treatment of PLA microcapsules at a temperature above its T_g would significantly improve their permeability, making them an excellent choice as microcarriers for medium sized molecules. However, the shell structure may not be compact enough to retain the small molecules even after heat treatment.

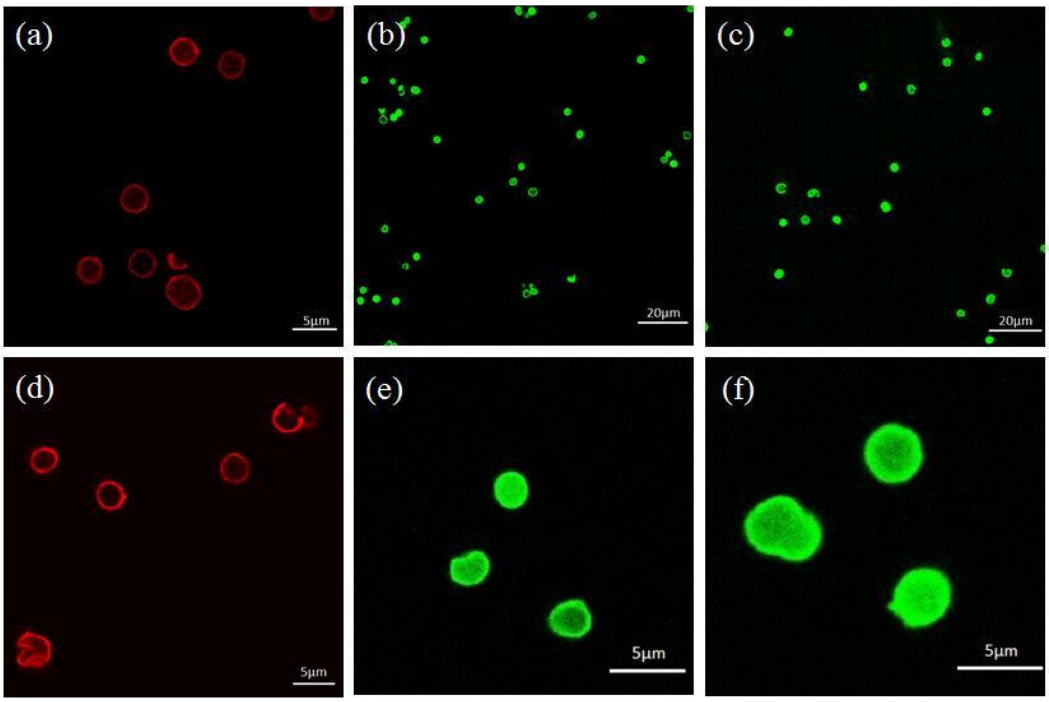

Figure 4.14 CLSM images of PLA stereocomplex microcapsules encapsulated with: (a), (d) RhB, (b), (e) FITC-dextran with MW 4400, (c), (f) FITC-dextran with MW 65,000-85,000 after heat treatment at 75 ℃.

4.5 **Conclusion**

PLA stereocomplex microcapsules were successfully fabricated by Layer-by-Layer technique using $CaCO_3$ and enantiomeric poly(lactic aicd)s as template and shell materials, respectively. PSS/PAH polyelectrolytes precursor has no effect on the

growth of PLA stereocomplex layers. The results of DSC, XRD as well as FTIR showed that the stereocomplex microcapsules were formed between two types of enantiomeric PLAs through van der Waals interactions. Compared with the microcapsule assembled through electrostatic interaction, more polymer layers and milder removal conditions of templates are needed in order to obtain intact microcapsules. At first, it was expected that PLA stereocomplex coating would be able to prevent EDTA from penetrating into the microparticles as PLA is hydrophobic. However, $CaCO_3$ cores were dissolved by EDTA. We suspect that the PLA coating still had some invisible defects from which EDTA could get into the shell. Unlike common polyelectrolytes, it takes much longer time for PLAs to form the stereocomplex multilayers through LbL process and requires stricter conditions for the deposition such as specific deposition temperature range. All these restrictions may lead to the imperfect structure of the PLA coatings, making them defective. Encouragingly, heat treatment at above glass transition temperature significantly enhanced the encapsulation ability of PLA microcapsules. This is because at higher temperature polymer molecules rearrange within the shell and eliminated the existing defects which results in the microcapsules being able to retain molecules that they could not trap before heat treatment.

5 Low permeable Poly(methyl methacrylate) shell grown from macroinitiator deposited inorganic templates via surface-initiated polymerization

The encapsulation and delivery of small molecules are of great importance. However, in spite of the efforts that have been made, the low permeability of microcarriers remains a major challenge. Due to the nature of polymers, microcarriers made of polymers are usually porous and water penetrable, which lead to the failure of retaining small molecules and narrows the applications of the micro polymeric containers. For example, micelles, which contain hydrophilic polymer chains around hydrophobic cores, are very likely to attract water molecules[253]. Previous work shows drug cargos trapped in the micelles assembled from amphiphilic polymers release in a linear pattern, suggesting that the micelle structure barely has the ability to prevent the rapid diffusion of small drugs[254]. Additionally, microcapsules made by Layer-by-Layer (LbL) technique usually carry charges and comprise hydrophilic polyelectrolytes, which again make them easy to be penetrated by surrounding water and loaded cargo molecules. One can deduce that hydrophilicity of the constituent polymer together with the charge groups some polymers bear are the major factors that lead to the failure of polymeric carriers in retaining small molecules. Thus, a non-charged hydrophobic shell is desired.

A popular way to fabricate such a shell is to generate a hydrophobic layer out of the pre-fabricated scaffold, such as polyelectrolytes multilayers and lipids. Some low permeable lipids covered with inorganic-organic hybrid particles have been manufactured by different groups using this process[122, 255, 256]. However, these

methods have disadvantages such as low stability and limited options of shell materials. Another emerging way is using surface initiated polymerization (SIP), typically Atom Transfer Radical Polymerization (ATRP), on particles that are pre-deposited with initiators.

Some mono initiator layers such as silane initiator are chosen to bind to the surface before growing the polymer brushes[257]. However, more initiators are required in order to get thicker polymer brush layers. Consequently, some copolymers which have a polyelectrolyte part that can adsorb onto the surface and a macroinitiator part that can initialize ATRP polymerization were developed[185, 258]. This enables researchers to create polymer layers with ideal thicknesses by adjusting the number of macroinitiator layers as well as the polymerization time. By tuning the thicknesses of the polymeric shells, one can control the permeability. Unlike polymer brushes that are generated from silane initiators and could possibly dissociate upon swelling caused by external stimulus, polymer brushes that are grafted from macroinitiator containing polyelectrolyte multilayers. They are more stable to swelling due to the stronger binding between polymer brushes and PEMs.

In comparison with other processes aforementioned that are used to fabricate composite shells, the shell made by polymer brush growth technique has active initiators remained on the surface which can be made use of to further propagate different functional polymer chains for various applications, such as specific binding and targeted delivery.

Many types of monomers have been synthesized into hydrophobic polymer brushes. For instance, Poly(methyl methacrylate), which has been widely used for biomedical applications due to its excellent biocompatibility, relatively low cost as well as

abundant sources[259-264], is suitable for our work. Moreover, PMMA shows hydrophobicity as there are no hydrophilic groups in its structure which makes it a competent choice for the purpose of growing charge-free polymer shells.

The aim of this work is to fabricate microparticles with low permeable shell as well as readily tunable shell thickness. Here, we explore the idea of combining LbL and SI-ATRP techniques for this purpose as LbL deposition could provide a tailored macroinitiator containing precursor, which leads to a polymer brush layer with optimized thickness after SI-ATRP process. We will study the kinetics of PMMA growth on macroinitiators containing polyelectrolytes pre-coated flat substrate with ellipsometer and then grow PMMA brush shell from the surface of macroinitiator covered $CaCO_3$ microparticles. Water contact angles are measured to compare the hydrophobicity of the surfaces with different coatings. The chemical composition of the obtained particles after polymerization and EDTA treatment is investigated by FTIR. The relationship between controlled shell thickness and permeability is also studied under electronic microscopes including SEM and TEM.

5.1 Synthesis of PMMA brushes on planar substrate and silica particles

Since any of the chemicals involved in ATRP could significantly change the speed of the reaction, a proper recipe should be ensured before growing PMMA brush from macroinitiators. Thereby, we first synthesized PMMA brush layer on silane initiator deposited silicon substrate and silica particles as there has similar research been done with which our results could be compared.

5.1.1 Kinetics of PMMA growth on planar substrate

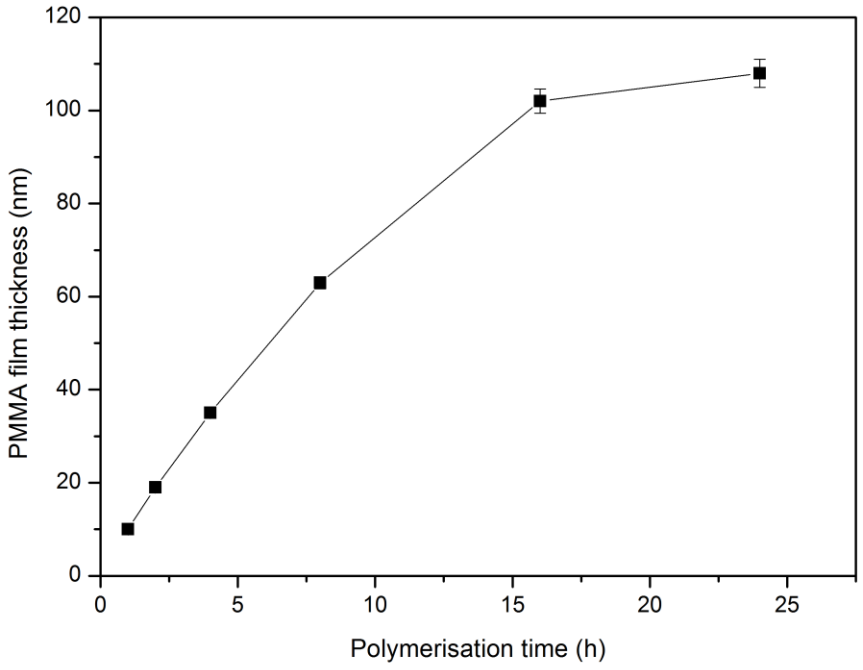

Figure 5.1 Kinetics of the growth of PMMA brush on silicon substrate

In order to perform well controlled polymerization, it is necessary to study the kinetics of PMMA growth on planar substrate before applying onto the particles. The polymerization time can be tuned to precisely control the thickness of polymer brushes as ATRP provides a more constant speed of polymer chain growth.

It is worth noting that although previous study showed that polymerization of MMA was conducted in the presence of inhibitors in the monomer[265], we found that monomers that contained inhibitors did not polymerize at all. Thus, the inhibitors were always removed prior to the polymerization by passing them through an Al_2O_3 column.

Figure 5.1 shows the kinetics of PMMA growth on silicon substrate, on which silane initiators has pre-assembled. The reaction was carried out for a duration of 24 hours and 6 time points were analysed. The kinetics plot shows an almost linear growth pattern as a function of reaction time at the first 16 hours due to the fact that only a small number of monomers were polymerized and that the polymer brush had limited steric repulsion, which resulted in a steady polymerization speed. However, the growth plateaued and slowed down after a certain period of time. These results are in accordance with those in previous study[266], demonstrating that our polymerization procedure was well managed and the parameters are suitable for the later reactions.

5.1.2 Synthesis and morphologies of PMMA coated silica particles

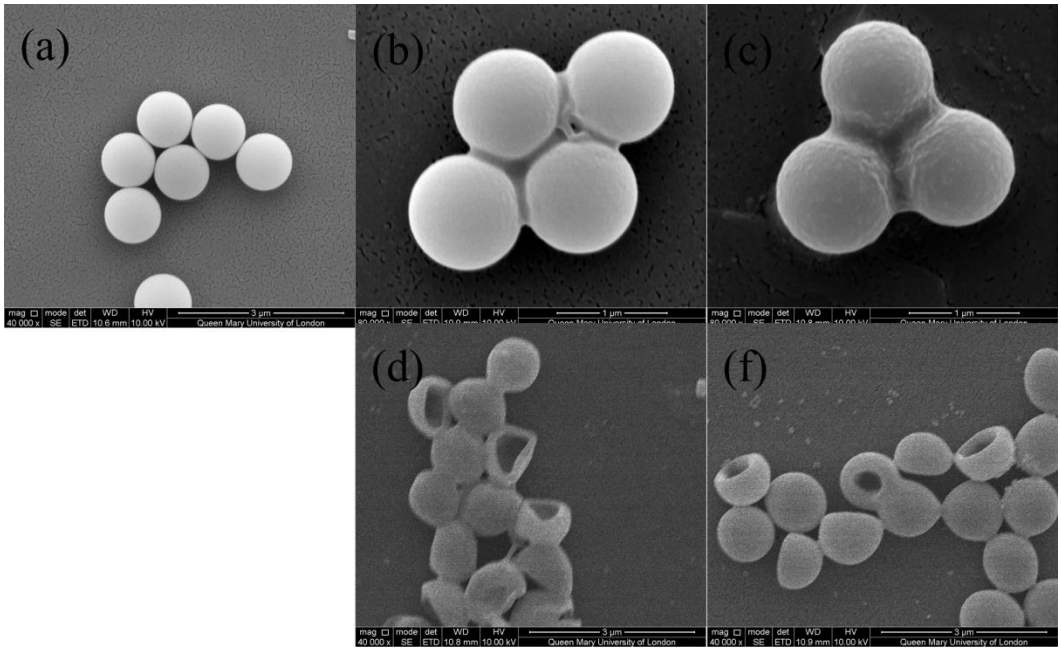

Figure 5.2 SEM images of (a) silica particles, (b) silica particles with PMMA brushes grown for 8 h, (c) silica particles with PMMA brushes grown for 24 h, (d) PMMA capsules of sample (b) after HF treatment, (f) PMMA capsules of sample (c) after HF treatment

After the kinetics of PMMA growth was studied on planar substrate, the polymerization was performed on the silica particles to generate the PMMA shell. As can be seen in Figure 5.2 (b) (c), polymer shells were formed after polymerization of

8 and 24 hours, with the 24 hours sample having obviously thicker outer layer. This was further proven by the samples of PMMA capsules after core removal, which is shown in Figure 5.2 (d) (f). Hollow capsules obtained after 8 hours of polymerization already had capsule shape whilst after 24 hours, the capsules showed fairly thick "bow-like" structure. The results indicate that the polymerization progressed well on silica particles over the entire period of polymerization.

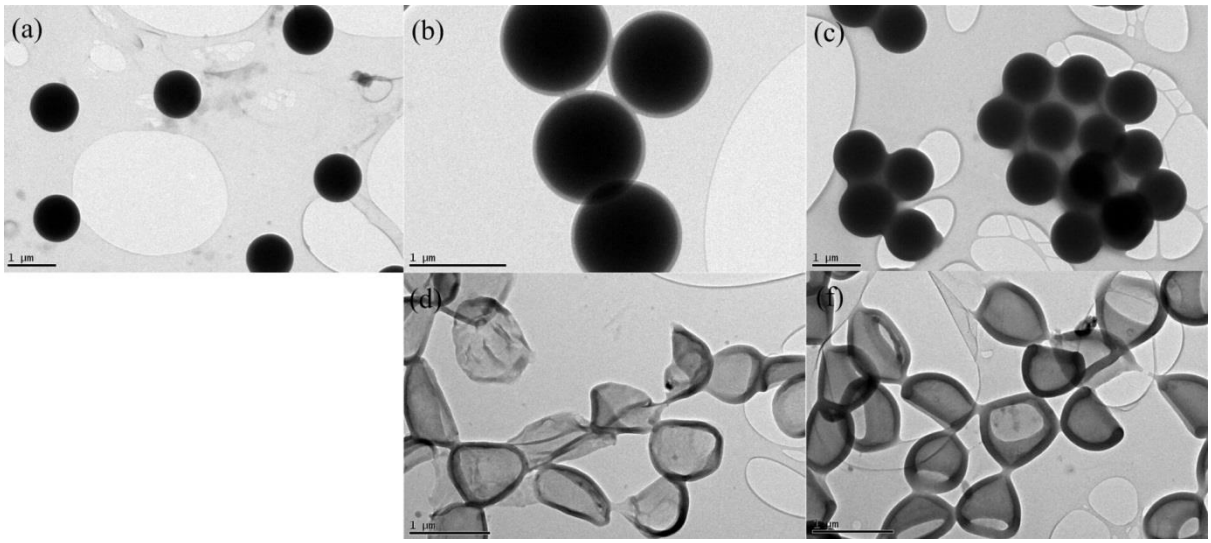

Figure 5.3 TEM images of (a) silica particles, (b) silica particles with PMMA brushes grown for 8 h, (c) silica particles with PMMA brushes grown for 24 h, (d) PMMA capsules of sample (b) after HF treatment, (f) PMMA capsules of sample (c) after HF treatment

TEM was also applied to further observe the internal structure of particles and PMMA capsules, Similarly in TEM images (Figure 5.3 (b) (c)), polymer shells were seen on silica particles after polymerization. Figure 5.3 (e) (f) show capsules obtained after 8 hours seemed to have some small defects and broken parts whereas those yielded after 24 hours have completely intact structures. These results demonstrate that structurally intact PMMA capsules can be obtained using "brush growth" technique after 24 hours of controlled ATRP from initiator covering particles.

5.2 Fabrication of PMMA coated microparticles with reduced permeability from macroinitiator

5.2.1 Synthesis of macroinitiator for ATRP

For polymer brush grown from mono silane initiator, the only way to tune its thickness is to change the duration of polymerization, which is very limited in terms of getting thicker polymer brush. Thus, a novel way to grow thicker polymer brush layer and tune its thickness more flexibly is to use macroinitiator, which can be stacked up through LbL assembly. By using macroinitiator multilayers precursor, one can easily obtain polymer brush layer with ideal thickness[8].

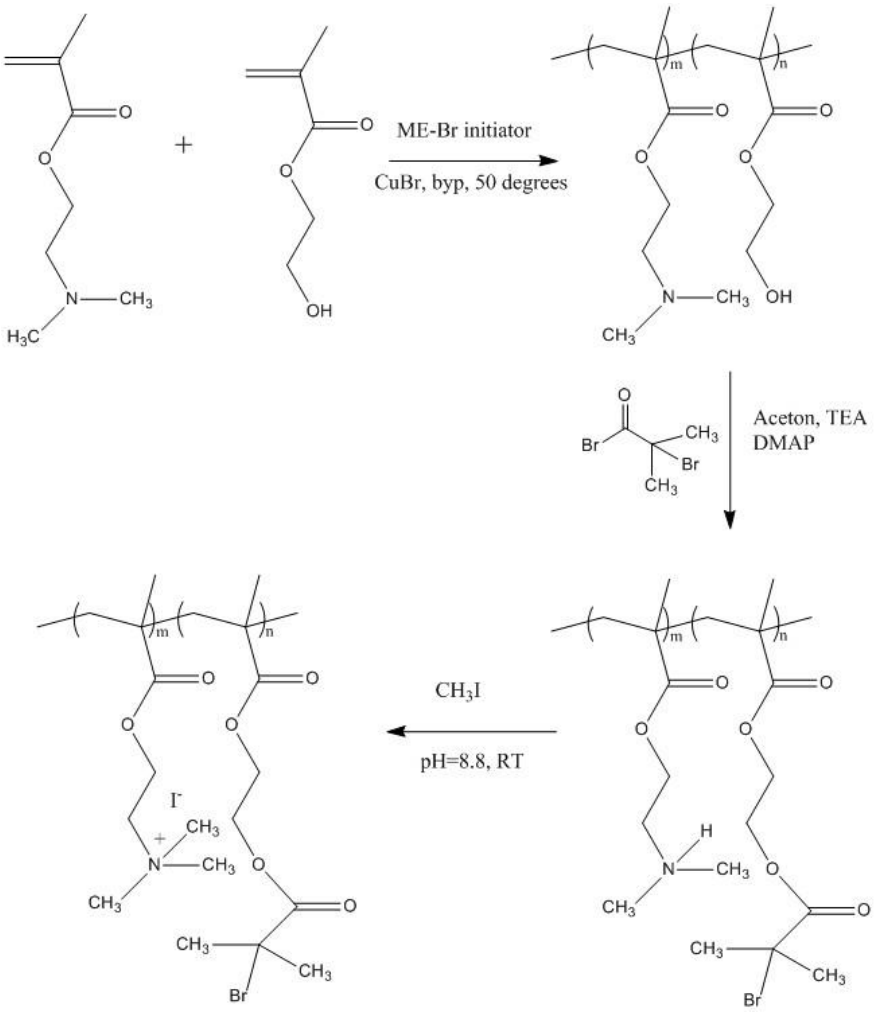

Figure 5.4 Synthesis route of macroinitiator for ATRP

The macroinitiator was synthesized via a three-step reaction process as described in Figure 5.4. In order to confirm the success of each step, NMR was applied to characterize the chemical composition of the purified products after each step. The NMR spectrum is shown in Figure 5.5. Peak (a), (b) and (c) belong to the $-CH_2$ and $-CH_3$ on the PDMAEMA part, respectively whereas peak (d), (e) are attributed to the $-CH_2$ groups on the PHEMA chains. Peak (a) (b) (c) shifted to (f) (g) (h) after esterification and further moved to (i) (j) after the copolymer being quaternized with methyl iodide, which was in agreement with the previous results[233].

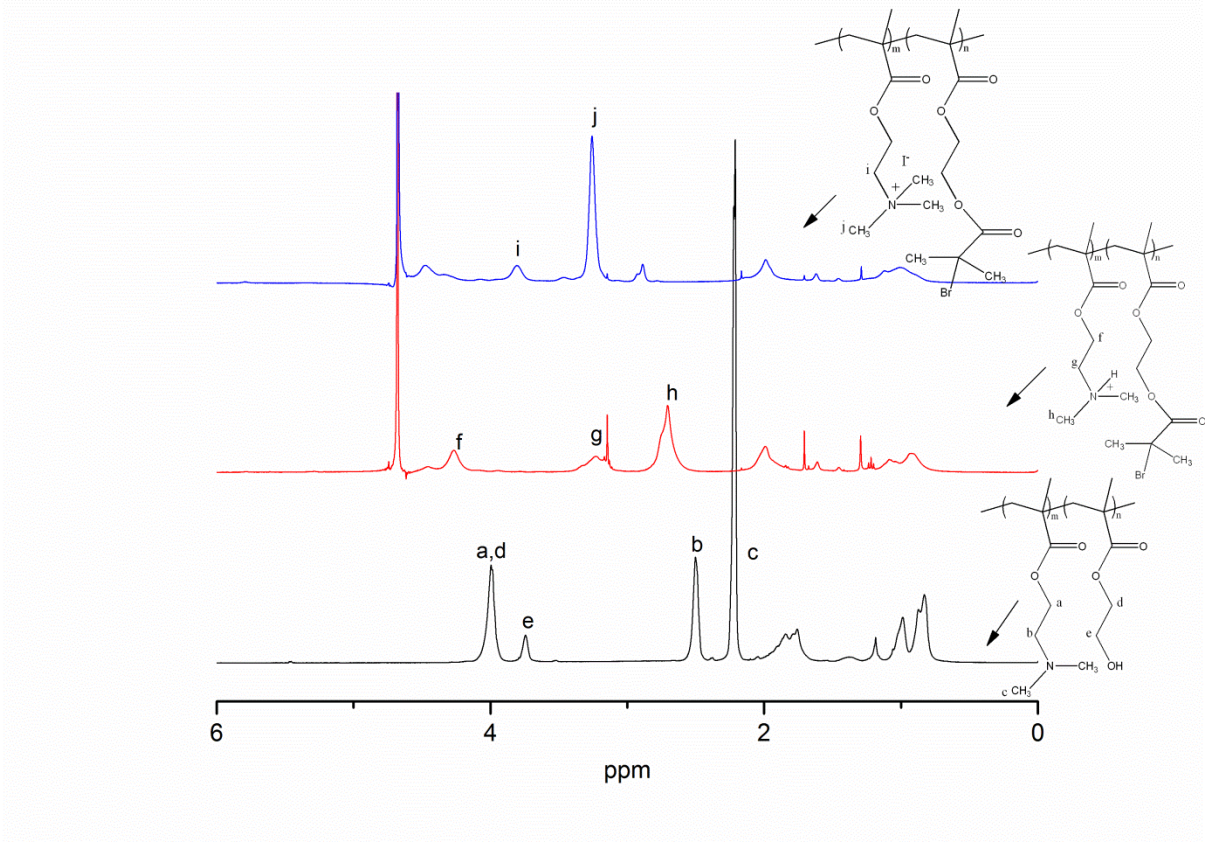

Figure 5.5 NMR spectrums of macroinitiators: (a) copolymer of HEMA and DMAEMA, (b) copolymer after grafting ATRP initiator, (c) copolymer after esterification and quaternization. Deuterated chloroform and deuterium oxide were used as solvents for (a) and (b), (c), respectively.

	Molecular Weight	PDI
Step 1 Copolymerization	22,400	1.77
Step 2 Esterification	23,200	1.51
Step 3 Quaternization	25,600	1.75

Table 5.1 Molecular weights and distributions of synthesized macroinitiator after each step.

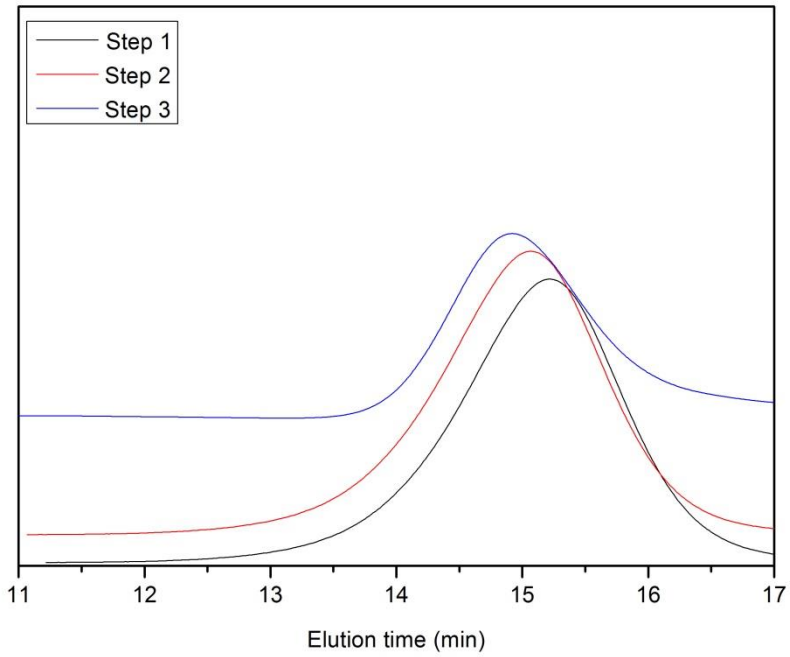

Figure 5.6 GPC curves of synthesized macroinitiator, step 1: Poly(DMAEMA-*co*-HEMA), step 2: initiators grafted Poly(DMAEMA-*co*-HEMA), step 3: Poly(DMAEMA-*co*-HEMA) after grafting initiator and quaternization.

The molecular weights and distributions of copolymers after each step were characterized by GPC. Table 1 shows the molecular weights of copolymers at three sequential steps, from which it is obvious that the molecular weights of the copolymers increased after each modification reaction from 22401 to 25581 as functional groups were grafted onto the polymer chains. The relatively low PDI

values and the mono peaks in the GPC curves (Figure 5.6) indicated that the molecular distributions are narrow and the copolymerization had been well controlled. Therefore, we used this macroinitiator for the synthesis of polymer brushes.

5.2.2 Fabrication and kinetics study of PMMA brushes from planar substrate

Before synthesizing the polymer shell on microparticles, we first studied kinetics of PMMA growth on planar substrates and compared the hydrophobicity of surfaces with different coatings. The general idea is illustrated in Figure 5.7. Macroinitiator containing multilayers are deposited on surfaces before the formation of PMMA layer through ATRP process.

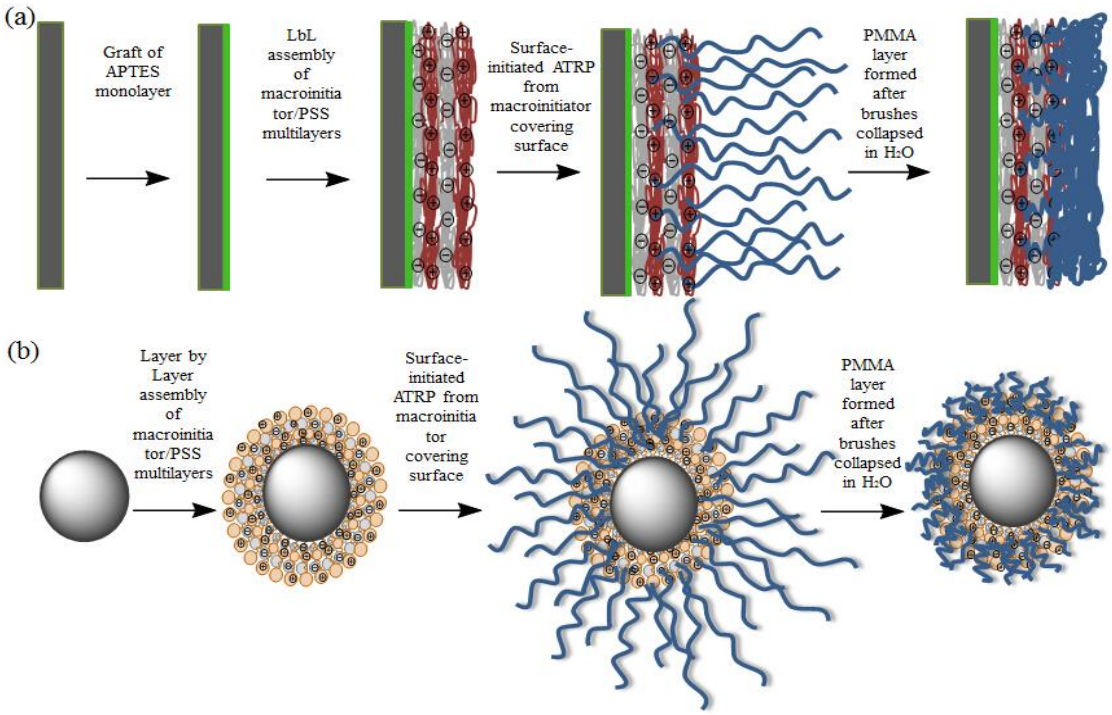

Figure 5.7 Schematic illustrations of (a) growth of PMMA brush from macroinitiator multilayers on planar substrate and (b) synthesis of PMMA low permeable macroparticles from macroinitiator multilayers covering inorganic cores.

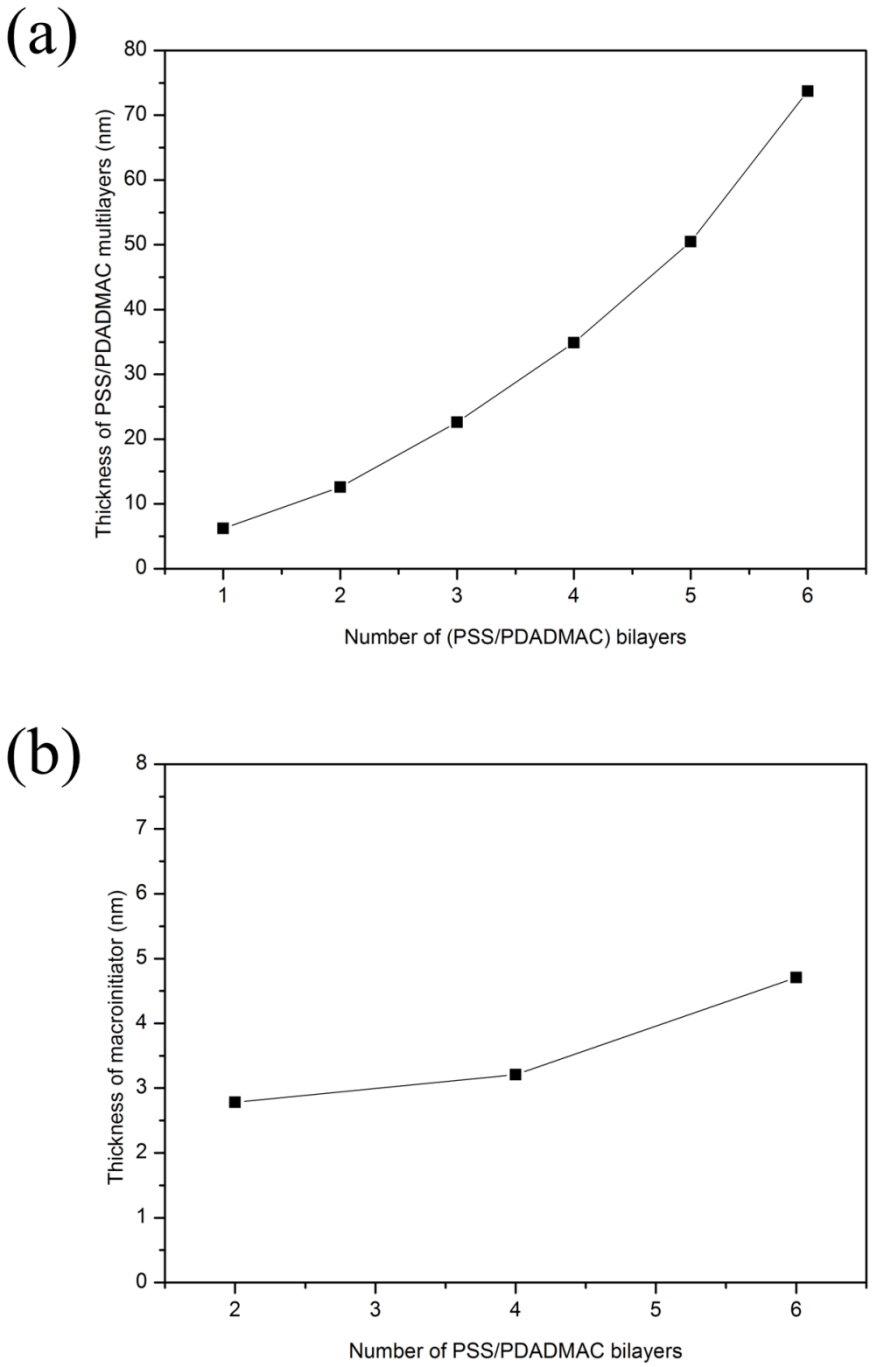

Figure 5.8 (a) Kinetics of growth, (b) thickness of macroinitiator deposited after certain number of PSS/PDADMAC multilayers.

A relatively thick and dense coverage of initiator is required for growing polymeric layer on substrate surface. As a result, macroinitiator containing multilayers were deposited onto the substrates via LbL process prior to the growth of PMMA brush

layer. There generally are two strategies to prepare these polyelectrolyte multilayers. One is, straightforwardly, deposition of (PSS/macroinitiator) multilayers while the other one is deposition of macroinitiator monolayer on exponentially grown polyelectrolyte multilayers. To be specified, here we used (PSS/PDADMAC) multilayers precursor. Previously study showed that when macroinitiator is deposited on (PSS/PDADMAC) multilayers, its thicknesses also increased exponentially as a function of the (PSS/PDADMAC) layer number[267]. This could potentially help us obtain thick macroinitiator layer from just one layer. Thus, two strategies were both carried out and the thicknesses of these multilayers were measured with ellipsometry. Figure 5.8 (a), (b) shows the kinetics of (PSS/PDADMAC) multilayers growth and thicknesses of macroinitiator on different number of (PSS/PDADMAC) multilayers, respectively. The exponential growth of the multilayers was observed, however, the thicknesses of macroinitiator from different multilayer precursor were all very thin which is different from the previous work. A possible explanation would be that the macroinitiators used in our work is different from that in literature which affected the growth. On the other hand, it can be seen from Figure 5.9 (a) that the thicknesses of (PSS/macroinitiator) multilayers are proportional to the number of macroinitiator layers, showing a nicely controlled polyelectrolytes deposition process. The average thickness of each PSS/MI bilayer was approximately 2.51 nm. Consequently, the PSS/MI multilayer precursor contains more initiator and thus was used for the growth of PMMA layer.

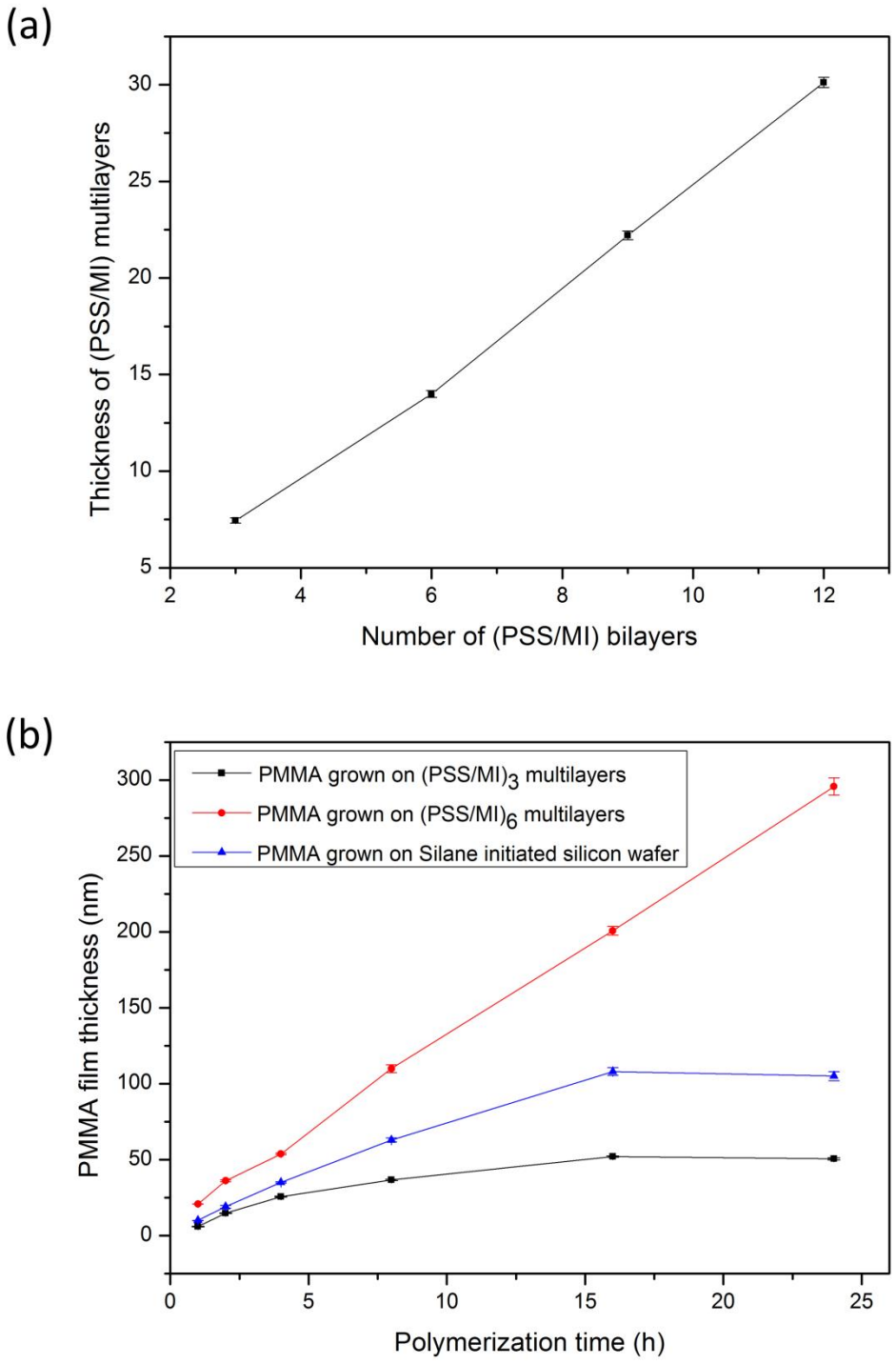

Figure 5.9 Kinetics of (a) Macroinitiator contained polyelectrolyte multilayers growth, (b) PMMA growth on different depositions of initiators.

Before synthesizing the polymer shell from the particle surfaces, the kinetics of polymer growth should be well studied. In order to grow polymer shell with ideal

thickness, it is essential to study the kinetics of the PMMA growth on certain amount of macroinitiators on flat substrate before grafting polymer brush layer from colloidal templates. After the deposition of silane initiator and macroinitiators on silicon substrates, the polymerizations of methyl methacrylate were carried out within a predetermined duration and samples were taken out at certain points of the reaction. As can be seen in Figure 5.9 (b), the thicknesses of PMMA film grown from silane initiators increased at a relatively stable speed before it slowed down after 16 hours and kept nearly unchanged until ending time, which was in correspondence with the results in literature[266], indicating that our procedure was well managed. The PMMA brush grew at a similar speed from $(PSS/macroinitiator)_3$ precursor in spite of having more initiator layers. Although rough surface of polyelectrolytes multilayers would possibly adsorb more initiator molecules in each layer, the amount of initiator in $(PSS/macroinitiator)_3$ is still not more than that in silane monolayer in overall. The main reason is that only about 20% of the macroinitiator chains have initiating sites with the rest majority of the chains being solely polyelectrolytes that are used for Layer-by-Layer assembly. The PMMA brushes grew much faster from $(PSS/macroinitiator)_6$ precursor with the thickness of it almost as much as three times that from silane monolayer and $(PSS/macroinitiator)_3$ multilayers. At the initial stage of (PSS/macroinitiator) precursor deposition, the attachment of polyelectrolytes on the substrate was relatively poor and during this time there might also be some areas on the substrate with no coverage of polyelectrolytes. As the deposition of polyelectrolytes goes on, the substrate is fully coated and each macroinitiator will have denser coverage and slightly more initiator molecules which results in greater grafting efficiency of $(PSS/macroinitiator)_6$ precursor in the same timescale.

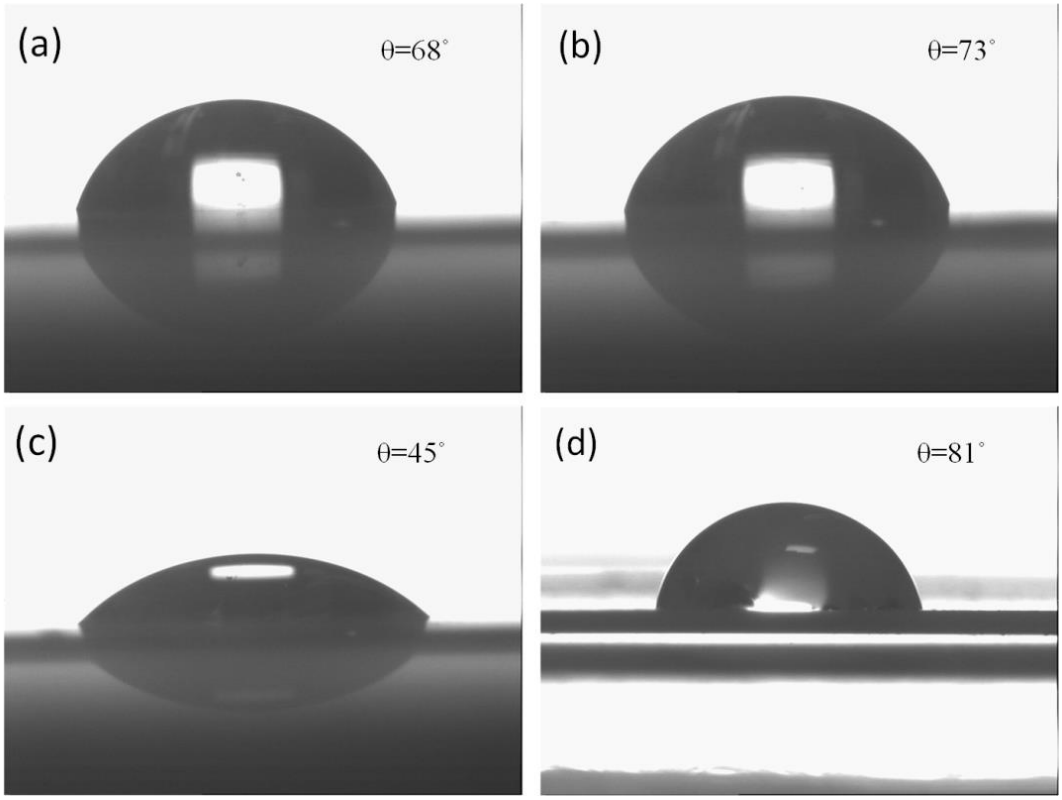

Figure 5.10 Water droplets on surfaces of (a) silicon wafer, (b) silicon wafer/APTES, (c) silicon wafer/APTES/$(PSS/MI)_6$ (d) silicon wafer/APTES/$(PSS/MI)_6$/PMMA. Each water droplet was 2 µl.

Hydrophobicity of surfaces with and without PMMA film is an important indicator that implies whether they are potentially competent to be a low permeable shell. Thus, water contact angles of surfaces with different coatings were measured and images are shown in Figure 5.10. An APTES monolayer was grafted on silicon substrate prior to the deposition of polyelectrolytes multilayers. This is because APTES is able to anchor on the silicon surface, forming more stable covalent bond and resulting in easier adsorption of the next polyelectrolyte layer. (PSS/MI) multilayers were then deposited successively until the desired number of layers were achieved, followed by ATRP of methyl methacrylate on the top.

From Figure 5.10 it can be seen that the water contact angles of bare silicon substrate and the same substrate with a thin (3-Aminopropyl)triethoxysilane (APTES) monolayer were 68˚ and 73˚, respectively. The water contact angle of APTES self-assembly monolayer (SAM) depends on different factors including the base material, the volume of water droplet, the measuring machine as well as the calculation model[268]. Both low and high water contact angles of APTES SAM have been experienced elsewhere[269]. In our study, the water contact angle slightly increased after the APTES SAM deposition. This is attributed to the NH_2- groups which are hydrophilic and other groups which are repellent to water, making the overall hydrophobicity of the substrate higher. After deposition of (PSS/macroinitiator) multilayers, the water contact angle of the planar surface reduced significantly to 45˚. It is easy to understand as polyelectrolytes carry numerous charged groups which can adsorb a large amount of water, resulting in a relatively hydrophilic surface. On the contrary, the water contact angle rose up to 81˚ after the growth of PMMA layer due to its nature of hydrophobicity, indicating that PMMA is able to build up a hydrophobic shell from the polyelectrolytes multilayers precursor.

5.2.3 Fabrication of PMMA coated microparticles with low permeability from macroinitiator

After having studied the growth behaviour of PMMA brushes on planar substrates, it was clear that $(PSS/MI)_6$ precursor could grow thicker polymer layer. In order to fabricate a thick and hydrophobic polymeric brush layer on inorganic template, PMMA brushes was grown after $(PSS/MI)_3$ and $(PSS/MI)_6$ being deposited on $CaCO_3$ cores.

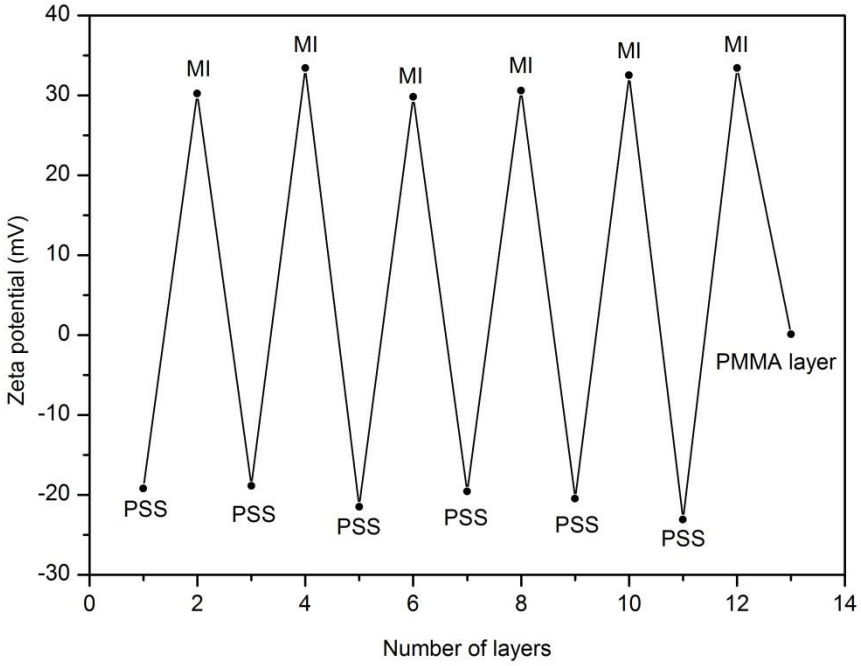

Figure 5.11 Zeta potential values of particles after each polymer coating

(All measurements were carried out in deionized water at pH=7)

To monitor the deposition of each polymer coating, zeta potential is an easy and convenient tool as it indicates the charge reversal after each polyelectrolyte layer. Figure 5.11 shows the zeta potential values of particles during our LbL deposition of $(PSS/MI)_6$ multilayers and after PMMA layer formation. Since PSS is universally used as the first layer due to its strong attachment with $CaCO_3$ particles, we also followed this rule in our procedure. Zeta potential measurement was performed using diluted particle dispersion. Normally, 30 μL of original microparticle dispersion is added into a standard Zetasizer cuvette followed by filling with deionized water to reach the minimum volume requirement.

There is a clear trend of charge reversal after each layer which confirms a successful deposition process of $(PSS/MI)_6$ multilayers onto $CaCO_3$ particles. After ATRP, the

zeta potential of particles became nearly neutral as the newly formed PMMA macromolecules do not carry any charges. The slightly positive zeta potential value may result from some defective particles which were not entirely covered by PMMA layers.

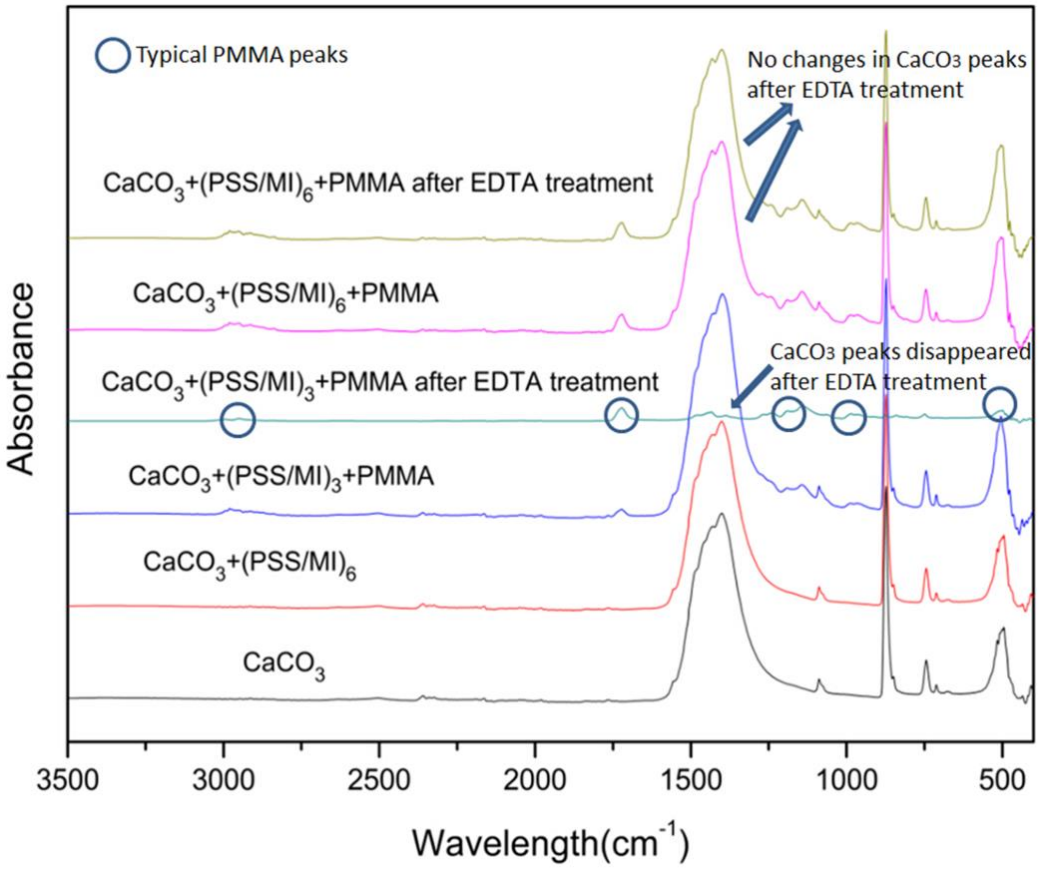

Figure 5.12 FTIR spectrums of $CaCO_3$ and polymer coated $CaCO_3$ before/after EDTA treatment

The chemical composition of obtained microparticles were then analysed by FTIR. Figure 5.12 shows the differences between the FTIR spectrums of $CaCO_3$ cores with and without polymer shells. In the spectrum of pure $CaCO_3$, the peak at 1399 cm^{-1} belongs to carbonate stretching. The peaks at 712 cm^{-1} and 874 cm^{-1} are attributed to the in-plane and out-of-plane carbonate bending, respectively. The spectrum of the $CaCO_3$ particles deposited by (PSS/MI) multilayers does not show any obvious

differences from the spectrum of pure $CaCO_3$. This is due to the significantly lesser amount of polyelectrolytes being deposited compared to that of the cores and therefore the characteristic peaks of the (PSS/MI) complex cannot be seen in the spectrum. After in situ polymerization of PMMA on the surface of $CaCO_3$, some typical PMMA peaks appeared on the spectrum. The peak at 986 cm^{-1} is the characteristic absorption vibration of PMMA while the peaks at 1150-1240 cm^{-1} and 1383 cm^{-1} are assigned to the C–O–C stretching vibration and α-methyl group vibration, respectively. Peak for Acrylate carboxyl group is shown at 1723 cm^{-1}. The stretching vibrations of the C-H bond of the $–CH_3$ and $–CH_2$ groups are overlapped, which are at 2995 cm^{-1} and 2952 cm^{-1}, respectively. The peaks of PMMA in the sample derived from $(PSS/MI)_6$ precursor are apparently bigger than those synthesized from $(PSS/MI)_3$ multilayers as there are more initiators in more precursor layers which leads to thicker PMMA layer.

After having proven the chemical composition of the polymer shells formed on the $CaCO_3$ cores, it is necessary to study whether they are low permeable as expected. Hence, these particles were treated with EDTA, which is a dissolution agent of $CaCO_3$ and has quite low molecular weight of 292.24, less than those of most small molecule drugs. Characteristic FTIR peaks of $CaCO_3$ disappeared in the sample of $CaCO_3/(PSS/MI)_3/PMMA$ after EDTA treatment, meaning that EDTA has penetrate into the polymeric shells and chelated Ca^+. In contrast, the spectrum of $CaCO_3/(PSS/MI)_6/PMMA$ particles remained the same after EDTA treatment.

Simultaneously, the morphologies and the elements composition of polyelectrolyte microcapsules and particles were analysed by different instruments including SEM, EDS as well as TEM. Figure 5.13 (a) (b) (c) (d) are $(PSS/MI)_3$ microcapsules, $CaCO_3/(PSS/MI)_3/PMMA$ particles before and after EDTA treatment and the cross

section of polymer coated particles without EDTA treatment respectively, whilst Figure 5.13 (e) (f) (g) (h) belong to their counterparts from $(PSS/MI)_6$ multilayers. From Figure 5.13 (a) (e), it is evident that the $(PSS/MI)_3$ microcapsules are thinner than $(PSS/MI)_6$ microcapsules, manifesting that the deposition of more polyelectrolyte multilayers was successful and that the PMMA to be synthesized on $CaCO_3/(PSS/MI)_6$ should be thicker than that on $CaCO_3/(PSS/MI)_3$. After polymerization of PMMA, it can be seen that both $CaCO_3/(PSS/MI)_3$ and $CaCO_3/(PSS/MI)_6$ particles became smoother, indicating that their surfaces had been covered by another layer. However, there were some defects on the new layer formed on $CaCO_3/(PSS/MI)_3$ particles where some areas of the surface were not coated by the synthesized layer. After further treatment in EDTA for enough time, most $CaCO_3/(PSS/MI)_3$/PMMA particles became hollow or collapsed, whereas $CaCO_3/(PSS/MI)_6$/PMMA particles were still free-standing and were without obvious difference from their status prior to EDTA treatment. These observation suggested that initiators in $(PSS/MI)_3$ precursor were not enough to grow a structurally perfect and low permeable polymer shell, whereas $CaCO_3/(PSS/MI)_6$/PMMA particles seemed to be resistible to treatment of small molecule dissolution agent.

The thickness of PMMA layer grown from colloid template are supposed to be different from that obtained from flat substrate as the brushes were grown from different base materials. Besides, the shapes and morphologies of the surfaces were also different. To gain a better understanding of how thick the brush layer is enough to form a low permeable shell, the thicknesses of the synthetic shells must be known.

Thus, the particles were broken as shown in Figure 5.13 (d) (h). The thicknesses of the PMMA layer grown from $CaCO_3/(PSS/MI)_3$ and $CaCO_3/(PSS/MI)_6$ were

approximately 70 nm and 200 nm, respectively, which were thicker than those grown from planar substrates.

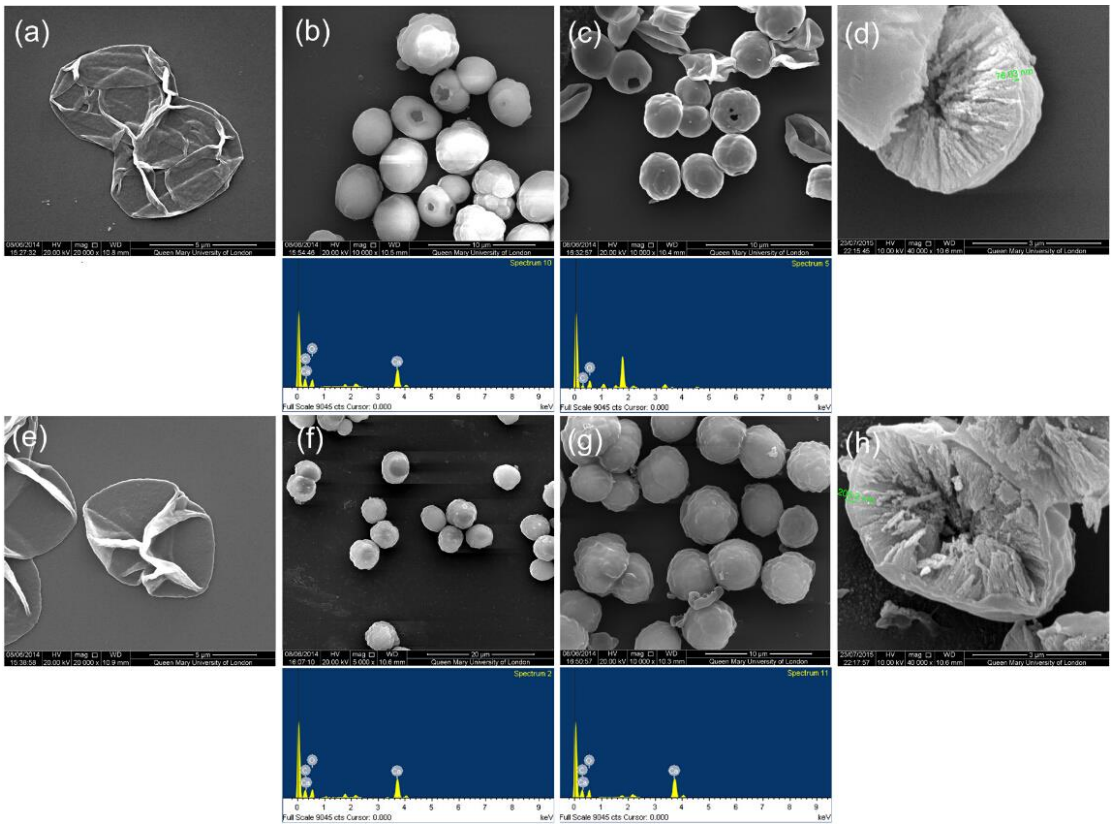

Figure 5.13 SEM images of (a) $(PSS/MI)_3$ microcapsules, (b) $CaCO_3/(PSS/MI)_3$/PMMA particles, (c) $CaCO_3/(PSS/MI)_3$/PMMA particles after EDTA treatment, (d) Cross section of $CaCO_3/(PSS/MI)_3$/PMMA particle, (e) $(PSS/MI)_6$ microcapsules, (f) $CaCO_3/(PSS/MI)_6$/PMMA particles, (g) $CaCO_3/(PSS/MI)_6$/PMMA particles after EDTA treatment, (h) Cross section of $CaCO_3/(PSS/MI)_6$/PMMA particle. EDS spectrums are below the corresponding SEM images.

Although the high roughness of $CaCO_3$ particles would help attract more macroinitiator containing polyelectrolyte precursor which will thereby lead to longer polymer brush layers, the fact that polymer brush is in favour of growing upwards may play a more important role in the shell formation should not be omitted. By

knowing the thickness of the synthetic low permeable shell, it enables us to further design other polymeric carriers with low permeability.

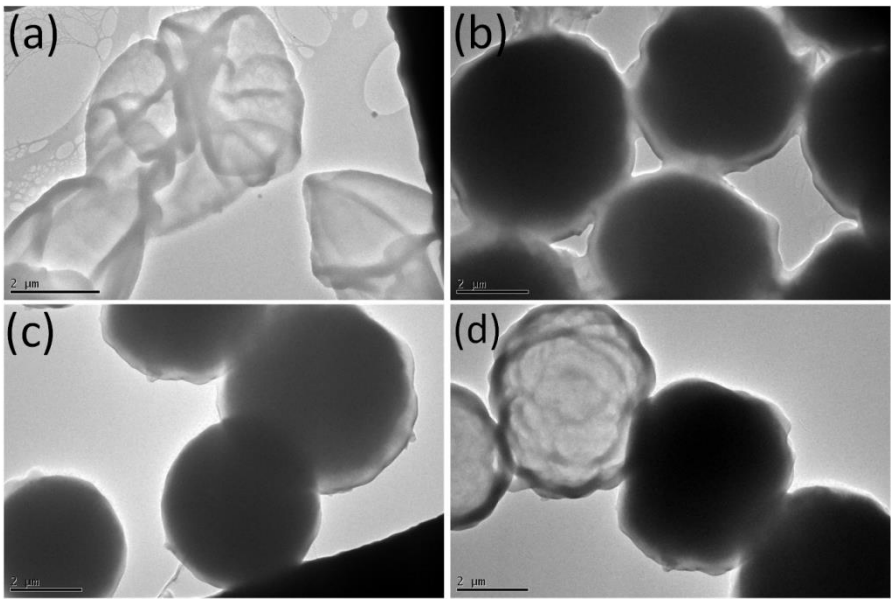

Figure 5.14 TEM images of (a) $(PSS/MI)_6$ microcapsules, (b) $CaCO_3/(PSS/MI)_6/PMMA$ particles, (c) (d) both are $CaCO_3/(PSS/MI)_6/PMMA$ particles after EDTA treatment

In addition to the SEM observation, EDS analysis was carried out in order to detect the elemental changes of different particles before and after EDTA treatment. The EDS spectrums in Figure 5.13 show elemental compositions of different particles. Not surprisingly, there was no trace of Calcium in $CaCO_3/(PSS/MI)_3/PMMA$ particles after EDTA treatment which was in accordance to the SEM analysis. In contrast, there were no obvious differences between the element compositions of $CaCO_3/(PSS/MI)_6/PMMA$ particles before and after EDTA treatment, indicating that small molecular dissolution agent had no effect on these particles.

To give more evidence, TEM as another tool was performed for internal morphology observation. As shown in figure 5.14 thin microcapsules and solid particles could be seen in the images of $(PSS/MI)_6$ microcapsules and $CaCO_3/(PSS/MI)_6/PMMA$

particles, respectively. The different contrasts in Figure 5.14 (b) which belongs the sample of $CaCO_3$/$(PSS/MI)_6$/PMMA particles demonstrate that the $CaCO_3$ cores had been surrounded by a relatively thick shell. Figure 5.14 (c) (d) show the sample of $CaCO_3$/$(PSS/MI)_6$/PMMA after EDTA treatment, in which particles still had the inorganic templates inside. Occasionally, few hollow microcapsules were observed in Figure 5.14 (d). These particles were presumably with defects that formed during shell formation. Moreover, the thickness of the shell was measured to be roughly 200 nm which is in good agreement with data from SEM images. These evidences from various characterization techniques indicate that PMMA shell grown from $(PSS/MI)_6$ precursor multilayers are non-permeable to EDTA dissolution agent. Thereby, it was confirmed that PMMA layer grown from $(PSS/MI)_6$ precursor via ATRP is an excellent barrier for small molecules.

5.3 **Conclusion**

PMMA brush layers were synthesized from both macroiniators deposited planar substrates and inorganic particles. The kinetics of PMMA growth on macroinitiator pre-deposited planar substrates was studied. It was found that a higher amount and denser coverage of $(PSS/macroinitiator)_6$ multilayers lead to a remarkably faster growth of polymer brush than that from 3 bilayers precursor. The surface with PMMA layer had significantly increased water contact angle than the surface without PMMA growth, showing PMMA layer is hydrophobic as anticipated for our aim. FTIR analysis suggested that PMMA shell was formed after polymerization on the $CaCO_3$ particles. Furthermore, FTIR, SEM, TEM as well as elemental analysis indicated that PMMA shell grown from $(PSS/macroinitiator)_6$ which has a thickness of about 200 nm are non-permeable to small molecules.

6 Fabrication of PLA coated microparticles with low permeability via emulsion process

In the previous two chapters, we have demonstrated two different methods to create microcarriers with low permeability. However, in spite of the encouraging results, these methods are relatively time-consuming. Thus, in this chapter a simple emulsion method is introduced to fabricate polymer coated microparticles with low permeability.

There are generally two categories of emulsion methods, single emulsion and double emulsion processes, with the former one being widely used for encapsulating hydrophobic molecules and the latter one being more efficient for loading of hydrophilic substances[231]. Thus, the method applied can be chosen according to the nature of the cargo molecules. However, regardless of the methods and the cargo molecules involved, an aqueous solution containing emulsifier is always used for the last emulsion step, during which a stabilizing layer would coat onto particles which is essential to prevent the aggregation of the resulting particles. When encapsulation of solid particles or instable water-soluble molecules is carried out, the desired cargo could be dispersed in oil phase as a solid-in-oil emulsion step, followed by second emulsion process in water[270]. Thus, the whole process is called solid-in-oil-in-water (S/O/W) double emulsion method. Unlike water-in-oil-in-water (W/O/W) and oil-in-water (O/W) emulsion processes where cargos are encapsulated directly during the formation of polymer shells, for the S/O/W technique molecules can be incorporated into the solid particles prior to the emulsion process. This could be used for encapsulation of a broader range of substances, especially those sensitive molecules for which a protective shelter is needed.

The aim of this work was to fabricate polymer coated microparticles with presumably low permeability using S/O/W emulsion method. Here we used $CaCO_3$ particle as a protective core for the encapsulated dextran. Micro-sized $CaCO_3$ particle has been intensively used as the template in LbL process. By using $CaCO_3$ particle, one can co-precipitate a wide range of desired substances during the formation of the particles from $CaCl_2$ and $NaCO_3$. Moreover, $CaCO_3$ has been clinically used for bone related disease as Calcium is one of the main components in bones. Therefore, PLA coated $CaCO_3$ particle with sealed bioactive molecules could be of great interest for biomedical applications, such as delivery of growth factors for bone regeneration.

6.1 Preparation process of PLA coated microparticles using S/O/W double emulsion technique

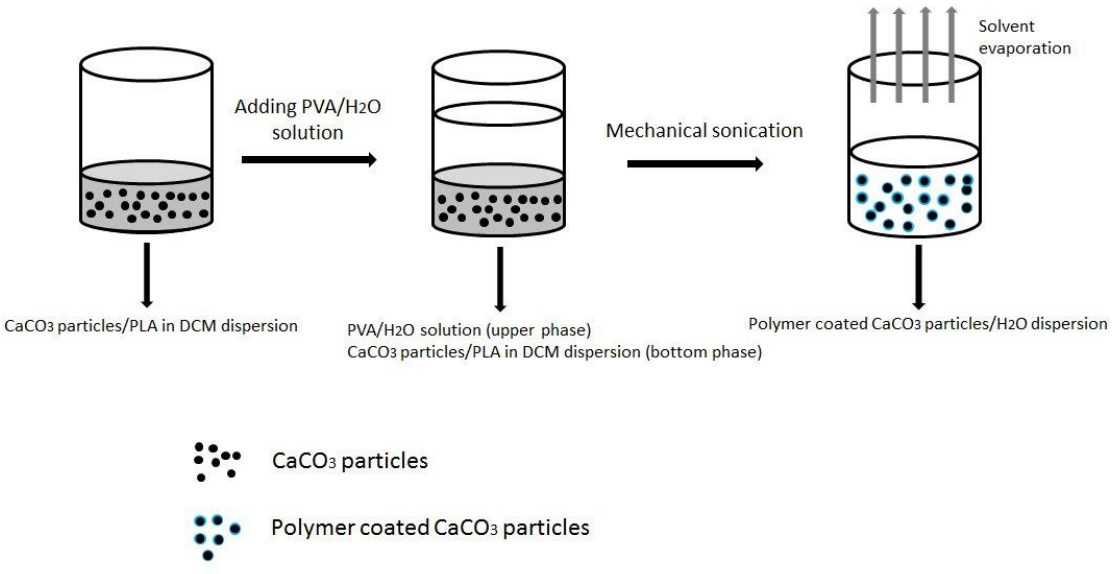

Figure 6.1 Schematic illustration of the preparation process of PLA coated $CaCO_3$ particle dispersion using emulsion method

Figure 6.1 shows the schematic illustration of the fabrication process of PLA coated microparticles using emulsion method. The concentration of PLA/DCM solution was 8% w/w and the ratio of organic phase and aqueous phase was 1/2 w/w throughout the experiments. Basically, PLA is present in organic phase along with $CaCO_3$ microparticles and is coated onto the particles when organic phase evaporates under vigorous mechnical sonication. Since PLA is hydrophobic in nature which would very likely lead to aggregation of the obtained microparticles in aqueous solution, Polyvinyl alcohol (PVA), a hydrophlic surfactant, is added into the aqueous phase and is also adsorbed onto the particles as an additional layer on top of PLA layer. This extra thin PVA layer would probably be helpful in yielding well-dispersed microparticles with polymer coating.

6.2 **Effect of PVA content on microparticles**

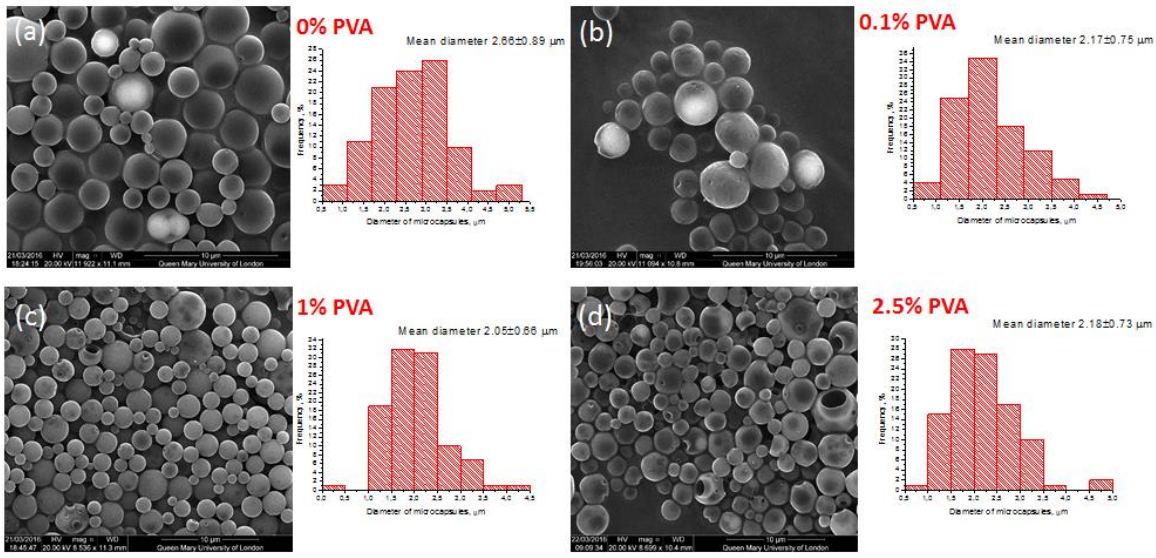

Figure 6.2 Back-scattered SEM images and size distributions of PLA coated microparticles prepared with (a) 0% (b) 0.1% (c) 1% (d) 2.5% w/v PVA solution. The mean particle diameter of each sample is based on the diameter of 80 particles.

In order to determine the optimal amount of PVA to be used, 4 different concentrations (0%, 0.1%, 1%, 2.5% w/v) of PVA solution were used for the preparation of polymer coated microparticles as these are commonly used PVA concentrations for emulsion process[271-273]. The mass of $CaCO_3$ particles were set at 20% of that of PLA for each sample. As can be seen in Figure 6.2, microparticles with spherical shapes are obtained in all samples where $CaCO_3$ particles are well encapsulated in polymer particles as observed in SEM images. Besides, there is no significant differences in morphologies of particles between each sample and the mean diameters of the resulting particles indicates that they are similar in size regardless of the concentration of PVA. However, the size distribution of microparticles narrows as the concentration of PVA increases, demonstrating a positve effect of PVA. More importantly, it was observed that as the content of PVA increased, less PLA precipitated in particles dispersion after emulsion process, indicating that more PLA polymer were stabilized on microparticles. Furthermore, PLA coated microparticles without PVA stabilizing layer tend to aggregate very quickly whereas the sample with PVA content of 2.5% dispersed fairly well. Thus, 2.5% w/v PVA aqueous solution was used throughout the rest experiments in this study.

6.3 Effect of $CaCO_3$ content on morphology and encapsulation of microparticles

In order to study the effect of $CaCO_3$ content on the polymer coated microparticles, 6 samples were prepared, with mass ratio of $CaCO_3$ relative to PLA being 0, 0.1, 0.2 0.4, 0.8 and 1.2 (sample 1-6). They were all prepared through a standard emulsion process described in Figure 6.1. BSA-FITC was incorporated into $CaCO_3$ cores during their

formation for the permeability study. The morphologies, elemental compositions, permeability of the resulting microparticles were then studied by SEM, EDS as well as CLSM.

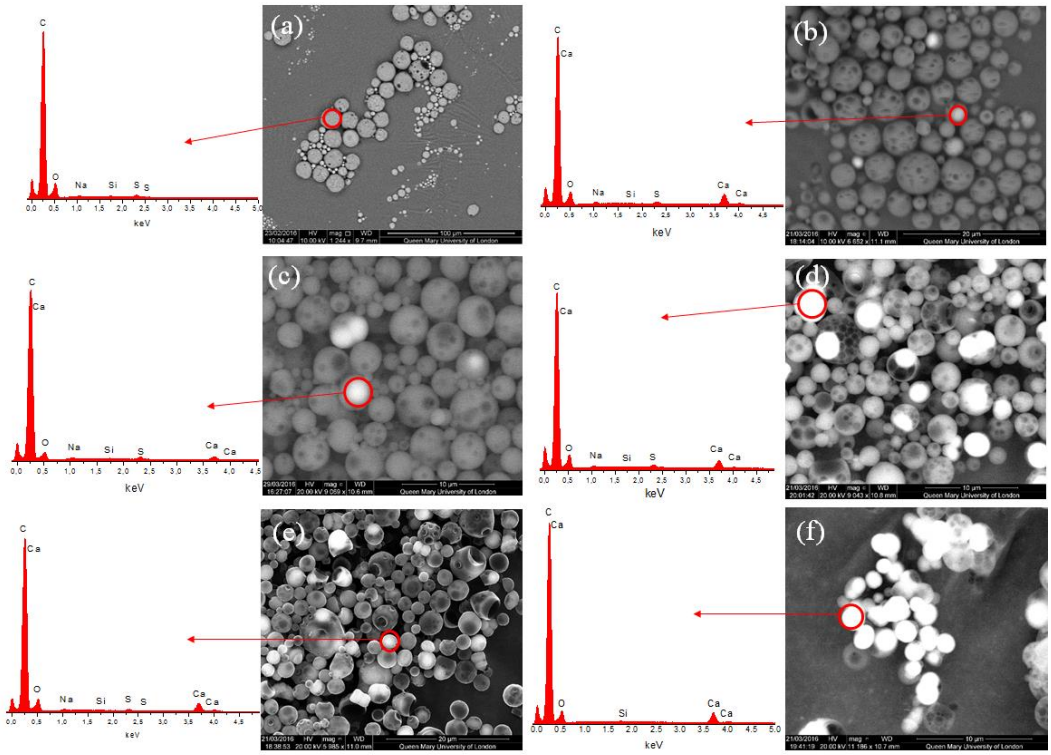

Figure 6.3 Back-scattered SEM images of PLA coated $CaCO_3$ microparticles with different $CaCO_3$ contents: (a) 0, (b) 0.1, (c) 0.2, (d) 0.4, (e) 0.8, (f) 1.2. Numbers are mass ratio of $CaCO_3$ particles relative to PLA. Carbon was used to coat the samples prior to SEM observation.

As the main task was encapsulation of $CaCO_3$ particles with PLA coating, one needs to know the positions of $CaCO_3$ particles after the emulsion process. Thus, back-scattered electrons SEM mode was used as it can determine the number of phases in a material and their mutual textural relationships. From Figure 6.3 we can see that spherical particles could be obtained in all samples and the diameters of the particles ranged from hundreds of nanometers to several micrometers. SEM image and EDS

spectrum of the sample 1 ($CaCO_3$/PLA ratio 0) suggested that there was no Calcium containing particles. Not suprisingly, white contrasts were observed in the particles in all of the rest samples. These white contrast were assumed to be $CaCO_3$ particles which was proven by EDS analysis shown in Figure 6.3 (b). As the amount of $CaCO_3$ particles increased, more white contrasts were found in the samples. It can be seen in Figure 6.3 (f) that most of the obtained microparticles contained $CaCO_3$ particles in sample 6 (ratio 1.2) which could also be proven by the corresponding EDS spectrum. Moreover, as more $CaCO_3$ particles in the sample, less small particles were formed after emulsion process. This is due to the majority of the PLA being deposited onto the $CaCO_3$ cores. Thereby, less amount of PLA was left to form pure polymer particles.

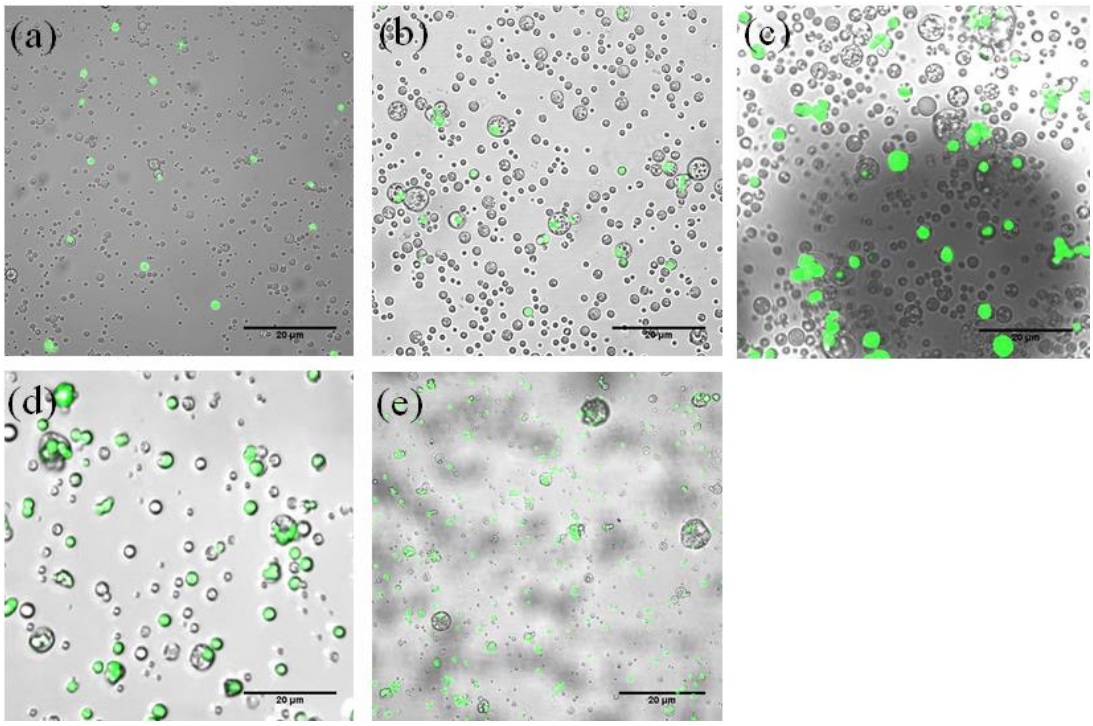

Figure 6.4 Overlayed CLSM images of PLA coated $CaCO_3$ microparticles with different $CaCO_3$ contents: (a) 0.1, (b) 0.2, (c) 0.4, (d) 0.8, (e) 1.2. Numbers are mass ratio of $CaCO_3$ particles relative to PLA

CLSM was also applied to check whether the incorporated FITC-BSA was still entrapped in the microparticles after the emulsion process. It shows clearly in Figure 6.4 that in all of the 5 samples FITC-BSA could be sealed within the microparticles as the fluerescent circles appeared to be solid. The overlayed CLSM images demonstrated that the amount of fluorescent particles increases as a function of the amount of $CaCO_3$ particles added during the sample preparation.

6.4 **Permeability study on PLA coated microparticles**

We then treated these PLA coated microparticles with EDTA in order to see if EDTA could dissolve the encapsulated $CaCO_3$ particles. Since EDTA has a much smaller molecular weight (292.24 g/mol) than FITC-BSA, being able to retain FITC-BSA within the polymer coated particles does not necessarily mean the polymer shells could stop EDTA penetrating into the particles. Each sample was then dispersed in 0.2 M EDTA solution for 2 h and was thoroughly washed with DI H_2O before further characterizations.

SEM, EDS and CLSM were again used to characterize these microparticles after them having been treated with EDTA. In general, reduced amount of $CaCO_3$ particles were observed in PLA coated particles in all of the 5 samples compared to those before EDTA treatment. This is because the morphologies and structures of the PLA particles are difficult to control which leads to more defects in the PLA shells in comparison to the shells syntheiszed by controlled polymerization. In spite of this, a great number of $CaCO_3$ particles were still retained within the PLA shells after EDTA treatment as shown in Figure 6.5, especially for sample 5 (ratio 0.8) where about half of the microparticles still contained $CaCO_3$ particles after EDTA treatment.

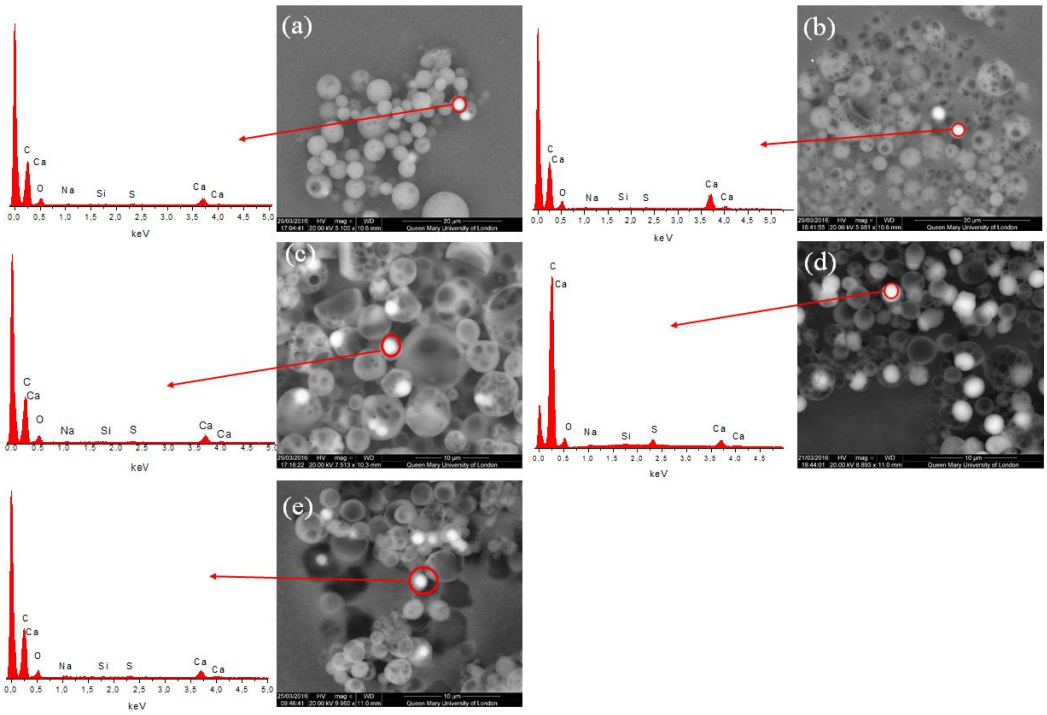

Figure 6.5 Back-scattered SEM images of PLA coated $CaCO_3$ microparticles with different $CaCO_3$ contents after EDTA treatment: (a) 0.1, (b) 0.2, (c) 0.4, (d) 0.8, (e) 1.2. Numbers are mass ratio of $CaCO_3$ particles relative to PLA. Carbon was used to coat the samples prior to SEM observation.

However, most of the $CaCO_3$ particles disappeared after EDTA treatment in sample 6 (ratio 1.2) where the remaining $CaCO_3$ particles were even less than those in sample 4 (ratio 0.4) and 5 (ratio 0.8). This is probably because higher $CaCO_3$ content would cause less amount of PLA polymer adsorbing onto each $CaCO_3$ particle, resulting in thinner PLA layer that is more permeable to EDTA molecules.

CLSM images (Figure 6.6) showed similar phenomenon as observed under SEM. Microparticles in Sample 2-5 (ratio 0.1, 0.2, 0.4, 0.8) could retain the fluorescent molecules after EDTA treatment whereas only few microparticles still showed fluorescent. Since FITC-BSA is much bigger molecules than EDTA, the PLA/ $CaCO_3$

hybrid particles in sample 6 (ratio 1.2) had much higher permeability compared to other samples.

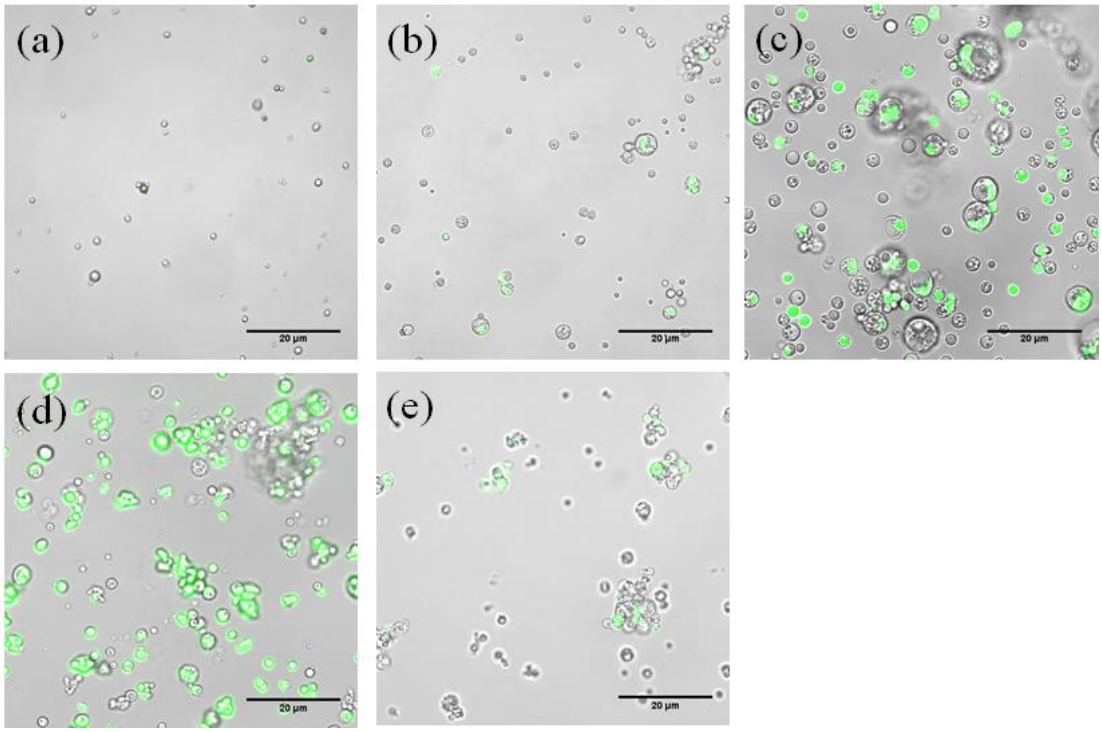

Figure 6.6 Overlayed CLSM images of PLA coated $CaCO_3$ microparticles with different $CaCO_3$ contents after EDTA treatment: (a) 0.1, (b) 0.2, (c) 0.4, (d) 0.8, (e) 1.2. Numbers are mass ratio of $CaCO_3$ particles relative to PLA

Thus, the SEM and CLSM results suggested that higher content of $CaCO_3$ particles help increase the amount of PLA used for coating, but it should not exceed a mass ratio of 0.8 between $CaCO_3$ particles and PLA as PLA layer would not be thick enough for low permeability purpose.

6.5 **Conclusion**

Low permeable PLA coated $CaCO_3$ microparticles with sealed bioactive molecules were successfully prepared via an emultion process. An additional PVA outmost layer was proven to be helpful in stablizing the obtained microparticles as well as

narrowing the size distribution of these particles, with 2.5% being the optimal PVA concentration. Different contents of $CaCO_3$ microparticles in each sample with fixed amount of PLA were also studied. All of the 5 samples could retain FITC-BSA within them. When the mass ratio of $CaCO_3$ relative to PLA is no more than 0.8, polymer coated microparticles are more likely to resist EDTA treatment and retain bioactive cargos, whereas the PLA coated particles can be penetrated by EDTA when mass of $CaCO_3$ is 1.2 times that of PLA. Therefore, 0.8 was the optimal mass ratio of $CaCO_3$ relative to PLA in terms of the high-usage of PLA as well as the low permeability of resulting microparticles. We believe that this PLA coated $CaCO_3$ microparticles with low permeability could be used for medical purposes such as drug delivery and bone regeneration.

7 PLA film synthesized via surface-initiated ring-opening polymerization and degradation study

A thin coating of biocompatible and biodegradable polymer on solid surface could lead to significant change in the surface properties as well as the permeability of the coated devices. For example, some hydrophilic polymer films such as Poly(ethylene glycol) (PEG) can act as a protective layer for implants to reduce the adhesion between implant surface and biomolecules or cells. Microchambers which are constructed by uniform polymer films could be used as drug reservoir. The release rate of drugs from such containers can be adjusted by coating an additional layer.

PLA is one of the most commonly used and clinically approved biodegradable polymers for biomedical applications. It can be grown on the surface of implants such as scaffolds where biodegradable/biocompatible coating is desired. Drug delivery devices could also use PLA films for controlled release. Furthermore, the investigation of the interaction between such biodegradable polymer coating and biomolecules or cells is of great importance for the design of biomedical devices.

In comparison to PLA films coated through physical interaction such as spin coating, dip coating, a chemically attached PLA film is more robust and even. Thus, Surface-initiated ring-opening polymerization (SI-ROP) has been intensively studied for the growth of PLA films. There have been a variety of surfaces from which PLA coating were grown for different applications. However, most of the PLA films are fairly thin (less than 100 nm) due to the limited initiating sites the initiator containing monolayers contain. This may restrict the application of PLA coatings where thicker PLA films are needed.

In chapter 5, we have successfully fabricated thick PMMA films by combining Layer-by-Layer and Surface-initiated polymerization techniques. In this work, we aim to prepare thick PLA film grown from macroinitiator via SI-ROP. Two different macroinitiators that contains hydroxyl groups as the initiator for SI-ROP are synthesized and used. Kinetics of the depositions of the macroinitiators onto the planar substrates is studied. PLA films are then synthesized from two macroinitators and the degradation behaviour of the obtained PLA films is also investigated.

7.1 Synthesis of PLA film via surface-initiated ROP from polyelectrolyte macroinitiator

7.1.1 Synthesis of polyelectrolyte macroinitiator for ring-opening polymerization

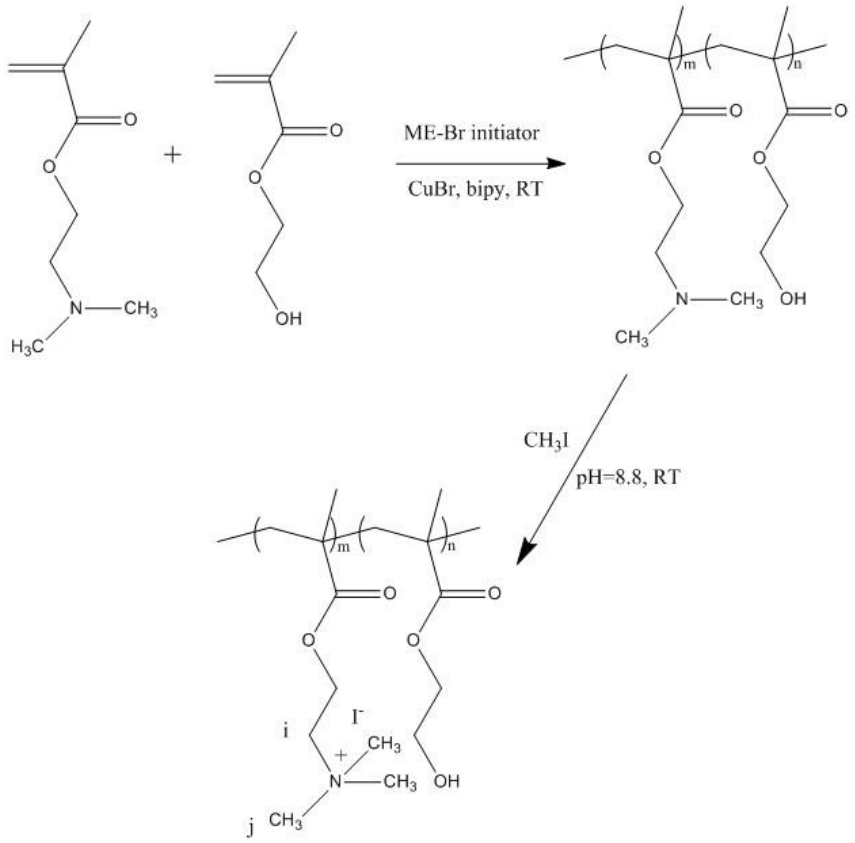

Figure 7.1 Schematic illustration of synthesis route of macroinitator for ROP

The macroinitiator was synthesized via a two-step reaction illustrated in Figure 7.1, which involves copolymerization of DMAEMA and HEMA as well as quaternization of the resulting copolymer. NMR was then used to analyse the chemical compositions of the purified products after each step. The NMR spectrum is shown in Figure 7.2, Peak (a), (b) and (c) belong to the $–CH_2$ and $–CH_3$ on the PDMAEMA part, respectively whereas peak (d), (e) are attributed to the $–CH_2$ groups on the PHEMA chains. After the copolymer was quaternized with methyl iodide, peak (b) (c) moved to (i) (j) which was in agreement with the previous results[233].

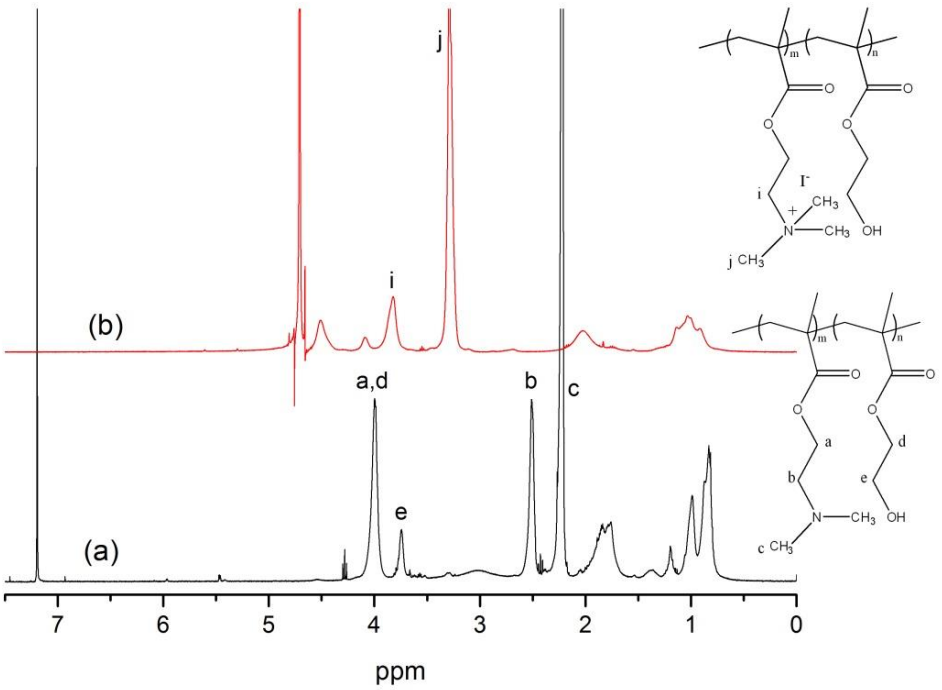

Figure 7.2 NMR spectrums of (a) Poly(DMAEMA-*co*-HEMA), (b) macroinitiator after quaternization of Poly(DMAEMA-*co*-HEMA). Deuterated chloroform and deuterium oxide were used as solvents for (a) and (b), respectively.

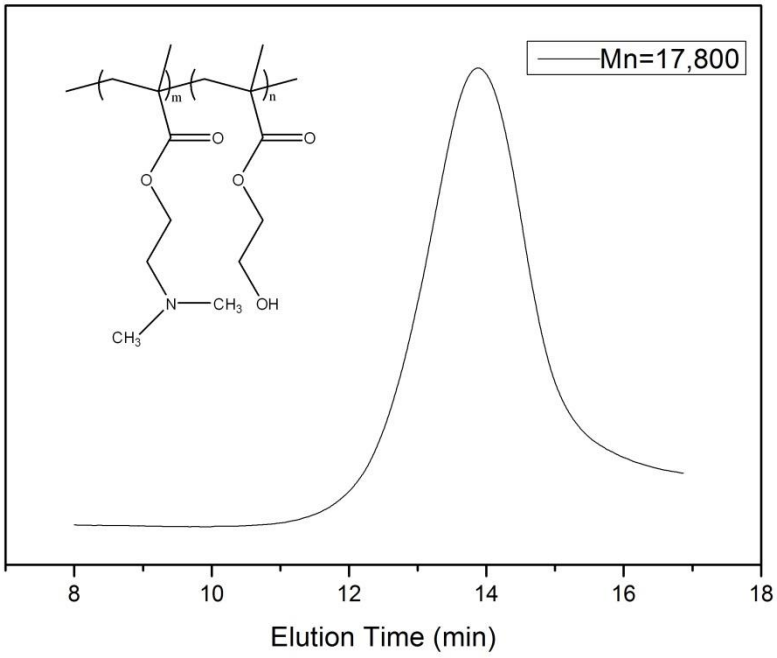

Figure 7.3 GPC curve of the polyelectrolyte macroinitiator

GPC was applied to acquire the information about the molecular weight of the macroinitiator. As can be seen in Figure 7.3, the molecular weight of the synthesized macroinitiator was 17,700，with a relatively narrow distribution.

7.1.2 Polymerization of L-lactide using macroinitiator

After having synthesized macroinitiator that bears –OH groups on the side chains, we used it to initiate ROP of L-lactide in bulk solution. This was done to test whether this macroinitiator was able to initiate ROP as different initiators may have significantly varied efficiencies. As shown in Figure 7.4 PLA chains are grafted onto the side chains of macroinitiator, forming a comb-like polymer structure.

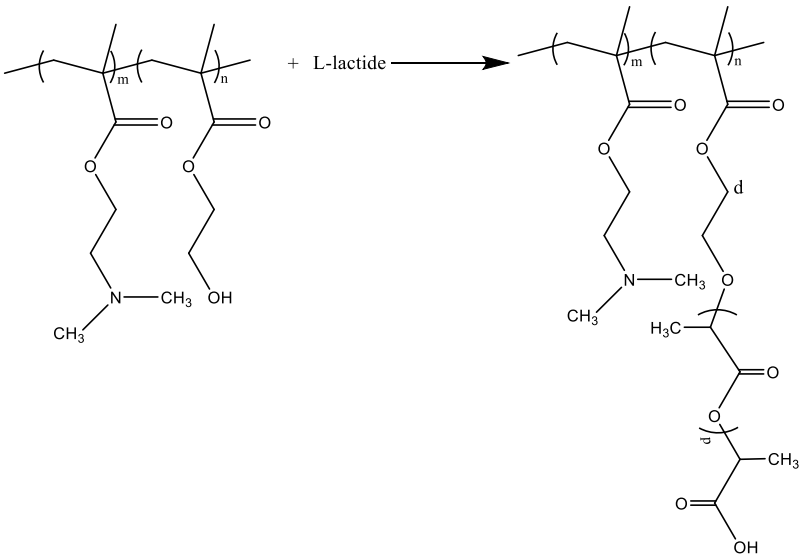

Figure 7.4 Schematic illustration of polymerization of L-lactide using macroinitiator

The polymerization was continued for 24 hours in anhydrous toluene at 100 ℃. This reaction condition will also be used later on for SI-ROP. After the reaction stopped, the crude product was dissolved in DCM and precipitated into cold diethyl ether. This was repeated for 3 times to get rid of unreacted monomers as well as other chemical residues.

NMR was used to determine the structure of the obtained polymer. As shown in Figure 7.5, peaks (a), (b), (c), (d), (e) belong to the macroinitiator which has already been presented in Figure 7.5. Peaks (f) and (g) are characteristic peaks for PLA. Therefore, PLA were successfully formed.

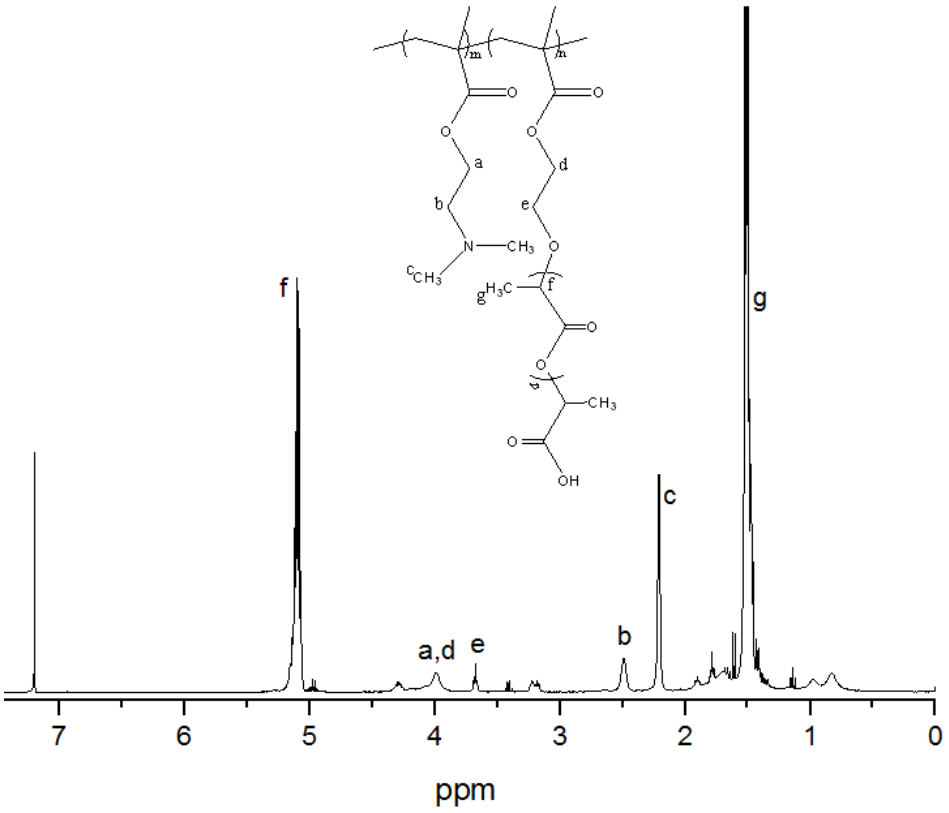

Figure 7.5 NMR spectrum of macroinitator-PLA

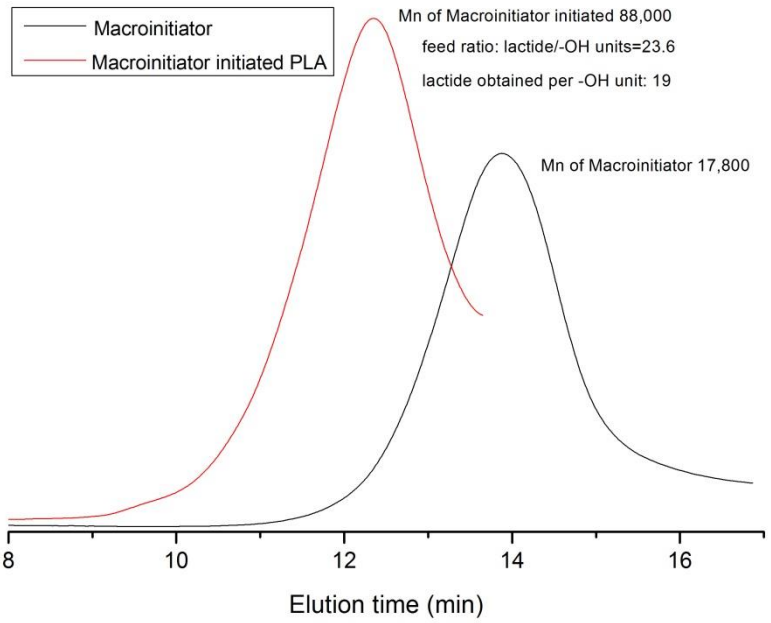

Figure 7.6 GPC curves of macroinitiator and macroinitator-PLA "comb-like" polymer

The purified macroinitator initiated PLA was then characterized with GPC in order to know the change in molecular weight after PLA chains having been grafted. The designed feed ratio of L-lactide to –OH groups was 23.6. GPC curve of the grafted polymer is shown in Figure 7.6. The molecular weight of the polymer shifted remarkably from 17,800 to 88,000, making the average grafting ratio 19, which indicates that the majority of the monomers were successfully polymerized by macroinitiator. Thus, this polyelectrolyte based macroinitiator was proven to be effective for ROP.

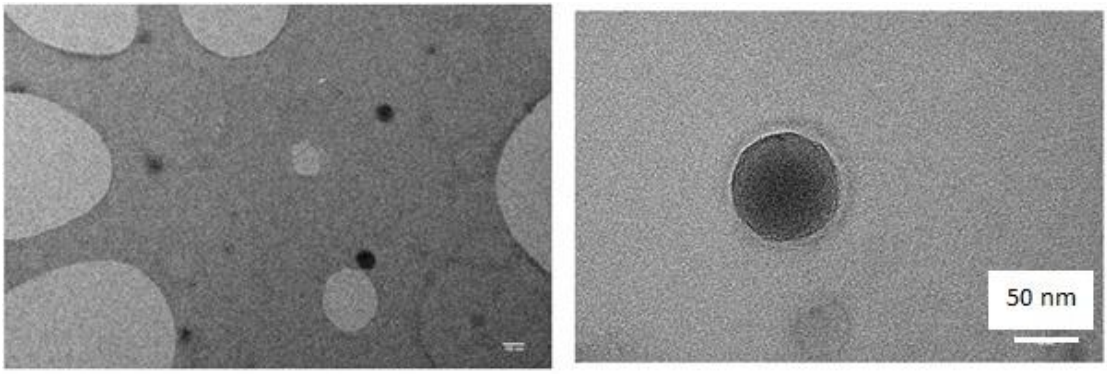

Figure 7.7 TEM images of micelles assembled from amphiphilic macroinitator-PLA "comb-like" polymer

In spite of the positive results from NMR and GPC, there was still a possibility that this polymer was initiated by trace water molecules, which could also act as an initiator for ROP. To rule out this potential problem, we found a way to identify the obtained polymer by testing its hydrophobicity-hydrophilicity. Since macroinitiator is amphiphilic whereas PLA chains are hydrophobic, the desired polymer should also be amphiphilic. In contrast, the obtained PLA polymer would be hydrophobic if it was initiated by water molecules. Hence, a self-assembly process of this polymer was performed in order to find out its hydrophobicity. A small amount of polymer was first dissolved in THF and then the solution was added dropwise into excess water.

After solvent evaporation, a light blue coloured solution was obtained. This is a typical phenomenon of micelle solution. We then observed a dried sample of this solution under TEM, the images of which are shown in Figure 7.7. These dark solid circles are typical morphologies of micelles as their hydrophobic chains form cores whilst the hydrophilic chains form outer shell. Thus, the resulting PLA polymer was proven to have been initiated by macroinitiator, which was then used for the surface-initiated ROP.

7.1.3 Synthesis of PLA film via surface-initiated ROP from polyelectrolyte macroinitiator

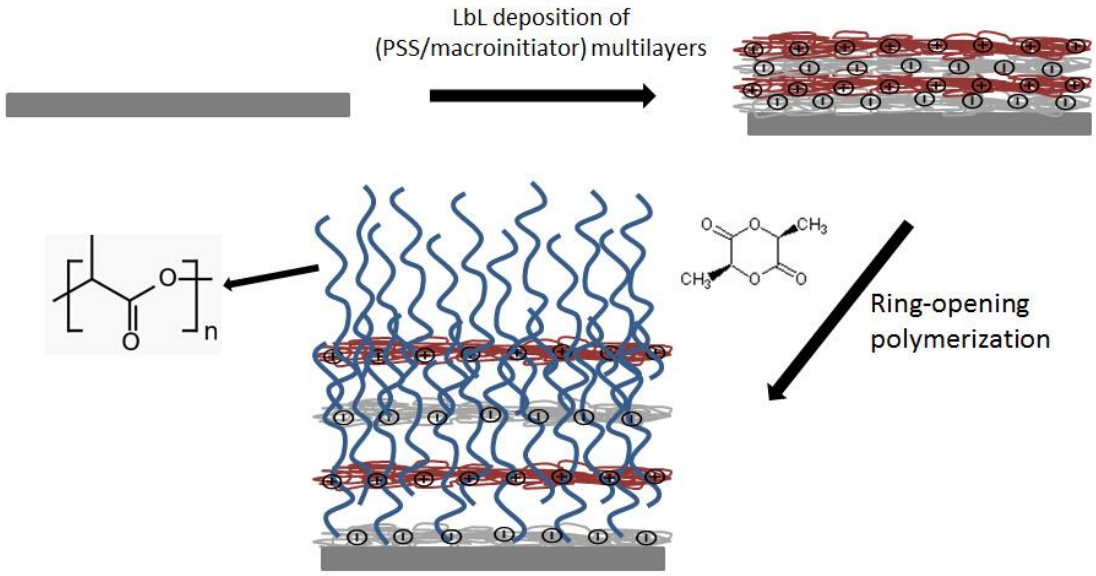

Figure 7.8 Schematic illustration of synthesizing of PLA brush from polyelectrolyte macroinitiator

7.1.3.1 Deposition of PSS/macroinitiator precursor on planar substrate

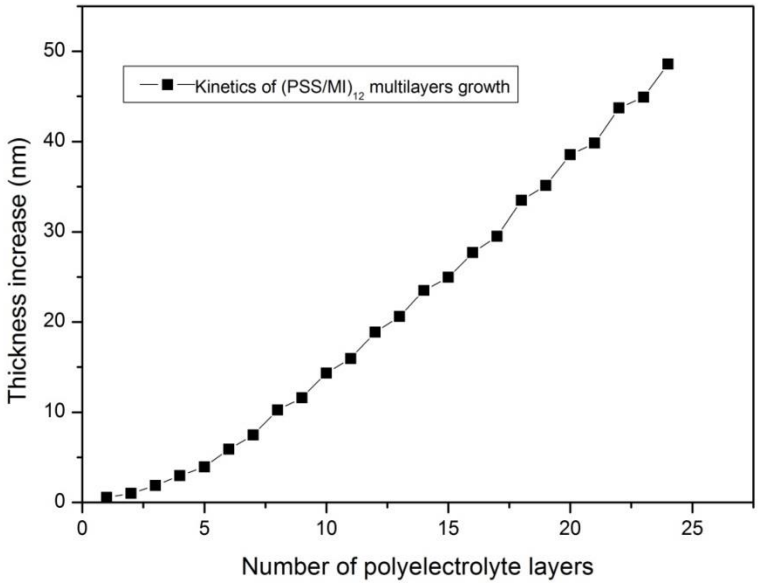

Figure 7.9 Kinetics of the growth of PSS/MI multilayers

Before growing PLA brush, the polyelectrolyte macroinitiator was deposited on silicon substrate through conventional LbL process along with PSS to create the macroinitiator precursor. As can be seen in Figure 7.9 the growth consists of two stages. The thickness of (PSS/MI) multilayers increased exponentially during the first 3 bilayers whereas after that this growth trend was replaced by a linear pattern until the end of the deposition. This phenomenon has been found in some polyelectrolyte multilayers. It is supposed that this two-stage growth pattern is caused by the restruction of the film that gradually obstruct one of the constituent polyelectrolytes diffusing through the multi-layered film. Once this polyelectrolyte can no longer diffuse into the formed film, a new growing zone forms and grows linearly underneath the formed film with the number of layers. Meanwhile, the thickness of the film constructed at the first exponential growing stage keeps constant and this part of film moves upward as the new growing zone continues to grow underneath it [37].

7.1.3.2 Kinetics of PLA brushes from PSS/macroinitiator precursor

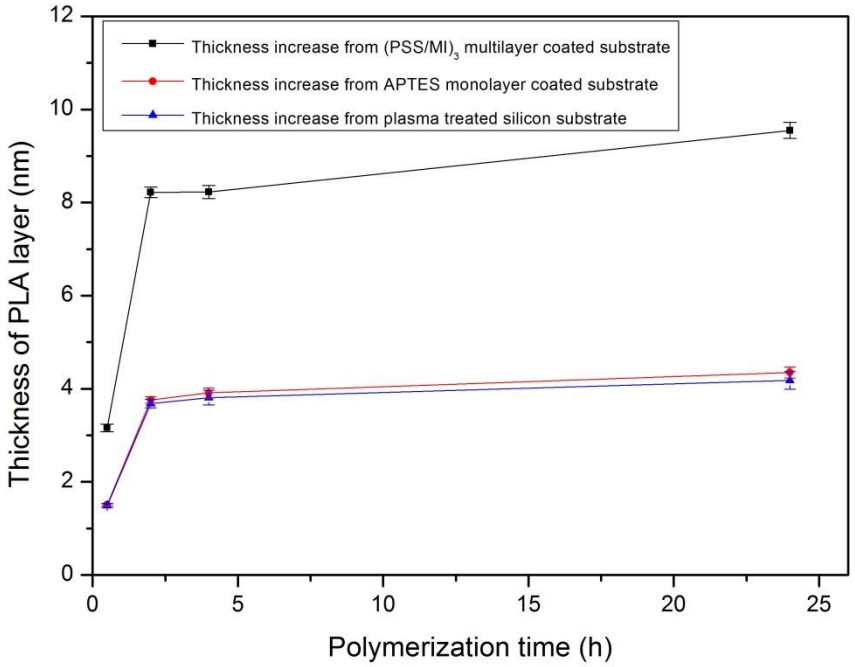

Figure 7.10 Kinetics of PLA brush growth from three different initiators, which are $(PSS/MI)_3$, APTES and native –OH on silicon substrate.

Afterwards, PLA brush layer was grown from three different initiators, which were native –OH groups on silicon substrate, $–NH_2$ groups on APTES monolayer and $(PSS/MI)_3$ multilayer precursor, through bulk polymerization. It is clearly shown in Figure 7.10 that PLA grew at nearly the same speed from –OH and $–NH_2$ initiating sites which indicates that these two functional groups have similar initiating efficiency for ROP. The kinetics of PLA growth from $(PSS/MI)_3$ multilayers was 2-3 times faster than that from monolayers due to the thicker initiator layers. All of these three samples showed very similar growth trends where PLA almost stopped growing after 2 hours. This could be explained by the phenomenon we observed that the polymerization solution had already become extremely viscous at 2-hour point which may indicate that most monomers had been polymerized by the trace water molecules.

This is because that water molecules contain hydroxyl groups, they can act as initiator for ROP as well. Thus, trace water could compete with macroinitiators to polymerize LLA monomers. Since macroinitiator was immobilised on the substrate, only a small amount of monomer could be accessed by them whereas trace water is able to reach all of the monomers in the bulk solution. In order to avoid this from happening, the use of a solvent would be helpful as it will reduce the concentration of monomers thus making it more difficult for the water molecules to access monomers.

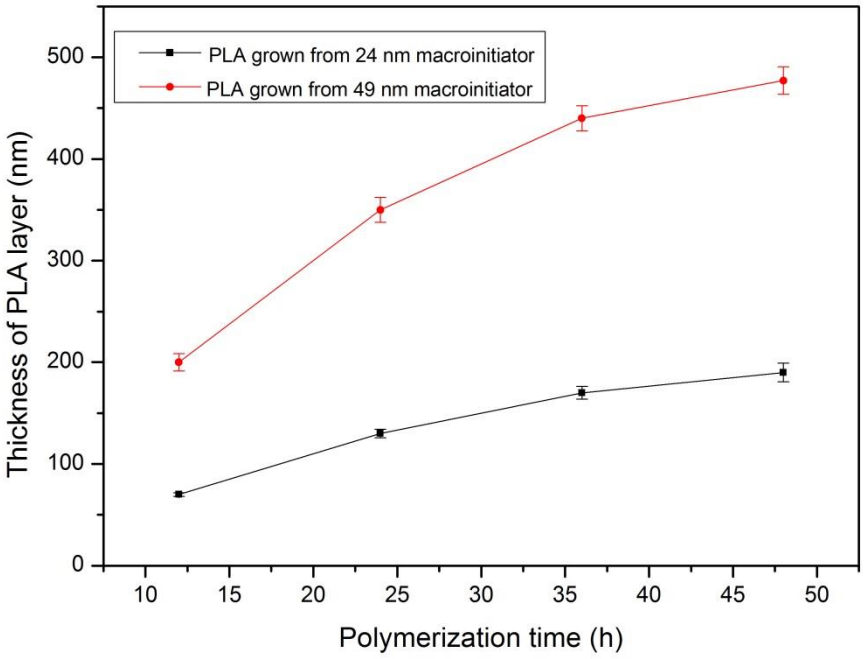

Figure 7.11 Kinetics of PLA growth from PSS/macroinitiator multilayer precursor

Two different heights (24, 49 nm) of macroinitiator multilayer precursors were then selected for PLA growth in solvent polymerization. The polymerization was carried out in anhydrous toluene at 100 °C using $Sn(Oct)_2$ as the catalyst. Prior to the polymerization, the schlenk flask should be dried properly by heat gun for at least 3 times to eliminate water moisture as it could act as a competing initiator.

The growth of PLA was monitored by measuring the thickness of each sample retrieved and washed after polymerization using ellipsometer. The thickness increase of the film contributed by PLA growth was calculated by subtracting the thickness of macroinitiator precursor from the total thickness of the obtained film.

As can be seen the kinetics of PLA growth in Figure 7.11, the growth rates gradually decreased over time for PLA films from both lengths of macroinitiator and the thicknesses almost plateaued after 48 h, with the thickness of PLA from thicker macroinitiator reaching 480 nm while the thickness of PLA from thinner macroinitiator ending at around 190 nm. The reason why the thickness of PLA layer grown from 49 nm precursor is more than twice that from 24 nm precursor is that the initial macroinitiator layers do not cover the substrate surface entirely. As macroinitiator multilayers grow and become thicker, each layer gets denser and covers the entire surface area which leads to more initiators in each layer. Thus, the 49 nm macroinitiator multilayers would have more than doubled amount of initiators the 24 nm precursor has which reflects in the thicknesses of polymer brushes initiated from these macroinitiator multilayers.

7.1.4 Synthesis of PLA coated microparticles from macroinitiator covering $CaCO_3$ cores

After having grown PLA brush on planar substrate, efforts were made to grow PLA shell from macroinitiator deposited $CaCO_3$ microparticles. Therefore, $(PSS/MI)_{12}$ multilayers were first deposited onto $CaCO_3$ cores through a LbL process followed by being washed with anhydrous ethanol to remove the water remaining in the particles. These particles were then transferred to anhydrous toluene before ring-opening polymerization of L-lactide was carried out for 2 days in the same manner as

described for planar substrates. Finally, the retrieved particles along with the particles before polymerization were treated with EDTA solution to remove the $CaCO_3$ cores.

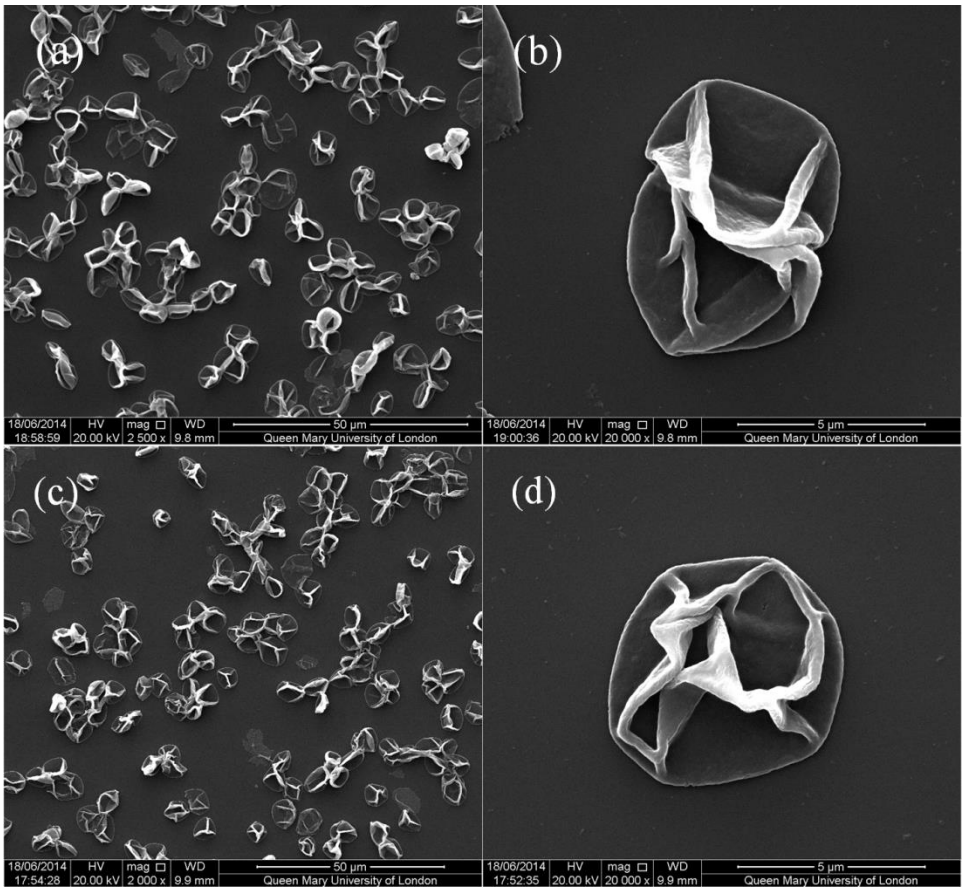

Figure 7.12 SEM images of (a) (b) $(PSS/MI)_{12}$ microcapsules, (c) (d) $(PSS/MI)_{12}$ microcapsules after EDTA treatment of microparticles retrieved from ROP polymerization

The resulting hollow capsules were imaged with SEM as shown in Figure 7.12. Figure 7.12 (a) (b) represent $(PSS/MI)_{12}$ microcapsules whilst (c) (d) are images of hollow capsules after EDTA treatment of microparticles retrieved from ROP. However, as seen in SEM images there are no obvious differences between these two samples, indicating that PLA brush did not grow from macroinitiaotor precursor during the polymerization. This is probably because of the water residue after sample being transferred from aqueous medium to the reaction solution which can easily stop the ROP. Although the ethanol and toluene used for washing step were anhydrous, the

entire handling procedure was done in ambient environment which would get water moisture absorbed into the microparticles dispersion. Even this tiny amount of water moisture could cease the polymerization by competing with macroinitiator and consuming monomers to generate oligomers.

7.2 Synthesis of PLA film via surface-initiated ROP from PHEMA brush macroinitiator

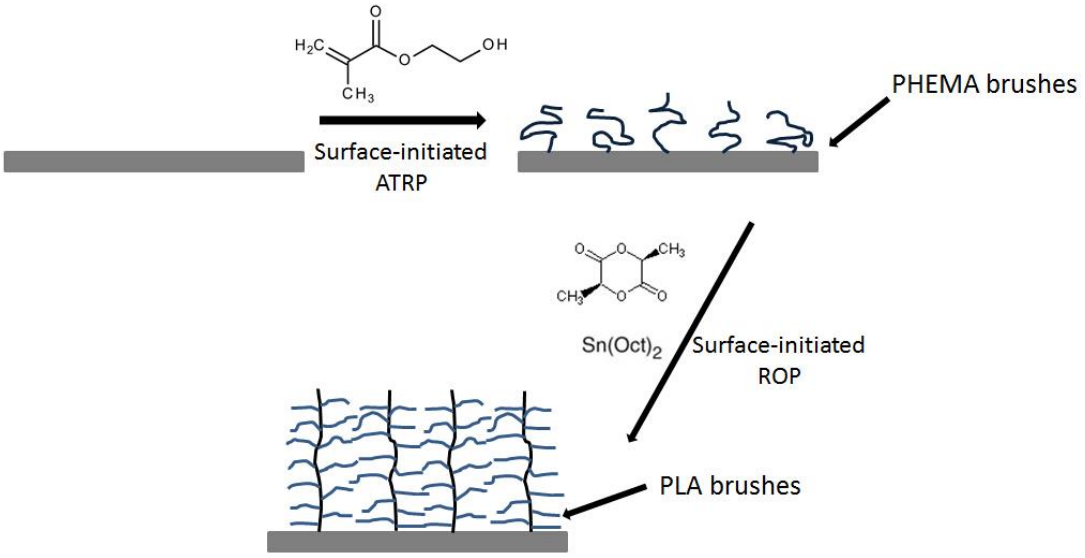

Figure 7.13 Schematic illustration of PLA brush layer grown from PHEMA precursor

The other macroinitiator used in this work was PHEMA brush layer which also contains –OH groups on the side of the chains. Unlike the polyelectrolyte macroinitiator which was assembly onto the substrate via LbL process, PHEMA precursor was grown from the substrate through an ATRP process. Afterwards, PLA layer was synthesized from PHEMA macroinitiator which is described in Figure 7.13.

7.2.1 Synthesis and kinetics of PHEMA brush layer from silicon substrate

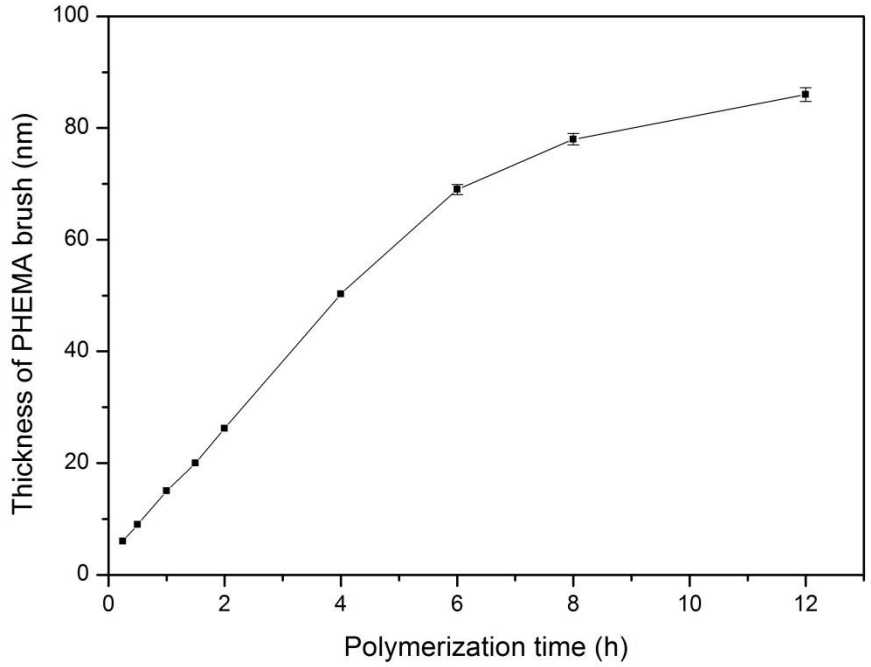

Figure 7.14 Kinetics of PHEMA brush growth on planar substrate

Figure 7.14 shows the kinetics of PHEMA growth on planar substrate. Similar to the growth patterns of most polymer brushes, PHEMA grew almost linearly at the first few hours and then plateaued after 8 h. Although the growth speed was much lower than that reported previously[274], the recipe of which was followed in our experiment, the thickness of the obtained PHEMA precursor was still enough for our study. Thereby, these PHEMA films were used as macroinitiator for ROP in next steps.

7.2.2 Synthesis and kinetics of PLA brushes from PHEMA macroinitiator

Two different heights (26, 50 nm) of PHEMA brush precursors were selected for PLA growth in accordance with the PLA growth from polyelectrolyte macroinitiator. The polymerization procedure as well as the thicknesses measurements after

polymerization was exactly the same as those carried out for PLA growth from polyelectrolyte macroinitiator.

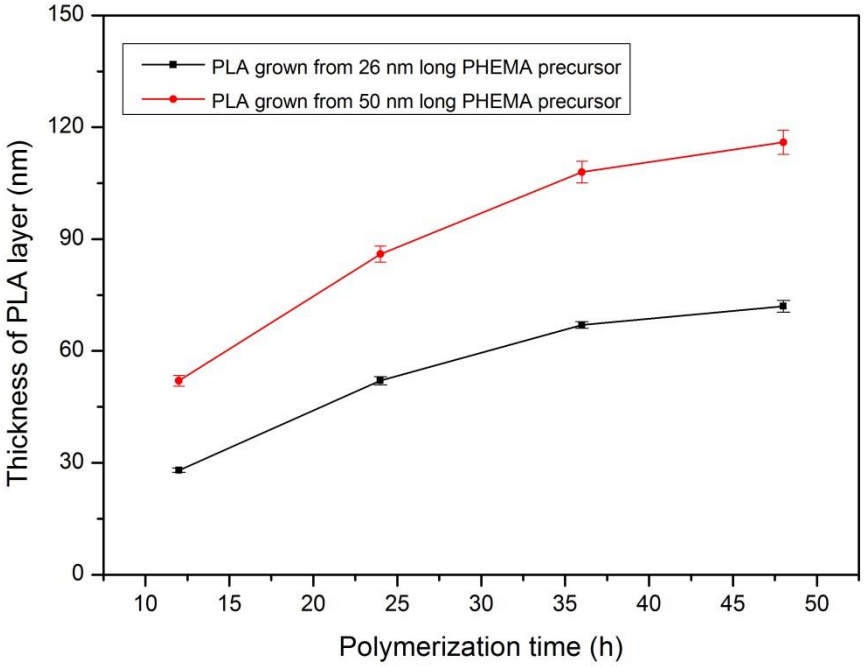

Figure 7.15 Kinetics of PLA growth from PHEMA brush precursor

As can be seen in Figure 7.15 the kinetics of PLA growth, the growth rates also gradually decreased over time which is similar to PLA growth from polyelectrolyte macroinitiator. The thickness of PLA grown from thicker macroinitiator eventually reached 120 nm whilst the thickness of PLA grown from thinner macroinitiator plateaued at around 70 nm. Noticeably, the thickness increases from 50 nm macroinitiator precursor at different time intervals are slightly less than twice those from 26 nm. It is assumed that the –OH groups in 50 nm macroinitiator precursor are slightly less accessible due to the denser structure of thicker PHEMA brush.

7.2.3 Degradation study of PLA brushes

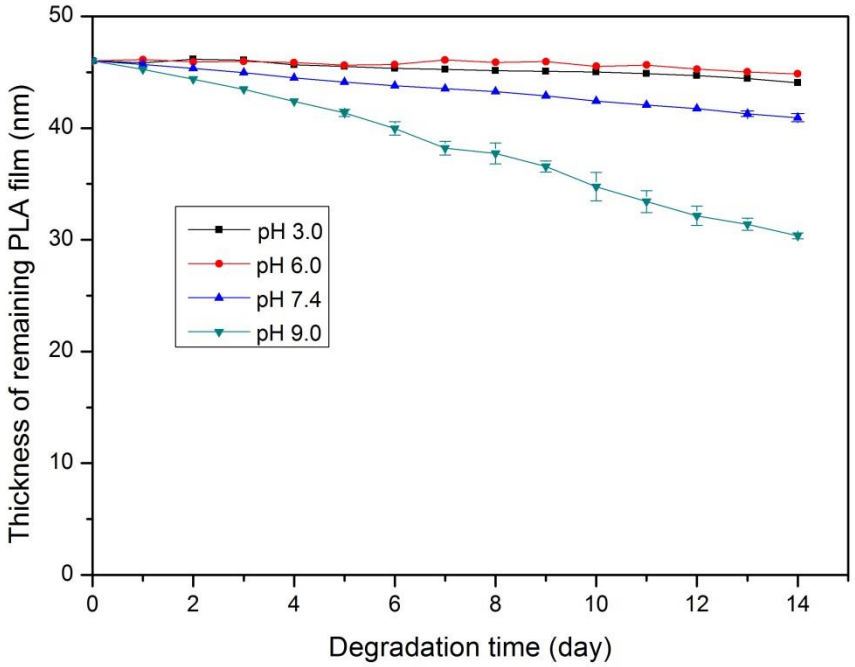

Figure 7.16 Degradation of PLA film in PBS solution at different pH values

The degradation of PLA films were conducted in phosphate-buffered saline (PBS) solution at 37 ℃ at different pH values. PLA brush (46 nm) grown from PHEMA (26 nm) brush precursor was used for this study. After a given amount of incubation time, samples were retrieved from the PBS solution， thoroughly washed with DI water and dried under nitrogen stream before being measured by ellipsometer. The ellipsometric thicknesses of PLA films versus the degradation time were plotted as in Figure 7.16.

PLA film degraded at a relatively fast rate at pH 9.0, losing a thickness of 13 nm in 14 days. At pH 7.4, the degradation was much slower. Only less than 4 nm decrease in thickness was observed over 14 days. When the degradation was performed in acidic conditions (pH 3.0 and 6.0), no obvious change was found in the PLA film thickness

over the entire degradation period. Thus, pH values play an important role in the degradation of PLA films, with basic condition being more effective.

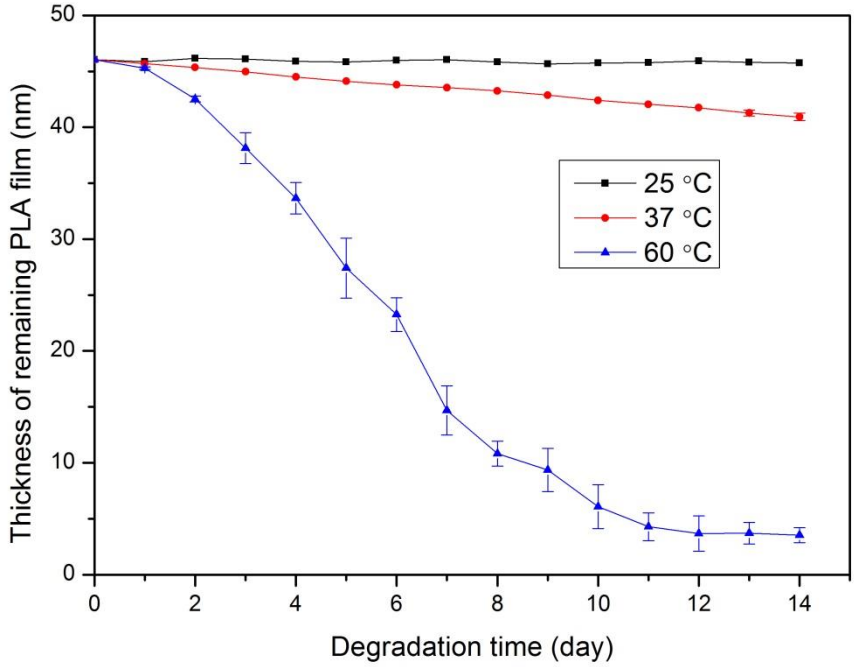

Figure 7.17 Degradation of PLA film in PBS solution at different temperatures

The effect of temperature on PLA degradation was also investigated in standard PBS solutions (pH=7.4) at different temperatures. The thicknesses of PLA films were measured by ellipsometer every 24 hours for 2 weeks and the results were plotted as seen in Figure 7.17. Not surprisingly, the degradation rate at lower temperatures was very slow. PLA film had no thickness loss at 25 ℃ over the entire period whereas only about 5 % decrease in the thickness of PLA film was observed at 37 ℃. However, when the degradation was conducted at 60 ℃, PLA film experienced a much quicker thickness loss. The film almost completely degraded within 12 days, with the thickness ending at about 4 nm which did not change for the last 2 days. This may be

due to the growth of PLA changed the structure of the PHEMA precursor, making its thickness slightly higher than that before PLA growth.

7.3 **Conclusion**

The polyelectrolyte macroinitiator synthesized from a two-step reaction was proven to be able to initiate ROP. The (PSS/MI) multilayers experienced an exponential-to-linear growth transition during LbL deposition. PLA films were then grown from polyelectrolyte based and PHEMA brush based macroinitiators, respectively. The thicknesses of PLA films grown from polyelectrolyte multilayers were thicker than those grown from PHEMA brush precursors. Both types of PLA films were thicker than previously synthesized PLA films from initiator containing self-assembly monolayers, providing a novel way to grow chemically attached PLA films with thickness of more than 100 nm. The degradation of PLA films was investigated at different pH values and temperatures. It was found that elevated temperature as well as basic pH environment would lead to accelerated degradation speed. While covering microparticle with the macroinitiator multilayers water cannot be completely eliminated from microparticles suspension prior to the polymerisation which makes it impossible to synthesize PLA layer on microparticles surface using LbL/SI-ROP binary technique.

8 Overall conclusions and outlook for future work

8.1 Overall conclusions

In order to respond to the increasing demand in encapsulation and delivery of drugs and other bioactive molecules, a variety of microcarriers have been developed in recent decades. Polymeric microcarriers are of particular importance due to the abundant sources, excellent versatility as well as functionalities. However, despite the efforts that have been made, the low permeability of microcarriers remain a challenge which costs massive waste across different fields. Therefore, this PhD thesis was devoted to develop several polymeric microcarrier systems with low permeability by using some state-of-the-art techniques.

There are mainly three techniques used in this PhD work, which are Layer-by-layer, surface-initiated polymerization and emulsion methods. These three approaches as well as their combination provide more options to be chosen for fabrication of microcarriers where certain properties are desired. The first approach used was Layer-by-Layer technique with which stereocomplex PLA microcapsules were fabricated in acetonitrile. It generally requires more layers to form intact capsule structure compared to the polyelectrolyte microcapsules. An appropriate temperature at which the deposition process is carried out is also a vital factor as either lower or higher temperature would lead to thinner polymer layer onto the templates. Different parameters were also compared to optimize the fabrication process. However, the resulting PLA coating on microparticles is not enough to prevent the penetration of EDTA molecules. It is assumed that these microcapsules have invisible defects due to the inhomogeneous adsorption of each layer. Encouragingly, heat treatment at above

T_g significantly lowered the permeability of these PLA microcapsules due to the rearrangement of the PLA molecules within the shell.

The second approach utilised both LbL and SI-ATRP techniques to synthesize PMMA coated microparticles. The kinetics of PMMA growth was first investigated on planar substrate in order to ensure the suitable reaction parameters. It was found that $(PSS/macroinitiator)_6$ multilayers lead to a remarkably faster growth of polymer brush than that from $(PSS/macroinitiator)_3$ precursor due to a higher amount and denser coverage of initiators. The surface with PMMA layer had significantly increased water contact angle than the surface without PMMAcoating, showing that PMMA layer is hydrophobic as anticipated for the aim of this work. PMMA brush layers were then synthesized from $CaCO_3$ particles, which had previously been deposited with different number of PSS/macroinitiator multilayers. Furthermore, FTIR, SEM, TEM as well as elemental analysis indicated that the PMMA shell grown from $(PSS/macroinitiator)_6$ are non-permeable to small molecules as EDTA cannot penetrate the PMMA layer. Afterwards, low permeable PLA coated $CaCO_3$ microparticles with sealed bioactive peptides were successfully prepared via an emulsion process. An additional PVA outmost layer was proven to be helpful in stablizing the obtained microparticles as well as narrowing the size distribution of these particles, with 2.5 % being the optimal PVA concentration. Different contents of $CaCO_3$ microparticles were also studied. Results show that most PLA coated microparticles are low permeable regardless of the $CaCO_3$ content when the mass ratio of $CaCO_3$ to PLA is no more than 0.8. However, PLA coated particles can be penetrated by EDTA when the $CaCO_3$ content in PLA solution exceeds a certain amount. This is probably due to the thinner layer of PLA on each $CaCO_3$ particle. In

general, 0.8 was found to be the optimal mass ratio of $CaCO_3$ relative to PLA in terms of the high-usage of PLA as well as the low permeability of resulting microparticles.

In addition to PMMA coated microparticles using LbL and SI-ATRP techniques, effort were also made to prepare PLA coated microparticles using LbL and surface-initiated polymerization techniques. Different from PMMA which is synthesized via ATRP process, the synthesis of PLA uses ROP. The general procedure was taken place in the same fashion as that for PMMA coated particles. PLA films were first grown from polyelectrolyte based and PHEMA brush based macroinitiators, respectively. The thicknesses of PLA films grown from polyelectrolyte multilayers were thicker than those grown from PHEMA brush precursors. Both types of PLA films were thicker than previously synthesized PLA films from initiator monolayer, providing a novel way to grow chemically attached PLA films with thickness of more than 100 nm. It was found that elevated temperature as well as basic pH environment would lead to accelerated degradation speed. This PLA brush layer can be made use of for various applications such as surface coating of biomedical devices and implants where biocompatible and biodegradable surfaces are required. After having grown PLA brushes on planar substrates, PLA layer were grown from macroinitiator covering particles as was done for PMMA coated microparticles. However, this was failed due to the difficulty in eliminating the remaining water in microparticles prior to ring-opening polymerization (ROP) of lactide. The remaining water can instantly stop the polymerization by acting as competing initiators.

In summary, three different types of microcarrier systems with reduced permeability have been developed using LbL, polymer brush as well as emulsion techniques. The preparation processes were optimized by adjusting various parameters. These low permeable microcarriers, which can be chosen according to the specific usages, are

strongly believed to be promising for encapsulation and delivery of molecules with different molecular weights. Potential applications could be found in a wide range of areas from medicine, coating, food to cosmetic industries.

8.2 Outlook for future work

Several novel polymeric microcarriers with low permeability and improved retention of loading cargo have successfully been prepared in this thesis. However, there certainly are some challenges need to be tackled and more progresses can be made.

Although the possibility of fabricating microcarriers with reduced permeability has been demonstrated, no active drug molecules were encapsulated in this work. Thus, in the next part of work attention could be paid to the encapsulation of small molecule drugs into the microcarriers as well as the release of the loaded drugs.

PLA is one of most widely used biodegradable polymers and biomedical materials source. The success in fabricating multilayered PLA stereocomplex microcapsules with enhanced retention for relatively small molecules after simple heat treatment above its glass transition temperature enables us to further develop a drug delivery system that is fully biodegradable and can deliver small molecular weight drugs. Certain release and delivery means could also be designed. For example, gold and silver nanoparticles could be incorporated between the multilayers and later use laser treatment to break the multi-layered shells. When magnesium nanoparticles are embedded between the multilayers, magnets could be used to direct the microcapsules to the desired area. In comparison with non-biodegradable delivery system, PLA stereocomplex microcapsules would degrade over a certain period of time which is also superior.

For the PMMA coated microparticles, the remaining initiators on the surface of the microparticles are mostly active after ATRP which means the microparticles and their surfaces could be further functionalized by growing other type of polymer brushes. Therefore, various modifications can be carried out to tailor the surface properties of these microcarriers. For example, hydrophilic or hydrophobic outmost layer could be synthesized according to the certain purposes. One can also use the remaining initiators to synthesize a thin anti-fouling layer such as polyoxazoline, which could prevent any non-spesific attachment to micro-organisms.

The emulsion approach used in this work takes advantage of both LbL and emulsion techniques. One of the most important advantages of this approach in comparion to the previsouly reported microcarriers obtained by emulsion processes is the use of $CaCO_3$ microparticles, which can be loaded with various desired molecules prior to the emulsion process. The traditional emulsion approach usually mix the target molecules directly with the solvent which significantly restricts the range of substances that are suitable for the emulsion method. The $CaCO_3$ microparticles basically create a shelter for the loading cargos during the emulsion process which is normally quite vigorous. In addition, the shortened formation duration in an emulsion process compared to that using LbL assembly greatly improved the efficiency of microcarrier prepartion. In future, a wide range of biactive molecules can be encapsulated and release profile as well as means can also be studied. Since emulsion method has been used to manufacture controlled drug release systems by pharmaceutical companies for a long time, this novel development could potentially benefit drugs that have not previously been able to load with this approach.

Unfortunately, PLA coated microparticles were not obtained via LbL/SI-ROP techniques due to the failure in completely removing existing water from

macroinitiator coated particles prior to polymerization. Thus, finding a proper way to remove the remaining water would be extremely important in terms of progressing further in this project. Compared to PLA microcarriers fabricated with LbL and emulsion methods, the PLA microcarriers resulted from LbL/SI-ROP binary technique would have some unique advantages such as more homogenous shell structure, completely tuneable thickness. However, the currently obtained PLA brush layer can still be used as a biodegradable protective coating for some biomedical devices. For example, when a medical device is needed to be put into human body, a homogeneous PLA layer would be a good candidate as a biocompatible coating to reduce the risk of foreign-body reaction to the implant.

After having developed all these improved delivery systems and emphasized to use them particularly for drug delivery purpose, one might wonder what biologically or chemically active substances we would use for the future study. Over the last several years, numerous studies have been focused on delivery of active ingradients, many of which had exclusively used drugs such as doxorubicin without any reasons. Therefore, when it comes to choosing what drug to use, the discussion should be carried out not only between the materials scientist but also with people from medical background in order to make a plan that is of real meanings. In addition to anti-cancer drugs, other type of drugs can also be studied. For example, oral health is also of great importance in our day-to-day life. To use some drugs such as chlorhexidine for the treatment of oral diseases would definitely expand the range of applications.

Apart from medical applications, one could also think of their use in the fields such as cosmetic industry. For example, fragrance products are often required long-lasting property. Our micro containers could be used to incorporate fragrance molecules to

reduce their release rate. Similar application can be found in food industry where these microcapsules could be used to store preservatives.

9 Bibliography

1. Decher, G., J. Hong, and J. Schmitt, *Buildup of ultrathin multilayer films by a self-assembly process: III. Consecutively alternating adsorption of anionic and cationic polyelectrolytes on charged surfaces.* Thin solid films, 1992. **210**: p. 831-835.
2. Decher, G., *Fuzzy nanoassemblies: toward layered polymeric multicomposites.* science, 1997. **277**(5330): p. 1232-1237.
3. *<Stepwise polyelectrolyte assembly on particle surfaces a novel approach to colloid design.PDF>.*
4. Sukhorukov, G.B., et al., *Stepwise polyelectrolyte assembly on particle surfaces: a novel approach to colloid design.* Polymers for Advanced Technologies, 1998. **9**(10‐11): p. 759-767.
5. Donath, E., et al., *Novel hollow polymer shells by colloid‐templated assembly of polyelectrolytes.* Angewandte Chemie International Edition, 1998. **37**(16): p. 2201-2205.
6. Volodkin, D.V., N.I. Larionova, and G.B. Sukhorukov, *Protein encapsulation via porous CaCO3 microparticles templating.* Biomacromolecules, 2004. **5**(5): p. 1962-1972.
7. Yu, A., et al., *Mesoporous Silica Particles as Templates for Preparing Enzyme‐Loaded Biocompatible Microcapsules.* Advanced Materials, 2005. **17**(14): p. 1737-1741.
8. Estillore, N.C. and R.C. Advincula, *Stimuli-responsive binary mixed polymer brushes and free-standing films by LbL-SIP.* Langmuir, 2011. **27**(10): p. 5997-6008.
9. *<pH-Controlled Permeability of Layered.pdf>.*
10. Déjugnat, C., D. Haložan, and G.B. Sukhorukov, *Defined picogram dose inclusion and release of macromolecules using polyelectrolyte microcapsules.* Macromolecular rapid communications, 2005. **26**(12): p. 961-967.
11. Raguzin, I., et al., *Single molecule investigation of complexes of oppositely charged bottle brushes.* Soft Matter, 2013. **9**(2): p. 359-364.
12. Lee, H., et al., *Inorganic analogs of Langmuir-Blodgett films: Adsorption of ordered zirconium 1, 10-decanebisphosphonate multilayers on silicon surfaces.* Journal of the American Chemical Society, 1988. **110**(2): p. 618-620.
13. Such, G.K., et al., *Assembly of ultrathin polymer multilayer films by click chemistry.* Journal of the American Chemical Society, 2006. **128**(29): p. 9318-9319.
14. Lvov, Y., G. Decher, and H. Moehwald, *Assembly, structural characterization, and thermal behavior of layer-by-layer deposited ultrathin films of poly (vinyl sulfate) and poly (allylamine).* Langmuir, 1993. **9**(2): p. 481-486.
15. Decher, G. and J. Hong, *Buildup of ultrathin multilayer films by a self‐assembly process: II. Consecutive adsorption of anionic and cationic bipolar amphiphiles and polyelectrolytes on charged surfaces.* Berichte der Bunsengesellschaft für physikalische Chemie, 1991. **95**(11): p. 1430-1434.
16. Xiang, Y. and S. Lu, *Layer-by-layer self-assembly in the development of electrochemical energy conversion and storage devices from fuel cells to supercapacitors.* Chemical Society Reviews, 2012. **41**(21): p. 7291-7321.
17. Lenahan, K.M., et al., *Novel Polymer Dyes for Nonlinear Optical Applications Using Ionic Self‐Assembled Monolayer Technology.* Advanced Materials, 1998. **10**(11): p. 853-855.
18. Chiarelli, P.A., et al., *Controlled Fabrication of Polyelectrolyte Multilayer Thin Films Using Spin‐Assembly.* Advanced Materials, 2001. **13**(15): p. 1167-1171.

19. Schlenoff, J.B., S.T. Dubas, and T. Farhat, *Sprayed polyelectrolyte multilayers.* Langmuir, 2000. **16**(26): p. 9968-9969.
20. Izquierdo, A., et al., *Dipping versus spraying: Exploring the deposition conditions for speeding up layer-by-layer assembly.* Langmuir, 2005. **21**(16): p. 7558-7567.
21. Jaber, J.A. and J.B. Schlenoff, *Polyelectrolyte multilayers with reversible thermal responsivity.* Macromolecules, 2005. **38**(4): p. 1300-1306.
22. Lvov, Y., G. Decher, and G. Sukhorukov, *Assembly of thin films by means of successive deposition of alternate layers of DNA and poly (allylamine).* Macromolecules, 1993. **26**(20): p. 5396-5399.
23. Borodina, T., et al., *Controlled Release of DNA from Self‐Degrading Microcapsules.* Macromolecular Rapid Communications, 2007. **28**(18‐19): p. 1894-1899.
24. Tiourina, O., et al., *Artificial cell based on lipid hollow polyelectrolyte microcapsules: Channel reconstruction and membrane potential measurement.* The Journal of membrane biology, 2002. **190**(1): p. 9-16.
25. Georgieva, R., et al., *Conductance and capacitance of polyelectrolyte and lipid-polyelectrolyte composite capsules as measured by electrorotation.* Langmuir, 2000. **16**(17): p. 7075-7081.
26. Skirtach, A.G., et al., *Remote activation of capsules containing Ag nanoparticles and IR dye by laser light.* Langmuir, 2004. **20**(17): p. 6988-6992.
27. Bédard, M.F., et al., *Assembling polyelectrolytes and porphyrins into hollow capsules with laser-responsive oxidative properties.* Journal of Materials Chemistry, 2009. **19**(15): p. 2226-2233.
28. Radziuk, D., et al., *Stabilization of silver nanoparticles by polyelectrolytes and poly (ethylene glycol).* Macromolecular rapid communications, 2007. **28**(7): p. 848-855.
29. Skirtach, A.G., et al., *Laser‐Induced Release of Encapsulated Materials inside Living Cells.* Angewandte Chemie International Edition, 2006. **45**(28): p. 4612-4617.
30. De Geest, B.G., et al., *Stimuli‐Responsive Multilayered Hybrid Nanoparticle/Polyelectrolyte Capsules.* Macromolecular rapid communications, 2007. **28**(1): p. 88-95.
31. Mamedov, A.A., et al., *Molecular design of strong single-wall carbon nanotube/polyelectrolyte multilayer composites.* Nature Materials, 2002. **1**(3): p. 190-194.
32. Schlenoff, J.B., G. Decher, and J.B. Schlenoff, *Multilayer thin films: sequential assembly of nanocomposite materials*. 2003: Wiley VCH.
33. Bertrand, P., et al., *Ultrathin polymer coatings by complexation of polyelectrolytes at interfaces: suitable materials, structure and properties.* Macromolecular Rapid Communications, 2000. **21**(7): p. 319-348.
34. Picart, C., et al., *Buildup mechanism for poly (L-lysine)/hyaluronic acid films onto a solid surface.* Langmuir, 2001. **17**(23): p. 7414-7424.
35. Kujawa, P., et al., *Effect of molecular weight on the exponential growth and morphology of hyaluronan/chitosan multilayers: A surface plasmon resonance spectroscopy and atomic force microscopy investigation.* Journal of the American Chemical Society, 2005. **127**(25): p. 9224-9234.
36. Elbert, D.L., C.B. Herbert, and J.A. Hubbell, *Thin polymer layers formed by polyelectrolyte multilayer techniques on biological surfaces.* Langmuir, 1999. **15**(16): p. 5355-5362.
37. Porcel, C., et al., *From exponential to linear growth in polyelectrolyte multilayers.* Langmuir, 2006. **22**(9): p. 4376-4383.
38. Picart, C., et al., *Molecular basis for the explanation of the exponential growth of polyelectrolyte multilayers.* Proceedings of the National Academy of Sciences, 2002. **99**(20): p. 12531-12535.

39. Michel, M., et al., *Layer by layer self-assembled polyelectrolyte multilayers with embedded phospholipid vesicles obtained by spraying: Integrity of the vesicles.* Langmuir, 2005. **21**(17): p. 7854-7859.
40. Salomäki, M., I.A. Vinokurov, and J. Kankare, *Effect of temperature on the buildup of polyelectrolyte multilayers.* Langmuir, 2005. **21**(24): p. 11232-11240.
41. Picart, C., et al., *Measurement of film thickness up to several hundreds of nanometers using optical waveguide lightmode spectroscopy.* Biosensors and Bioelectronics, 2004. **20**(3): p. 553-561.
42. McAloney, R.A., et al., *Atomic force microscopy studies of salt effects on polyelectrolyte multilayer film morphology.* Langmuir, 2001. **17**(21): p. 6655-6663.
43. Ogawa, Y., et al., *Fabrication of Novel Layer-by-Layer Assembly Films Composed of Poly (lactic acid) and Polylysine through Cation− Dipole Interactions.* Langmuir, 2008. **24**(16): p. 8606-8609.
44. Kovtyukhova, N.I., et al., *Layer-by-layer assembly of ultrathin composite films from micron-sized graphite oxide sheets and polycations.* Chemistry of Materials, 1999. **11**(3): p. 771-778.
45. Zhang, J., et al., *Multilayered films fabricated from plasmid DNA and a side-chain functionalized poly (β-amino ester): surface-type erosion and sequential release of multiple plasmid constructs from surfaces.* Langmuir, 2007. **23**(22): p. 11139-11146.
46. Sun, J., et al., *Fabrication of a covalently attached multilayer via photolysis of layer-by-layer self-assembled films containing diazo-resins.* Chemical Communications, 1998(17): p. 1853-1854.
47. Sukhorukov, G.B., et al., *Layer-by-layer self assembly of polyelectrolytes on colloidal particles.* Colloids and Surfaces A: physicochemical and engineering aspects, 1998. **137**(1): p. 253-266.
48. Voigt, A., et al., *Membrane filtration for microencapsulation and microcapsules fabrication by layer-by-layer polyelectrolyte adsorption.* Industrial & engineering chemistry research, 1999. **38**(10): p. 4037-4043.
49. Peyratout, C.S. and L. Dähne, *Tailor‐Made Polyelectrolyte Microcapsules: From Multilayers to Smart Containers.* Angewandte Chemie International Edition, 2004. **43**(29): p. 3762-3783.
50. De Koker, S., et al., *In vivo cellular uptake, degradation, and biocompatibility of polyelectrolyte microcapsules.* Advanced Functional Materials, 2007. **17**(18): p. 3754-3763.
51. Sukhorukov, G.B., et al., *Porous calcium carbonate microparticles as templates for encapsulation of bioactive compounds.* Journal of Materials Chemistry, 2004. **14**(14): p. 2073-2081.
52. Volodkin, D.V., et al., *Matrix polyelectrolyte microcapsules: new system for macromolecule encapsulation.* Langmuir, 2004. **20**(8): p. 3398-3406.
53. Itoh, Y., et al., *Preparation of biodegradable hollow nanocapsules by silica template method.* Chemistry Letters, 2004. **33**(12): p. 1552-1553.
54. Adalsteinsson, T., W.-F. Dong, and M. Schönhoff, *Diffusion of 77 000 g/mol dextran in submicron polyelectrolyte capsule dispersions measured using PFG-NMR.* The Journal of Physical Chemistry B, 2004. **108**(52): p. 20056-20063.
55. Fernandes, P.A., et al., *Quantitative analysis of scanning transmission X-ray microscopy images of gas-filled PVA-based microballoons.* Langmuir, 2008. **24**(23): p. 13677-13682.
56. Shchukin, D.G., et al., *Gas‐Filled Polyelectrolyte Capsules.* Angewandte Chemie International Edition, 2005. **44**(21): p. 3310-3314.
57. Gedanken, A., *Preparation and properties of proteinaceous microspheres made sonochemically.* Chemistry-A European Journal, 2008. **14**(13): p. 3840-3853.

58. Neu, B., et al., *Biological cells as templates for hollow microcapsules.* Journal of microencapsulation, 2001. **18**(3): p. 385-395.
59. Moya, S., et al., *Polyelectrolyte multilayer capsules templated on biological cells: core oxidation influences layer chemistry.* Colloids and Surfaces A: Physicochemical and Engineering Aspects, 2001. **183**: p. 27-40.
60. Kreft, O., et al., *Red blood cell templated polyelectrolyte capsules: a novel vehicle for the stable encapsulation of DNA and proteins.* Macromolecular rapid communications, 2006. **27**(6): p. 435-440.
61. Schneider, G. and G. Decher, *From functional core/shell nanoparticles prepared via layer-by-layer deposition to empty nanospheres.* Nano Letters, 2004. **4**(10): p. 1833-1839.
62. Antipov, A.A., et al., *Carbonate microparticles for hollow polyelectrolyte capsules fabrication.* Colloids and Surfaces A: Physicochemical and Engineering Aspects, 2003. **224**(1): p. 175-183.
63. Manning, G.S., *Limiting laws and counterion condensation in polyelectrolyte solutions. III. An analysis based on the Mayer ionic solution theory.* The Journal of Chemical Physics, 1969. **51**: p. 3249.
64. Klitzing, R.v. and H. Möhwald, *A realistic diffusion model for ultrathin polyelectrolyte films.* Macromolecules, 1996. **29**(21): p. 6901-6906.
65. Gao, C., et al., *Melamine formaldehyde core decomposition as the key step controlling capsule integrity: optimizing the polyelectrolyte capsule fabrication.* Macromolecular Chemistry and Physics, 2002. **203**(7): p. 953-960.
66. Gao, G., et al., *The decomposition process of melamine formaldehyde cores: the key step in the fabrication of ultrathin polyelectrolyte multilayer capsules.* Macromolecular Materials and Engineering, 2001. **286**(6): p. 355-361.
67. Köhler, K. and G.B. Sukhorukov, *Heat treatment of polyelectrolyte multilayer capsules: a versatile method for encapsulation.* Advanced Functional Materials, 2007. **17**(13): p. 2053-2061.
68. Kreft, O., et al., *Polymer microcapsules as mobile local pH-sensors.* J. Mater. Chem., 2007. **17**(42): p. 4471-4476.
69. Caruso, F., et al., *Enzyme encapsulation in layer-by-layer engineered polymer multilayer capsules.* Langmuir, 2000. **16**(4): p. 1485-1488.
70. Hua, F., Y. Lvov, and T. Cui, *A lithographic approach of spatial separation for multiple types of layer-by-layer self-assembled nanoparticles.* Thin solid films, 2004. **449**(1): p. 222-225.
71. Kreft, O., et al., *Shell‐in‐Shell Microcapsules: A Novel Tool for Integrated, Spatially Confined Enzymatic Reactions.* Angewandte Chemie International Edition, 2007. **46**(29): p. 5605-5608.
72. Kreft, O., et al., *Remote control of bioreactions in multicompartment capsules.* Advanced Materials, 2007. **19**(20): p. 3142-3145.
73. Mauser, T., C. Déjugnat, and G.B. Sukhorukov, *Reversible pH‐Dependent Properties of Multilayer Microcapsules Made of Weak Polyelectrolytes.* Macromolecular rapid communications, 2004. **25**(20): p. 1781-1785.
74. Georgieva, R., et al., *Influence of different salts on micro-sized polyelectrolyte hollow capsules.* Journal of Materials Chemistry, 2005. **15**(40): p. 4301-4310.
75. Heuvingh, J., M. Zappa, and A. Fery, *Salt softening of polyelectrolyte multilayer capsules.* Langmuir, 2005. **21**(7): p. 3165-3171.
76. Déjugnat, C. and G.B. Sukhorukov, *pH-responsive properties of hollow polyelectrolyte microcapsules templated on various cores.* Langmuir, 2004. **20**(17): p. 7265-7269.

77. Itano, K., J. Choi, and M.F. Rubner, *Mechanism of the pH-induced discontinuous swelling/deswelling transitions of poly (allylamine hydrochloride)-containing polyelectrolyte multilayer films.* Macromolecules, 2005. **38**(8): p. 3450-3460.
78. Biesheuvel, P.M., et al., *Micromechanical theory for pH-dependent polyelectrolyte multilayer capsule swelling.* Macromolecules, 2006. **39**(24): p. 8480-8486.
79. Gao, C., et al., *Swelling and shrinking of polyelectrolyte microcapsules in response to changes in temperature and ionic strength.* Chemistry-A European Journal, 2003. **9**(4): p. 915-920.
80. Gao, C., H. Möhwald, and J.C. Shen, *Enhanced biomacromolecule encapsulation by swelling and shrinking procedures.* ChemPhysChem, 2004. **5**(1): p. 116-120.
81. Dong, W.-F., et al., *Controlled permeability in polyelectrolyte films via solvent treatment.* Chemistry of materials, 2005. **17**(20): p. 4992-4999.
82. Lvov, Y., et al., *Urease encapsulation in nanoorganized microshells.* Nano Letters, 2001. **1**(3): p. 125-128.
83. Köhler, K., et al., *Drastic morphological modification of polyelectrolyte microcapsules induced by high temperature.* Macromolecules, 2004. **37**(25): p. 9546-9550.
84. Büscher, K., et al., *Influence of adsorption conditions on the structure of polyelectrolyte multilayers.* Langmuir, 2002. **18**(9): p. 3585-3591.
85. Tan, H.L., et al., *Temperature dependence of polyelectrolyte multilayer assembly.* Langmuir, 2003. **19**(22): p. 9311-9314.
86. Köhler, K., H. Möhwald, and G.B. Sukhorukov, *Thermal behavior of polyelectrolyte multilayer microcapsules: 2. Insight into molecular mechanisms for the PDADMAC/PSS system.* The Journal of Physical Chemistry B, 2006. **110**(47): p. 24002-24010.
87. Köhler, K., et al., *Thermal behavior of polyelectrolyte multilayer microcapsules. 1. The effect of odd and even layer number.* The Journal of Physical Chemistry B, 2005. **109**(39): p. 18250-18259.
88. Déjugnat, C., et al., *Membrane Densification of Heated Polyelectrolyte Multilayer Capsules Characterized by Soft X‐ray Microscopy.* Advanced Materials, 2007. **19**(10): p. 1331-1336.
89. Yi, Q., D. Wen, and G.B. Sukhorukov, *UV-cross-linkable multilayer microcapsules made of weak polyelectrolytes.* Langmuir, 2012. **28**(29): p. 10822-10829.
90. Bedard, M.F., et al., *Polymeric microcapsules with light responsive properties for encapsulation and release.* Adv Colloid Interface Sci, 2010. **158**(1-2): p. 2-14.
91. Esser-Kahn, A.P., et al., *Triggered release from polymer capsules.* Macromolecules, 2011. **44**(14): p. 5539-5553.
92. Bédard, M.F., et al., *Toward self-assembly of nanoparticles on polymeric microshells: near-IR release and permeability.* Acs Nano, 2008. **2**(9): p. 1807-1816.
93. Yu, T., Z. Wang, and T.J. Mason, *A review of research into the uses of low level ultrasound in cancer therapy.* Ultrasonics sonochemistry, 2004. **11**(2): p. 95-103.
94. Skirtach, A.G., et al., *Ultrasound stimulated release and catalysis using polyelectrolyte multilayer capsules.* Journal of Materials Chemistry, 2007. **17**(11): p. 1050-1054.
95. Schroeder, A., et al., *Ultrasound triggered release of cisplatin from liposomes in murine tumors.* Journal of controlled release, 2009. **137**(1): p. 63-68.
96. Goldenstedt, C., et al., *Delivery by shock waves of active principle embedded in gelatin-based capsules.* Ultrasonics sonochemistry, 2008. **15**(5): p. 808-814.
97. Caruso, F., et al., *Magnetic CoreqShell Particles: Preparation of Magnetite Multilayers on Polymer Latex Microspheres*.* Adv. Mater, 1999. **11**(11).

98. Zebli, B., et al., *Magnetic targeting and cellular uptake of polymer microcapsules simultaneously functionalized with magnetic and luminescent nanocrystals.* Langmuir, 2005. **21**(10): p. 4262-4265.
99. Lu, Z., et al., *Magnetic switch of permeability for polyelectrolyte microcapsules embedded with Co@Au nanoparticles.* Langmuir, 2005. **21**(5): p. 2042-2050.
100. Hu, S.-H., et al., *Controlled rupture of magnetic polyelectrolyte microcapsules for drug delivery.* Langmuir, 2008. **24**(20): p. 11811-11818.
101. She, Z., et al., *Mechanism of protein release from polyelectrolyte multilayer microcapsules.* Biomacromolecules, 2010. **11**(5): p. 1241-1247.
102. De Cock, L.J., et al., *Polymeric multilayer capsules in drug delivery.* Angewandte Chemie International Edition, 2010. **49**(39): p. 6954-6973.
103. Beyer, S., W.C. Mak, and D. Trau, *Reverse-Phase LbL Encapsulation of Highly Water Soluble Materials by Layer-by-Layer Polyelectrolyte Self-Assembly.* Langmuir, 2007. **23**(17): p. 8827-8832.
104. Beyer, S., et al., *Assembly of biomacromolecule loaded polyelectrolyte multilayer capsules by using water soluble sacrificial templates.* Soft Matter, 2012. **8**(9): p. 2760-2768.
105. Matsusaki, M., et al., *Layer‐by‐Layer Assembly Through Weak Interactions and Their Biomedical Applications.* Advanced Materials, 2012. **24**(4): p. 454-474.
106. Feitsma, E., A. De Boer, and G. Challa, *Association of stereoregular poly (methyl methacrylates): 2. Formation of stereocomplex in bulk.* Polymer, 1975. **16**(7): p. 515-519.
107. De Boer, A. and G. Challa, *Association of stereoregular poly (methyl methacrylates): 3. Thermal behaviour and composition of stereocomplex.* Polymer, 1976. **17**(7): p. 633-637.
108. Vorenkamp, E., F. Bosscher, and G. Challa, *Association of stereoregular poly (methyl methacrylates): 4. Further study on the composition of the stereocomplex.* Polymer, 1979. **20**(1): p. 59-64.
109. Bosscher, F., D. Keekstra, and G. Challa, *The influence of ester groups on the stereocomplex formation between different polyalkylmethacrylates.* Polymer, 1981. **22**(1): p. 124-126.
110. Ikada, Y., et al., *Stereocomplex formation between enantiomeric poly (lactides).* Macromolecules, 1987. **20**(4): p. 904-906.
111. Baba, Y. and A. Kagemoto, *Heats of dissociation of mixture of poly (γ-benzyl L-and D-glutamate).* Macromolecules, 1977. **10**(2): p. 458-460.
112. Takahashi, T., et al., *Dielectric Behavior of DL Mixtures of Poly (γ-benzyl glutamates).* Macromolecules, 1974. **7**(6): p. 806-809.
113. Serizawa, T., et al., *Stepwise stereocomplex assembly of stereoregular poly (methyl methacrylate) s on a substrate.* Journal of the American Chemical Society, 2000. **122**(9): p. 1891-1899.
114. Liquori, A., et al., *Complementary stereospecific interaction between isotactic and syndiotactic polymer molecules.* Nature, 1965. **206**: p. 358-362.
115. Arikawa, Y., et al., *Layer-by-layer crystallization of enantiomeric poly (lactide) s.* Journal of nanoscience and nanotechnology, 2006. **6**(12): p. 3863-3866.
116. Kida, T., M. Mouri, and M. Akashi, *Fabrication of hollow capsules composed of poly (methyl methacrylate) stereocomplex films.* Angewandte Chemie, 2006. **118**(45): p. 7696-7698.
117. Kondo, K., et al., *Nanotube formation through the continuous one-dimensional fusion of hollow nanocapsules composed of layer-by-layer poly (lactic acid) stereocomplex films.* Journal of the American Chemical Society, 2010. **132**(24): p. 8236-8237.

118. Yan, S., et al., *Layer-by-layer assembly of poly (L-glutamic acid)/chitosan microcapsules for high loading and sustained release of 5-fluorouracil.* European Journal of Pharmaceutics and Biopharmaceutics, 2011. **78**(3): p. 336-345.
119. Shi, X. and F. Caruso, *Release behavior of thin-walled microcapsules composed of polyelectrolyte multilayers.* Langmuir, 2001. **17**(6): p. 2036-2042.
120. Tong, W., et al., *Micelles‐Encapsulated Microcapsules for Sequential Loading of Hydrophobic and Water‐Soluble Drugs.* Macromolecular rapid communications, 2010. **31**(11): p. 1015-1019.
121. Huang, C.-J. and F.-C. Chang, *Using click chemistry to fabricate ultrathin thermoresponsive microcapsules through direct covalent layer-by-layer assembly.* Macromolecules, 2009. **42**(14): p. 5155-5166.
122. Gao, H., D. Wen, and G.B. Sukhorukov, *Composite silica nanoparticle/polyelectrolyte microcapsules with reduced permeability and enhanced ultrasound sensitivity.* Journal of Materials Chemistry B, 2015. **3**(9): p. 1888-1897.
123. Liu, L., et al., *Fully printable mesoscopic perovskite solar cells with organic silane self-assembled monolayer.* Journal of the American Chemical Society, 2015. **137**(5): p. 1790-1793.
124. Rühe, J., *Polymer brushes: on the way to tailor-made surfaces.* Polymer Brushes, 2004: p. 1-31.
125. Kong, X., et al., *Amphiphilic polymer brushes grown from the silicon surface by atom transfer radical polymerization.* Macromolecules, 2001. **34**(6): p. 1837-1844.
126. Kim, J.-B., M.L. Bruening, and G.L. Baker, *Surface-initiated atom transfer radical polymerization on gold at ambient temperature.* Journal of the American Chemical Society, 2000. **122**(31): p. 7616-7617.
127. Rodriguez‐Emmenegger, C., et al., *Controlled/Living Surface‐Initiated ATRP of Antifouling Polymer Brushes from Gold in PBS and Blood Sera as a Model Study for Polymer Modifications in Complex Biological Media.* Macromolecular bioscience, 2012. **12**(4): p. 525-532.
128. Li, W., Q. Liu, and L. Liu, *Antifouling Gold Surfaces Grafted with Aspartic Acid and Glutamic Acid Based Zwitterionic Polymer Brushes.* Langmuir, 2014. **30**(42): p. 12619-12626.
129. Haloi, D.J., S. Ata, and N.K. Singha, *Synthesis and characterization of all acrylic block copolymer/clay nanocomposites prepared via surface initiated atom transfer radical polymerization (SI-ATRP).* Industrial & Engineering Chemistry Research, 2012. **51**(29): p. 9760-9768.
130. Jia, X., et al., *Tuning the low critical solution temperature of polymer brushes grafted on single‐walled carbon nanotubes and temperature dependent loading and release properties.* Journal of Polymer Science Part A: Polymer Chemistry, 2014. **52**(13): p. 1807-1814.
131. Huang, Y., et al., *Synthesis of Iron Oxide Rods Coated with Polymer Brushes and Control of Their Assembly in Thin Films.* Langmuir, 2015. **31**(3): p. 1172-1179.
132. Yameen, B., et al., *Surface Initiated Polymerization on Pulsed Plasma Deposited Polyallylamine: A Polymer Substrate‐Independent Strategy to Soft Surfaces with Polymer Brushes.* Macromolecular rapid communications, 2011. **32**(21): p. 1735-1740.
133. Belder, G., G. Ten Brinke, and G. Hadziioannou, *Influence of anchor block size on the thickness of adsorbed block copolymer layers.* Langmuir, 1997. **13**(15): p. 4102-4105.
134. Balazs, A.C., et al., *Theory of polymer chains tethered at interfaces.* Progress in surface science, 1997. **55**(3): p. 181-269.
135. Rühe, J. and W. Knoll, *FUNCTIONAL POLYMER BRUSHES*.* Journal of Macromolecular Science, Part C: Polymer Reviews, 2002. **42**(1): p. 91-138.

136. Prucker, O. and J. Rühe, *Synthesis of poly (styrene) monolayers attached to high surface area silica gels through self-assembled monolayers of azo initiators.* Macromolecules, 1998. **31**(3): p. 592-601.
137. Ma, H., et al., *"Non‐Fouling" Oligo (ethylene glycol)‐Functionalized Polymer Brushes Synthesized by Surface‐Initiated Atom Transfer Radical Polymerization.* Advanced Materials, 2004. **16**(4): p. 338-341.
138. Brinks, M.K. and A. Studer, *Polymer Brushes by Nitroxide‐Mediated Polymerization.* Macromolecular rapid communications, 2009. **30**(13): p. 1043-1057.
139. Ranjan, R. and W.J. Brittain, *Synthesis of high density polymer brushes on nanoparticles by combined RAFT polymerization and click chemistry.* Macromolecular Rapid Communications, 2008. **29**(12‐13): p. 1104-1110.
140. Edmondson, S., V.L. Osborne, and W.T. Huck, *Polymer brushes via surface-initiated polymerizations.* Chemical society reviews, 2004. **33**(1): p. 14-22.
141. Husseman, M., et al., *Controlled synthesis of polymer brushes by "living" free radical polymerization techniques.* Macromolecules, 1999. **32**(5): p. 1424-1431.
142. Ohno, K., et al., *Suspensions of silica particles grafted with concentrated polymer brush: effects of graft chain length on brush layer thickness and colloidal crystallization.* Macromolecules, 2007. **40**(25): p. 9143-9150.
143. Rahane, S.B., et al., *Synthesis of multifunctional polymer brush surfaces via sequential and orthogonal thiol-click reactions.* Journal of Materials Chemistry, 2012. **22**(3): p. 932-943.
144. Börner, H.G., et al., *Synthesis of molecular brushes with block copolymer side chains using atom transfer radical polymerization.* Macromolecules, 2001. **34**(13): p. 4375-4383.
145. Olivier, A., et al., *Surface-initiated controlled polymerization as a convenient method for designing functional polymer brushes: From self-assembled monolayers to patterned surfaces.* Progress in polymer science, 2012. **37**(1): p. 157-181.
146. Wu, L., U. Glebe, and A. Böker, *Surface-initiated controlled radical polymerizations from silica nanoparticles, gold nanocrystals, and bionanoparticles.* Polymer Chemistry, 2015. **6**(29): p. 5143-5184.
147. Huang, X. and M.J. Wirth, *Surface-initiated radical polymerization on porous silica.* Analytical chemistry, 1997. **69**(22): p. 4577-4580.
148. Xiao, D. and M.J. Wirth, *Kinetics of surface-initiated atom transfer radical polymerization of acrylamide on silica.* Macromolecules, 2002. **35**(8): p. 2919-2925.
149. Xia, J., S.G. Gaynor, and K. Matyjaszewski, *Controlled/"living" radical polymerization. Atom transfer radical polymerization of acrylates at ambient temperature.* Macromolecules, 1998. **31**(17): p. 5958-5959.
150. Devaux, C., et al., *Controlled structure and density of "living" polystyrene brushes on flat silica surfaces.* The European Physical Journal E: Soft Matter and Biological Physics, 2002. **7**(4): p. 345-352.
151. Wang, X., et al., *Chem Commun 1999, 1817.* CrossRef| CAS| Web of Science® Times Cited. **130**.
152. Wang, X.-S. and S. Armes, *Facile atom transfer radical polymerization of methoxy-capped oligo (ethylene glycol) methacrylate in aqueous media at ambient temperature.* Macromolecules, 2000. **33**(18): p. 6640-6647.
153. Jones, D.M. and W.T. Huck, *Controlled Surface‐Initiated Polymerizations in Aqueous Media.* Advanced Materials, 2001. **13**(16): p. 1256-1259.
154. Huang, W., et al., *Functionalization of surfaces by water-accelerated atom-transfer radical polymerization of hydroxyethyl methacrylate and subsequent derivatization.* Macromolecules, 2002. **35**(4): p. 1175-1179.

155. Matyjaszewski, K., et al., *Utilizing halide exchange to improve control of atom transfer radical polymerization.* Macromolecules, 1998. **31**(20): p. 6836-6840.
156. Ejaz, M., et al., *Controlled graft polymerization of methyl methacrylate on silicon substrate by the combined use of the Langmuir-Blodgett and atom transfer radical polymerization techniques.* Macromolecules, 1998. **31**(17): p. 5934-5936.
157. Ejaz, M., et al., *Fabrication of patterned high-density polymer graft surfaces. 1. Amplification of phase-separated morphology of organosilane blend monolayer by surface-initiated atom transfer radical polymerization.* Macromolecules, 2002. **35**(4): p. 1412-1418.
158. Zhao, H., X. Kang, and L. Liu, *Comb-coil polymer brushes on the surface of silica nanoparticles.* Macromolecules, 2005. **38**(26): p. 10619-10622.
159. Bombalski, L., et al., *Preparation of well-defined hybrid materials by ATRP in miniemulsion.* Macromolecules, 2007. **40**(21): p. 7429-7432.
160. Esteves, A.C., et al., *Polymer grafting from CdS quantum dots via AGET ATRP in miniemulsion.* Small, 2007. **3**(7): p. 1230-1236.
161. Wischerhoff, E., et al., *Controlled cell adhesion on PEG‐based switchable surfaces.* Angewandte Chemie International Edition, 2008. **47**(30): p. 5666-5668.
162. Bao, Z., M.L. Bruening, and G.L. Baker, *Rapid growth of polymer brushes from immobilized initiators.* Journal of the American Chemical Society, 2006. **128**(28): p. 9056-9060.
163. Ayres, N., C.D. Cyrus, and W.J. Brittain, *Stimuli-responsive surfaces using polyampholyte polymer brushes prepared via atom transfer radical polymerization.* Langmuir, 2007. **23**(7): p. 3744-3749.
164. Perrier, S. and P. Takolpuckdee, *Macromolecular design via reversible addition–fragmentation chain transfer (RAFT)/xanthates (MADIX) polymerization.* Journal of Polymer Science Part A: Polymer Chemistry, 2005. **43**(22): p. 5347-5393.
165. Chiefari, J., et al., *Living free-radical polymerization by reversible addition-fragmentation chain transfer: the RAFT process.* Macromolecules, 1998. **31**(16): p. 5559-5562.
166. Baum, M. and W.J. Brittain, *Synthesis of polymer brushes on silicate substrates via reversible addition fragmentation chain transfer technique.* Macromolecules, 2002. **35**(3): p. 610-615.
167. Zhao, Y. and S. Perrier, *Synthesis of well-defined homopolymer and diblock copolymer grafted onto silica particles by Z-supported RAFT polymerization.* Macromolecules, 2006. **39**(25): p. 8603-8608.
168. Hong, C.-Y., Y.-Z. You, and C.-Y. Pan, *Synthesis of water-soluble multiwalled carbon nanotubes with grafted temperature-responsive shells by surface RAFT polymerization.* Chemistry of materials, 2005. **17**(9): p. 2247-2254.
169. Skaff, H. and T. Emrick, *Reversible addition fragmentation chain transfer (RAFT) polymerization from unprotected cadmium selenide nanoparticles.* Angewandte Chemie, 2004. **116**(40): p. 5497-5500.
170. Tsujii, Y., et al., *Mechanism and kinetics of RAFT-mediated graft polymerization of styrene on a solid surface. 1. Experimental evidence of surface radical migration.* Macromolecules, 2001. **34**(26): p. 8872-8878.
171. Hawker, C.J., et al., *Initiating systems for nitroxide-mediated "living" free radical polymerizations: synthesis and evaluation.* Macromolecules, 1996. **29**(16): p. 5245-5254.
172. Husseman, M., et al., *D. Mecerreyes. DG Benoît. JL Hedrick. P. Mansky. E. Huang. TP Russell, and CJ. Hawker.* Macromolecules, 1999. **32**: p. 1424.

173. Voccia, S., et al., *Controlled free radical polymerization of styrene initiated from alkoxyamine attached to polyacrylate chemisorbed onto conducting surfaces.* Chemistry of materials, 2003. **15**(4): p. 923-927.
174. Zhao, X., et al., *Water soluble multi-walled carbon nanotubes prepared via nitroxide-mediated radical polymerization.* Journal of Materials Chemistry, 2006. **16**(47): p. 4619-4625.
175. Matsuno, R., et al., *Polystyrene-grafted magnetite nanoparticles prepared through surface-initiated nitroxyl-mediated radical polymerization.* Chemistry of materials, 2003. **15**(1): p. 3-5.
176. Matsuno, R., et al., *Polystyrene-and poly (3-vinylpyridine)-grafted magnetite nanoparticles prepared through surface-initiated nitroxide-mediated radical polymerization.* Macromolecules, 2004. **37**(6): p. 2203-2209.
177. Zhao, X.D., et al., *Surface modification of multiwalled carbon nanotubes via nitroxide‐mediated radical polymerization.* Journal of Polymer Science Part A: Polymer Chemistry, 2006. **44**(15): p. 4656-4667.
178. Benoit, D., et al. *Controlled free-radical polymerization in the presence of a novel asymmetric nitroxyl radical*. in *ABSTRACTS OF PAPERS OF THE AMERICAN CHEMICAL SOCIETY*. 1997. AMER CHEMICAL SOC 1155 16TH ST, NW, WASHINGTON, DC 20036.
179. Benoit, D., et al., *Development of a universal alkoxyamine for "living" free radical polymerizations.* Journal of the American Chemical Society, 1999. **121**(16): p. 3904-3920.
180. Benoit, D., et al., *Kinetics and mechanism of controlled free-radical polymerization of styrene and n-butyl acrylate in the presence of an acyclic β-phosphonylated nitroxide.* Journal of the American Chemical Society, 2000. **122**(25): p. 5929-5939.
181. Köthe, M., et al., *Examination of poly (butadiene epoxide)-coatings on inorganic surfaces.* Colloids and Surfaces A: Physicochemical and Engineering Aspects, 1999. **154**(1): p. 75-85.
182. Advincula, R.C., et al., *Polymer brushes*. 2004: Wiley Online Library.
183. Jones, D.M., A.A. Brown, and W.T. Huck, *Surface-initiated polymerizations in aqueous media: effect of initiator density.* Langmuir, 2002. **18**(4): p. 1265-1269.
184. Matyjaszewski, K., et al., *Polymers at interfaces: using atom transfer radical polymerization in the controlled growth of homopolymers and block copolymers from silicon surfaces in the absence of untethered sacrificial initiator.* Macromolecules, 1999. **32**(26): p. 8716-8724.
185. Edmondson, S., et al., *Surface polymerization from planar surfaces by atom transfer radical polymerization using polyelectrolytic macroinitiators.* Macromolecules, 2007. **40**(15): p. 5271-5278.
186. Carlsson, L., et al., *Surface-initiated ring-opening polymerization from cellulose model surfaces monitored by a Quartz Crystal Microbalance.* Soft Matter, 2012. **8**(2): p. 512-517.
187. Voccia, S., et al., *Preparation of poly (ε-caprolactone) brushes at the surface of conducting substrates.* Langmuir, 2004. **20**(24): p. 10670-10678.
188. Ma, J., et al., *Functionalization of multiwalled carbon nanotubes with polyesters via bergman cyclization and "grafting from" strategy.* Journal of Polymer Science Part A: Polymer Chemistry, 2010. **48**(23): p. 5541-5548.
189. Choi, I.S. and R. Langer, *Surface-initiated polymerization of L-lactide: coating of solid substrates with a biodegradable polymer.* Macromolecules, 2001. **34**(16): p. 5361-5363.
190. Hans, M., et al., *Novel biodegradable heterografted polymer brushes prepared via a chemoenzymatic approach.* Macromolecular Chemistry and Physics, 2009. **210**(9): p. 736-746.

191. Zhang, K. and G.N. Tew, *Cyclic brush polymers by combining ring-expansion metathesis polymerization and the "grafting from" technique.* ACS Macro Letters, 2012. **1**(5): p. 574-579.
192. Park, S., Y.S. Chi, and I.S. Choi, *Immobilization of Ti (OiPr) 4 onto silicon oxide surfaces and surface‐initiated polymerization of ϵ‐caprolactone.* Journal of Polymer Science Part A: Polymer Chemistry, 2006. **44**(11): p. 3711-3716.
193. Grubbs III, J.B., et al., *Degradable Polycaprolactone and Polylactide Homopolymer and Block Copolymer Brushes Prepared by Surface-Initiated Polymerization with Triazabicyclodecene and Zirconium Catalysts.* Langmuir, 2015. **31**(37): p. 10183-10189.
194. Hu, X., et al., *Comparison of the growth and degradation of poly (glycolic acid) and poly (ε‐caprolactone) brushes.* Journal of Polymer Science Part A: Polymer Chemistry, 2013. **51**(21): p. 4643-4649.
195. Barbey, R., et al., *Polymer brushes via surface-initiated controlled radical polymerization: synthesis, characterization, properties, and applications.* Chemical reviews, 2009. **109**(11): p. 5437-5527.
196. Bantz, M.R., et al., *Effect of fractional fluorination on the properties of ATRP surface-initiated poly (hydroxyethyl methacrylate) films.* The Journal of Physical Chemistry B, 2004. **108**(28): p. 9787-9794.
197. Zhai, G., Y. Cao, and J. Gao, *Covalently tethered comb‐like polymer brushes on hydrogen‐terminated Si (100) surface via consecutive aqueous atom transfer radical polymerization of methacrylates.* Journal of applied polymer science, 2006. **102**(3): p. 2590-2599.
198. Tugulu, S., et al., *RGD—Functionalized polymer brushes as substrates for the integrin specific adhesion of human umbilical vein endothelial cells.* Biomaterials, 2007. **28**(16): p. 2536-2546.
199. Hojjati, B., R. Sui, and P.A. Charpentier, *Synthesis of TiO 2/PAA nanocomposite by RAFT polymerization.* Polymer, 2007. **48**(20): p. 5850-5858.
200. Navarro, M., et al., *Buried, covalently attached RGD peptide motifs in poly (methacrylic acid) brush layers: the effect of brush structure on cell adhesion.* Langmuir, 2008. **24**(19): p. 10996-11002.
201. Dai, J., et al., *High-capacity binding of proteins by poly (acrylic acid) brushes and their derivatives.* Langmuir, 2006. **22**(9): p. 4274-4281.
202. Cullen, S.P., et al., *Polymeric brushes as functional templates for immobilizing ribonuclease A: study of binding kinetics and activity.* Langmuir, 2008. **24**(3): p. 913-920.
203. Sanjuan, S. and Y. Tran, *Synthesis of random polyampholyte brushes by atom transfer radical polymerization.* Journal of Polymer Science Part A: Polymer Chemistry, 2008. **46**(13): p. 4305-4319.
204. Edmondson, S. and W.T. Huck, *Controlled growth and subsequent chemical modification of poly (glycidyl methacrylate) brushes on silicon wafers.* Journal of Materials Chemistry, 2004. **14**(4): p. 730-734.
205. Xu, F., et al., *Thermoresponsive comb-shaped copolymer-Si (100) hybrids for accelerated temperature-dependent cell detachment.* Biomaterials, 2006. **27**(8): p. 1236-1245.
206. Xu, F., et al., *Covalent immobilization of glucose oxidase on well-defined poly (glycidyl methacrylate)-Si (111) hybrids from surface-initiated atom-transfer radical polymerization.* Biomacromolecules, 2005. **6**(2): p. 1012-1020.
207. Kim, J.-B., et al., *Synthesis of triblock copolymer brushes by surface-initiated atom transfer radical polymerization.* Macromolecules, 2002. **35**(14): p. 5410-5416.

208. Lee, H.J., Y. Nakayama, and T. Matsuda, *Spatio-resolved, macromolecular architectural surface: highly branched graft polymer via photochemically driven quasiliving polymerization technique.* Macromolecules, 1999. **32**(21): p. 6989-6995.
209. Huang, W., G.L. Baker, and M.L. Bruening, *Controlled Synthesis of Cross‐Linked Ultrathin Polymer Films by Using Surface‐Initiated Atom Transfer Radical Polymerization.* Angewandte Chemie, 2001. **113**(8): p. 1558-1560.
210. Yu, W., E. Kang, and K. Neoh, *Controlled grafting of well-defined epoxide polymers on hydrogen-terminated silicon substrates by surface-initiated ATRP at ambient temperature.* Langmuir, 2004. **20**(19): p. 8294-8300.
211. Xu, C., et al., *Synthesis and characterization of tapered copolymer brushes via surface-initiated atom transfer radical copolymerization.* Langmuir, 2005. **21**(24): p. 11136-11140.
212. Chaudhury, M.K. and G.M. Whitesides, *How to make water run uphill.* Science, 1992. **256**(5063): p. 1539-1541.
213. Harris, B.P. and A.T. Metters, *Generation and characterization of photopolymerized polymer brush gradients.* Macromolecules, 2006. **39**(8): p. 2764-2772.
214. Bhat, R.R., M.R. Tomlinson, and J. Genzer, *Orthogonal surface‐grafted polymer gradients: A versatile combinatorial platform.* Journal of Polymer Science Part B: Polymer Physics, 2005. **43**(23): p. 3384-3394.
215. LeMieux, M., et al., *Adaptive nanomechanical response of stratified polymer brush structures.* Langmuir, 2007. **23**(1): p. 265-273.
216. Zhou, F., et al., *Multicomponent polymer brushes.* Journal of the American Chemical Society, 2006. **128**(50): p. 16253-16258.
217. Marutani, E., et al., *Surface-initiated atom transfer radical polymerization of methyl methacrylate on magnetite nanoparticles.* Polymer, 2004. **45**(7): p. 2231-2235.
218. Kim, J.B., et al., *Kinetics of surface‐initiated atom transfer radical polymerization.* Journal of Polymer Science Part A: Polymer Chemistry, 2003. **41**(3): p. 386-394.
219. Gorman, C.B., R.J. Petrie, and J. Genzer, *Effect of substrate geometry on polymer molecular weight and polydispersity during surface-initiated polymerization.* Macromolecules, 2008. **41**(13): p. 4856-4865.
220. Farhan, T., O. Azzaroni, and W.T. Huck, *AFM study of cationically charged polymer brushes: switching between soft and hard matter.* Soft Matter, 2005. **1**(1): p. 66-68.
221. Azzaroni, O., et al., *Switching the properties of polyelectrolyte brushes via "hydrophobic collapse".* Macromolecules, 2005. **38**(24): p. 10192-10199.
222. Lee, B.S., et al., *Functionalization of poly (oligo (ethylene glycol) methacrylate) films on gold and Si/SiO2 for immobilization of proteins and cells: SPR and QCM studies.* Biomacromolecules, 2007. **8**(12): p. 3922-3929.
223. Li, D., et al., *Fabrication of pH-responsive nanocomposites of gold nanoparticles/poly (4-vinylpyridine).* Chemistry of materials, 2007. **19**(3): p. 412-417.
224. Choi, E.-Y., et al., *Electrochemical characteristics of polyelectrolyte brushes with electroactive counterions.* Langmuir, 2007. **23**(20): p. 10389-10394.
225. Spruijt, E., E.-Y. Choi, and W.T. Huck, *Reversible electrochemical switching of polyelectrolyte brush surface energy using electroactive counterions.* Langmuir, 2008. **24**(19): p. 11253-11260.
226. El-Aasser, M., J. Ugelstad, and J. Vanderhoff, *Polymer Emulsification Process.* US4177177 A, 1979.
227. Staff, R.H., et al., *Phase behavior of binary mixtures of block copolymers and a non-solvent in miniemulsion droplets as single and double nanoconfinement.* Soft Matter, 2011. **7**(21): p. 10219-10226.
228. Sansdrap, P. and A.-J. Moës, *Influence of manufacturing parameters on the size characteristics and the release profiles of nifedipine from poly (DL-lactide-co-*

glycolide) microspheres. International journal of pharmaceutics, 1993. **98**(1): p. 157-164.
229. Mainardes, R. and R. Evangelista, *Praziquantel-loaded PLGA nanoparticles: preparation and characterization.* Journal of microencapsulation, 2005. **22**(1): p. 13-24.
230. Staff, R.H., K. Landfester, and D. Crespy, *Recent advances in the emulsion solvent evaporation technique for the preparation of nanoparticles and nanocapsules*, in *Hierarchical Macromolecular Structures: 60 Years after the Staudinger Nobel Prize II*. 2013, Springer. p. 329-344.
231. Clegg, P.S., J.W. Tavacoli, and P.J. Wilde, *One-step production of multiple emulsions: microfluidic, polymer-stabilized and particle-stabilized approaches.* Soft matter, 2016. **12**(4): p. 998-1008.
232. Takada, S., et al., *Sustained release of human growth hormone from microcapsules prepared by a solvent evaporation technique.* Journal of Controlled Release, 2003. **88**(2): p. 229-242.
233. Chen, X., et al., *Synthesis of hydrophilic polymer-grafted ultrafine inorganic oxide particles in protic media at ambient temperature via atom transfer radical polymerization: use of an electrostatically adsorbed polyelectrolytic macroinitiator.* Langmuir, 2004. **20**(3): p. 587-595.
234. Radley company, Available from: http://www.radleys.com/products/our-products/parallel-reaction-stations/carousel-12-plus-reaction-station.
235. Michigan State University, Department of Chemistry, Available from: www2.chemistry.msu.edu/faculty/reusch/virttxtjml/spectrpy/nmr/nmr1.htm.
236. Malvern company, Available from: http://www.malvern.com/en/products/technology/gel-permeation-chromatography/.
237. Polymer Science Learning Center, Available from: http://pslc.ws/macrog/dsc.htm.
238. Kumar, S., S. Chaudhary, and D.C. Jain, *Vibrational Studies of Different Human Body Disorders Using FTIR Spectroscopy.* Open Journal of Applied Sciences, 2014. **4**(03): p. 103.
239. University of California, Berkeley, Available from: http://undsci.berkeley.edu/article/0_0_0/dna_04.
240. Wikipedia. Available from: https://en.wikipedia.org/wiki/Zeta_potential.
241. Silver Colloids, Available from: http://www.silver-colloids.com/Tutorials/Intro/pcs18A.html.
242. Nanoscience Instruments, Available from: http://www.nanoscience.com/technology/sem-technology/how-sem-works/.
243. Material Evaluation and Engineering, inc., Available from: http://www.mee-inc.com/hamm/energy-dispersive-x-ray-spectroscopyeds/.
244. University of Warwick, Department of Physics, Available from: https://www2.warwick.ac.uk/fac/sci/physics/current/postgraduate/regs/mpags/ex5/techniques/structural/tem/.
245. Pechenkin, M.A., H. Möhwald, and D.V. Volodkin, *pH-and salt-mediated response of layer-by-layer assembled PSS/PAH microcapsules: fusion and polymer exchange.* Soft Matter, 2012. **8**(33): p. 8659-8665.
246. She, S., et al., *Fabrication of Red‐Blood‐Cell‐Like Polyelectrolyte Microcapsules and Their Deformation and Recovery Behavior Through a Microcapillary.* Advanced Materials, 2013. **25**(40): p. 5814-5818.
247. Athanasiou, K.A., G.G. Niederauer, and C. Agrawal, *Sterilization, toxicity, biocompatibility and clinical applications of polylactic acid/polyglycolic acid copolymers.* Biomaterials, 1996. **17**(2): p. 93-102.

248. Schliephake, H., et al., *Mandibular bone repair by implantation of rhBMP-2 in a slow release carrier of polylactic acid—an experimental study in rats.* Biomaterials, 2008. **29**(1): p. 103-110.
249. Serizawa, T., et al., *Stepwise assembly of enantiomeric poly (lactide) s on surfaces.* Macromolecules, 2001. **34**(6): p. 1996-2001.
250. Hasırcı, V., et al., *Versatility of biodegradable biopolymers: degradability and an in vivo application.* Journal of biotechnology, 2001. **86**(2): p. 135-150.
251. Zhang, J., et al., *Investigation of phase transitional behavior of poly (L-lactide)/poly (D-lactide) blend used to prepare the highly-oriented stereocomplex.* Macromolecules, 2007. **40**(4): p. 1049-1054.
252. Zhao, L., et al., *A poly (ethylene glycol)-brush decorated magnetic polymer for highly specific enrichment of phosphopeptides.* Chemical Science, 2012. **3**(9): p. 2828-2838.
253. Fredenberg, S., et al., *The mechanisms of drug release in poly (lactic-co-glycolic acid)-based drug delivery systems—a review.* International journal of pharmaceutics, 2011. **415**(1): p. 34-52.
254. Cheng, Y., et al., *Thermally controlled release of anticancer drug from self-assembled γ-substituted amphiphilic poly (ε-caprolactone) micellar nanoparticles.* Biomacromolecules, 2012. **13**(7): p. 2163-2173.
255. Moya, S., et al., *Lipid coating on polyelectrolyte surface modified colloidal particles and polyelectrolyte capsules.* Macromolecules, 2000. **33**(12): p. 4538-4544.
256. Katagiri, K., et al., *Tunable UV-responsive organic− inorganic hybrid capsules.* Chemistry of Materials, 2008. **21**(2): p. 195-197.
257. Krishnamoorthy, M., et al., *Surface-Initiated Polymer Brushes in the Biomedical Field: Applications in Membrane Science, Biosensing, Cell Culture, Regenerative Medicine and Antibacterial Coatings.* Chemical reviews, 2014. **114**(21): p. 10976-11026.
258. Chen, X. and S.P. Armes, *Surface polymerization of hydrophilic methacrylates from ultrafine silica sols in protic media at ambient temperature: a novel approach to surface functionalization using a polyelectrolytic macroinitiator.* Advanced Materials, 2003. **15**(18): p. 1558-1562.
259. Cho, D.-Y., W.-Y. Lee, and P.-C. Sheu, *Treatment of thoracolumbar burst fractures with polymethyl methacrylate vertebroplasty and short-segment pedicle screw fixation.* Neurosurgery, 2003. **53**(6): p. 1354-1361.
260. Jaeblon, T., *Polymethylmethacrylate: properties and contemporary uses in orthopaedics.* Journal of the American Academy of Orthopaedic Surgeons, 2010. **18**(5): p. 297-305.
261. Hayashi, K., et al., *Decentration and tilt of polymethyl methacrylate, silicone, and acrylic soft intraocular lenses.* Ophthalmology, 1997. **104**(5): p. 793-798.
262. Hollick, E.J., et al., *The effect of polymethylmethacrylate, silicone, and polyacrylic intraocular lenses on posterior capsular opacification 3 years after cataract surgery.* Ophthalmology, 1999. **106**(1): p. 49-55.
263. Cuijpers, V.M., et al., *Resolution, sensitivity, and in vivo application of high‐resolution computed tomography for titanium‐coated polymethyl methacrylate (PMMA) dental implants.* Clinical oral implants research, 2014. **25**(3): p. 359-365.
264. John, J., S.A. Gangadhar, and I. Shah, *Flexural strength of heat-polymerized polymethyl methacrylate denture resin reinforced with glass, aramid, or nylon fibers.* The Journal of prosthetic dentistry, 2001. **86**(4): p. 424-427.
265. Rzhepishevska, O., et al., *The surface charge of anti-bacterial coatings alters motility and biofilm architecture.* Biomaterials Science, 2013. **1**(6): p. 589-602.
266. Pinto, J.C., et al., *Organic thin film transistors with polymer brush gate dielectrics synthesized by atom transfer radical polymerization.* Advanced Functional Materials, 2008. **18**(1): p. 36-43.

267. Wischerhoff, E., et al., *Tuning the thickness of polymer brushes grafted from nonlinearly growing multilayer assemblies.* Langmuir, 2009. **25**(10): p. 5949-5956.
268. Zeng, X., et al., *Surface wettability of (3-aminopropyl) triethoxysilane self-assembled monolayers.* The Journal of Physical Chemistry B, 2010. **115**(3): p. 450-454.
269. Tang, L. and N.Y. Lee, *A facile route for irreversible bonding of plastic-PDMS hybrid microdevices at room temperature.* Lab on a Chip, 2010. **10**(10): p. 1274-1280.
270. Morita, T., et al., *Protein encapsulation into biodegradable microspheres by a novel S/O/W emulsion method using poly (ethylene glycol) as a protein micronization adjuvant.* Journal of controlled release, 2000. **69**(3): p. 435-444.
271. Katare, Y.K., T. Muthukumaran, and A.K. Panda, *Influence of particle size, antigen load, dose and additional adjuvant on the immune response from antigen loaded PLA microparticles.* International journal of pharmaceutics, 2005. **301**(1): p. 149-160.
272. Panyam, J., et al., *Solid‐state solubility influences encapsulation and release of hydrophobic drugs from PLGA/PLA nanoparticles.* Journal of pharmaceutical sciences, 2004. **93**(7): p. 1804-1814.
273. Rosca, I.D., F. Watari, and M. Uo, *Microparticle formation and its mechanism in single and double emulsion solvent evaporation.* Journal of Controlled Release, 2004. **99**(2): p. 271-280.
274. Fang, Y., et al., *Poly (2-hydroxyethyl methacrylate) Brush Surface for Specific and Oriented Adsorption of Glycosidases.* Langmuir, 2012. **28**(37): p. 13318-13324.

10 **Publications**

1. Fabrication and characterization of novel multilayered structures by stereocomplexion of poly(D-lactic acid)/poly(L-lactic acid) and self-assembly of polyelectrolytes,
Elena Dellacasa‡, Li Zhao‡, Gesheng Yang, Laura Pastorino and Gleb B. Sukhorukov, Beilstein J. Nanotechnol, 2016, 7, 81–90. (DOI):10.3762/bjnano.7.10. ‡ Equal contribution

2. Fabrication of PLA coated composite microparticles with low permeability, Li Zhao‡, Valeriya Kudryavtseva‡, Gleb B. Sukhorukov, ‡ Equal contribution, submitted to Particle & Particle Systems Characterization

3. Synthesis of low permeable Poly(methyl methacrylate) shell from macroinitiator deposited inorganic templates via surface-initiated atom transfer radical polymerization, Li Zhao, Julien E. Gautrot, Gleb B. Sukhorukov, In preparation